

DISS. ETH NO. 29909

ADVANCING DYNAMIC TRAJECTORY RADIOTHERAPY

EXPLORING ROBUSTNESS FOR
TREATMENT PLANNING AND MANAGING
MOTION FOR DELIVERY

A thesis submitted to attain the degree of

DOCTOR OF SCIENCES
(Dr. sc. ETH Zurich)

presented by

HANNES ANTON LOEBNER
MSc ETH Physics
born on 28.06.1995

accepted on the recommendation of

Prof. Dr. Marco F.M. Stampanoni
Prof. Dr. Peter Manser
Prof. Dr. Per R. Poulsen

2024

Tout est bien qui finit bien.

french proverb, attributed to
William Shakespeare



ABSTRACT

About one in three individuals will develop cancer during their lives which makes cancer a leading cause of death. Fortunately, advances in diagnosing and treating cancer in the last century have improved patient survival and treatment outcome. Modern cancer treatment is based on three pillars. Radiotherapy, alongside surgery and chemotherapy, is prescribed to almost every second cancer patient as a single or combined treatment modality. As a local treatment technique, radiotherapy uses ionizing radiation to treat the tumor. In this context, the term dose is used as a surrogate for the tumor and healthy tissue cell damage induced by the radiation. Although there are other types of ionizing radiation, such as electron-, proton- and heavy ion-based ionizing radiation, photon-based external radiotherapy is the main treatment modality with about 15'000 photon treatment machines worldwide. The external application of photon-based radiotherapy provides cancer patients with a localized, non-invasive treatment method. However during tumour irradiation, healthy tissue will also receive some dose, especially in cases involving deep seated tumours. The resulting radiation induced toxicities can greatly affect a patient's prognosis and quality of life. As a combined result of the advances in imaging, computation and the introduction of new machine equipment in the last decades, treatment outcomes of external radiotherapy could be improved and side effects reduced. Since the early 2000s, the C-arm clinical linear accelerator (linac) has been the workhorse of photon-based radiotherapy. With its multi-leaf collimator (MLC) it enables to efficiently shape the radiation beam and to modulate its intensity, leading to improved healthy tissue sparing. Today's main treatment techniques for external, photon-based radiotherapy treatments are three dimensional conformal radiotherapy, intensity modulated radiotherapy (IMRT) and volumetric modulated arc therapy (VMAT). The introduction of these techniques refined the quality of photon-based radiotherapy

treatment plans by improving target coverage and dose conformity to the tumor as well as reducing dose to healthy tissue and reducing delivery time. Building on these advancements, the pre-clinical research technique dynamic trajectory radiotherapy (DTRT) has been recently developed. DTRT extends VMAT by dynamic table and dynamic collimator rotation during beam-on. DTRT indicates a potential to improve the dosimetric plan quality. Healthy tissue can be spared by avoiding critical organs in the beam path, while maintaining similar tumor coverage and similar delivery times as VMAT. However, the term plan quality is not limited to dosimetric plan quality. It is rather an overriding concept and further includes robustness (to uncertainties on the planning, delivery and patient side), plan complexity, deliverability of and planning protocols for the treatment technique. With the aim to advance DTRT plan quality, each of these aspects must be investigated.

The first study presented in this work, describes the development of a flexible Monte Carlo based robustness tool, to calculate and evaluate the robustness of treatment plans of different treatment techniques. With the intention to characterize robustness of DTRT plans, this tool also enables the plan robustness comparison with other treatment techniques.

The dynamic table rotation during delivery, specifically the gradient in gantry-table rotation, is a main characteristic of DTRT. The second study investigates DTRT plan quality, in terms of dosimetric plan quality, complexity, robustness, deliverability and delivery time as a function of the freedom in the gantry-table rotation gradient for three example cases in the brain and head and neck region. Furthermore, it provides a path finding algorithm for the gantry-table paths of the DTRT plans that includes a maximal user-specified freedom in the gantry-table rotation gradient. The findings of this study are employed in the following studies to generate DTRT plans with appropriate restrictions in the gantry-table rotation gradient.

Head and neck cancer is one of the most complex treatment sites due to the several organs at risk in close proximity to the tumor. The third study facilitates DTRT treatment planning for this cancer entity. It provides and investigates a

standardized but patient-specific DTRT treatment planning protocol, which is used in the fourth study to generate the DTRT treatment plans.

The fourth study is a retrospective comparative study of 46 head and neck cases to assess the dosimetric robustness of DTRT and VMAT plans. The impact of different patient-setup and machine position related uncertainties are investigated.

Intra-fraction patient motion can influence the dosimetric plan quality and lead to a difference between the planned and delivered dose. In the fifth and last study, the technical feasibility and dosimetric performance of free-breathing gating as an active motion mitigation strategy for DTRT is explored.

In conclusion, a tool to assess robustness was successfully developed and employed to compare the robustness of different treatment techniques. DTRT plan quality as a function of the freedom in the gantry-table rotation gradient was investigated, first protocols to generate DTRT plans for head and neck cancer patients were established and free-breathing gating for DTRT was successfully performed for the first time. Together, these findings advance DTRT on the different fronts of treatment plan quality and pave the way for a clinical implementation of DTRT with the long-term goal of improving cancer care and treatment outcome for the patients.

ZUSAMMENFASSUNG

In den letzten Jahren haben sich Krebserkrankungen zu einer der häufigsten Todesursachen entwickelt. Statistiken zeigen, dass etwa ein Drittel der Bevölkerung im Laufe ihres Lebens an Krebs erkrankt. Moderne Therapieansätze gegen Krebs stützen sich dabei auf drei Säulen. Nebst der chirurgischen Intervention und der Chemotherapie wird fast jedem zweiten Krebspatienten eine Strahlentherapie als alleinige oder kombinierte Behandlungsmethode verschrieben. Als lokales Therapieverfahren nutzt die Strahlentherapie ionisierende Strahlung, um den Tumor mit einer bestimmten Dosis zu bestrahlen und die Tumorzellen zu sterilisieren. In diesem Zusammenhang wird der Begriff Dosis als Surrogat für die durch die Strahlung verursachte Schädigung von Tumor- und gesunden Gewebezellen verwendet. Unter den verschiedenen Strahlentherapieoptionen, einschliesslich Elektronen, Protonen und schwere Ionen, ist die externe Photonen-Strahlentherapie die häufigste Behandlungsmethode mit weltweit etwa 15'000 Photonen-Strahlentherapie-Behandlungsgeräten. Sie wird extern angewendet und bietet eine nicht-invasive, lokalisierte Behandlungsmethode für Krebspatienten. Bei der Bestrahlung des Tumors wird jedoch stets auch gesundes Gewebe mitbestrahlt, insbesondere bei tiefsitzenden Tumoren. Dies führt unweigerlich zu Nebenwirkungen, sogenannten strahleninduzierten Toxizitäten, die die Lebensqualität der Patienten erheblich beeinträchtigen können. In den letzten Jahrzehnten konnten in Kombination mit den Entwicklungen in der Bildgebung, der Computertechnik und der Einführung neuer Bestrahlungsgeräte grosse Fortschritte bei den Behandlungsergebnissen und eine Reduzierung der Nebenwirkungen der Strahlentherapie erzielt werden. Seit Anfang der 2000er Jahre hat sich der klinische C-arm Linearbeschleuniger (Linac) als Hauptapplikationsgerät für die externe Photonenbasierte Strahlentherapie etabliert. Mit Hilfe des Multilamellen-Kollimators (MLC) ist er in der Lage, den Photonenstrahl effizient und präzise auf den Tumor zu

formen und die Intensität der Strahlung zu modulieren. Die wichtigsten externen, Photonen-basierten Behandlungstechniken sind heute die konforme 3D-Strahlentherapie, die intensitätsmodulierte Strahlentherapie (IMRT) und die volumetrisch modulierte Bogen-Therapie (VMAT). Mit Einführung dieser Techniken hat sich die Qualität der Photonenbestrahlung und damit die Planqualität verbessert. Neben Verbesserungen im Bereich der Tumor Dosis und ihrer Konformität ermöglichen diese Techniken die Dosis für gesundes Gewebe zu reduzieren und zusätzlich die Behandlungsgenauigkeit und -dauer zu verbessern. Darauf aufbauend, wurde in den letzten Jahren die prä-klinische Forschungstechnik Dynamic Trajectory Radiotherapy (DTRT) entwickelt. DTRT erweitert VMAT durch die Einführung dynamischer Tisch und Kollimator Rotationen während der Bestrahlung. Dies bietet ein Verbesserungspotenzial im Bereich der dosimetrischen Planqualität, d.h. eine bessere Schonung des gesunden Gewebes durch Vermeidung kritischer Organe im Strahlengang, bei gleichzeitiger Beibehaltung der Tumorabdeckung und ähnlicher Bestrahlungszeiten wie VMAT. Der Begriff Planqualität ist jedoch nicht nur auf die dosimetrischen Aspekte beschränkt. Es handelt sich vielmehr um ein übergeordnetes Konzept, das zusätzlich Robustheit (in Bezug auf Planungsunsicherheiten, Abstrahlungsunsicherheiten und patientenbezogene Unsicherheiten), Plan-Komplexität, Applizierbarkeit und standardisierte Planungsprotokolle für die Behandlungstechnik umfasst. Zusammenfassend, um die gesamte Planqualität von DTRT Plänen zu verbessern, bedarf es einer ausführlichen Untersuchung all dieser Aspekte.

Die erste Studie, die in dieser Arbeit vorgestellt wird, beschreibt die Entwicklung eines flexiblen Monte-Carlo basierten Tools zur Berechnung und Bewertung der Robustheit von Behandlungsplänen verschiedener Bestrahlungstechniken. In Bezug auf DTRT soll dieses Tool die Robustheit von DTRT-Plänen charakterisieren und den Vergleich mit anderen Behandlungstechniken ermöglichen.

Die dynamische Tischrotation während der Bestrahlung ist eines der Hauptmerkmale von DTRT. Die zweite Studie untersucht daher die Planqualität der DTRT-Pläne in Bezug auf die dosimetrische Planqualität, die Komplexität, die Robustheit, die Applizierbarkeit und die Bestrahlungszeit als Funktion der Freiheit in dem Gradienten zwischen Gantry- und Tischrotation. Zusätzlich wird ein

Pfadfindungsalgorithmus für die Gantry-Tisch Pfade der DTRT Pläne vorgestellt, der eine benutzerdefinierter Freiheit in dem Gantry-Tischrotationsgradienten respektiert. Die Ergebnisse dieser Studie werden in den folgenden Studien verwendet, um DTRT Behandlungspläne mit angemessenen Restriktionen bezüglich Gantry-Tischrotationsgradienten zu generieren.

Kopf- und Hals-Tumore sind eine der komplexesten Behandlungsstellen aufgrund der verschiedenen gesunden Organen in der Nähe dieser Tumore. Die dritte Studie erleichtert die DTRT-Behandlungsplanung für diese Krebsart, indem sie ein standardisiertes, aber patientenspezifisches DTRT Planungsprotokoll für Kopf und Hals Krebspatienten bereitstellt und untersucht. Dieses Protokoll wird in der folgenden Studie angewandt, um die DTRT Behandlungspläne zu generieren.

Die vierte Studie präsentiert eine retrospektive Studie für 46 Kopf- und Hals-Krebspatienten, um die dosimetrische Robustheit von DTRT und VMAT Behandlungspläne zu bewerten. Die Studie konzentriert sich auf die Untersuchung und den Vergleich der Auswirkungen verschiedener Unsicherheiten beim Patientensetup und der Genauigkeit von verschiedenen Maschinenkomponenten auf DTRT und VMAT Behandlungspläne.

Intra-fractionelle Patientenbewegungen beeinflussen die dosimetrische Planqualität und können zu Unterschieden zwischen der geplanten und der applizierten Dosis führen. In der fünften und letzten Studie wird die technische Durchführbarkeit und die dosimetrische Performance des Free-Breathing Gating als aktive Strategie zur Minderung negativer Effekte der Patientenbewegung auf die dosimetrische Planqualität für DTRT untersucht.

Zusammenfassend wurde ein Tool zur Bewertung der Robustheit erfolgreich entwickelt und angewandt, um die Robustheit verschiedener Behandlungstechniken zu vergleichen. Weiter wurde die Qualität von DTRT Behandlungspläne in Abhängigkeit von der Freiheit in dem Gantry-Tischrotationsgradienten untersucht. Erste Protokolle zur Erstellung von DTRT Behandlungsplänen für Kopf- und Hals-Tumore wurden entwickelt und die Durchführung von Free-Breathing Gating für DTRT wurde erstmals erfolgreich getestet. Diese Ergebnisse bringen DTRT an

den verschiedenen Fronten der Planqualität voran und ebnen den Weg für die klinische Umsetzung von DTRT mit dem langfristigen Ziel, die externe Photonenbasierte Krebsbehandlung und das Behandlungsergebnis für die Patienten zu verbessern.

ACKNOWLEDGEMENTS

My interest in the research field of medical physics was awakened in lectures at ETH Zürich and abroad at KTH Stockholm which introduced me to the topic of medical physics. Following a semester project at the Paul Scherrer Institute (PSI) and a Master's thesis at the Division of Medical Radiation Physics (AMS), I knew I found my passion. Finally, with medical physics, I had found a topic in which I could apply my knowledge of physics in a practical manner and help people. It became clear to me that I wanted to deepen my knowledge in the field and pursue a doctorate in this field, ideally right here in Bern at the AMS.

I would like to begin by thanking Prof. Dr. Marco Stampanoni for the supervision of the thesis and Prof. Dr. Per Poulsen for agreeing to co-examine the dissertation.

My sincerest gratitude goes to Prof. Dr. Peter Manser and Prof. Dr. Michael Fix, for offering me the possibility to conduct the doctoral thesis at AMS, for guiding me along the project and for encouraging me to learn, and to try out new ideas. Even though, their schedules were busy, there was always an open door and ear for my questions and ideas. From research to personal life, I could always count on your sincere interest and support. Throughout my PhD, I learned a lot, but maybe the most profound lesson I learned from you, is the assurance that ultimately, everything will work out, just as the Shakespearean quote at the beginning of the thesis suggests. Thank you, for letting me being part of your team, for your mentoring, and helping me to form this thesis to what it is today.

The research presented in this thesis would not have been possible without the continuous support, insightful discussions, and input from my friends and col-

ACKNOWLEDGEMENTS

leagues. My warmest thanks go to Dr. Jenny Bertholet, who dedicated a lot of her time to help me improve numerous abstracts and paper drafts, even amidst her full days. The conversations, ping-ponging of ideas, and in general working with you, particularly on the robustness and gating study, have been a pleasure and truly rewarding. To Dr. Silvan Mueller, teaching me the art of being a discerning researcher, being "picky" precisely on the right aspects, and for all the conversations about medical physics, but also about general topics like when we were at conferences. To Dr. Paul-Henry Mackeprang for his curiosity to push for new approaches in research and for always listening to my questions from medical to research to general life. To Dr. Werner Volken and Dr. Daniel Frei, whose guidance in studying C++ programming, code/software design, and Monte Carlo improved my studies a lot and helped me progress. To Gian, for his input on shaping research questions and for the insightful discussions. To Chengchen, who I got to know towards the end of my PhD. Thank you, for your input and always being so cheerful and brightening everybody's mood. To Florian, even though not directly connected to this work, but for the infectious optimism and interest in our research.

And of course, I would like to extend my heartfelt gratitude to the whole AMS team, including clinical medical physicists, secretaries, IT-specialists, technicians, planners, physicians and radiation therapy technologist, with whom I had the pleasure working alongside with during the last four years. From the very first day, you welcomed me with open arms. I could always count on your advice, and could profit from your interest in my research and your professional experience.

During the course of my PhD journey, I had the pleasure to supervise several semester and Master's thesis. Supervising the students, designing and managing the project layout and working with them has definitely helped me to mature in my own research journey. Particularly, I want to mention Lisa Fankhauser, Raphael Joost and Björn Zobrist. Their work and the discussions we had contributed to shaping this thesis.

Last but not least, I want to express my love and gratitude to my friends and family, who continuously supported me during my studies and my research jour-

ney. I am thankful to my friends, who welcomed me in Switzerland, and on whose support I could always rely since the first semester. Together we have gone through long periods of learning, researched during our PhD journeys, relaxed during travels and holidays and celebrated on dinners, parties and weddings. A heartfelt thank you goes to Mike and Maria, who proof-read for the English, agreed to several haircuts, and made me feel welcome in their family. I also want to thank my grandparents, for their steadfast faith in me, whenever there was an exam or handing-in of a paper, I knew they were thinking of me. To my parents Judith and Hans, who always support me, quizzing me in long hours for exams since primary school, taking the time to listen to my explanations about physics, but most of all, encouraging me in all my interests and endeavours. To my sister Helen, who always has my back, even when I get on her nerves and who always makes me laugh. And finally I want to thank my wife Sarah, who supported me through my studies at ETH, my research and all other challenges. You always believe in me and you are my rock. Without your continuous love and support, this thesis would not have been possible.

ACKNOWLEDGEMENTS

CONTENTS

Abstract	v
Zusammenfassung	ix
Acknowledgements	xiii
1 Introduction	1
2 Loebner et al.: Monte Carlo based robustness tool	39
3 Loebner et al.: Impact of G-T rotation on DTRT plans	81
4 Bertholet et al.: OAR sparing with DTRT	131
5 Loebner et al.: DTRT & VMAT plan robustness for H&N cancer	179
6 Loebner et al.: Gated dynamic trajectory radiotherapy	219
7 Discussion and outlook	249
8 Concluding remarks	275
Student projects	277
Publications, conference proceedings and grants	279
Peer review	285
Curriculum vitae	287



1

INTRODUCTION

1.1 Cancer today

The term cancer describes a group of diseases in which abnormal cells proliferate uncontrollably [1] and invade adjacent body parts or other organs [2]. With a total number of 19.2 million new cancer cases worldwide in the year 2020, and a total of 9.9 million cancer deaths, cancer is today's second leading cause of death [3]. The global incidence of cancer is predicted to increase by 47% to 28.4 million cases by 2024 [4]. In Western Europe, the cancer burden is substantially larger as compared to the world average. In 2020, the age-standardized incidence rate (ASIR) for all cancer types, excluding non-melanoma skin cancer, was 296.9 for Western Europe as compared to 190.0 for the world average per 100'000. Likewise, in Switzerland the ASIR is 317.6 [3]. Before the age of 70 years, more than one out of five people in Switzerland fall ill from cancer resulting in 46'409 new cases and 17'192 deaths in the year 2019 [5].

The increasing cancer case rate can be partly explained by the developments in imaging and early detection [6]. For instance, the introduction of screening mammography for breast cancer is associated with a doubling of the number of early-stage breast cancer in the United States from 112 to 234 incidences per 100'000 [7, 8]. Similarly for prostate cancer, introducing regular testing for PSA levels led to an increase in prostate cancer incidence [9, 10]. On the bright side, it is most likely that this early detection and diagnosis also improved the cancer survival rates [11–13]. Figure 1.1 shows, that for all illustrated cancer types, age-

INTRODUCTION

standardized five-year overall survival increased between the periods 1997-2001 and 2012-2016 [14], sometimes by more than 10 percentage points. However, there are still cancer types, such as pancreatic cancer, presenting a low overall survival.

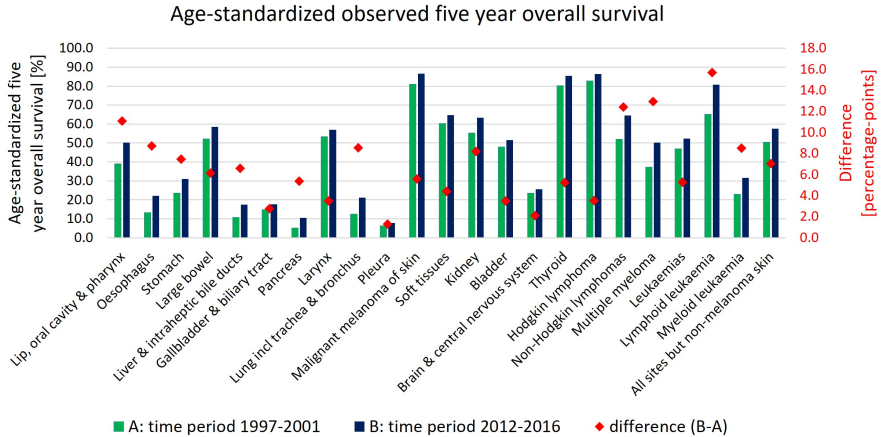


Figure 1.1: Age-standardized observed five-year overall survival in Switzerland for two time periods (1997-2001 and 2012-2016).

To improve the chance of recovery, cancer is often treated using a multi-disciplinary approach consisting of surgery, chemotherapy and radiotherapy [15–17]. Approximately every second patient will receive radiotherapy during cancer treatment [18] and in the future, similar to the incidence rates, the number of cancer patients requiring radiotherapy is expected to increase [19]. Radiotherapy can be delivered using various techniques. A typical distinction is made between internal and external radiotherapy [20]. Internal radiotherapy refers to delivering the radiation from the inside of the body. This is achieved by using radioactive liquid treatment (radioisotope or radionuclide therapy) or using brachytherapy [21]. In brachytherapy a sealed radioactive source is used to administer radiation at a short distance [20]. In external radiotherapy the radiation is delivered from the "outside" of the patient. Different types of highly energetic particles (pho-

tons, electrons, protons, or heavy ions) are produced using various accelerators to deliver the radiation in external radiotherapy [22].

1.2 The principles of radiotherapy

Radiotherapy uses ionizing radiation to sterilize cancer cells. It can be described as "targeted DNA damage" [23]. The DNA damage is induced by direct or indirect ionizing radiation. Photon-based radiotherapy uses indirect ionizing radiation to produce free radicals which in turn can ultimately damage the DNA of the cell. Charged particle radiation, such as electrons or protons, can directly ionize atoms. If the DNA damage is not repaired through DNA damage recognition and repair pathways, the cell will not proliferate and die.

A surrogate for the radiation induced damage is the dose. The physical dose is given in units of Gray (Gy) with $1 \text{ Gy} = 1 \frac{\text{J}}{\text{kg}}$. It is defined as the differential of the mean energy absorbed by a unit mass element of a material and can be measured using ionization chambers. In radiotherapy, it is customary to report the dose to water [24]. The goal of radiotherapy is to deliver a lethal dose to the tumor using ionizing radiation. However, to deliver the dose to tumors within the body, healthy tissue usually receives also some dose and DNA damage can occur, potentially leading to radiation-induced toxicities and treatment complications.

The response of the tumor and healthy tissue to the dose in terms of cell damage, has a sigmoidal shape (figure 1.2). Fortunately, in most cases the curve for the tumor tissue, the tumor control probability (TCP), is located left of the one for healthy tissue, the normal tissue complication probability (NTCP). Between the curves there is the so-called therapeutic window [25, 26]. The goal is to deliver a dose to the tumor sufficient enough to achieve a high TCP, while limiting the NTCP to an acceptable level. Attention has to be paid for these probability curves. The curves usually represent an average over multiple cases of the same tumor or healthy tissue type and contain uncertainties (e.g., due to tissue heterogeneity). Furthermore, there are also uncertainties regarding the dose axis, the accuracy

requirements for the delivery of the absorbed dose are only within $\pm 5\%$ [27].

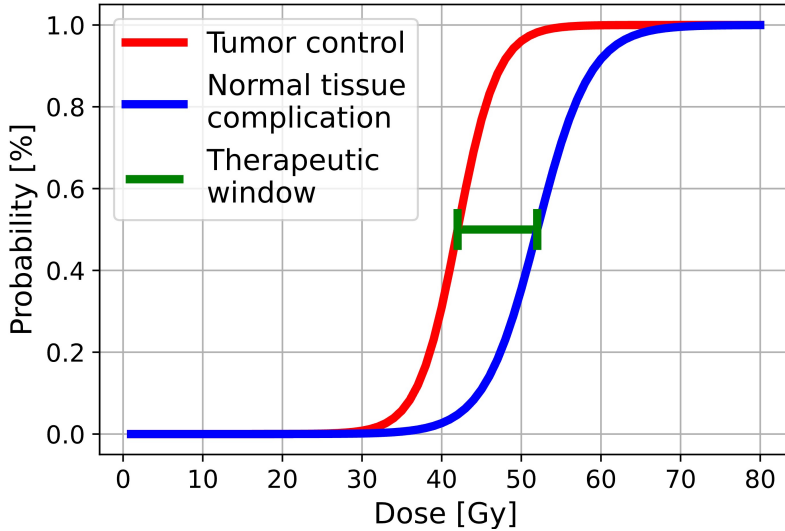


Figure 1.2: Schematic representation of tumor control probability, normal tissue complication probability and therapeutic window.

To widen the therapeutic window, the full treatment is usually not applied within one session but distributed over several treatment sessions. This principle is called fractionation [28, 29] and describes the delivery of multiple sub-lethal doses, usually in the order of 2 Gy. Fractionation exploits the better repair mechanisms of healthy tissue cells as compared to tumor cells. Together, the multiple sub-lethal damages accumulate and lead to sterilization of the cell or cell death of the tumor cells, while they can be repaired in the healthy tissue cells.

1.3 A brief overview of the evolution of radiotherapy

From past to present

The journey of radiotherapy as a pillar of modern cancer treatments began in 1895, with the accidental discovery of Wilhelm Röntgens "new kind of rays". Unsure about their nature, he proceeded to call them X-rays [30, 31], the name they are called by to this day. Shortly after, Henry Becquerel conducted research on fluorescing minerals, and discovered the phenomenon of natural radioactivity [32]. His studies were further advanced by Marie and Pierre Curie, studying radioactive elements. Awarded with two Nobel Prizes [33, 34], their research led to the discovery of polonium and radium in 1898 and laid the foundation of our understanding of radioactivity.

These discoveries quickly found their way into medicine. Only one year after the discovery of X-rays, physicians applied them first for imaging purposes, thus using them for the first diagnostic application [35, 36]. The therapeutic application of X-rays followed shortly after: In 1899 the first cancer patient, a woman with breast cancer, was treated by the physicians Grubb and Ludlam using X-rays, ringing in the era of external radiotherapy [37, 38].

In the following decades, the therapeutic application of ionizing radiation saw the development of several new treatment modalities. On one hand, there were discoveries and developments in the field of internal (interstitial) radiotherapy; in 1903 brachytherapy was first used by Margareth Cleaves to treat cervical cancer [39]. In brachytherapy, a radioactive source is placed directly or in the near proximity of the tumor. On the other hand, in external radiotherapy, the developments of devices to generate of high-energy X-rays in the 1910s allowed the treatment of deep seated tumors. However, due to the severe side effects of ionizing radiation, its clinical application remained at a low level [40, 41].

Next to photon-based treatments, electron therapy emerged in the 1950s [42], and proton therapy labeled as a "precision therapy" [43] was first applied in 1954 to treat a breast cancer patient. While pion therapy was already discussed in 1961 [44] and subsequently applied to several hundred patients at the Paul Scherrer Institute (PSI) in Switzerland, it remained a very specialized therapy modality and was not applied to a wider range of patients. By contrast, in the 1950s, the development of cobalt-60 machines introduced radiotherapy to a greater public. Based on the work of Harold Johns [45], cobalt-60 machines allowed the delivery of higher doses with improved accuracy.

The invention of the clinical computed tomography (CT) scanner by Godfrey Hounsfield in 1967 revolutionized radiotherapy planning [46]. As the cost of computing technology decreased in the following years, CT was applied more in the clinical setting. Due to this switching from two dimensional radiographs to the CT, the tumor and healthy organs could be delineated in three dimensions and thus better considered during treatment planning [47].

In 1956, the medical linear accelerator was finally introduced by Edward Ginzton and Henry Kaplan [48]. Together with the multi-leaf collimator (MLC, 1965) [49, 50], this revolutionary machine enables modulating and efficiently shaping the radiotherapy beam to conform the dose to difficult tumor shapes. This allowed to reduce the dose to the healthy tissue and thus to decrease the occurrence of radiation-induced side effects. The MLC facilitated and improved three-dimensional conformal radiotherapy (3D-CRT) [51]. Combining the MLC with advances in computer science, particularly computational optimization algorithms, intensity modulated radiotherapy (IMRT) [52] was introduced. In IMRT, the intensities of multiple treatment fields are optimized together to enable steeper dose gradients, more homogeneous dose distributions in the tumor region, and improved healthy tissue sparing. However, the application of multiple treatment fields including the different shapes of the intensity modulated fields, can be time consuming. Therefore, volumetric modulated arc therapy (VMAT) was introduced in 2008. In the original paper, VMAT was called "IMRT in a single gantry

arc", thus improving delivery time as compared to multiple IMRT fields [53]. Today VMAT is the state-of-the-art treatment technique due to combining efficient delivery and the dosimetric benefits of IMRT over 3D-CRT. Nonetheless, several treatments are still performed with 3D-CRT and IMRT. In figure 1.3, this evolution of external photon-based radiotherapy is visualized: starting from 2D planning based on radiographs, to 3D-CRT on CT images and finally reaching IMRT/VMAT. With a wood-carved figure it is illustrated how the dose can be shaped more precisely to account for tumor details and spare healthy tissue, by including three dimensional information about the patient and tumor geometry and beam shaping/modulation by means of the MLC.

Evolution of Radiotherapy

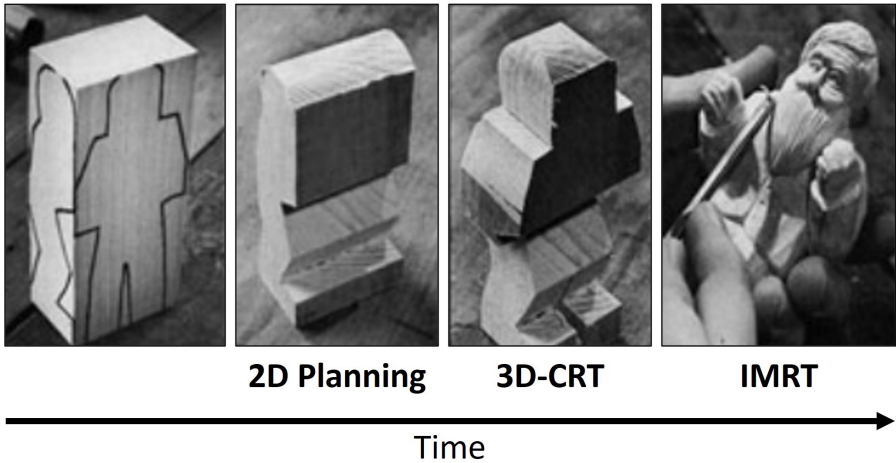


Figure 1.3: Schematic representation of the evolution of photon-based external radiotherapy, adapted from Schreiner [54] and Rock Mackie, IC3D, 2010.

The present - the linear accelerator

Since the early 2000's the linear accelerator (linac) is considered the workhorse in radiotherapy [55]. In Switzerland there are currently approximately 85 linacs for

patient treatment [56] (figure 1.4).

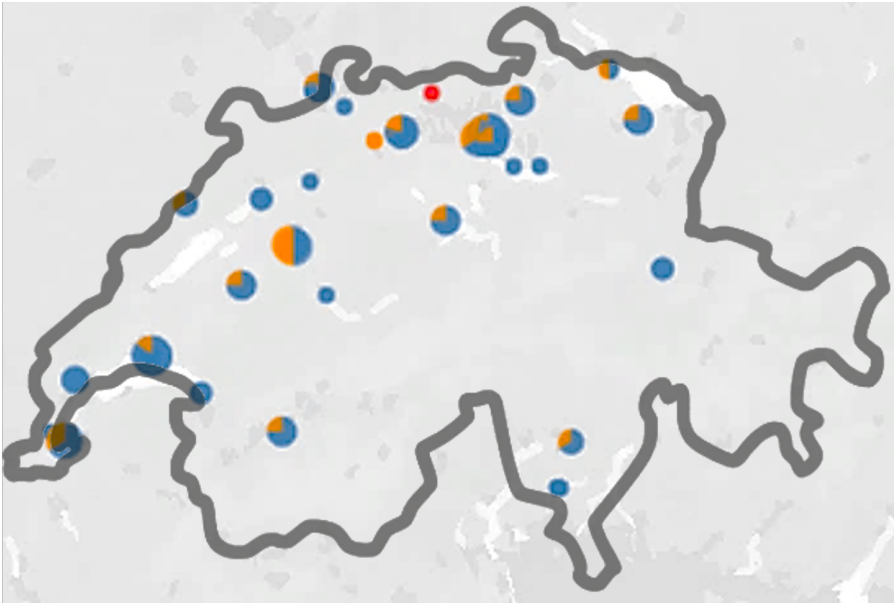


Figure 1.4: Distribution of MV therapy (blue), brachytherapy (orange) and proton therapy (red) centers across Switzerland, adapted from [56]. The size of the circle schematically represents the number of devices in the different places. Linacs are categorized into the MV therapy group due to the energy range of the applied radiation.

Figure 1.5 is a picture of a linac available at Bern University Hospital, Inselspital. From an electron gun mounted in the gantry (figure 1.5, 1), the electrons are accelerated using a wave guide to roughly mono-energetic electron beams with mega-voltage (MV) energy. Using magnets, they are bent (commonly 270°) and focused in the direction of the patient. The linac can be used in photon or electron mode. For the photon mode, a target is placed in the beam path. The focused electrons hit the target and produce MV Bremsstrahlung with a broad spectrum. For the electron mode, there is no target in the beam path. The first shaping of the beam is achieved by a tungsten primary collimator. Next, a flattening filter is introduced to counter the mainly forward peaked angular distribution of the beam

to produce a homogeneous field intensity over commonly used field widths in radiotherapy treatments. Following the flattening filter, a dual ion chamber, called monitor chamber, is mounted to control the to-be-delivered dose. The monitor chamber measures the dose in so-called monitor units (MU) and thus enables beam control. The monitor chamber is calibrated so that 1 MU corresponds to 1 cGy in a phantom under reference conditions [29]. Within the collimator (figure 1.5, 3), the second shaping of the beam is done by the secondary collimators, two sets of jaws, perpendicular to each other, shape the beam into a rectangular field. To enable further beam shaping, a MLC consisting of multiple 0.25-1 cm thick (depending on the MLC model) tungsten leaf pairs that can move independently are introduced (figure 1.5, 4). It enables more conformal radiotherapy but also allows to modulate the intensity of the beam. The secondary collimator jaws and the MLC can be rotated around the beam axis.

The accelerator including the beam-defining system is mounted on a gantry. The patient lies on the treatment table (figure 1.5, 2) and the gantry can be rotated around the patient. In addition, the table can be rotated to enable additional beam directions.

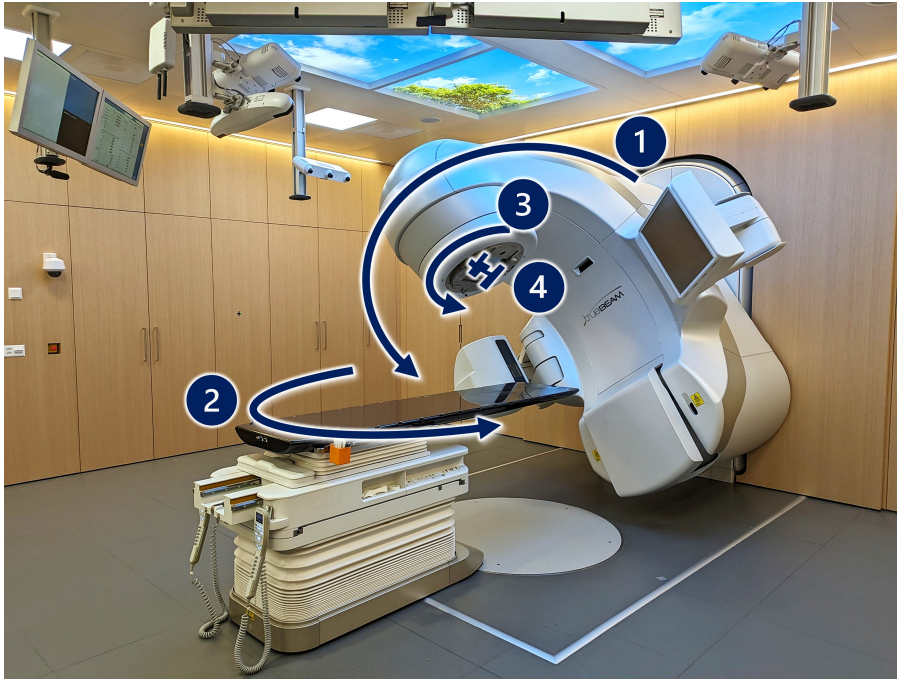


Figure 1.5: Linac (TrueBeam[®], Varian, a Siemens Healthineers Company, Erlangen, Germany) available at Bern University Hospital, Inselspital. The main machine components are indicated by numbers: 1) gantry, including electron gun, waveguide, magnets and target, 2) table, 3) collimator and 4) MLC.

To the future

The state-of-the-art technique, VMAT, involves a dynamic gantry rotation around the patient to deliver the radiotherapy. However, during VMAT the machine is usually restricted to one or a few coplanar plane(s) defined by the beam directions. Modern linacs, as seen in figure 1.5, also enable table or collimator rotation. In pre-clinical research, it was demonstrated that table and collimator could be even rotated dynamically during delivery [57, 58]. The inclusion of non-coplanar beam directions increases the degrees of freedom in treatment planning and organs-at-risk (OARs) in the beam path can be avoided. This has the potential to

improve the sparing of healthy tissue and the dose conformality to the target, as compared to coplanar techniques [59–64]. Particularly, in the brain and head and neck region, non-coplanar radiotherapy has been investigated in the past, due to the increased collision-free space (between gantry and patient, and gantry and treatment table).

In the clinical setting, these promising results lead to the introduction of HyperArc™ (Varian, a Siemens Healthineers Company, Erlangen, Germany), where multiple non-coplanar (and sometimes partial) arcs are used to deliver radiation mostly to brain tumors [65]. However, HyperArc employs a set of fixed non-coplanar partial arcs. The potential of adapting the table angle specifically to the patient is not fully used. There exists also dedicated systems, such as the CyberKnife (Accuray, Sunnyvale, CA, USA) or the discontinued VERO (Brainlab, Munich, Germany and Mitsubishi Heavy Industries, Tokyo, Japan), which are specifically designed to employ non-coplanar beam angles. However, they are not as widely available as the commonly used C-arm linacs [66, 67].

On the research side, the dosimetric benefits of non-coplanar radiotherapy encouraged investigations to include more dynamic machine axis on standard C-arm linacs. With the aim of improving dosimetric plan quality and efficient delivery, dynamic trajectory radiotherapy (DTRT) has been developed [57, 61]. DTRT extends VMAT by dynamic table and dynamic collimator rotation during beam-on, to efficiently bring together the benefits of intensity modulation and non-coplanarity in combination with similar delivery times as VMAT. Next to DTRT, there exist several other non-coplanar treatment techniques, which include (dynamic) table and/or collimator rotation. A common distinction is made based on the inclusion of the table rotation [68]: *static non-coplanar VMAT* refers to VMAT with non-zero static table angles [65, 69, 70], *coronal VMAT* describes arcs with dynamic table rotation but fixed or limited gantry rotation [71, 72], and *trajectory VMAT* is characterized as VMAT with dynamic table and gantry rotation [60, 73]. HyperArc and DTRT can be assigned to the first and last group, respectively. While some of these approaches use geometrical information

to determine the non-coplanar beam paths, by projecting the patient geometry in the beam's eye view plane [59, 74] or using raytracing [75, 76], other approaches include fluence [60, 77–79] or dosimetric [80] information.

The DTRT plans in this work are based on the workflow proposed by Fix et al. [57] (figure 1.6). In short: Upon the acquisition of the CT and the structure delineation, the target-OAR overlap in beam's eye view for every gantry-table (GT) combination is determined to generate a GT map. The GT-map penalizes regions where there is a great overlap of target and OARs. Next, collision and restriction zones are excluded in the GT-map. On the GT-map, an A* path finding [81], to determine the GT-path with the lowest cost for a full gantry rotation. This process can be repeated on different GT-maps focusing on sparing of different OARs to obtain multiple paths. Next, A* path finding is performed on a gantry-collimator (GC) map, which can for instance quantify the field width in the leaf travel direction of a target-conformal and jaw-defined field for each position along the previously determined GT-paths for all possible collimator rotations. Other possibilities include path finding on a map that quantifies the area instead of the field width or the collimator could be aligned with a user-defined axis (e.g., superior-inferior axis). Finally, intensity modulation optimization along the obtained gantry-table-collimator (GTC) paths is performed to obtain the dynamic trajectories. The intensity modulation optimization is followed by the calculation of the dose distribution. This workflow allows for manual planner input at several stages. Particularly, in step 2 (figure 1.6) the selection of OARs to consider to generate the GT-maps substantially impacts the resulting trajectories. Up to now, there is no protocol for this approach proposing a standardized selection of OARs to consider in the GT maps, the number of GTC paths, or consensus on how to determine the collimator rotation. Likewise, apart from general dose limits, there is no protocol for the intensity modulation optimization. Additional structures need to be delineated and optimization objectives need to be specified to ensure sparing of OARs, which might receive more dose with DTRT as compared to VMAT due to the non-coplanar beam directions.

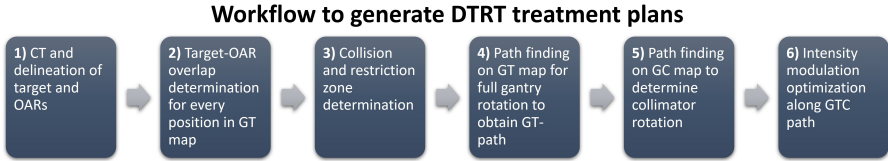


Figure 1.6: DTRT treatment planning as proposed by Fix et al. [57].

In figure 1.7, a VMAT arc setup, a HyperArc partial arc setup, and DTRT dynamic trajectory setup for a nasopharynx carcinoma case are visualized in a research version of the Eclipse (Varian, a Siemens Healthineers Company, Erlangen, Germany) treatment planning system. The red bands around patient phantom indicate the arc/dynamic trajectories. The dynamic trajectories of the DTRT plan are generated according to the approach of Fix et al. [57].

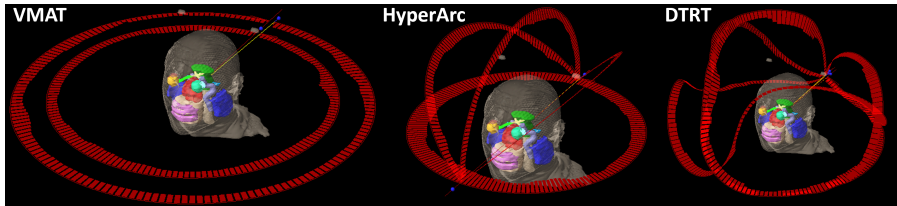


Figure 1.7: VMAT, HyperArc, and DTRT arc/trajectory setup for a nasopharynx carcinoma case. The red bands around the patient indicate the arcs/dynamic trajectories, the target is shown in red, the organs at risk are shown in different colors.

Despite the encouraging dosimetric results and the technical feasibility for delivery, DTRT has not yet been introduced in clinics and is still a research technique.

1.4 Plan quality in radiotherapy

What makes a good radiotherapy treatment plan? To enable the evaluation of treatment plans, the term plan quality needs to be defined in the context of

radiotherapy.

To evaluate plan quality, the focus is usually on the dosimetric properties of the plan. The voxelized three-dimensional dose distribution within the patient of the treatment plan is assessed using dose metrics such as dose volume histograms. To this end the dose distribution needs to be calculated. Dose calculation algorithms can be generally divided into three categories with the trade-off of complexity vs. accuracy: correction-based, model-based, and Monte Carlo (MC) simulations [82]. Correction-based algorithms use dose measurements in water and apply corrections for tissue heterogeneity and surface curvature. Greatest differences to the actual delivered dose are observed at beam borders and inhomogeneous tissues. Model-based approaches, like convolution-superposition, rely on pre-calculated dose kernels to calculate the dose distributions stemming from the interactions of primary radiation particles. The most accurate, however most complex, are MC simulations, simulating and taking into account individual particle transport, different cross-section interactions, backscattering, and electronic disequilibrium in tissue inhomogeneities and interfaces. In clinical practice, algorithms of the the second category and simplified MC methods are common, balancing accuracy and computational efficiency. In our research group the Swiss Monte Carlo Plan (SMCP) has been developed [83, 84]. It interfaces a research version of a standard clinical treatment planning system. It is a user-friendly MC framework for dose distribution calculations for for state-of-the-art treatment techniques, as well as ones under current research [57, 58, 85]. In the studies presented in this work, SMCP is employed for MC dose calculation.

However, even when using MC methods, there can be a discrepancy between the planned and the delivered dose due to various uncertainties. There can be uncertainties in the dose calculation algorithm, delivery uncertainties on the machine side due to the limited accuracy of the treatment machine, as well as uncertainties on the patient side due to variations in the patient anatomy and patient-setup during the course of the treatment. Moreover, there is a knowledge gap connecting the planned dose to a personalized prediction of the clinical outcome.

Due to this reason, Hernandez et al. [86] defined plan quality in their work "as the clinical suitability of the delivered dose distribution that can be realistically expected from a treatment plan". They argue, that plan quality is a multi-faceted topic and the dimension of plan quality is at least threefold:

- *Dosimetric plan quality*, assessed by dose metrics such as dose volume histograms.
- *Robustness*, to dose calculation algorithm-, delivery-, machine- and patient-related uncertainties.
- *Complexity*, with regard to machine movements and ability to deliver the treatment plan as planned.

Also Kaplan et al. agree in their 2020 ESTRO survey, that complexity and robustness are closely interlinked with the plan quality [87]. Hansen et al. [88] extend this definition by *Deliverability* of the treatment plan, as well as by *Protocols*, i.e. the need for standardization in treatment planning and documentation. They admit that there will always be cases where patient-specific customization is needed, however this should be stated and documented. Plan quality is therefore a complex, multi-faceted topic extending beyond the dosimetric aspects of the planned dose distribution.

DTRT has the potential to improve or at least maintain plan quality with regards to each of these points. On the one hand, it could be shown, that DTRT has potential to improve the dosimetric plan quality by improving OAR sparing while maintaining similar target coverage as compared to state-of-the-art VMAT [57, 68]. DTRT has also been shown to efficiently combine non-coplanar beam directions with intensity modulation, resulting in slightly increased but still similar delivery times as VMAT [57]. On the other hand, profound robustness investigations, or assessments of the DTRT plan complexity have not yet been conducted. Furthermore, the current DTRT planning process proposed by Fix et al. [57] is individual to each patient and protocols or standardized planning

procedures have not been proposed and agreed upon. Additionally, there is no strategy, especially no active motion management, to handle patient-motion such as breathing during DTRT delivery. There are still many open questions for investigation to improve plan quality on each of the before-mentioned fronts.

1.5 Uncertainties, robustness and motion management

Uncertainties

In radiotherapy, there is a great variety of uncertainties which can impact the treatment plan quality and thus the treatment outcome. As seen before, there is usually a differentiation between uncertainties related to the patient (e.g., uncertainties in setup [89], contouring [90, 91], motion [92–94], tumor and healthy tissue biology [95]), uncertainties related to the machine (e.g., delivery uncertainties [96, 97], miss-calibration [98, 99]) and uncertainties related to the dose calculation algorithm [100]. The uncertainties on the patient side, particularly setup and motion uncertainties are often described with the term geometric uncertainties [101–103].

Usually, a radiotherapy treatment is administered in multiple fractions. Uncertainties that vary (arbitrarily) in magnitude and direction over all fractions are considered random, while systematic uncertainties occur in each fraction [104, 105]. As an example, a slightly different positioning of the patient on the treatment table each fraction is considered a random uncertainty, whereas a contouring uncertainty of the target is a systematic uncertainty, as this uncertainty is present to the same extent in each fraction. It is important to note, that in this context, the number of treatment fractions influences the classification in systematic and random setup uncertainties. Random uncertainties are considered random in standard fractionated treatments, while they become more systematic in hy-

po-fractionated treatments.

While some uncertainties result in a difference between the planned and the delivered dose (e.g., a patient-setup or a machine calibration uncertainties), some influence the treatment outcome (uncertainties in the dose response) and other uncertainties can impact the treatment plan design. A contouring uncertainty might lead to a different field setup for instance in tangential breast radiotherapy, or a dose calculation algorithm uncertainty might deem a plan not acceptable due to falsely breaching dose limits, leading to unnecessary re-planning.

What all uncertainties have in common is that they impact treatment plan quality. In line with the IAEA report on accuracy requirements and uncertainties in radiotherapy [104], to limit and mitigate the uncertainties to an acceptable level, it is necessary to: first, identify uncertainties relevant to the specific radiotherapy workflow and clinical setting and determine their magnitudes. Second, to assess the impact of the uncertainties and third, to develop quality assurance (QA) procedures, protocols and reporting systems to detect and mitigate the impact of the uncertainties.

A robustness assessment enables quantification of the impact of an uncertainty. This is particularly important when introducing a new treatment technique such as DTRT. Before introducing DTRT to the clinics, it needs to be investigated, if the potential benefits in dosimetric plan quality are not lost in the presence of common uncertainties.

The wide variety of available treatment techniques and machines, dose calculation algorithms in addition to inter-patient anatomical and biological variations, do not generally allow for universal conclusions that relate a specific type of uncertainty to a dosimetric or clinical outcome. It is therefore necessary to evaluate the robustness of the individual treatment plan on a patient-specific level.

Robustness

Radiotherapy plan quality strongly depends the robustness, more specifically, on the dosimetric robustness, of the treatment plan to the before-mentioned uncertainties. Historically, these uncertainties are dealt with using margins [106] and to apply margins, the target needs to be specified. To this end, the international commission on radiation units and measurements (ICRU) has standardized the target definition [107, 108]. First, the gross target volume (GTV), the visible tumor is contoured on the CT or MRI images. Second, the GTV is expanded to the clinical target volume (CTV) to account for likely microscopic spread. This volume is further expanded by a margin to the internal target volume (ITV) to consider motion of the CTV. In the case of breathing motion, the ITV could be defined as the sum of the CTV of all breathing phases. Lastly, to account for setup uncertainties, the CTV or ITV is further expanded to the so-called planning target volume (PTV), to ensure the entire treatment of the CTV in the presence of uncertainties. The prescription of the treatment is usually based on the PTV.

There exist different approaches to determine the necessary margins, particularly the one for the CTV-PTV expansion. Next to literature values, or observations from clinical practice, a formula has been introduced by van Herk [105] to calculate the CTV-PTV margin (M). To cover the CTV for 90% of the patients with 95% of the prescribed dose following margin needs to be selected.

$$M = 2.5\Sigma + 0.7\sigma, \quad (1.1)$$

where Σ is the quadratic sum of all systematic uncertainties and σ is the quadratic sum of all random uncertainties. Although this formula is based on several limitations, such as assuming a rather spherical target or water equivalent densities, it is commonly used in clinical practice. By assigning different weights to the uncertainty types, systematic uncertainties are deemed more important than random ones as random ones have the possibility to average out.

On the downside, adding or increasing margins leads to an increase in the total irradiated volume, particularly the high-dose volume. As per definition margins also include healthy tissue, side effects and radiation-induced toxicities become then more pronounced. The goal is therefore to select appropriate margins, and shape the dose as conformal as possible to the the tumor plus the margin region to minimize the side effects.

To select reasonable margins, the relevant uncertainties need to be identified and their impact needs to be assessed. Apart from the above mentioned formula or literature values, a robustness assessment can be conducted to determine the necessary margins, or to test whether the selected margins are appropriate. During a robustness assessment, the impact of the uncertainty on the planned dose distribution or on the treatment outcome is assessed. In 1985, Goitein [109] proposed a method to calculate the uncertainty in the delivered dose, but there is no consensus, on which uncertainties should be considered or how to summarize treatment plan robustness. In 2021, Sterpin et al. [110] suggested different robustness evaluation procedures to enable statistically consistent reporting, including confidence levels. They propose different procedures to select and evaluate uncertainties, however, they assume knowledge about the probability density functions of the uncertainties. This knowledge is in general not given for any type of uncertainty. To assess the impact of the uncertainties, the dose distribution can be recalculated including the uncertainty. These robustness assessments are computationally expensive and not routinely done in clinical practice for photon-based treatments. There are some approximations to reduce the computational burden, such as the static dose cloud approximation [111, 112]. This approximation suggests that the dose distribution can be shifted within the patient geometry according to the uncertainty. However, not all uncertainties, can be approximated by shifting the dose distribution (e.g., a MLC position uncertainty for a VMAT plan). Moreover, in the case of more complex techniques, such as DTRT, it is not clear how uncertainties impact the dosimetric plan quality, especially when they occur in combination (e.g., a collimator rotation position uncertainty combined

with a table rotation position uncertainty).

Usually, evaluation of the impact of the uncertainty is mainly focused on target [105]. However, some OARs have precedence over target coverage (e.g., the brainstem or the spinal cord), or treatment technique decisions are based on OAR sparing (e.g., the allocation of proton or photon treatment slots according to the Landelijk Indicatie Protocol Protontherapie [113]). It is therefore clear, that a robustness assessment should also consider the robustness of OARs.

Summarizing above mentioned points, an ideal robustness assessment should include the following aspects: *First*, flexible selection of the treatment technique; *Second*, freedom in the selection of uncertainties; *Third*, evaluation the impact of the uncertainty as accurately as possible; *Fourth*, consideration of target and OAR robustness; *Fifth*, reasonably fast calculation and evaluation of the impact of the uncertainty; and *Sixth*, be able to summarize robustness. This coincides with the conclusion of the ESTRO 2020 survey [87], which further highlights the need for commercial tools with these properties to evaluate the treatment plan robustness.

Motion management

The term motion in radiotherapy commonly refers to intra-fraction patient motion, such as breathing, bladder filling/emptying or organ drifts during the treatment delivery. There exists also inter-fraction patient motion, which describes changes in the patient anatomy over the course of the treatment or differences in patient-setup.

A frequently employed passive strategy to address the challenges posed by motion is the introduction of margins [101, 105, 106]. As mentioned before, a common approach is to construct an ITV to encompass the CTV, including all its positions along the motion path based on pre-treatment imaging, to ensure sufficient coverage of the CTV. Opposed to fixed margins, there exist also a probabilistic margin approach that considers the motion as a random positioning

uncertainty and the PTV-construction is based on the mean time-weighted tumor position in the so-called mid-ventilation approach [114, 115]. However, both approaches have two disadvantages, namely that they increase the irradiated high dose volume leading to increased dose to OARs [114] and they cannot ensure target dose coverage, particularly for motion including a target drift that exceeds the margin.

To address these challenges, active motion mitigation strategies have been developed [116]. These strategies directly relate to the principle to 'see what we treat as we treat' [117]. They can be categorized into two different approaches: gating delivers the radiation only when the target is in a pre-defined window and tracking moves the treatment table or the beam-defining parameters (e.g., MLC) to counteract target motion and thus ensuring target coverage [100, 118–123]. The successful implementation of gating and tracking strategies however is dependent on available machine equipment, accurate real-time motion monitoring, fast processing of this monitoring signal and the treatment machines capability to allow for triggering beam on/off or tracking. To apply active motion mitigation strategies for non-coplanar techniques such as DTRT, particularly with the non-coplanar beam directions and the additional dynamic machine axis, several questions arise. It is not clear if patient motion can be monitored for the (dynamic) non-coplanar table positions. Moreover, there is no information about the capabilities of the treatment machine, about its mechanical accuracy and its dosimetric performance for active motion mitigation strategies during DTRT delivery.

1.6 Aim and outline of the thesis

The aim of this thesis is to advance external radiotherapy, in particular, DTRT. By addressing the open questions, challenges and needs mentioned before, with a special focus on robustness and motion management, we aim to explore DTRT plan quality beyond the dosimetric aspects of the planned dose distribution, with the goal to bring DTRT closer to clinical implementation.

The core of this thesis consists of five studies published or submitted to peer-reviewed journals. In the following, the aim and background of these five studies are defined and discussed.

PAPER 1

The first study aims to develop a versatile robustness tool to calculate and evaluate the treatment plan robustness to a wide range of patient- and machine-related uncertainties, individually and in combination. The tool is designed for user-friendly operation. Likewise, a sophisticated code design and data-structure permits the handling of large amounts of data in a multi-dimensional robustness space to extract the desired robustness information, including the robustness summary by the novel robustness index. To ensure accurate calculation of the dose distributions including the uncertainties, MC dose calculation, using the SMCP, serves as the backbone for the robustness tool. The robustness tool is applicable to a wide range of treatment techniques and used to evaluate and compare their robustness.

Keywords: *monte carlo, plan evaluation, robustness (to patient and machine-related uncertainties)*

PAPER 2

The dynamic table rotation is a main characteristic of DTRT. The question arises, how this dynamic table rotation influences the different aspects of DTRT plan

quality. In a comprehensive investigation, this study aims to assess the DTRT plan quality as a function of the gantry-table rotation gradient, in terms of dosimetric plan quality, robustness, deliverability and delivery time. The findings of this study regarding the gantry-table rotation gradient influence the DTRT treatment plan generation which is used in the following studies.

Keywords: *dynamic trajectory radiotherapy, non-coplanar radiotherapy, treatment plan quality*

PAPER 3

In the head and neck area, DTRT has a great potential to improve the dosimetric plan quality. The collision-free space between patient and machine is larger in the head and neck region compared to treatment sites located in the middle and lower body region. DTRT can exploit these non-coplanar beam directions to improve OAR sparing as compared to VMAT, while maintaining target coverage. This study aims to establish DTRT path finding strategies, demonstrate deliverability and dosimetric accuracy of DTRT plans on a standard C-arm linac and compare DTRT to VMAT for common head and neck cancer cases on a publicly available library of common head and neck cancer cases using an anthropomorphic phantom.

Keywords: *treatment planning, non-coplanar radiotherapy, head and neck cancer, VMAT, OAR sparing*

PAPER 4

Robustness is an essential part of the treatment plan quality. The objective of this study is to conduct a comprehensive analysis of the treatment plan robustness to patient-setup and machine position uncertainties for DTRT and VMAT plans for head and neck cancer using the previously developed robustness tool. In this study, the impact of uncertainties on dosimetric endpoints, NTCP values, and fulfilment of planning-goals is analyzed, to identify potential strengths and

limitations of each technique.

Keywords: *head and neck cancer, dynamic trajectory radiotherapy, VMAT, robustness, machine and setup uncertainties*

PAPER 5

Motion management is an essential part of radiotherapy to ensure the delivery of the planned dose. Free-breathing gating is an established motion management strategy. However, in the context of DTRT several challenges related to the specific capabilities of the machine to perform gating during DTRT delivery arise. The aim of this work is therefore to assess the technical feasibility of gating during DTRT delivery, and to evaluate mechanical accuracy and dosimetric performance with and without gating.

Keywords: *dynamic trajectory, gating, motion management*

REFERENCES

1. National Cancer Institute. *Definition of cancer - NCI Dictionary of Cancer Terms*, accessed on 25.10.2023 2023. <https://www.cancer.gov/publications/dictionaries/cancer-terms/def/cancer>.
2. World Health Organization. *Cancer*, accessed on 25.10.2023 https://www.who.int/health-topics/cancer#tab=tab_1.
3. World Health Organization. *Cancer Today*, accessed on 25.10.2023 <https://gco.iarc.fr/today/home>.
4. Sung, H. *et al.* Global Cancer Statistics 2020: GLOBOCAN Estimates of Incidence and Mortality Worldwide for 36 Cancers in 185 Countries. *CA: A Cancer Journal for Clinicians* **71**. ISSN: 0007-9235 (2021).
5. Bundesamt für Statistik. *Krebs*, accessed on 25.10.2023 <https://www.bfs.admin.ch/bfs/de/home/statistiken/gesundheit/gesundheits%20zustand/krankheiten/krebs.html>.
6. Torre, L. A. *et al.* Global cancer statistics, 2012. *CA: A Cancer Journal for Clinicians* **65**. ISSN: 1542-4863 (2015).
7. Bleyer, A. & Welch, H. G. Effect of Three Decades of Screening Mammography on Breast-Cancer Incidence. *New England Journal of Medicine* **367**. ISSN: 0028-4793 (2012).
8. Miller, B. A., Feuer, E. J. & Hankey, B. F. The increasing incidence of breast cancer since 1982: relevance of early detection. *Cancer Causes and Control* **2**. ISSN: 09575243 (1991).

REFERENCES

9. Center, M. M. *et al.* International variation in prostate cancer incidence and mortality rates. *European Urology* **61**. ISSN: 03022838 (2012).
10. Bray, F., Lortet-Tieulent, J., Ferlay, J., Forman, D. & Auvinen, A. Prostate cancer incidence and mortality trends in 37 European countries: An overview. *European Journal of Cancer* **46**. ISSN: 09598049 (2010).
11. Allemani, C. *et al.* Global surveillance of trends in cancer survival 2000–14 (CONCORD-3): analysis of individual records for 37513025 patients diagnosed with one of 18 cancers from 322 population-based registries in 71 countries. *The Lancet* **391**. ISSN: 1474547X (2018).
12. Miller, K. D. *et al.* Cancer treatment and survivorship statistics, 2019. *CA: A Cancer Journal for Clinicians* **69**. ISSN: 0007-9235 (2019).
13. Miller, K. D. *et al.* Cancer treatment and survivorship statistics, 2022. *CA: A Cancer Journal for Clinicians* **72**. ISSN: 0007-9235 (2022).
14. *National statistics on cancer survival, accessed on 25.10.2023* <https://www.nicer.org/en/statistics-atlas/cancer-survival/>.
15. Berardi, R. *et al.* Benefits and limitations of a multidisciplinary approach in cancer patient management. *Cancer Management and Research* **12**. ISSN: 11791322 (2020).
16. Arruebo, M. *et al.* Assessment of the evolution of cancer treatment therapies. *Cancers* **3**. ISSN: 20726694 (2011).
17. Lo Nigro, C., Denaro, N., Merlotti, A. & Merlano, M. Head and neck cancer: Improving outcomes with a multidisciplinary approach. *Cancer Management and Research* **9**, 363–371. ISSN: 11791322 (2017).
18. DKFZ - Deutsches Krebsforschungszentrum. *Strahlentherapie und Nuklearmedizin: Überblick, accessed on 25.10.2023* <https://www.krebsinformationsdienst.de/behandlung/strahlentherapie-nuklearmedizin/>.

19. Borras, J. M. *et al.* How many new cancer patients in Europe will require radiotherapy by 2025? An ESTRO-HERO analysis. *Radiotherapy and Oncology* **119**. ISSN: 18790887 (2016).
20. Sadeghi, M., Enferadi, M. & Shirazi, A. External and internal radiation therapy: Past and future directions. *Journal of Cancer Research and Therapeutics* **6**, 239–248. ISSN: 09731482 (July 2010).
21. Cancer Research UK. *What is internal radiotherapy?* *Cancer treatment*, accessed on 25.10.2023 <https://www.cancerresearchuk.org/about-cancer/treatment/radiotherapy/internal/what-is-internal-radiotherapy>.
22. National Cancer Institute. *External Beam Radiation Therapy for Cancer*, accessed on 25.20.2023 <https://www.cancer.gov/about-cancer/treatment/types/radiation-therapy/external-beam>.
23. Evans, E. & Staffurth, J. Principles of cancer treatment by radiotherapy. *Surgery (Oxford)* **36**, 111–116. ISSN: 0263-9319 (Mar. 2018).
24. Goitein, M. Radiation Oncology: A Physicist's-Eye View. *Biological and Medical Physics, Biomedical Engineering* (2007).
25. SM Bentzen. *Basic Clinical Radiobiology Fourth Edition* (2009).
26. Chang, D. S., Lasley, F. D., Das, I. J., Mendonca, M. S. & Dynlacht, J. R. Therapeutic Ratio. *Basic Radiotherapy Physics and Biology*, 307–312 (2021).
27. IAEA - International Atomic Energy Agency. Determination of absorbed dose in a patient irradiated by beams of X or gamma rays in radiotherapy procedures. ICRU report 24. *ICRU report* (1987).
28. Fowler, J. F. Brief summary of radiobiological principles in fractionated radiotherapy. *Seminars in Radiation Oncology* **2**. ISSN: 10534296 (1992).

REFERENCES

29. Mayles, P., Nahum, A. E. & Rosenwald, J. *Handbook of Radiotherapy Physics: Theory and Practice* ISBN: 9780367192075 (CRC Press, June 2007).
30. Röntgen, W. C. Ueber eine neue Art von Strahlen: vorläufige Mitteilung. *Sitzungsberichten der Würzburger Physikal.-medic. Gesellschaft* (1895).
31. Röntgen, W. C. On a new kind of rays. *Nature* **53**. ISSN: 00280836 (1896).
32. Nobel Prize organization. *Henri Becquerel*, accessed on 25.10.2023 <https://www.nobelprize.org/prizes/physics/1903/becquerel/facts/>.
33. Nobel Prize organization. *The Nobel Prize in Chemistry 1911*, accessed on 25.10.2023 <https://www.nobelprize.org/prizes/chemistry/1911/summary/>.
34. Nobel Prize organization. *The Nobel Prize in Physics 1903*, accessed on 25.10.2023 <https://www.nobelprize.org/prizes/physics/1903/summary/>.
35. Spiegel, P. K. The first clinical X-ray made in America—100 years. *AJR. American journal of roentgenology* **164**. ISSN: 0361803X (1995).
36. Feldman, A. A sketch of the technical history of radiology from 1896 to 1920. *Radiographics* **9**. ISSN: 02715333 (1989).
37. Huh, H. D. & Kim, S. History of Radiation Therapy Technology. *Progress in Medical Physics* **31**. ISSN: 2508-4445 (2020).
38. Lederman, M. The early history of radiotherapy: 1895-1939. *International Journal of Radiation Oncology, Biology, Physics* **7**. ISSN: 03603016 (1981).
39. Mayer, C., Gasalberti, D. P. & Kumar, A. *Brachytherapy* (StatPearls, 2023).
40. Lawrence, E. O. & Livingston, M. S. The production of high speed light ions without the use of high voltages. *Physical Review* **40**. ISSN: 0031899X (1932).

41. Gianfaldoni, S. *et al.* An overview on radiotherapy: From its history to its current applications in dermatology. *Open Access Macedonian Journal of Medical Sciences* **5**. ISSN: 18579655 (2017).
42. Ronga, M. G. *et al.* Back to the future: Very high-energy electrons (vhees) and their potential application in radiation therapy. *Cancers* **13**. ISSN: 20726694 (2021).
43. Hu, M., Jiang, L., Cui, X., Zhang, J. & Yu, J. Proton beam therapy for cancer in the era of precision medicine. *Journal of Hematology and Oncology* **11**. ISSN: 17568722 (2018).
44. Fowler, P. H. & Perkins, D. H. The possibility of therapeutic applications of beams of negative π -mesons. *Nature* **189**. ISSN: 00280836 (1961).
45. Elford Johns, H. O. & John Robert Cunningham, D. *Physics of Radiology* 4th ed. ISBN: 0398046697 (1983).
46. Richmond, C. Sir Godfrey Hounsfield. *BMJ* **329**. ISSN: 0959-8138 (2004).
47. Bucci, M. K., Bevan, A. & Roach, M. Advances in Radiation Therapy: Conventional to 3D, to IMRT, to 4D, and Beyond. *CA: A Cancer Journal for Clinicians* **55**. ISSN: 0007-9235 (2005).
48. Ginzton, E. L., Mallory, K. B. & Kaplan, H. S. The Stanford medical linear accelerator. I. Design and development. *Stanford medical bulletin* **15**. ISSN: 03762602 (1957).
49. Takahashi, S. Conformation radiotherapy. Rotation techniques as applied to radiography and radiotherapy of cancer. *Acta radiologica: diagnosis*. ISSN: 05678056 (1965).
50. Kallman, P., Lind, B., Eklof, A. & Brahme, A. Shaping of arbitrary dose distributions by dynamic multileaf collimation. *Physics in Medicine and Biology* **33**. ISSN: 00319155 (1988).

51. Brewster, L. *et al.* Three dimensional conformal treatment planning with multileaf collimators. *International Journal of Radiation Oncology, Biology, Physics* **33**. ISSN: 03603016 (1995).
52. Bortfeld, T., Bürkelbach, J., Boesecke, R. & Schlegel, W. Methods of image reconstruction from projections applied to conformation radiotherapy. *Physics in Medicine and Biology* **35**. ISSN: 00319155 (1990).
53. Otto, K. Volumetric modulated arc therapy: IMRT in a single gantry arc. *Medical Physics* **35**, 310–317. ISSN: 2473-4209 (Aug. 2008).
54. Schreiner, L. J. *True 3D chemical dosimetry (gels, plastics): Development and clinical role* in *Journal of Physics: Conference Series* **573** (2015).
55. Thwaites, D. I. & Tuohy, J. B. Back to the future: The history and development of the clinical linear accelerator. *Physics in Medicine and Biology* **51**. ISSN: 00319155 (2006).
56. DIRAC - Directory of Radiotherapy Centres. *Division for Human Health: DIRAC, accessed on 25.20.2023* <https://dirac.iaea.org/Query/Countries>.
57. Fix, M. K. *et al.* Part 1: Optimization and evaluation of dynamic trajectory radiotherapy. *Medical Physics* **45**, 4201–4212. ISSN: 00942405 (Aug. 2018).
58. Mueller, S. *et al.* Part 2: Dynamic mixed beam radiotherapy (DYMBER): Photon dynamic trajectories combined with modulated electron beams. *Medical Physics* **45**, 4213–4226. ISSN: 00942405 (Aug. 2018).
59. Yang, Y. *et al.* Choreographing couch and collimator in volumetric modulated arc therapy. *International Journal of Radiation Oncology Biology Physics* **80**. ISSN: 03603016 (2011).
60. Wild, E., Bangert, M., Nill, S. & Oelfke, U. Noncoplanar VMAT for nasopharyngeal tumors: Plan quality versus treatment time. *Medical Physics* **42**, 2157–2168. ISSN: 2473-4209 (Aug. 2015).

61. Smyth, G. *et al.* Dosimetric accuracy of dynamic couch rotation during volumetric modulated arc therapy (DCR-VMAT) for primary brain tumours. *Physics in Medicine and Biology* **64**. ISSN: 13616560 (2019).
62. Park, J., Park, J. W. & Yea, J. W. Non-coplanar whole brain radiotherapy is an effective modality for parotid sparing. *Yeungnam University Journal of Medicine* **36**, 36 (Aug. 2019).
63. Kim, S.-T. *et al.* Non-coplanar VMAT plans for lung SABR to reduce dose to the heart: a planning study. *The British Journal of Radiology* **93**, 20190596. ISSN: 0007-1285 (Aug. 2020).
64. Sheng, K. & Shepard, D. M. Point/Counterpoint. Noncoplanar beams improve dosimetry quality for extracranial intensity modulated radiotherapy and should be used more extensively. *Medical physics* **42**, 531–533. ISSN: 2473-4209 (Aug. 2015).
65. Ohira, S. *et al.* HyperArc VMAT planning for single and multiple brain metastases stereotactic radiosurgery: a new treatment planning approach. *Radiation Oncology 2018 13:1* **13**, 1–9. ISSN: 1748-717X (Aug. 2018).
66. Dieterich, S. & Gibbs, I. C. The cyberknife in clinical use: Current roles, future expectations. *Frontiers of Radiation Therapy and Oncology* **43**. ISSN: 00719676 (2011).
67. Depuydt, T. *et al.* Treating patients with real-time tumor tracking using the Vero gimbaled linac system: Implementation and first review. *Radiotherapy and Oncology* **112**. ISSN: 18790887 (2014).
68. Smyth, G., Evans, P. M., Bamber, J. C. & Bedford, J. L. Recent developments in non-coplanar radiotherapy. *Brit J Radiol* **92**. ISSN: 1748880X (Aug. 2019).
69. Audet, C. *et al.* Evaluation of volumetric modulated arc therapy for cranial radiosurgery using multiple noncoplanar arcs. *Medical Physics* **38**. ISSN: 00942405 (2011).

70. Clark, G. M. *et al.* Plan quality and treatment planning technique for single isocenter cranial radiosurgery with volumetric modulated arc therapy. *Practical Radiation Oncology* **2**. ISSN: 18798500 (2012).
71. Shaitelman, S. F. *et al.* Continuous arc rotation of the couch therapy for the delivery of accelerated partial breast irradiation: A treatment planning analysis. *International Journal of Radiation Oncology Biology Physics* **80**. ISSN: 03603016 (2011).
72. Fahimian, B., Yu, V., Horst, K., Xing, L. & Hristov, D. Trajectory modulated prone breast irradiation: A LINAC-based technique combining intensity modulated delivery and motion of the couch. *Radiotherapy and Oncology* **109**. ISSN: 01678140 (2013).
73. Krayenbuehl, J., Davis, J. B. & Ciernik, I. F. Dynamic intensity-modulated non-coplanar arc radiotherapy (INCA) for head and neck cancer. *Radiotherapy and Oncology* **81**. ISSN: 01678140 (2006).
74. Lee MacDonald, R. & Thomas, C. G. Dynamic trajectory-based couch motion for improvement of radiation therapy trajectories in cranial SRT. *Medical Physics* **42**. ISSN: 24734209 (2015).
75. Smyth, G., Bamber, J. C., Evans, P. M. & Bedford, J. L. Trajectory optimization for dynamic couch rotation during volumetric modulated arc radiotherapy. *Physics in Medicine and Biology* **58**. ISSN: 13616560 (2013).
76. Smyth, G. *et al.* Non-coplanar trajectories to improve organ at risk sparing in volumetric modulated arc therapy for primary brain tumors. *Radiotherapy and Oncology* **121**, 124–131. ISSN: 0167-8140 (Aug. 2016).
77. Papp, D., Bortfeld, T. & Unkelbach, J. A modular approach to intensity-modulated arc therapy optimization with noncoplanar trajectories. *Physics in medicine and biology* **60**, 5179–5198. ISSN: 1361-6560 (Aug. 2015).

78. Langhans, M., Unkelbach, J., Bortfeld, T. & Craft, D. Optimizing highly noncoplanar VMAT trajectories: the NoVo method. *Physics in Medicine & Biology* **63**, 25023. ISSN: 0031-9155 (Aug. 2018).
79. Lyu, Q. *et al.* A novel optimization framework for VMAT with dynamic gantry couch rotation. *Physics in Medicine & Biology* **63**, 125013. ISSN: 0031-9155 (Aug. 2018).
80. Mackeprang, P. *et al.* MO-0544 4pi-IMRT based path-finding for dynamic trajectory radiotherapy. *Radiotherapy and Oncology* **170**, S469–S470. ISSN: 01678140 (Aug. 2022).
81. Hart, P. E., Nilsson, N. J. & Raphael, B. A Formal Basis for the Heuristic Determination of Minimum Cost Paths. *IEEE Transactions on Systems Science and Cybernetics* **4**, 100–107 (1968).
82. Speer, T. W. *et al.* in *Encyclopedia of Radiation Oncology* 158–166 (Springer Berlin Heidelberg, Berlin, Heidelberg, 2013).
83. Fix, M. K. *et al.* An efficient framework for photon Monte Carlo treatment planning. *Physics in Medicine and Biology* **52**, 425–437. ISSN: 00319155 (2007).
84. Fix, K. *et al.* Efficient photon treatment planning by the use of Swiss Monte Carlo Plan. *Journal of Physics: Conference Series* **74**, 21004. ISSN: 1742-6596 (Aug. 2007).
85. Guyer, G. *et al.* Enabling non-isocentric dynamic trajectory radiotherapy by integration of dynamic table translations. *Physics in Medicine and Biology* **67**. ISSN: 13616560 (2022).
86. Hernandez, V. *et al.* What is plan quality in radiotherapy? The importance of evaluating dose metrics, complexity, and robustness of treatment plans. *Radiother Oncol* **153**, 26–33. ISSN: 18790887 (2020).

87. Kaplan, L. P. *et al.* Plan quality assessment in clinical practice: Results of the 2020 ESTRO survey on plan complexity and robustness. *Radiotherapy and Oncology* **173**. ISSN: 18790887 (2022).
88. Hansen, C. R., Hussein, M., Bernchou, U., Zukauskaitė, R. & Thwaites, D. *Plan quality in radiotherapy treatment planning – Review of the factors and challenges* 2022.
89. Schmidhalter, D. *et al.* Assessment of patient setup errors in IGRT in combination with a six degrees of freedom couch. *Zeitschrift für Medizinische Physik* **24**, 112–122. ISSN: 0939-3889 (Aug. 2014).
90. Segedin, B. & Petric, P. Uncertainties in target volume delineation in radiotherapy - Are they relevant and what can we do about them? *Radiology and Oncology* **50**. ISSN: 15813207 (2016).
91. Hamilton, C. S. & Ebert, M. A. Volumetric uncertainty in radiotherapy. *Clinical Oncology* **17**. ISSN: 09366555 (2005).
92. Bertholet, J., Worm, E. S., Fledelius, W., Høyer, M. & Poulsen, P. R. Time-resolved intrafraction target translations and rotations during stereotactic liver radiation therapy: Implications for marker-based localization accuracy. *International Journal of Radiation Oncology Biology Physics* **95**. ISSN: 1879355X (2016).
93. Schmidt, M. L. *et al.* Cardiac and respiration induced motion of mediastinal lymph node targets in lung cancer patients throughout the radiotherapy treatment course. *Radiotherapy and Oncology* **121**, 52–58. ISSN: 0167-8140 (Aug. 2016).
94. Van Herk, M. *et al.* Quantification of organ motion during conformal radiotherapy of the prostate by three dimensional image registration. *International Journal of Radiation Oncology, Biology, Physics* **33**. ISSN: 03603016 (1995).

95. Vū Bezin, J. *et al.* *A review of uncertainties in radiotherapy dose reconstruction and their impacts on dose-response relationships* 2017.
96. Imae, T. *et al.* Retrospective dose reconstruction of prostate stereotactic body radiotherapy using cone-beam CT and a log file during VMAT delivery with flattening-filter-free mode. *Radiological Physics and Technology* 2020 **13:3** **13**, 238–248. ISSN: 1865-0341 (Aug. 2020).
97. Loebner, H. A. *et al.* Technical note: Feasibility of gating for dynamic trajectory radiotherapy – Mechanical accuracy and dosimetric performance. *Medical Physics* **50**, 6535–6542. ISSN: 0094-2405 (Aug. 2023).
98. Fraass, B. A. Impact of complexity and computer control on errors in radiation therapy. *Annals of the ICRP* **41**, 188–196. ISSN: 01466453 (Oct. 2012).
99. LoSasso, T., Chui, C.-S. & Ling, C. C. Physical and dosimetric aspects of a multileaf collimation system used in the dynamic mode for implementing intensity modulated radiotherapy. *Medical Physics* **25**, 1919–1927. ISSN: 2473-4209 (Aug. 1998).
100. Keall, P. J., Siebers, J. V., Jeraj, R. & Mohan, R. The effect of dose calculation uncertainty on the evaluation of radiotherapy plans. *Medical Physics* **27**. ISSN: 00942405 (2000).
101. Stroom, J. C. & Heijmen, B. J. M. Geometrical uncertainties, radiotherapy planning margins, and the ICRU-62 report. *Radiother Oncol* **64**, 75–83. ISSN: 01678140 (2002).
102. Landberg, T. *et al.* ICRU Report 62, Prescribing, Recording and Reporting Photon Beam Therapy (Supplement to ICRU 50). *Journal of the ICRU* **32** (1999).
103. Wilkinson, J. M. Geometric uncertainties in radiotherapy. *British Journal of Radiology* **77**. ISSN: 00071285 (2004).

REFERENCES

104. Van der Merwe, D. *et al.* Accuracy requirements and uncertainties in radiotherapy: a report of the International Atomic Energy Agency. *Acta Oncologica* **56**. ISSN: 1651226X (2017).
105. Herk, M. V. Errors and Margins in Radiotherapy. *Seminars in Radiation Oncology* **14**, 52–64. ISSN: 10534296 (2004).
106. Unkelbach, J. *et al.* Robust radiotherapy planning. *Physics in Medicine and Biology* **63**. ISSN: 13616560 (Aug. 2018).
107. Lens, E. *et al.* ICRU Report 50. Prescribing, recording, and reporting photon beam therapy. Bethesda, MD: The International Commission on Radiation Units and Measurements; 1993. *Int J Radiat Oncol Biol Phys* **7**. ISSN: 0167-8140 (2019).
108. Berthelsen, A. K. *et al.* What's new in target volume definition for radiologists in ICRU Report 71? How can the ICRU volume definitions be integrated in clinical practice? *Cancer Imaging* **7**. ISSN: 14707330 (2007).
109. Goitein, M. Calculation of the uncertainty in the dose delivered during radiation therapy. *Medical Physics* **12**. ISSN: 00942405 (1985).
110. Sterpin, E. *et al.* Development of robustness evaluation strategies for enabling statistically consistent reporting. *Physics in Medicine & Biology* **66**, 45002. ISSN: 0031-9155 (Aug. 2021).
111. Karlsson, K., Lax, I., Lindbäck, E. & Poludniowski, G. Accuracy of the dose-shift approximation in estimating the delivered dose in SBRT of lung tumors considering setup errors and breathing motions. *Acta Oncologica* **56**. ISSN: 1651226X (2017).
112. Unkelbach, J., Bortfeld, T., Martin, B. C. & Soukup, M. Reducing the sensitivity of IMPT treatment plans to setup errors and range uncertainties via probabilistic treatment planning. *Medical Physics* **36**. ISSN: 00942405 (2009).

113. Nederslandse Vereniging voor Radiotherapie en Oncologie. *Landelijk Indicatie Protocol Protonentherapie (versie 2.2) (LIPPv2.2)*, accessed on 25.10.2023 2019. <https://docplayer.nl/195792198-Landelijk-indicatie-protocol-protonentherapie-versie-2-2-lippv2-2.html>.
114. Wolthaus, J. W. *et al.* Comparison of Different Strategies to Use Four-Dimensional Computed Tomography in Treatment Planning for Lung Cancer Patients. *International Journal of Radiation Oncology Biology Physics* **70**. ISSN: 03603016 (2008).
115. Bellec, J., Arab-Ceschia, F., Castelli, J., Lafond, C. & Chajon, E. ITV versus mid-ventilation for treatment planning in lung SBRT: A comparison of target coverage and PTV adequacy by using in-treatment 4D cone beam CT. *Radiation Oncology* **15**. ISSN: 1748717X (2020).
116. Keall, P. J. *et al.* The management of respiratory motion in radiation oncology report of AAPM Task Group 76. *Medical physics* **33**, 3874–3900. ISSN: 0094-2405 (2006).
117. Bertholet, J. *et al.* Real-time intrafraction motion monitoring in external beam radiotherapy. *Physics in Medicine and Biology* **64**. ISSN: 13616560 (2019).
118. Colvill, E. *et al.* DMLC tracking and gating can improve dose coverage for prostate VMAT. *Medical Physics* **41**. ISSN: 00942405 (2014).
119. Green, O. L. *et al.* First clinical implementation of real-time, real anatomy tracking and radiation beam control. *Medical Physics* **45**. ISSN: 24734209 (2018).
120. Yamada, T. *et al.* Optimization and evaluation of multiple gating beam delivery in a synchrotron-based proton beam scanning system using a real-time imaging technique. *Physica Medica* **32**. ISSN: 1724191X (2016).

REFERENCES

121. Wan, H., Bertholet, J., Ge, J., Poulsen, P. & Parikh, P. Automated patient setup and gating using cone beam computed tomography projections. *Physics in Medicine and Biology* **61**. ISSN: 13616560 (2016).
122. Poulsen, P. R. *et al.* Respiratory gating based on internal electromagnetic motion monitoring during stereotactic liver radiation therapy: First results. *Acta Oncologica* **54**. ISSN: 1651226X (2015).
123. Booth, J. *et al.* MLC tracking for lung SABR is feasible, efficient and delivers high-precision target dose and lower normal tissue dose. *Radiotherapy and Oncology* **155**. ISSN: 18790887 (2021).

DEVELOPMENT OF A MONTE CARLO BASED ROBUSTNESS CALCULATION AND EVALUATION TOOL

H.A. Loebner¹, W. Volken¹, S. Mueller¹, J. Bertholet¹,
P.-H. Mackeprang¹, G. Guyer¹, D.M. Aebersold¹,
M.F.M. Stampanoni², P. Manser¹, M.K. Fix¹

¹ Division of Medical Radiation Physics and Department of Radiation Oncology, Inselspital, Bern University Hospital, University of Bern, Bern, Switzerland

² Institute for Biomedical Engineering, ETH Zürich and PSI, Villigen, Switzerland

published in
Medical Physics

July 2022, Volume 49, Issue 7

<https://doi.org/10.1002/mp.15683>

©American Association of Physicists in Medicine

Open access article distributed under the terms of the Creative Commons CC BY-NC-ND 4.0 license.

2.1 Abstract

Background

Evaluating plan robustness is a key step in radiotherapy.

Purpose

To develop a flexible Monte Carlo (MC)-based robustness calculation and evaluation tool to assess and quantify dosimetric robustness of intensity modulated radiotherapy treatment plans by exploring the impact of systematic and random uncertainties resulting from patient setup, patient anatomy changes, and mechanical limitations of machine components.

Methods

The robustness tool consists of two parts: the first part includes automated MC dose calculation of multiple user-defined uncertainty scenarios to populate a robustness space. An uncertainty scenario is defined by a certain combination of uncertainties in patient setup, rigid intra-fraction motion and in mechanical steering of the following machine components: angles of gantry, collimator, table-yaw, table-pitch, table-roll, translational positions of jaws, multi-leaf-collimator (MLC) banks, and single MLC leaves. The Swiss Monte Carlo Plan (SMCP) is integrated in this tool to serve as the backbone for the MC dose calculations incorporating the uncertainties. The calculated dose distributions serve as input for the second part of the tool, handling the quantitative evaluation of the dosimetric impact of the uncertainties. A graphical user interface (GUI) is developed to simultaneously evaluate the uncertainty scenarios according to user-specified conditions based on dose-volume histogram (DVH) parameters, fast and exact gamma analysis, and dose differences. Additionally, a robustness index (RI) is introduced with the aim to simultaneously evaluate and condense dosimetric robustness against multiple uncertainties into one number. The RI is defined as the ratio of scenarios passing the conditions on the dose distributions. Weighting of the scenarios in the robustness space is possible to consider their likelihood of occurrence. The robust-

ness tool is applied on an intensity modulated radiotherapy (IMRT), a volumetric modulated arc therapy (VMAT), a dynamic trajectory radiotherapy (DTRT) and a dynamic mixed beam radiotherapy (DYMBER) plan for a brain case to evaluate the robustness to uncertainties of gantry-, table-, collimator angle, MLC, and intra-fraction motion. Additionally, the robustness of the IMRT, VMAT and DTRT plan against patient setup uncertainties are compared. The robustness tool is validated by Delta4 measurements for scenarios including all uncertainty types available.

Results

The robustness tool performs simultaneous calculation of uncertainty scenarios, and the GUI enables their fast evaluation. For all evaluated plans and uncertainties, the PTV margin prevented major clinical target volume (CTV) coverage deterioration (maximum observed standard deviation of $D_{98\%CTV}$ was 1.3 Gy). OARs close to the PTV experienced larger dosimetric deviations (maximum observed standard deviation of $D_{2\%chiasma}$ was 14.5 Gy. Robustness comparison by RI evaluation against patient setup uncertainties revealed better dosimetric robustness of the VMAT and DTRT plans as compared to the IMRT plan. Delta4 validation measurements agreed with calculations by >96% gamma-passing rate (3%/2 mm).

Conclusions

The robustness tool was successfully implemented. Calculation and evaluation of uncertainty scenarios with the robustness tool were demonstrated on a brain case. Effects of patient and machine specific uncertainties and the combination thereof on the dose distribution are evaluated in a user-friendly GUI to quantitatively assess and compare treatment plans and their robustness.

2.2 Introduction

A key step in the radiotherapy treatment workflow is the treatment plan evaluation both in terms of dose parameters and in terms of robustness [1]. In recent years, evaluating robustness to uncertainties on the patient side (e.g., setup uncertainty [2]) or in the mechanical accuracy of the treatment machine (e.g., multi-leaf-collimator (MLC) leaf positioning accuracy [3]) has become an essential part of plan quality assessment [4].

To quantify the impact of an uncertainty on the plan robustness, its influence on the dosimetric quality of the plan has to be determined. Due to interpatient anatomical variations and the large variety of treatment techniques available, it is difficult to make a general statement relating a specific type of uncertainty to a dosimetric consequence.

Treatment plan robustness depends on the applied technique. Particularly, the complexity of the techniques impedes the straightforward understanding of the dosimetric impact of a type of uncertainty. Developments in intensity modulated treatment techniques for C-arm treatment units aim to improve plan quality by using increased degrees of freedom (DoF) and consequently increasing the plan complexity for the novel techniques. Volumetric modulated arc therapy (VMAT) increases the DoF by including dynamic gantry rotation as compared to intensity modulated radiotherapy (IMRT) and has become standard of care of radiotherapy [5–7]. Dynamic trajectory radiotherapy (DTRT), which extends VMAT by dynamic table and collimator rotations during delivery, adds two additional DoF, while ensuring acceptable delivery times [8, 9]. An additional DoF, and additional complexity, is introduced in mixed beam radiotherapy (MBRT [10]) and dynamic MBRT (DYMBER [11]) by combining photon and electron beams to use the radiation type specific advantages of sharp beam penumbra (photons), and distal dose fall-off (electrons). Treatment plan robustness therefore depends on the treatment technique. For instance, uncertainties in gantry position have

different effects on the dose distribution for the dynamic gantry rotation in VMAT as compared to the static gantry in IMRT and patient setup uncertainties have different effects on photon treatment compared to electron treatments.

Usually, a differentiation between systematic and random uncertainties is made [12]. Uncertainties in patient set-up have both systematic and random components. On the machine side, systematic uncertainties such as calibration errors, and intra-fraction uncertainties of each machine component, influence the delivery accuracy and thus the delivered dose distribution. In recent years, the study of machine logfiles has been a focus topic in research. Logfiles contain time-resolved information of the machine status during delivery and are used to calculate the fraction-specific uncertainty of the machine. In routine clinical practice, logfiles are used to monitor the performance of treatment machines, improve efficiency in quality assurance (QA) workflows [13–17] and examine the robustness of treatment plans [14, 17].

With this increasing variety and complexity in treatment techniques, it is not sufficient anymore to assess e.g., MLC positioning uncertainty [18, 19] or uncertainties in patient setup [2] alone. These investigated uncertainty scenarios have to be extended to account for the added DoF of new techniques and the uncertainties must be assessed in combination to achieve a more comprehensive robustness assessment of a treatment plan. There is a need for simple and comprehensive calculation and evaluation tools of the dosimetric impact of all patient and machine related uncertainties, including their interplay.

Therefore, this work aims to develop a robustness tool to evaluate the dosimetric robustness of treatment plans. The robustness tool will be applicable to a wide range of treatment techniques and used to investigate the impact of patient and machine component related uncertainties on the dose distribution individually and in combination. To ensure the accurate calculation of the dose distributions including the aforementioned uncertainties, Monte Carlo (MC) dose calculation [20] using the Swiss Monte Carlo Plan (SMCP) [21, 22] will serve as the backbone of this tool.

Finally, following the idea of a plan quality index [23], we introduce a robustness index (RI), which condenses dosimetric robustness to multiple uncertainties into one number. This streamlines the robustness evaluation and robustness comparison of different treatment plans, for the considered uncertainties.

2.3 Materials and Methods

The robustness tool consists of two components: the calculation and the evaluation part. In the calculation part, the dose distribution including the desired uncertainties are calculated. In the evaluation part, the dosimetric impact of the uncertainties on the dose distribution is assessed. Dose calculation uses SMCP on a high-performance computing cluster for efficient calculation [21]. To evaluate the dosimetric impact of the uncertainties, a GUI is developed. The workflow is illustrated in figure 2.1.

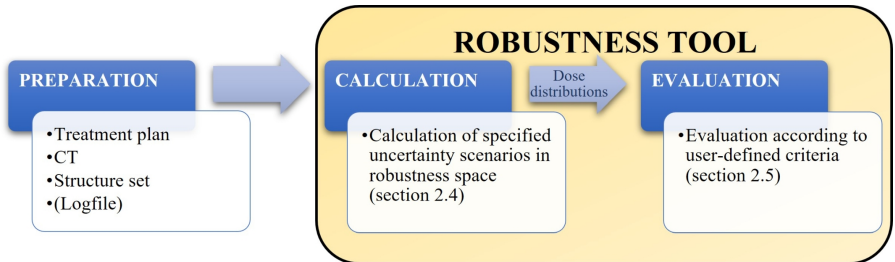


Figure 2.1: Workflow for the robustness tool. *PREPARATION*: The treatment plan is created in a treatment planning system (TPS) based on the CT and structure set. To include logfile and time resolved information, the created treatment plan must be delivered first and the logfile recorded. *Part 1, CALCULATION*: user defines the robustness space in terms of uncertainty scenarios. Subsequently, the respective dose distributions incorporating the desired uncertainties are calculated (see section 2.4). *Part 2, EVALUATION*: Evaluation of the dose distributions of the robustness space (see section 2.5).

2.3.1 Terminology

To assess robustness of a treatment plan, a so-called robustness space is evaluated. The robustness space has the dimensionality N , related to the N uncertainty types considered for the evaluation. The robustness space is spanned up by N *uncertainty axes* a_i , $i \in \{1 \dots N\}$, with z_i uncertainty scenarios at $n_{a_i}^1, n_{a_i}^2, \dots, n_{a_i}^{z_i}$ along the axis a_i . The location of a single scenario in the robust-

ness space is given by $n_{a_1, \dots, a_N}^{x \in \{1 \dots z_1\}, \dots, x \in \{1 \dots z_N\}}$. Thus, each scenario represents a combination of uncertainties. An uncertainty axis is characterized by the origin of the considered uncertainty: It can be patient (e.g., setup, motion) or machine (e.g., gantry uncertainty) related. The uncertainty axes and scenarios for calculation and evaluation are specified by the user of the robustness tool. A scenario is associated with the dose distribution including the corresponding uncertainties. In the centre of the robustness space, the reference scenario represents the nominal plan with the planned dose distribution involving no uncertainty, the reference CT, and the reference structure set. For example, the robustness space considering patient setup uncertainties with respective scenarios in longitudinal, lateral, and vertical patient setup direction and their combination, has scenarios in three dimensions.

The following uncertainty axes are implemented in the tool: patient setup uncertainties (longitudinal, lateral, vertical, table rotation angle, table pitch angle, table roll angle) are modelled by table translations and rotations. Further uncertainty axes consider the mechanical accuracy of machine components (gantry angle, collimator angle, MLC leaf positions, translational jaws position), monitor units, and rigid three DoF intra-fraction patient motion in longitudinal, lateral, and vertical direction. Additionally, the tool supports the re-calculation of the plan on different CTs to account for anatomical changes. If requested, each scenario has its own CT and structure set. Further not yet considered uncertainty axes are easily integrated in the tool.

2.3.2 Data structure

Scenarios in the robustness space are structured according to two options: in the Gridded Data (GD) option, where the scenarios are ordered in a regular grid. Thus, the dose distributions of all possible combinations of the considered uncertainty axes are calculated: Together, the N uncertainty axes define a set of $z_1 \times z_2 \times \dots \times z_N$ scenarios in the robustness space. The Spotted Data

(SD) option requires the specification of each individual uncertainty scenario at $x \in \{1 \dots z_1\}, \dots, x \in \{1 \dots z_N\}$, for calculation of the respective dose distribution. The SD option potentially limits the number of calculations and subsequent evaluations, which becomes particularly useful to probe the robustness space, e.g., for the most sensitive uncertainty axes.

2.3.3 Uncertainty type

The robustness tool enables to calculate and evaluate patient and machine related uncertainties. For the purpose of patient related setup uncertainties, a Gaussian distribution is used [12]. Thereby the mean and the standard deviation (sigma) represents the systematic and the random component of the uncertainty. During the Monte Carlo dose calculation, a shift is sampled from the Gaussian (mean, sigma) and applied to the particle exiting the linac head. Thus, for each particle exiting the linac head such a shift is applied following the Gaussian distribution. As this distribution is applied on a particle-by-particle base, there is no need to simulate several fractions for a specific setup uncertainty. The obtained dose distribution directly accounts for the setup uncertainty distribution. This approach saves substantial computational resources but assumes a sufficient number of fractions (>10), as shown by van Herk et al. [24]. In the context of robust optimization, the effect of number of fractions on the simulation of random setup uncertainties and robustness has been investigated previously by Fredriksson [25].

For machine related uncertainties, the robustness tool models global systematic uncertainties by constant offsets in the respective machine components. To simulate treatment plan and machine specific uncertainty combinations, information of the machine logfile is used. To this end, the plan has to be delivered at least once prior to application to record the logfile, which e.g., could be done during pre-treatment quality assurance. In the logfile of a TrueBeam[®] (Varian Medical Systems, Palo Alto, CA), the status of all machine components is logged as expected and actual value during delivery at a rate of 50 Hz with absolute time

stamp. The difference between *expected* and *actual* for each control-point can be assigned as control-point specific local systematic uncertainty. The robustness tool enables to consider and to scale these uncertainties for the subsequent respective dose calculation.

The time-resolved machine logfile information can be further used to synchronize a time-series of intrafraction patient-related motion (e.g., breathing) with machine parameters.

2.3.4 Calculation

The reference treatment plan is generated with EclipseTM (Varian Medical Systems, Palo Alto, CA), research version 15.6.99. An input file, defining the treatment machine axis at all control points of the treatment for the nominal scenario, is created. The user specifies the desired robustness space, and the input file is automatically adapted accordingly using a python framework to serve as an input for the subsequent calculation of the dose distributions of the scenarios in the robustness space, using SMCP [21, 22, 26]. Calculation voxel size is $0.25 \times 0.25 \times 0.25 \text{ cm}^3$. The statistical uncertainty of the Monte Carlo calculated dose distributions presented in this work is $<1.2\%$ (one standard deviation). The number of simulated primary particles per calculation is in the order of 10^8 .

2.3.5 Evaluation

Evaluation of the uncertainty scenarios dose distributions is performed according to *DVHs*, *Gamma Passing Rate* and *Dose differences*. To provide a flexible and user-friendly robustness evaluation of treatment plans, a GUI is developed. The read-in of the input of the GUI, loading of the robustness space data (dose distributions, CTs, structures), and the calculation of DVHs and gamma passing rate is parallelized on the number of available CPU cores. The computer memory required for the evaluation is roughly proportional to the size of the dose distribution times the number of scenarios. The GUI is implemented in C++ utilizing

the Qt toolkit [27] and has a dynamic structure.

The user of the robustness tool interactively defines the evaluation conditions including thresholds for acceptance to evaluate the robustness of a scenario in the robustness space. Possible conditions are based on $Dx\%$, $Vx\%$, D_{mean} or gamma passing rate, evaluated for selected structures. To assess the “distance” of the individual quantity to the specified acceptable threshold, a conditions meter c is introduced as follows:

$$c = \frac{Q_{current} - Q_{ref}}{Q_{acceptable} - Q_{ref}} \quad (2.1)$$

where c is the ordinate for a given quantity Q (e.g., D_{mean}). $Q_{current}$ and Q_{ref} are the parameter values for the current and reference scenario, respectively. $Q_{acceptable}$ is the threshold for the parameter value used to determine if Q is robust. For $c > 1$ the scenario is not considered robust and for $c < 1$ it is robust. For $c = 0$ the scenario fulfils the condition equally well as the reference scenario and for $c < 0$ the scenario achieves the condition better than the reference scenario.

The calculation of the gamma passing rate is based on the algorithm of Ju et al. [28], which calculates the gamma without using a linear interpolator and discretization of the search space (supplementary material A1). This has the advantage that the time needed for calculating the gamma passing rate is independent of the distance- and dose difference criteria and an exact gamma value is calculated: the common limitation of lacking an infinite resolution grid is overcome by calculating the gamma passing rate values of each reference dose point as the closest geometric distance between this point to the hypersurface defined by the evaluation dose distribution. Additionally, a maximal gamma threshold value, representing the maximal difference in gamma value to the nominal scenario is set, after which the calculation is automatically terminated to save calculation time. The robustness tool employs a global gamma analysis with the reference scenario set as the reference dose in each evaluation. The dose criterion is given relative to a user-defined value. The default is the prescribed dose. Additionally,

a low-dose threshold relative to the beforementioned value is used.

Visual evaluation of the difference between dose distributions of any scenarios in the robustness space is conducted in three dimensions (lateral, sagittal, coronal), with an adjustable dose difference threshold.

2.3.6 Interpolation between scenarios

Evaluation of the treatment plan robustness is not limited to the initially defined uncertainty scenarios. The scenarios populating the robustness space serve as sampling points, between which interpolation is applied. To this end, a metric defining the distance d between two scenarios at b and c in the robustness space is specified as

$$d^2 = \sum_{l=1}^N \left(\frac{b_l - c_l}{m_l} \right)^2 \quad (2.2)$$

with the uncertainty normalization $M = (m_1, m_2, \dots, m_N)$. The uncertainty normalization is defined by default as

$$m_l = \left(\frac{n_{a_l}^{z_l} - n_{a_l}^1}{z_l - 1} \right) \quad (2.3)$$

but is adjustable. The resulting distance is unitless. The evaluation quantity Q can then be interpolated based on the nearest neighbours.

2.3.7 Robustness Index

To summarize the information of treatment plan robustness considering multiple uncertainties, the *Robustness Index (RI)* is introduced. When all scenarios in the robustness space are considered equally important, the RI describes the fraction of scenarios passing the conditions: $RI = \frac{N_p}{N_{all}}$, where N_p is the number of scenarios passing all robustness conditions and N_{all} is the number of all scenarios in the present robustness space.

However, a greater distance to the location of the reference scenario, usually

represents a decrease in the likelihood of occurrence of such a scenario. Therefore, a second option to calculate RI is introduced, given by $RI = \frac{\sum_{t=1}^{N_p} w_t}{\sum_{t=1}^{N_{all}} w_t}$ with $w_t \exp \frac{-d_t^2}{2R_E^2}$. d_t is the distance between the location of scenario t and the reference scenario in the robustness space and R_E is the evaluation range, the standard deviation of this scenario distribution. The maximal value of the RI is 100% (in the weighted and unweighted case) and states that all scenarios pass the conditions. In the unweighted case, a RI of 10% means that 10% of the scenarios in the robustness space pass the conditions. In the weighted case, a RI of 10% describes that the fraction of the summed weights of the passing scenarios is 10%. Thereby the scenarios are weighted according to a Gaussian distribution $G(\mu = 0, \sigma = R_E)$ centred around the reference scenario (supplementary material A2). The mean and standard deviation of a quantity Q evaluated on the whole robustness space change to a weighted *mean*, $\mu_Q = \frac{\sum_t w_t Q_t}{\sum_t w_t}$ and a weighted *standard deviation*, Σ_Q with $\Sigma_Q^2 = \frac{\sum_t w_t Q_t^2 \sum_t w_t - (\sum_t w_t Q_t)^2}{(\sum_t w_t)^2 - \sum_t w_t^2}$ where w_t is the Gaussian weighted distance factor from the reference as defined above and Q_t is the value of the quantity Q at scenario t .

2.3.8 Application and demonstration of the robustness tool

Application of the robustness tool and the GUI is demonstrated on different treatment plans for a right sided brain case (figure 2.2), namely an IMRT, a VMAT, a DTRT and a DYMBER plan (table 2.1). Prescribed dose is 60 Gy to 50% of the PTV volume. The CTV-PTV margin is 0.5 cm. The respective plans are optimized according to clinical goals applied in our institute. Application of the main functionalities of the GUI are demonstrated on the DTRT plan. To conduct the robustness comparison against uncertainties in patient setup of different treatment techniques, application 1 to 6 (table 2.1), are assessed. To demonstrate the flexibility of the robustness tool in terms of different treatment techniques and uncertainty scenarios, application 7 to 12 are investigated.

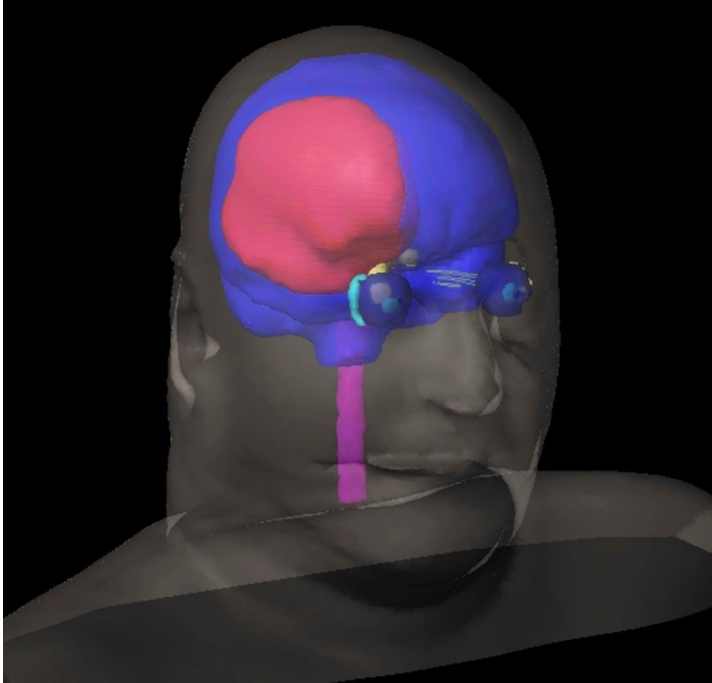


Figure 2.2: Right sided glioblastoma brain case. The PTV is shown in red.

The robustness conditions are set to: 98% and $D2\%$ of the CTV are not allowed to be reduced or increased by more than 1 Gy, respectively. Additionally, $D2\%$ and mean dose are not allowed to be increased by more than 1 Gy for serial and parallel OARs, respectively. The plan robustness is then quantified by the RI: once for all scenarios weighted equally and once with $R_E=0.5$ to increase the weight of the more likely scenarios.

Table 2.1: Application situation of the robustness tool, demonstrated on different treatment techniques. Application 1-6 evaluate systematic and random patient-setup uncertainty, application 7-12 evaluate different robustness spaces for different treatment techniques.

#Application	Treatment technique	Description of uncertainty axes and Scenarios	#Scenarios
1	IMRT (3 fields)	Systematic patient setup uncertainty: Longitudinal, lateral, and vertical direction modelled with Gaussian distribution $G(\mu, 0)$, $\{\mu = -0.5, -0.2, 0.0, 0.2, 0.5\text{cm}\}$ Vaxes, and combinations of them	125
2	IMRT (3 fields)	Random patient setup uncertainty: Longitudinal, lateral, and vertical direction modelled with Gaussian distribution $G(0, \sigma)$, $\{\sigma = 0.0, 0.1, 0.2, 0.3, 0.5\text{cm}\}$ Vaxes, and combinations of them	125
3	VMAT (2 arcs)	Systematic patient setup uncertainty: Longitudinal, lateral, and vertical direction modelled with Gaussian distribution $G(\mu, 0)$, $\{\mu = -0.5, -0.2, 0.0, 0.2, 0.5\text{cm}\}$ Vaxes, and combinations of them	125
4	VMAT (2 arcs)	Random patient setup uncertainty: Longitudinal, lateral, and vertical direction modelled with Gaussian distribution $G(0, \sigma)$, $\{\sigma = 0.0, 0.1, 0.2, 0.3, 0.5\text{cm}\}$ Vaxes, and combinations of them	125
5	DTRT (3 trajectories)	Systematic patient setup uncertainty: Longitudinal, lateral, and vertical direction modelled with Gaussian distribution $G(\mu, 0)$, $\{\mu = -0.5, -0.2, 0.0, 0.2, 0.5\text{cm}\}$ Vaxes, and combinations of them	125
6	DTRT (3 trajectories)	Random patient setup uncertainty: Longitudinal, lateral, and vertical direction modelled with Gaussian distribution $G(0, \sigma)$, $\{\sigma = 0.0, 0.1, 0.2, 0.3, 0.5\text{cm}\}$ Vaxes, and combinations of them	125
7	IMRT (3 fields)	Global systematic uncertainty counter-moving jaws X1&X2 and Y1&Y2, $\{-1.0, -0.5, 0.0, 0.5, 1.0\text{cm}\}$; Globals systematic uncertainty leaf bank A&B, $\{-0.1, -0.05, 0.0, 0.05, 0.1\text{cm}\}$, and combinations of them	625
8	DTRT (3 trajectories)	Global systematic uncertainty in gantry-, table-, collimator angle $\{-4.0, -2.0, -1.0, 0.0, 1.0, 2.0, 4.0^\circ\}$, and combinations of them	343
9	DYMBER (3 photon trajectories & 1 electron field (6, 9, 12, 15, 18, 22 MeV))	Systematic patient setup uncertainty for electron fields: Longitudinal, lateral, and vertical direction, modelled with Gaussian distribution $G(\mu, 0)$, $\{\mu = -0.5, 0.0, 0.5\}$, Vaxes, and combinations of them	27
10	VMAT (2 arcs)	Rigid intra-fraction motion in transversal and sagittal plane, Rotation amplitude of isocenter around dens axis in transversal & sagittal plane, $\{0.0, 0.5, 1.0, 2.0, 3.0^\circ\}$ and combinations of them	25
11	VMAT (2 arcs)	Global systematic collimator and table angle uncertainty $\{-4.0, -2.0, -1.0, 0.0, 1.0, 2.0, 4.0^\circ\}$; Local systematic gantry uncertainty: mean absolute gantry logfile difference between expected and actual scaled to $\{0.0, 1.0, 2.0, 3.0, 4.0^\circ\}$ and combinations of them	245
12	VMAT (2 arcs)	Global systematic uncertainty in table and gantry angle $\{-1.0, 0.0, 1.0^\circ\}$; Local systematic gantry uncertainty: mean absolute gantry logfile difference between expected and actual scaled to $\{0.0, 1.0^\circ\}$; Systematic and random lateral patient setup uncertainty: modelled with Gaussian distribution $G(\mu, \sigma)$, $\{\mu = -1.0, 0.0, 1.0\text{cm}; \sigma = 0.0, 0.5\text{cm}\}$	10

2.3.9 Validation of the robustness tool

Extensive validation of the SMCP dose calculation framework has been conducted in the past [8, 10, 11, 21, 26, 29]. This included validation of photon-based treatment techniques such as IMRT, VMAT, DTRT, as well as mixed beam treatment techniques, such as DYMBER. Measurements are conducted with the Delta4 device (ScandiDos, Uppsala, Sweden). First 10×10 cm² fields and 5×5 cm² fields at different gantry angles (0° , 90° , 180°) are delivered and the measured dose is compared to the calculation. Second, to validate the accuracy of the dose calculation of selected scenarios (table 2.2) in the robustness space of the VMAT plan for the brain case (figure 2), the scenario are calculated with the robustness tool and the corresponding XML files needed for delivery on a TrueBeam[®] (Varian Medical Systems, Palo Alto, CA) in developer mode are created, the plans are delivered, and the delivered dose is measured and compared against the calculation.

To validate the calculation of quantities Q , e.g., DVH parameters such as volume, $Dx\%$ and D_{mean} , the robustness tool calculations are compared to the results of the corresponding Eclipse implementation. The dose distribution of the reference VMAT plan is loaded into Eclipse and the DVH parameters for several organs are compared to the evaluation returned by the robustness tool. The gamma passing rate calculations of the robustness tool are validated against the open-source gamma passing rate calculation of pymedphys 0.37.1, an implementation based on the work of Wendling et al. [30]: gamma passing rates of the reference scenario of the VMAT plan and the scenarios in the robustness space incorporating systematic setup uncertainties in lateral, longitudinal and vertical direction between -0.5 to 0.5 cm, are calculated and compared.

Table 2.2: Validation Scenarios 1-2: Validation of $10 \times 10 \text{ cm}^2$ and $5 \times 5 \text{ cm}^2$ open fields at different gantry angles. Validation Scenarios 3-13: Specific uncertainty scenarios for validation of the robustness space of the VMAT plan.

Validation Scenario	Description
1	$10 \times 10 \text{ cm}^2$ field at gantry angle $0^\circ, 90^\circ, 180^\circ$
2	$5 \times 5 \text{ cm}^2$ field at gantry angle $0^\circ, 90^\circ, 180^\circ$
3	Reference scenario (no uncertainty)
4	Systematic patient setup uncertainty of +1 cm in lateral, longitudinal and vertical direction
5	Systematic uncertainty of 1° in gantry
6	Systematic uncertainty of 1° in gantry and collimator
7	Systematic uncertainty of 1° in gantry, collimator, and table rotation
8	Systematic uncertainty of 1 mm for MLC leaf 40 in leafbank B
9	Systematic uncertainty of 3 cm in Jaw X1
10	Intra-fraction motion of 1 cm in longitudinal direction during treatment
11	Systematic 10% more MU
12	Gantry logfile uncertainty scaled up by factor 10
13	Systematic gantry uncertainty of 1° combined with systematic patient setup uncertainty of +1 cm in lateral, longitudinal and vertical direction

2.4 Results

2.4.1 GUI for evaluation

Robustness evaluation with the GUI is shown in figure 2.3 for the DTRT plan table 2.1, application 8. The DVH viewer (figure 2.3, number 1) represents the DVH distributions of the selected structures over all scenarios in the robustness space as DVH bands. The boundaries of the DVH bands correspond to the scenarios which induce the maximal deviations in terms of dose distribution for this structure. The reference DVH is indicated by a solid line and the DVH of the current scenario is shown with a dashed line. In the axes selection window (figure 2.3, number 3), the user switches the uncertainty axes of the robustness space to select a two-dimensional plane in the robustness space. The selected plane is displayed in the robustness map (figure 2.3, number 2) in real time. Additionally, the evaluation range is superimposed on the robustness map: in figure 2.3 an R_E of 1.5 and standard metric, is chosen to emphasize the smaller uncertainties. The evaluation range is visualized by the shaded area. The conditions meter for the selected conditions set in the conditions list is shown on the bottom right of figure 2.3.

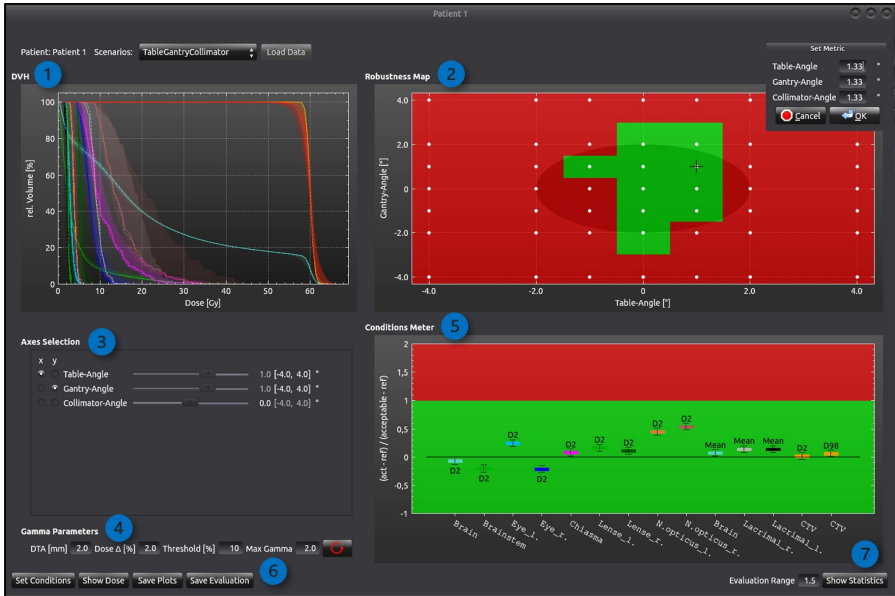


Figure 2.3: Main GUI of the robustness evaluation tool. Top left, 1: *DVH Viewer* with DVH bands of all scenarios of the robustness space of the DTRT plan (table 2.2, application 8), top right, 2: *Robustness Map* displaying 2D plane of the robustness space and pop-up metric window to change the metric if needed, bottom left, 3: *Axes Selection* window to select a plane in the robustness space for closer inspection, bottom left, 4: *Specification* of parameters Gamma Passing Rate calculation, bottom right, 5: *Conditions Meter* for evaluating structure specific conditions, 6&7: Opens pop-up windows: *conditions list* (definition of robustness conditions), *dose view* (shows dose distribution and dose difference) and *statistics window* (summarizes key quantities of the robustness space).

Conditions List

The conditions from section 2.3.9 are specified in the conditions list (figure 2.3, number 5 opens the conditions list seen in figure 2.4) and are adjustable on the fly according to the interest of the user. The following structures are part of the evaluation: brain, brainstem, left and right eye (Eye l./r.), chiasma, left and right lens (Lense l./r.), left and right optic nerve (N.opticus l./r.), left and right

lacrimal glands (Lacrimal l./r.), CTV, and PTV.

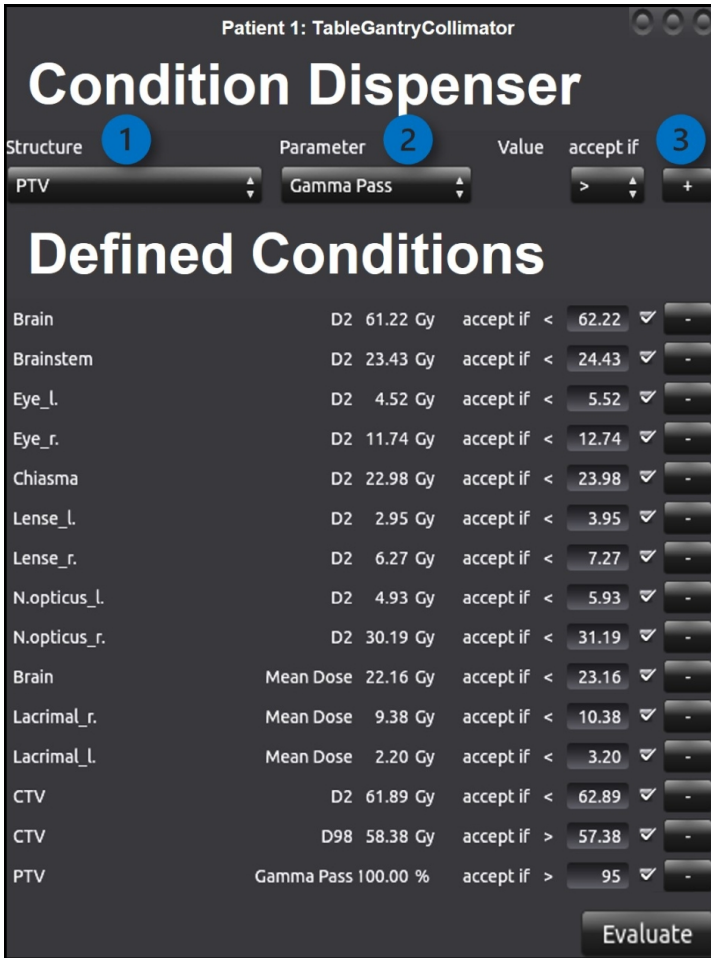


Figure 2.4: Conditions list opened by figure 2.3, number 6. 1: Select structure, 2: Select parameter, 3: Add to evaluation.

Conditions meter

The conditions meter in figure 2.3, number 5, displays how well the current scenario is fulfilling the user-defined conditions. If all conditions are passed, the

respective rectangle in the robustness map (figure 2.3, number 2) is marked green, and red, if one condition is not fulfilled. To evaluate changes in the distance or dose difference criteria in the calculation of gamma passing rate, the gamma passing rate calculation needs to be restarted by ticking the red circle in the main GUI window (figure 2.3, number 4).

Dose window

The dose window (figure 2.5) displays the dose distributions of the selected scenario (systematic uncertainty of one degree in table and gantry angle, figure 2.5, number 2.5), the reference scenario (figure 2.5, number 2) and the dose difference (figure 2.5, number 3) superimposed on the respective CT. The dose difference is always superimposed on the CT of the reference scenario and the structures of the underlying anatomy are visualized by their contours. The user explores the dose distributions in the transversal, coronal, and sagittal plane by scrolling through them, and switches from one plane to the other with the help of the crosshairs. Additionally, an adjustable dose threshold is implemented to visualize dose differences in a desired range.

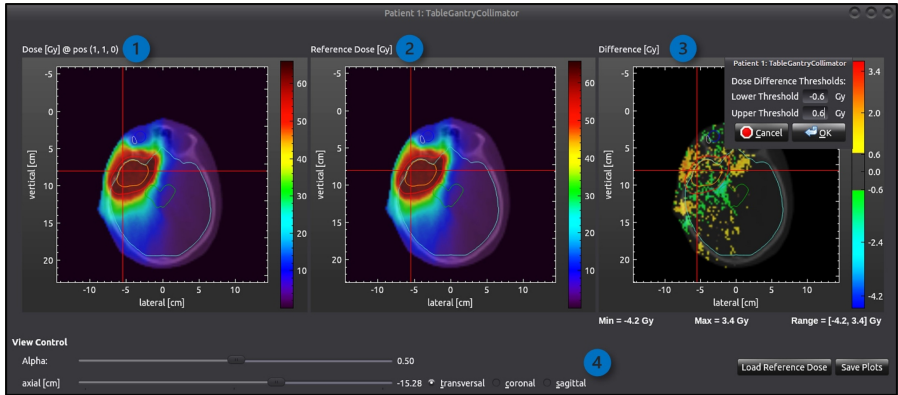


Figure 2.5: The dose window (opened by figure 2.3, number 6) displays dose distributions superimposed on the CT. Structures are indicated by the fine lines (PTV and CTV in red and orange here). 1: Dose of current scenario, 2: Reference dose, 3: Dose difference between reference and current dose, includes a user-defined threshold to visualize relevant dose ranges, 4: View control to switch through transversal, coronal, and sagittal plane. The red cross serves as a guideline when switching planes from transversal (shown here) to coronal or sagittal.

Statistics window

Parameter Statistics		Evaluation Range = 1.5			
- CTV		Min	Max	Mean	Sigma
V95 [%]		94.0	100.0	99.8	0.5
D2 [Gy]		61.8	64.4	62.2	0.3
Min Dose [Gy]		48.5	57.1	56.1	0.8
Max Dose [Gy]		64.5	69.5	66.0	0.8
Mean Dose [Gy]		60.2	60.7	60.5	0.1
Median Dose [Gy]		59.8	60.3	60.1	0.1
Gamma Pass [%]		54.7	100.0	86.3	7.7
Volume [cm3]		166.4	166.4	166.4	0.0
D98 [Gy]		56.0	58.6	58.2	0.4
Robustness Index	33.6 %				

Figure 2.6: Statistics window (opened by figure 2.3, number 7) displays key quantities and RI for all selected structures in the current evaluation range.

The statistics window, displayed in figure 2.6, summarizes dosimetric key quantities for all OARs. Additionally, the RI for the selected evaluation range is displayed at the bottom.

Interpolation

A robustness map of SD and corresponding GD is shown in figure 2.7. Here only some scenarios are available (shown as white dots). Green and red areas indicate whether a scenario is considered robust and acceptable or not, respectively. Between the available scenarios the robustness map displays grey rectangles (figure 2.7, number 1). So far, no information on the robustness of these areas in the robustness space is available. These empty spaces are filled by interpolation. Besides interpolation, the zoom functionality is implemented in the GUI. It inspects a single two-dimensional slice through the robustness space in greater detail. The

zoom function increases the number of scenarios along the uncertainty axes of this slice by a factor of two, thus leading to additional combinations of these uncertainty axes in the selected plane and performs an interpolation on all inserted scenarios. Interpolation and zooming, are implemented on a multithreaded basis.

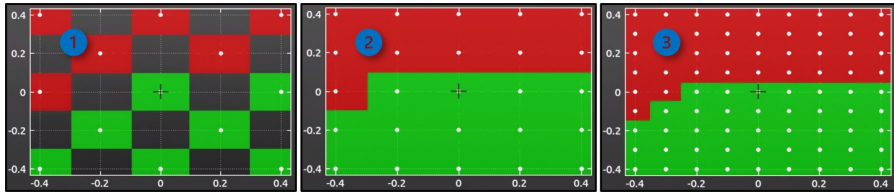


Figure 2.7: 1: Robustness map of robustness space with SD, with scenarios at every other combination (white dots), 2: Robustness map of robustness space with GD, 3: Zoom functionality: doubles resolution of scenarios in this slice and interpolates on all inserted scenarios.

2.4.2 Robustness evaluation of different treatment plans

The results of the applications 1-13 from table 2.1 are shown in table 2.3. The default uncertainty normalization is chosen. Furthermore, the standard deviation Σ of the $D_{98\%CTV}$ and $D_{2\%CTV}$ as well as the structure with the greatest standard deviation in mean dose and in $D_{2\%}$ are displayed. RI is higher for a weighted analysis ($R_E = 1.5$), compared to equal weighting of the scenarios. Due to the Gaussian weighted evaluation method, RI increases, since scenarios located closer to the reference have more weight compared to scenarios located further away from the reference scenario and they usually pass the conditions better.

Evaluating application 1 to 6, compares the robustness of different treatment techniques to patient setup uncertainties. The RI indicates better dosimetric robustness to setup uncertainties for the VMAT and the DTRT plan as compared to the IMRT plan. Assessing RI and the standard deviation of $D_{98\%CTV}$ and $D_{2\%CTV}$ show, that the CTV-PTV margin compensates for the uncertainties to maintain CTV coverage, but some of the OARs are strongly affected by setup uncertainties, potentially leading to reject the plan completely when clinical

constraints are no longer met.

In figure 2.8 the DVH bands of the robustness space including random setup uncertainties of the IMRT, VMAT and DTRT plan, are shown. Especially the OARs near the PTV experience a great variation in their dose, as seen by the width of the DVH bands compared to the ones of PTV and CTV.

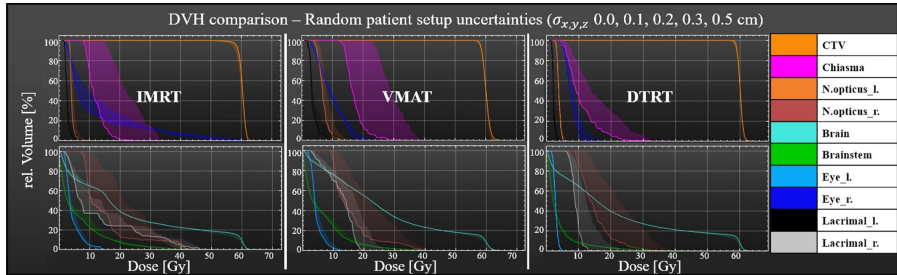


Figure 2.8: DVH bands for the IMRT, VMAT and DTRT plan, including random uncertainties ($G(0, \sigma_{x,y,z} = 0.0, 0.1, 0.2, 0.3, 0.5 \text{ cm})$) in patient setup.

Table 2.3: Evaluation of applications 1 to 12. RI for all scenarios weighted equally and $R_E=1.5$. Standard deviations for $D_{98\%CTV}$ and $D_{2\%CTV}$ and structure with greatest standard deviation in mean dose and D2%. The calculation of standard deviations is based on the default metric and $R_E=1.5$.

#Application, Description	RI (all scenarios equally weighted)	RI (R_E 1.5)	Σ of D_{98CTV} , Σ [Gy]	Σ of D_{2CTV} , Σ [Gy]	Structure with greatest Σ for mean dose, Σ [Gy]	Structure with greatest Σ for D2%, Σ [Gy]
1, IMRT Setup (systematic)	0.8%	2.2%	1.3	0.5	Optic nerve r.: 8.8	Optic nerve r.: 15.1
2, IMRT Setup (random)	9.6%	31.3%	0.1	0.1	Chiasma: 1.8	Eye_r.: 2.4
3, VMAT Setup (systematic)	8.0%	12.5%	0.5	0.3	Optic nerve r.: 7.3	Optic nerve r.: 14.4
4, VMAT Setup (random)	14.4%	49.5%	0.1	0.2	Chiasma: 2.2	Chiasma: 1.8
5, DTRT Setup (systematic)	16.8%	23.2%	0.5	0.4	Optic nerve r.: 6.2	Chiasma: 14.5
6, DTRT Setup (random)	5.6%	23.4%	0.1	0.1	Optic nerve r.: 0.8	Chiasma: 1.5
7, IMRT MLC / Jaws	21.0%	29.9%	1.7	1.7	PTV: 1.9	Lacrimal gland r.: 1.9
8, DTRT Gantry, Table, Collimator	12.0%	33.5%	0.4	0.3	Lacrimal gland r.: 0.9	Optic nerve r.: 1.5
9, DYMBER electron setup	25.9%	31.2%	0.9	0.7	Lacrimal gland r.: 0.4	PTV: 0.7
10, VMAT rigid intrafraction motion	16.0%	43.2%	0.2	0.8	Chiasma: 0.6	Optic nerve r.: 1.2
11, VMAT logfile	5.1%	15.3%	0.2	0.2	Chiasma: 1.6	Lacrimal gland l.: 3.5
12, VMAT systematic & random patient & machine uncertainties	13.9%	16.9	0.1	0.2	Optic nerve r.: 1.6	Chiasma: 3.6

2.4.3 Validation

In table 2.4, the dose measurements of the selected scenarios (table 2.2) are compared against the calculation. For the gamma analysis, dose difference /distance criteria of 2% (global)/1 mm for validation scenario 1-2 and 3% (global)/2 mm for validation scenario 3-13, including a 20% low-dose threshold, are applied in the evaluation for all measurements. All measurements agree with the calculation of the robustness tool with a gamma passing rate of >96.4%.

Table 2.4: Gamma Passing Rate evaluation of scenarios specified in table 1. 2% (global)/1 mm dose difference and distance criteria, including a 20% dose threshold was applied to evaluate scenario 1-2. The clinical dose difference and distance criteria, 3% (global)/2 mm, including a 20% dose threshold was applied for the evaluation of scenario 3-13.

Validation Scenario	Gamma Passing Rate (2% global/1 mm)	
1	Average 98.5%	
2	Average 99.0%	
	Gamma Passing Rate (3% global/2 mm) Arc 1	Gamma Passing Rate (3% global/2 mm) Arc 2
3	97.8%	99.6%
4	98.7%	97.8%
5	97.0%	99.8%
6	96.4%	99.6%
7	97.0%	99.6%
8	97.2%	99.8%
9	98.7%	99.6%
10	99.8%	100.0%
11	97.4%	99.4%
12	99.0%	99.4%
13	99.4%	100.0%

In table 2.5, the results of the Eclipse implementation to calculate volume, $Dx\%$ and D_{mean} agree with the calculation of the robustness tool (e.g., PTV volume differentiates by 0.2%). For small structures greater differences (e.g., chiasma volume) occur. To validate the accuracy of the gamma passing rate calculation, a total of 64 scenarios are evaluated (2% of prescribed dose /2mm, 20% threshold). The results cover a range of 91% to 100% passing rate. The robustness tool and pymedphys deviate by a maximum of 0.8%. However, pymedphys needs substantially longer calculation time for the same number of CPU cores (on average: 5 min as compared to 2 seconds for the robustness tool).

Table 2.5: Comparison of the DVH parameter evaluation: Robustness tool (**bold**) and Eclipse.

	PTV		CTV		Brain		Brainstem		Chiasma		Body	
Volume [cm ³]	272.9	272.4	166.4	165.5	1479.5	1479.1	39.8	39.3	0.5	0.1	7599.6	7508.2
D2% [Gy]	63.3	62.5	62.2	62.1	61.8	61.3	28.7	27.7	27.3	24.1	59.8	59.9
D98% [Gy]	55.4	56.6	57.4	58.2	0.0	1.3	0.0	0.4	13.7	14.6	0.0	0.1
<i>D_{mean}</i> [Gy]	59.5	59.9	60.5	60.1	25.7	26.2	7.4	6.4	18.1	16.8	7.6	8.0

2.5 Discussion

In this work, a novel robustness tool is developed and implemented to evaluate the robustness of treatment plans of different techniques to patient and machine related uncertainties. In contrast to usually applied robustness evaluation procedures (e.g., evaluation limited to consider only setup uncertainties [2]), this tool has a great flexibility in terms of accurately calculating and evaluating different uncertainty scenarios and types (individually and in combination), in terms of simultaneously evaluating multiple uncertainty scenarios according to various criteria for the target and the OARs, and in terms of its applicability to different treatment techniques.

Accurate dose calculation of uncertainty scenarios is ensured by employing validated MC dose calculation with SMCP. It is necessary to simulate a sufficient number of primary particles for each MC dose calculation to achieve a reasonable statistical uncertainty [31] and hence reliable robustness results within the statistical uncertainty of the Monte Carlo calculated dose distributions. As MC dose calculations are usually computational expensive, the tool is constructed in a modular way, and the dose calculation algorithm is interchangeable.

The robustness tool provides high flexibility to the user to enter specific scenarios for the robustness space. Owing to this flexibility in the calculation and evaluation of the robustness space, the developed robustness tool efficiently overcomes the restriction of standardised uncertainty scenarios – e.g., limited robustness spaces, such as only considering MLC [32] or only patient setup [2, 33] uncertainties. The user of the robustness tool defines the robustness space incorporating a variety of uncertainty types and their combinations. With the help of this tool, the dosimetric impact of systematic and random uncertainties in patient setup and uncertainties in the mechanical accuracy of machine components on the reference scenario are quantified. The robustness tool offers the possibility to simulate systematic and random setup uncertainties of Gaussian distributions.

This reflects that e.g., the user can determine up to what level of uncertainty the given treatment plan is robust for the conditions considered, which then trigger e.g., an appropriate setup strategy. Additionally, it incorporates machine logfile information for realistic fraction-specific modelling of the uncertainties in each machine component, which has been determined to be a useful tool to assess machine specific delivery uncertainties [17, 34–36]. The robustness tool therefore permits comprehensive robustness evaluation adaptable to different use cases.

The flexibility to evaluate different treatment techniques, as for example described by Quian et al. [35], is fundamental to the design of the robustness tool. Owing to the availability of validated dose calculation for various treatment techniques, robustness comparison of different treatment techniques, including different radiation sources, is possible with the robustness tool. This has the potential to redefine and restructure the treatment planning process to already include robustness evaluation at the stage of appropriate treatment technique and treatment plan selection.

The robustness tool assesses robustness according to multiple criteria. The dosimetric impact of uncertainties on target and OARs is investigated visually and quantitatively on a scenario-by-scenario base as well as in summary. The DVH viewer with the DVH bands including all investigated scenarios, the robustness maps and the RI contextualize the detailed evaluation according to dose-volume parameters, dose difference and gamma passing rate of the individual scenarios. The gamma passing rate calculation is successfully validated against pmedphys and permits efficient assessment of the dosimetric impact of an uncertainty type. Differences in DVH parameter calculation, especially for small structures arise due to the different volume calculations and the dose value: the triangular meshes are not constructed in the exact same way in the robustness tool and in Eclipse. Furthermore, Eclipse interpolates the dose between the voxels for DVH calculation and the robustness tool does not. In literature more complex interpolation methods, e.g., the polynomial chaos expansion [37] or (quasi-) Monte Carlo methods [38], as compared to our interpolation method are described, usually operating

on the level of dose distributions. However, these methods assume, that the probability distribution function of the uncertainties is known beforehand, and that the uncertainties are independent of each other. In general, the independence of the uncertainties cannot be guaranteed and there is limited knowledge, especially about the cumulative probability distribution of several uncertainties. The presented applications of the robustness tool confirm that restricting robustness investigations on the target volume [12] gives a misleading picture of the plan robustness and simultaneous evaluation of dosimetric robustness on OARs is needed for a comprehensive robustness analysis of a treatment plan.

The application of the robustness tool fits into existing evaluation strategies: the flexibility in incorporating numerous uncertainty scenarios in the dose calculation and their evaluation makes it compatible with existing robustness approaches such as the “good practice scenario selection” and the “statistically sound scenario selection” evaluated by Sterpin et al. [39]. However, the tool extends these strategies by considering new potential scenarios, various uncertainties, different treatment techniques and flexible evaluation including the RI. The RI facilitates the robustness evaluation, summarizes, and efficiently compares the robustness of competing treatment plans and techniques for a given robustness space. Robustness evaluation is directly depending on the selected robustness space along with the conditions as robustness acceptance criteria. The RI is consequently also depending on those settings. Robustness evaluation by means of RI should always be reported with information about robustness space and the robustness conditions. Additionally, if the user of the robustness tool has knowledge about the probability distribution of the scenarios, a confidence interval for the RI can be reported.

We understand that the full potential of the RI only unfolds, when standardized robustness spaces in terms of uncertainty axes, scenarios, and evaluation range, as well as relevant evaluation conditions such as $D_{98\%}$, $D_{2\%}$ or D_{mean} for the structures are defined. This standardization facilitates and streamlines the comparison of RI of different robustness studies in various radiotherapy centres.

Furthermore, the RI has the potential to serve as a threshold action level for replanning, discarding the plan or recommending specific QA tests.

The robustness tool is expected to play a key role in our group in the field of robust optimization, the margin concept, and the implementation of new treatment techniques. With the help of this tool, we aim to gain an understanding of meaningful robust plan optimization by investigating treatment type specific correlations between different uncertainties and by studying the sensitivity of a plan to different uncertainty types. Additionally, with the tool there is the potential to investigate the margin concept of target volumes and OARs towards flexible margins [40]. Finally, the robustness of new treatment techniques is explorable in order to facilitate their safe clinical implementation.

2.6 Conclusion

In conclusion, by combining dose calculation of treatment plans using different treatment techniques, including patient and machine related uncertainties, flexible evaluation according to user-defined criteria, this robustness tool provides accurate comprehensive robustness evaluation and fills the need for an overarching robustness evaluation tool to determine plan quality.

2.7 Acknowledgements

This work was supported by Varian Medical Systems. The MC dose calculations were performed on UBELIX (www.id.unibe.ch/hpc), the high-performance-computing cluster at the University of Bern. Open access funding provided by Universitat Bern.

2.8 Conflict of interest statement

The authors have no relevant conflicts of interest to disclose.

REFERENCES

1. Hernandez, V. *et al.* What is plan quality in radiotherapy? The importance of evaluating dose metrics, complexity, and robustness of treatment plans. *Radiother Oncol* **153**, 26–33. ISSN: 18790887 (2020).
2. Schmidhalter, D. *et al.* Assessment of patient setup errors in IGRT in combination with a six degrees of freedom couch. *Zeitschrift für Medizinische Physik* **24**, 112–122. ISSN: 0939-3889 (Aug. 2014).
3. Kerns, J. R., Childress, N. & Kry, S. F. A multi-institution evaluation of MLC log files and performance in IMRT delivery. *Radiation Oncology* **9**, 1–10. ISSN: 1748717X (Aug. 2014).
4. Yock, A. D. *et al.* Robustness Analysis for External Beam Radiation Therapy Treatment Plans: Describing Uncertainty Scenarios and Reporting Their Dosimetric Consequences. *Practical Radiation Oncology* **9**. ISSN: 18798500 (2019).
5. Teoh, M., Clark, C. H., Wood, K., Whitaker, S. & Nisbet, A. Volumetric modulated arc therapy: A review of current literature and clinical use in practice. *Brit J Radiol* **84**, 967–996. ISSN: 00071285 (2011).
6. Unkelbach, J. *et al.* Optimization approaches to volumetric modulated arc therapy planning. *Medical Physics* **42**. ISSN: 00942405 (2015).
7. Pigorsch, S. U. *et al.* Report on planning comparison of VMAT, IMRT and helical tomotherapy for the ESCALOX-trial pre-study. *Radiation Oncology* **15**. ISSN: 1748717X (2020).

8. Fix, M. K. *et al.* Part 1: Optimization and evaluation of dynamic trajectory radiotherapy. *Medical Physics* **45**, 4201–4212. ISSN: 00942405 (Aug. 2018).
9. Smyth, G., Evans, P. M., Bamber, J. C. & Bedford, J. L. Recent developments in non-coplanar radiotherapy. *Brit J Radiol* **92**. ISSN: 1748880X (Aug. 2019).
10. Mueller, S. *et al.* Simultaneous optimization of photons and electrons for mixed beam radiotherapy. *Physics in Medicine and Biology* **62**. ISSN: 13616560 (2017).
11. Mueller, S. *et al.* Part 2: Dynamic mixed beam radiotherapy (DYMBER): Photon dynamic trajectories combined with modulated electron beams. *Medical Physics* **45**, 4213–4226. ISSN: 00942405 (Aug. 2018).
12. Herk, M. V. Errors and Margins in Radiotherapy. *Seminars in Radiation Oncology* **14**, 52–64. ISSN: 10534296 (2004).
13. Katsuta, Y. *et al.* Patient-Specific Quality Assurance Using Monte Carlo Dose Calculation and Elekta Log Files for Prostate Volumetric-Modulated Arc Therapy. *Technology in Cancer Research and Treatment* **16**. ISSN: 15330346 (2017).
14. Katsuta, Y. *et al.* Log file-based patient dose calculations of double-arc VMAT for head-and-neck radiotherapy. *Phys Med* **48**, 6–10. ISSN: 1120-1797 (Aug. 2018).
15. Pan, Y. *et al.* National survey of patient specific IMRT quality assurance in China. *Radiation Oncology* **14**. ISSN: 1748717X (2019).
16. Wojtasik, A. M., Bolt, M., Clark, C. H., Nisbet, A. & Chen, T. Multivariate log file analysis for multi-leaf collimator failure prediction in radiotherapy delivery. *Physics and Imaging in Radiation Oncology* **15**. ISSN: 24056316 (2020).

17. Imae, T. *et al.* Retrospective dose reconstruction of prostate stereotactic body radiotherapy using cone-beam CT and a log file during VMAT delivery with flattening-filter-free mode. *Radiological Physics and Technology* 2020 **13:3** **13**, 238–248. ISSN: 1865-0341 (Aug. 2020).
18. LoSasso, T., Chui, C.-S. & Ling, C. C. Physical and dosimetric aspects of a multileaf collimation system used in the dynamic mode for implementing intensity modulated radiotherapy. *Medical Physics* **25**, 1919–1927. ISSN: 2473-4209 (Aug. 1998).
19. Luo, W. *et al.* Monte Carlo based IMRT dose verification using MLC log files and R/V outputs. *Medical Physics* **33**, 2557–2564. ISSN: 2473-4209 (Aug. 2006).
20. Andreo, P. Monte Carlo simulations in radiotherapy dosimetry. *Radiation Oncology* **13**. ISSN: 1748717X (2018).
21. Fix, K. *et al.* Efficient photon treatment planning by the use of Swiss Monte Carlo Plan. *Journal of Physics: Conference Series* **74**, 21004. ISSN: 1742-6596 (Aug. 2007).
22. Fix, M. K. *et al.* An efficient framework for photon Monte Carlo treatment planning. *Physics in Medicine and Biology* **52**, 425–437. ISSN: 00319155 (2007).
23. Giglioli, F. R. *et al.* Dosimetric Multicenter Planning Comparison Studies for Stereotactic Body Radiation Therapy: Methodology and Future Perspectives. *International Journal of Radiation Oncology Biology Physics* **106**, 403–412. ISSN: 1879355X (Aug. 2020).
24. Herk, M. V., Witte, M., Geer, J. V. D., Schneider, C. & Lebesque, J. V. Biologic and physical fractionation effects of random geometric errors. *International journal of radiation oncology, biology, physics* **57**, 1460–1471. ISSN: 0360-3016 (Aug. 2003).

25. Fredriksson, A. A characterization of robust radiation therapy treatment planning methods—from expected value to worst case optimization. *Medical Physics* **39**, 5169–5181. ISSN: 2473-4209 (Aug. 2012).
26. Magaddino, V. *et al.* Validation of the Swiss Monte Carlo Plan for a static and dynamic 6 MV photon beam. *Zeitschrift fur Medizinische Physik* **21**. ISSN: 09393889 (2011).
27. Blanchette, J. *C++ GUI Programming with Qt 4, Second Edition* (2008).
28. Ju, T., Simpson, T., Deasy, J. O. & Low, D. A. Geometric interpretation of the γ dose distribution comparison technique: Interpolation-free calculation. *Medical Physics* **35**. ISSN: 00942405 (2008).
29. Manser, P. *et al.* Dose calculation of dynamic trajectory radiotherapy using Monte Carlo. *Zeitschrift fur Medizinische Physik* **29**. ISSN: 18764436 (2019).
30. Wendling, M. *et al.* A fast algorithm for gamma evaluation in 3D. *Medical Physics* **34**, 1647–1654. ISSN: 2473-4209 (Aug. 2007).
31. Jeraj, R. & Keall, P. The effect of statistical uncertainty on inverse treatment planning based on Monte Carlo dose calculation. *Physics in Medicine & Biology* **45**, 3601. ISSN: 0031-9155 (Aug. 2000).
32. Pogson, E. M. *et al.* Multi-institutional comparison of simulated treatment delivery errors in sIMRT, manually planned VMAT and autoplan-VMAT plans for nasopharyngeal radiotherapy. *Physica Medica* **42**, 55–66. ISSN: 1120-1797 (Aug. 2017).
33. Jensen, C. A., Roa, A. M. A., Johansen, M., Lund, J. Å. & Frengen, J. Robustness of VMAT and 3DCRT plans toward setup errors in radiation therapy of locally advanced left-sided breast cancer with DIBH. *Physica Medica* **45**, 12–18. ISSN: 1120-1797 (Aug. 2018).

34. Lee, L., Le, Q. T. & Xing, L. Retrospective IMRT Dose Reconstruction Based on Cone-Beam CT and MLC Log-File. *International Journal of Radiation Oncology, Biology, Physics* **70**, 634–644. ISSN: 0360-3016 (Aug. 2008).
35. Qian, J. *et al.* Dose reconstruction for volumetric modulated arc therapy (VMAT) using cone-beam CT and dynamic log files. *Physics in Medicine & Biology* **55**, 3597–3610. ISSN: 0031-9155 (Aug. 2010).
36. Katsuta, Y. *et al.* Quantification of residual dose estimation error on log file-based patient dose calculation. *Phys Med* **32**, 701–705. ISSN: 1120-1797 (Aug. 2016).
37. Xiu, D. & Hesthaven, J. S. High-Order Collocation Methods for Differential Equations with Random Inputs. *SIAM Journal on Scientific Computing* **27**, 1118–1139. ISSN: 10648275 (Aug. 2005).
38. Lemieux, C. *Monte Carlo and Quasi-Monte Carlo Sampling* ISBN: 978-0-387-78164-8 (Springer New York, 2009).
39. Sterpin, E. *et al.* Development of robustness evaluation strategies for enabling statistically consistent reporting. *Physics in Medicine & Biology* **66**, 45002. ISSN: 0031-9155 (Aug. 2021).
40. Ahmad, R. *et al.* A margin-of-the-day online adaptive intensity-modulated radiotherapy strategy for cervical cancer provides superior treatment accuracy compared to clinically recommended margins: A dosimetric evaluation. *Acta Oncologica* **52**, 1430–1436 (Aug. 2013).

2.9 Appendix

A1 Comparison of gamma passing rate calculation algorithms

The gamma passing rate calculation of two dose distributions by our tool and by pymedphys open-source calculation is compared in figure 2.9. The pymedphys algorithm uses an interpolation fraction to calculate the gamma passing rate. The interpolation fraction is the fraction, which the gamma distance criteria is divided into for interpolation. If a 2 mm distance criteria is chosen, and the interpolation fraction is set to 10, the evaluation grid is consequently interpolated at a step size of 0.2 mm. With increasing interpolation fraction, the gamma passing rate asymptotically approaches the result of the robustness tool, however, on the cost of increased calculation time. After calculation with 20 interpolation fractions, the passing rates differed by less than 0.5%. The robustness tool does not need interpolation fractions as it calculates the closest geometric distance between a reference dose point and the hypersurface defined by the evaluation dose distribution. Pymedphys approximates this distance by sampling this hypersurface.

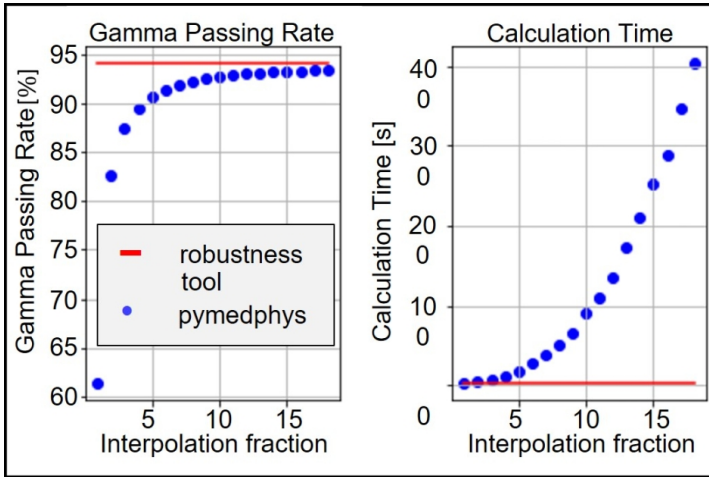


Figure 2.9: Gamma passing rate and calculation time as a function of interpolation fraction for pymedphys (blue). Gamma passing rate calculation with the robustness tool (red) is independent of the interpolation fraction and is shown as reference.

A2 Robustness Index calculation

In figure 2.10 the weight of the scenarios for an unweighted RI and a weighted RI are visualized. Here, we assume uncertainty scenarios in only one dimension equally spaced at 0, 1, 2, 3, 4 and 5. The reference scenario is located at 0. Green scenarios are considered robust, red scenarios are not robust. If the evaluation range is set to 2, scenarios closer to the reference scenario receive a

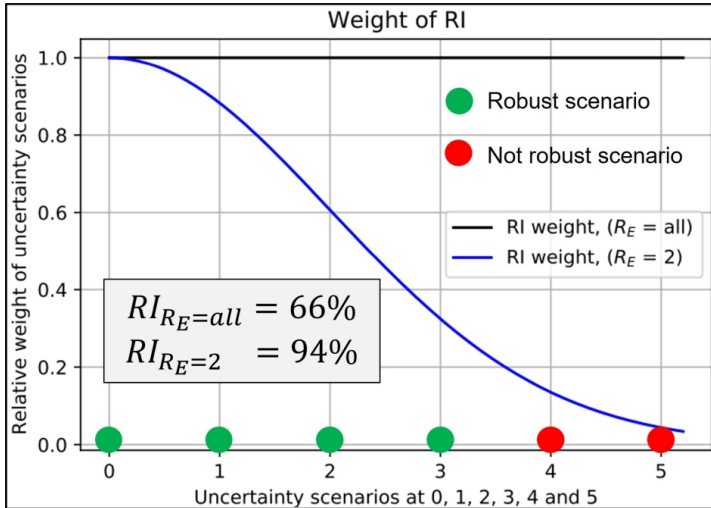


Figure 2.10: RI for scenarios at 0 to 5, when all scenarios are equally weighted (black), and RI with $R_E=2$ (blue).

higher weight (blue curve) in the calculation of the RI: in the illustrated example, the RI increases from 66%, in the unweighted, to 94%, in the weighted case. This weighting is intended for situations in which scenarios closer to the reference scenario are more likely than those further from the reference scenario. For these situations the weighted RI reflects this probability by means of a Gaussian distribution (mean=0, sigma= R_E).

IMPACT OF THE GRADIENT IN GANTRY-TABLE ROTATION ON DYNAMIC TRAJECTORY RADIO-THERAPY PLAN QUALITY

H.A. Loebner¹, S. Mueller¹, W. Volken¹, P. Wallimann¹,
D.M. Aebbersold¹, M.F.M. Stampanoni², M.K. Fix¹,
P. Manser¹

¹ Division of Medical Radiation Physics and Department of Radiation
Oncology, Inselspital, Bern University Hospital, University of Bern, Bern,
Switzerland

² Institute for Biomedical Engineering, ETH Zürich and PSI, Villigen,
Switzerland

published in
Medical Physics

September 2023, Volume 50, Issue 11
<https://doi.org/10.1002/mp.16749>

©American Association of Physicists in Medicine

Open access article distributed under the terms of the Creative Commons CC BY-NC-ND 4.0 license.

3.1 Abstract

Background

To improve organ at risk (OAR) sparing, dynamic trajectory radiotherapy (DTRT) extends VMAT by dynamic table and collimator rotation during beam-on. However, comprehensive investigations regarding the impact of the gantry-table (GT) rotation gradient on the DTRT plan quality have not been conducted.

Purpose

To investigate the impact of a user-defined GT rotation gradient on plan quality of DTRT plans in terms of dosimetric plan quality, dosimetric robustness, deliverability, and delivery time.

Methods

The dynamic trajectories of DTRT are described by GT and gantry-collimator paths. The GT path is determined by minimizing the overlap of OARs with planning target volume (PTV). This approach is extended to consider a GT rotation gradient by means of a maximum gradient of the path (G_{max}) between two adjacent control points ($G = |\Delta \text{table angle} / \Delta \text{gantry angle}|$) and maximum absolute change of G (ΔG_{max}). Four DTRT plans are created with different maximum G & ΔG : $G_{max} \& \Delta G_{max} = 0.5 \& 0.125$ (DTRT-1), $1 \& 0.125$ (DTRT-2), $3 \& 0.125$ (DTRT-3) and $3 \& 1$ (DTRT-4), including 3-4 dynamic trajectories, for three clinically motivated cases in the head and neck and brain region (A, B and C). A reference VMAT plan for each case is created. For all plans, plan quality is assessed and compared. Dosimetric plan quality is evaluated by target coverage, conformity, and OAR sparing. Dosimetric robustness is evaluated against systematic and random patient-setup uncertainties between ± 3 mm in the lateral, longitudinal, and vertical directions, and machine uncertainties between $\pm 4^\circ$ in the dynamically rotating machine components (gantry, table, collimator rotation). Delivery time is recorded. Deliverability and delivery accuracy on a TrueBeam are assessed by logfile analysis for all plans and additionally verified by film measure-

ments for one case. All dose calculations are Monte Carlo based.

Results

The extension of the DTRT planning process with user-defined G_{max} & ΔG_{max} to investigate the impact of the GT rotation gradient on plan quality is successfully demonstrated. With increasing G_{max} & ΔG_{max} , slight (case C, $D_{mean,parotid}$: up to -1 Gy), and substantial (case A, $D_{0.03cm^3,opticnerver}$: up to -9.3 Gy, case B, $D_{mean,brain}$: up to -4.7 Gy) improvements in OAR sparing are observed compared to VMAT, while maintaining similar target coverage. All plans are delivered on the TrueBeam. Expected and actual machine position values recorded in the logfiles deviated by $<0.2^\circ$ for gantry, table and collimator rotation. The film measurements agreed by $>96\%$ (2% global/2 mm Gamma passing rate) with the dose calculation. With increasing G_{max} & ΔG_{max} , delivery time is prolonged by <2 min/trajectory (DTRT-4) compared to VMAT and DTRT-1. The DTRT plans for case A and B and the VMAT plan for case C plan reveal the best dosimetric robustness for the considered uncertainties.

Conclusions

The impact of the GT rotation gradient on DTRT plan quality is comprehensively investigated for three cases in the head and neck and brain region. Increasing freedom in this gradient improves dosimetric plan quality at the cost of increased delivery time for the investigated cases. No clear dependency of GT rotation gradient on dosimetric robustness is observed.

3.2 Introduction

To improve organ at risk (OAR) sparing and target coverage, research in intensity modulated radiotherapy on C-arm linear accelerators (linacs) has explored the possibility to increase the degrees of freedom (DoF) during treatment planning and delivery compared to three-dimensional conformal radiotherapy. C-arm linacs have the possibility to dynamically move multiple machine axes simultaneously: volumetric modulated arc therapy (VMAT) combines multi-leaf collimation (by means of the photon multi-leaf collimator, MLC) and dynamic gantry rotation to efficiently deliver intensity modulated photon beams. VMAT has become standard of care in radiotherapy [1–3]. For a typical VMAT plan, the beam directions reside within a two-dimensional plane. Previous studies confirm however, that by deviating from this plane, improvements in dosimetric plan quality, particularly in OAR sparing, are achievable [4–8]. Consequently, several treatment techniques employing non-coplanar beam directions have been developed, such as non-coplanar partial VMAT arcs (e.g., Hyper Arc [9, 10]) or 4π -IMRT [11–14]. Moreover, dedicated systems such as the CyberKnife[®] (Accuray, Sunnyvale, CA, USA) or the discontinued VERO[®] (Brainlab, Munich, Germany and Mitsubishi Heavy Industries, Tokyo, Japan) are explicitly developed to use non-coplanar beam angles. However, these systems are not as widely available as C-arm linacs.

On the downside, non-coplanar treatment techniques present a challenge in preventing collisions between gantry and table, as well as between gantry and patient. Furthermore, diverging from the coplanar plane is usually connected with increased delivery times, especially for 4π -IMRT [11, 15, 16] which can negatively impact patient comfort. Hence, more efficient delivery is desired and can be achieved by combining dynamic gantry and table rotation with intensity modulation [17, 18]: Dynamic trajectory radiotherapy (DTRT) [19, 20] is an extension of VMAT that involves dynamic table and collimator rotations during delivery, allowing for treatment times similar to VMAT.

A comprehensive assessment of the plan quality of DTRT compared to VMAT requires the characterization of the dynamics of DTRT, particularly the gantry-table (GT) rotations, and the evaluation of the following aspects of plan quality [21]:

- *Dosimetric plan quality*
- *Plan complexity*
- *Dosimetric robustness*
- *Deliverability*
- *Delivery time*

Dosimetric treatment plan comparisons considering different treatment sites already indicated substantially improved sparing of OARs for DTRT as compared to VMAT [18, 19]. With the added DoF and the associated increased complexity, the dosimetric robustness of DTRT plans could be compromised. The number of robustness studies including DTRT are limited, and usually focus on patient setup uncertainties [22, 23]. Uncertainties in the now dynamically rotating machine components have not been evaluated. A comprehensive robustness assessment needs to additionally investigate how uncertainties in gantry, table, and collimator, impact the dosimetric plan quality. To ensure deliverability, the treatment machine must meet additional requirements compared to VMAT. Namely, the accurate dynamic rotation of the treatment table and the collimator in combination with the gantry rotation and MLC modulation needs to be verified. On the patient side, the delivery time can impact patient comfort. Delivery time is therefore another key quantity to assess when determining plan quality.

Finally, as DTRT trajectories are patient-specific and not limited to a specific GT path, it is crucial to consider and characterize their dynamics when evaluating and comparing the plan quality. For this purpose, we extended the inhouse developed DTRT planning process [19] to consider a user-specified GT rotation

gradient. In this work, the extended DTRT planning process is applied to generate DTRT plans with different GT rotation gradients for three clinically motivated cases: two head and neck cases and one brain case. The VMAT and DTRT plans were used to study the trade-offs between dosimetric plan quality, plan complexity, dosimetric robustness, deliverability and delivery time as a function of the GT rotation gradient.

3.3 Materials and Methods

A GT rotation gradient is introduced to characterize the dynamics of DTRT trajectories. The GT rotation gradient is defined as the ratio of the change in table angle to the change in gantry angle between two adjacent control points of the DTRT trajectory.

3.3.1 DTRT treatment planning process

To investigate the impact of the GT rotation gradient on plan quality, the underlying idea for the DTRT treatment planning process (TPP), described by Fix et al. [19], is extended. In the following the TPP is summarized, and the extended path finding is described in more detail (figure 3.1).

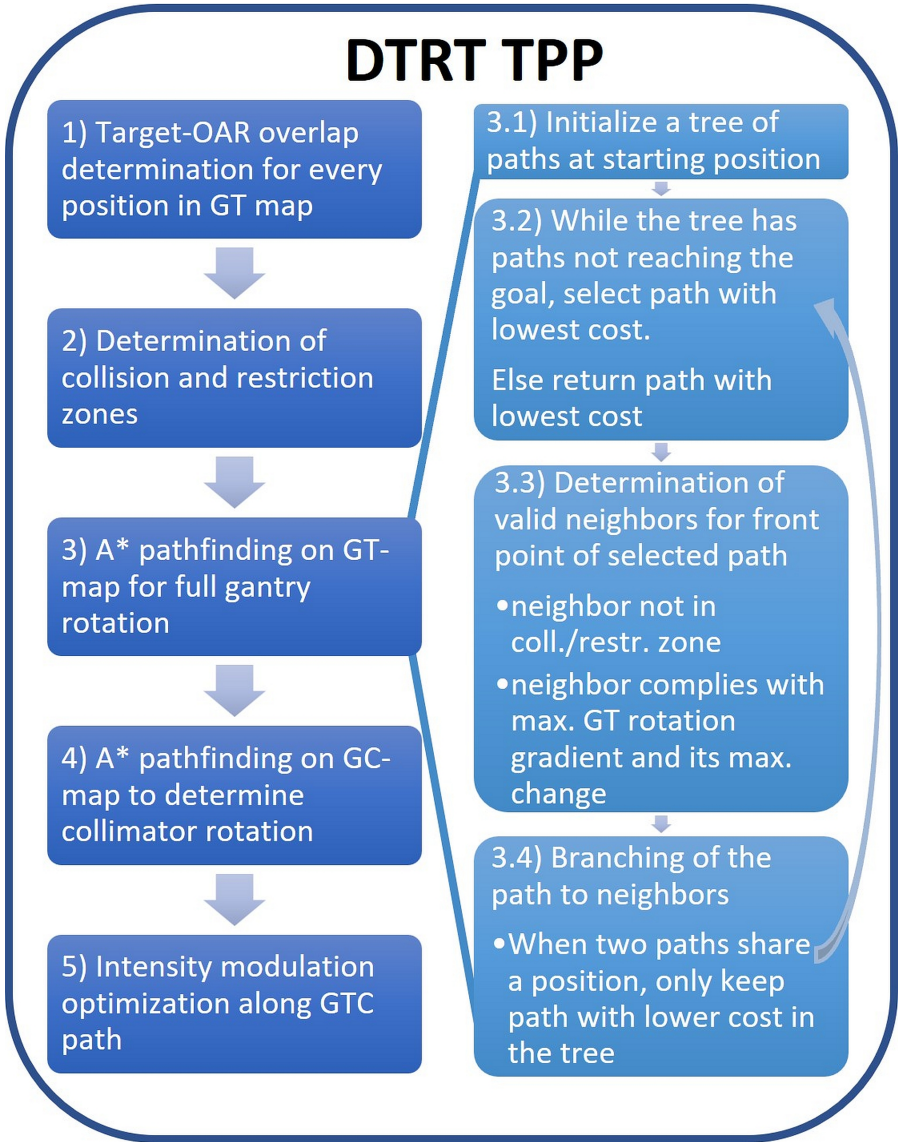


Figure 3.1: Steps of the DTRT TPP, with the path finding in detail shown on the right.

The DTRT TPP is started by creation of the target-OAR overlap maps, based

on the structure set (figure 3.1, 1). The target-OAR overlap in the beam's-eye-view is determined geometrically for a set of 400 uniformly [24] distributed beam directions defined by a gantry and table angle using an in-house software. First, the 2D overlap of the projection is calculated. Second, the corresponding fractional volume of target and OAR is determined using the mesh of the structures and raytracing. The fractional volumes are weighted according to their depth within the patient body ($\text{weight} = e^{-\text{depth}/22}$), which corresponds to an approximation of the depth dose curve of a 6 MV photon beam in water, neglecting build-up. Third the weighted fractional volume overlap is determined. OARs located in front of the target are therefore penalized more than those located behind. The weighted overlaps are then projected on a two-dimensional GT map of gantry (x-axis) and table angles (y-axis), ranging from -180° to 180° and -90° to 90° , respectively. Summed maps can be generated for multiple user-selected OARs to emphasize the sparing of OAR groups (target-OARs overlap). The GT map is interpolated to a resolution of $r_g = 2^\circ$ in gantry and $r_t = 0.25^\circ$ in table angle. Beam directions in collision zones (between gantry-patient or GT), as well as CT restriction zones (beam entering through the end of the CT), are excluded in the GT maps (figure 3.1, 2). An A* algorithm [25] is employed to find the GT path for a full gantry rotation in this map, which minimizes the target-OARs overlap (figure 3.1, 3). The A* algorithm is deterministic and provides the path with the lowest cost on a given cost map. The GT path finding can be repeated on different target-OAR overlap maps to obtain multiple paths. In a next step, the dynamic collimator rotation is determined (figure 3.1, 4). To this end, a gantry-collimator (GC) map is generated for the previously determined GT path using an inhouse software: The GC map quantifies the width in the leaf travel direction of a target-conformal and jaw-defined field for each position along the GT path and all possible collimator rotations. On the GC map, an A* algorithm determines the dynamic collimator rotation along the GT path with minimal summed field width. This dynamic collimator rotation reduces potential leaf travel in the later intensity modulation optimization.

The resulting gantry-table-collimator (GTC) paths are transferred back into a research version of Eclipse® embedded in the Aria 15.6 framework (Varian Medical Systems, Palo Alto, CA, USA) via the Eclipse Scripting Application Programming Interface (ESAPI). In Eclipse, the GTC paths are then defined by the standard control point resolution for a full VMAT arc (178 control points). A research version of the Eclipse photon optimizer is used to optimize the intensity modulation and generate the treatment plan according to dosimetric clinical guidelines (figure 3.1, 5).

The dose calculations in this work are Monte Carlo (MC) based using the Swiss Monte Carlo Plan (SMCP) [26]. SMCP employs VMC++ [27] for the radiation transport through the beam modifiers and the dose distribution calculation within the patient. Calculation voxel size is $0.25*0.25*0.25\text{ cm}^3$. The number of simulated primary particles per calculation is in the order of 10^8 , leading to an actual mean statistical uncertainty of $<1.2\%$ (one standard deviation) for the voxels with dose values higher than 50% of the maximum dose for all presented dose distributions.

To steer the path finding of the GT path, step 3 of the DTRT TPP is expanded to consider user-defined limitations given by a maximal GT rotation gradient G_{max} and its change ΔG_{max} between two adjacent positions of the GT path along the gantry axis (pseudo code in Supplementary Material 0). G_{max} restricts the steepness of the resulting path. The motivation to introduce G_{max} is to control the maximal slow-down of the gantry rotation speed due to the table rotation. Introducing G_{max} gives the possibility of aiming for similar delivery times as VMAT. ΔG_{max} limits the maximal directional change and enables granular adjustment of the smoothness of the resulting path. Limiting unsmooth behavior in the table rotation can increase machine durability and can reduce unwanted patient motion during delivery.

GT path finding is performed in a three-dimensional map, where the third dimension is used to consider the change in table angle and thus to enable finding the optimal path under the additional restriction of ΔG_{max} . A position in this

map is given by $p_{i,j,k}$:

- $i \in \left[1, I = \frac{360}{r_g} + 1\right]$ corresponds to the gantry angle $g_i = -180 + (i-1) * r_g$.
- $j \in \left[1, j = \frac{1800}{r_t} + 1\right]$ corresponds to the gantry angle $t_j = -90 + (j-1) * r_t$.
- $k \in \left[1, K = \frac{2G_{max} * r_g}{r_t} + 1\right]$ is an index whose value range defines the permissible table positions. The change in table angle $\Delta t_k = (-G_{max} * r_g + (k-1) * r_t)$ (Equation 1) between two adjacent positions along the GT path is dependent on k .

Owing to the third dimension, the potential neighbors of each position can be determined independently of the path finding while respecting the constraints of G_{max} and ΔG_{max} . Each $p_{i,j,k}$ has an associated cost $c_{i,j}$ (independent of k , which refers to permissible table position at gantry-table position indexed by i and j). The cost corresponds to the target-OARs overlap for the respective beam direction and is independent of index k , and thus the notation of this cost can be reduced to $c_{i,j} = c_{i,j,k}$.

γ^a is the GT path with index a for a full gantry rotation and consists of I positions with the assigned labels $(j_1^a, j_2^a, \dots, j_I^a)$, which can be translated to the respective table angle for each $i = 1, \dots, I$. For a path, $\Delta t_{k_i^a}$ can directly be calculated by $\Delta t_{k_i^a} = t_{j_{i-1}^a} - t_{j_i^a}$ and index k_i^a can be obtained by solving equation 1 for k . A path γ^a needs to comply with the following restrictions for all i :

- All p_{i,j_i^a,k_i^a} of path γ^a cannot be in a collision or restriction zone
- $G_i = \left| \frac{t_{j_i^a} - t_{j_{i+1}^a}}{g_i - g_{i+1}} \right| \leq G_{max}$
- $\Delta G_i = \left| \frac{t_{j_{i-1}^a} - t_{j_i^a}}{g_{i-1} - g_i} - \frac{t_{j_i^a} - t_{j_{i+1}^a}}{g_i - g_{i+1}} \right| = \left| \frac{\Delta t_{k_i^a}}{g_{i-1} - g_i} - \frac{\Delta t_{k_{i+1}^a}}{g_i - g_{i+1}} \right| \leq \Delta G_{max}$

Additionally, an artificial start p_0 and end position p_{I+1} with no cost ($c_0 = c_{I+1} = 0$) are introduced. Gantry and table angle and k are not defined for p_0 and p_{I+1} . All p_{1,j_1,k_1} neighbor p_0 and p_{I+1} neighbors all p_{I,j_I,k_I} . Introducing

an artificial start and end position enables finding the path with the optimal start and end position on the map, without introducing a bias by an arbitrary selection of the start and end table angle (figure 3.2).

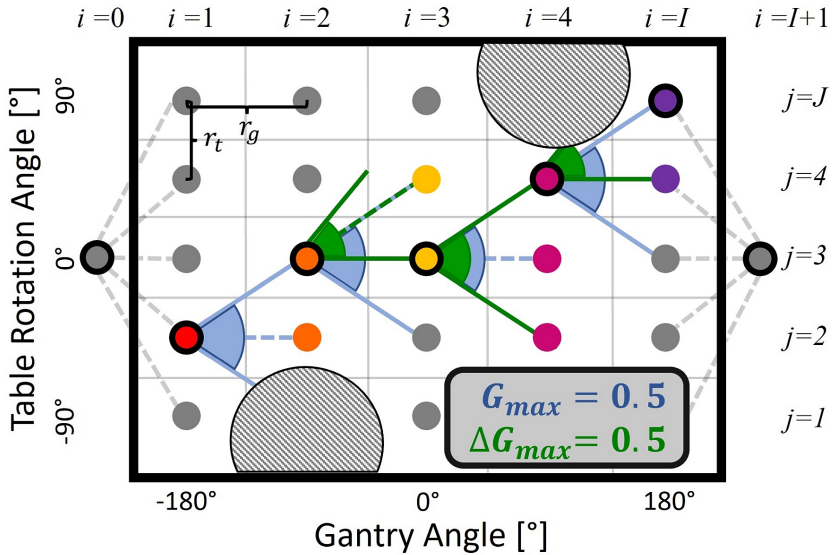


Figure 3.2: Schematic representation to determine the neighbors of specific positions within the GT map. The resolution in table and gantry angle is adapted for demonstration purpose. To the left and right side of the map, artificial start and end positions are shown. The black encircled points have neighboring candidates that are exemplary shown in different colors: the neighbors of the red points are displayed in orange, the orange points' neighbors are displayed in yellow, the yellow points' neighbors are displayed in magenta, and the purple points neighbor the magenta points. The blue and green cones represent the G_{max} and ΔG_{max} restriction, respectively. The dashed half-circles indicate collision and CT-restriction zones. Per definition, the ΔG_{max} restriction is only applicable starting from $i=2$.

The path cost between two positions is given by the mean of the position costs. The goal is to find the GT path γ^* which has the minimal path cost C_{γ^*} out of all paths A which comply with the above criteria. The optimization problem reads as follows:

$$\text{find } \gamma^*, \text{ such that } C_{\gamma^*} = \min_{\gamma^* \in A} \left(\sum_{i'=0}^I \frac{1}{2} * (c_{i',j_{i'}^a} + c_{i'+1,j_{i'+1}^a}) \right) \quad (3.1)$$

The A* algorithm starts at p_0 . From there, it establishes and iteratively expands a tree of paths to find the path with the lowest cost for a full gantry rotation. A priority queue is used to expand only the paths with the current lowest path cost. The extended path finding considers the above-mentioned restrictions at the stage of neighbor determination $p_{i+1\#}, j_{i+1\#}, k_{i+1\#}$ of p_{i,j_i^a, k_i^a} prior to the path finding.

An essential feature of the A* algorithm to substantially improve efficiency is the bookkeeping which enables discarding paths from the tree of paths when two paths share a position (equal in all three coordinates). Only the path corresponding to the lower path cost is kept. The suspension of paths of higher cost substantially reduces the number of paths that are expanded during the path finding.

3.3.2 Clinically motivated cases

Three representative cases in the head and neck and brain region are investigated: a nasopharynx case (A), a glioblastoma case (B), and a bilateral oropharynx case (C) (figure 3.3). For each case, a coplanar VMAT plan is created as a reference plan. To investigate the impact of the GT rotation gradient, four DTRT plans conforming to different G_{max} & ΔG_{max} are created for each case (table 3.1).

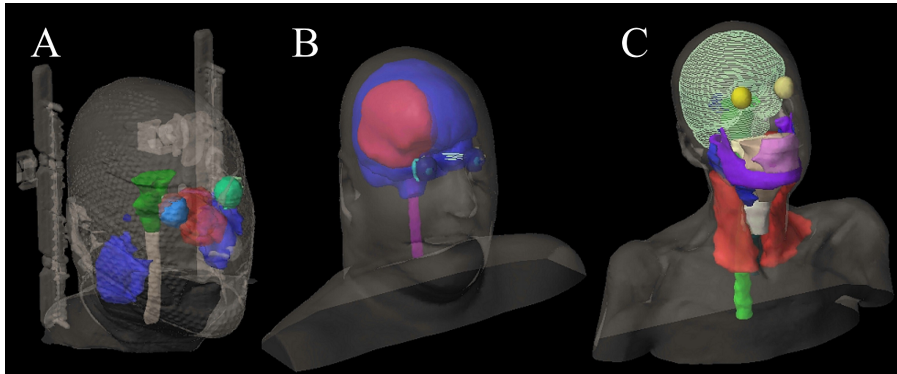


Figure 3.3: The investigated nasopharynx (A), glioblastoma (B) and bilateral oropharynx case (C) are shown. The PTV is shown in red, the OARs are visualized in different colors.

Table 3.1: G_{max} and ΔG_{max} specifications for the considered VMAT and DTRT plans.

	VMAT	DTRT-1	DTRT-2	DTRT-3	DTRT-4
G_{max}	0	0.5	1	3	3
ΔG_{max}	0	0.125	0.125	0.125	1

A suitable set of optimization objectives is determined for each case to optimize the VMAT and DTRT plans alike, aiming for similar target coverage between the plans (Supplementary Material 1). VMAT and DTRT plans are optimized using the same optimizer (i.e., a research version of the Eclipse photon optimizer, which allows for additional dynamic machine components, table and collimator rotation, during the optimization).

In table 3.2, the prescription, VMAT arc setup and DTRT strategy are described for case A, B and C. The different dynamic trajectories focus on the sparing of different OAR groups by considering the overlap of the target with different OARs. In cases, where the field width of the arc/dynamic trajectory in the leaf travel direction would exceed 10 cm, field splitting is performed to enable more MLC leaf modulation. Field splitting is always performed in leaf-travel

direction by dividing the field-of-view with an overlap of 2 cm in the center to generate two arcs/dynamic trajectories. For cases A, B and C, the CTV-PTV expansion is 0.3 cm, 0.5 cm and 0.5 cm, respectively. When a distance between PTV to skin surface of 0.5 cm could not be maintained, the CTV-PTV expansion is reduced accordingly.

Table 3.2: Prescription and VMAT and DTRT strategy for case A, B and C.

Treatment site	Prescription	VMAT strategy	DTRT strategy
Case A, glioblastoma	50 Gy to 95% of the PTV, delivered in 25 fractions	3 arcs, with rotated collimator (45° and 90°) for the second and third arc with respect to the first arc	3 dynamic trajectories, <i>first</i> : all OARs, <i>second</i> : optic nerve, <i>third</i> : chiasm – second and third focus on sparing of small important structures
Case B, nasopharynx	60 Gy to 50% of the PTV, delivered in 30 fractions	2 arcs, with the second one duplicated by means of field splitting, with rotated collimator for the first arc (90°) with respect to the second arc	2 dynamic trajectories, with the first one being duplicated by 90° collimator rotation, <i>first</i> : brain – sparing healthy brain tissue, <i>second</i> : right optic nerve – due to its proximity to the target
Case C, bilateral oropharynx	50 Gy to 95% of the PTV, delivered in 25 fractions	2 arcs, duplicated using field splitting, with rotated collimator for (90°) with respect to each other	2 dynamic trajectories, which are duplicated by field splitting, <i>first</i> : brain, brainstem, parotids, and oral cavity – OARs in the upper head region, <i>second</i> : pharynx, spinal cord – OARs close to the PTV

3.3.3 Evaluation

Plan complexity

Plan complexity is evaluated using the average G and ΔG of the final paths, as well as the modulation complexity score (MCS). The MCS was originally introduced for IMRT [28], and then extended to VMAT [29]. In this work, the concept is applied to DTRT plans by transferring the definition of MCS along the control points of the VMAT arc to the control points along the DTRT trajectory. The MCS ranges from 0 to 1, with a higher score indicating a “less complex” plan.

Dosimetric plan quality

Dosimetric plan quality is assessed by three aspects:

- evaluating target coverage, conformity and OAR sparing in terms of DVH comparison
- comparing the Paddick Index [30] for the prescription isodose (PI) and for 50% of the prescription ($PI_{50\%}$). The PI is given by: $PI = \frac{TV_{PI}^2}{TV * PIV}$, with TV as target volume, PIV as prescription isodose volume and TV_{PI} as target volume covered by prescription isodose
- assessing the low dose bath in the normal tissue ($NT = Body - PTV$) by evaluating $V_5 Gy, NT$, and $V_{10 Gy, NT}$ for the respective plans [8].

Additionally, a comparison of the objective function values of the dose distributions after optimization and final dose calculation for each case can be found in the Supplementary Material 2.

Dosimetric robustness

A previously developed robustness tool [31] is used to assess the impact of patient- and machine-related uncertainties on the dose distributions of the plans. On the patient side, systematic patient-setup uncertainties (-0.3 cm, 0.0 cm, 0.3 cm), the combination thereof, and random patient setup uncertainties sampled from a Gaussian distribution ($\sigma = 0.0$ cm and 0.3 cm) and the combination thereof in longitudinal, lateral and vertical direction, are investigated. This leads to a total of $3 \times 3 \times 3 - 1$ (nominal scenario) = 26 systematic and $2 \times 2 \times 2 - 1 = 7$ random patient-setup uncertainty scenarios per plan. On the machine side, systematic uncertainties (-4°, -2°, -1°, 0°, 1°, 2°, 4°) in gantry, table and collimator rotation and the combination thereof are investigated, leading to a total of $7 \times 7 \times 7 - 1 = 342$ machine-related uncertainty scenarios per plan.

Patient-setup uncertainties are selected to include extreme cases observed in clinical practice [32]. Furthermore, setup shifts up to 0.3 cm are often not corrected for in clinical practice [33]. Machine uncertainties are selected to evaluate miscalibration scenarios: systematic miscalibrations of the machine components

are not visible in the machine logfiles. For DTRT, investigations of uncertainties in these machine components are of particular interest, as:

- DTRT extends VMAT by the combination of dynamic rotations in these machine components
- The beam direction is defined by both gantry and table angles, and the effect of uncertainties in these components are difficult to predict due to their dynamic movement
- The complexity of DTRT treatment plans obstructs how the combination of uncertainties in the dynamic movement of gantry, table and collimator affects the dosimetric plan quality

In this work, a plan is defined to be dosimetrically robust when $D_{98\%CTV}$ of the clinical target volume (CTV) is not decreased and $D_{2\%CTV}$ is not increased by more than 1 Gy compared to the nominal scenario (no uncertainty). Additionally, $D_{2\%serialOAR}$ and $D_{mean_{parallelOAR}}$ are not increased by 1 Gy compared to the nominal scenario. The robustness tool returns a robustness summary of all uncertainty scenarios using the robustness index (RI). RI is given by the fraction of uncertainty scenarios passing the beforementioned criteria.

Deliverability and delivery accuracy

To demonstrate the deliverability of DTRT plans of different G_{max} & ΔG_{max} , all plans are translated into XML-files and delivered in Developer Mode on a TrueBeam (Varian Medical Systems, Palo Alto, CA, USA).

It is first assessed whether the plans can be delivered collision and interlock free. Second, a machine logfile analysis is then conducted to assess the accuracy of the delivery with respect to G_{max} & ΔG_{max} . In the logfile, the *expected* and *actual* machine positions of gantry angle, table rotation angle, collimator angle and MLC are recorded at a rate of 50 Hz. The differences between expected and actual are compared, and correlations between the differences and the re-

spective machine component speed are investigated. Third, the accuracy of the dose calculation for the extended TPP is verified by means of an end-to-end test using film validation measurements for all DTRT plans of case A (Supplementary Material 3).

Delivery time

The delivery time of a plan is extracted from the machine logfiles, defined as the total beam-on time.

3.4 Results

3.4.1 Path generation and complexity

In figure 3.4 the path costs of the target-OAR overlap maps of the different plans are displayed. With increasing G_{max} and ΔG_{max} a greater reduction of the cost is achieved as expected.

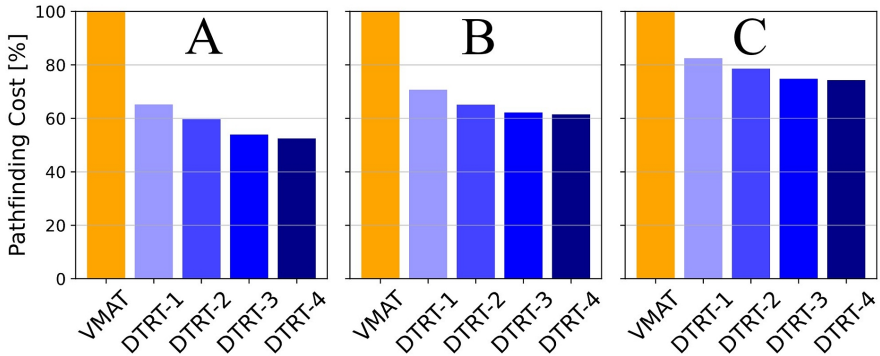


Figure 3.4: A* path finding costs on the target-OAR overlap maps for the investigated cases A, B and C, normalized to the VMAT plan as reference. The VMAT cost is calculated on each of the respective target-OAR overlap maps and summed together.

In figure 3.5, the paths of the three dynamic trajectories of DTRT-1, 2, 3 and 4 are shown for case A. Increasing G_{max} enabled the A* algorithm to find paths with greater GT rotation gradients: For instance, shortly after gantry angle = 0° , path 1 and path 3 of DTRT-3 and DTRT-4 include a greater table rotation range to avoid a high-cost region. By increasing ΔG_{max} , the A* algorithm is free to select a more “unsmooth” path, which is particularly seen around table = 60° and gantry = -90° of the GT map of path 1 and 2. Furthermore, several direction changes occur at the end of the path.

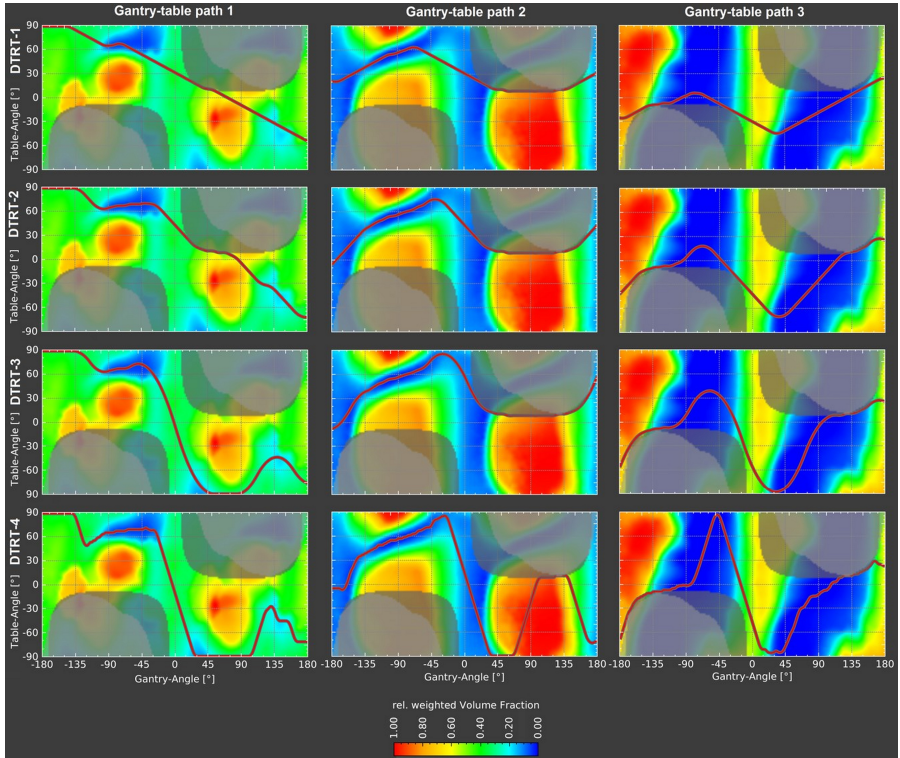


Figure 3.5: Target-OAR overlap maps with respective DTRT-1 to DTRT-4 paths for case A. With increasing freedom in the GT rotation gradient, the cost for one path is minimized more. In light grey collision zones (between gantry-patient or GT) and in dark grey CT restriction zones are marked.

Regarding complexity (Supplementary Material 4), the average and maximal $G\&\Delta G$ increased from DTRT-1 to DTRT-4 plans. The average $G\&\Delta G$ are $0.421\&0.002$, $0.778\&0.003$, $1.284\&0.003$ and $1.953\&0.009$ and the maximal $G\&\Delta G$ are $0.580\&0.049$, $1.083\&0.077$, $3.048\&0.178$ and $3.077\&0.499$ for DTRT-1 to DTRT-4, respectively. The logfile reported maximal G and ΔG values are slightly greater than specified in the path finding, which is explained by rounding uncertainties and the internal machine translation of the XML plan-file into the application of the plan. The median MCS decreases from VMAT to the

DTRT plans (0.24 to 0.19 ± 0.15).

3.4.2 Dosimetric plan quality and robustness

To analyze the dosimetric plan quality, first the DVHs are compared. In figure 3.6 DVHs of the plans for case A are shown. The greater freedom in the GT rotation gradient is reflected in the DVH: while PTV coverage and homogeneity is similar between all plans, OAR sparing, particularly sparing of the optic chiasm and the right optic nerve are improved substantially with increasing $G_{max} \& \Delta G_{max}$ ($D_{0.03cm^3, opticnerver.} -9.3$ Gy). The DTRT-2 plan for case B improves the OAR sparing the best: $D_{0.03cm^3, opticnerver.} -1.6$ Gy, $D_{0.03cm^3, eyel.} -6.0$ Gy, $D_{0.03cm^3, chiasm} -7.7$ Gy, $D_{mean, brain} -4.7$ Gy compared to VMAT (Supplementary Material 5). Only slight improvements with increasing $G_{max} \& \Delta G_{max}$ are observed for the plans of case C ($D_{mean, parotid.} -1.0$ Gy) at the cost of increased mean dose (>5 Gy) to the brain. (Supplementary Material 6).

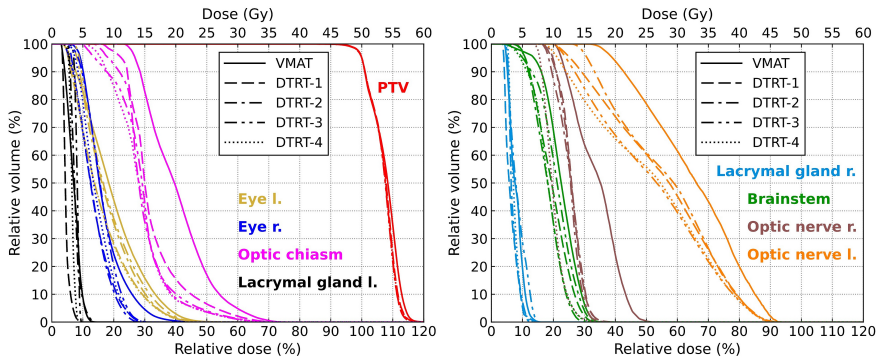


Figure 3.6: DVH comparison of the VMAT and DTRT plans for case A. While target coverage is comparable, increased OAR sparing for the OARs considered in the target overlap maps is observed with increased GT rotation gradient.

The low dose bath in terms of $V_{10 Gy, NT}$ is reduced for case A and case B from VMAT to DTRT, but increases for case C. Except for case A, $V_{5 Gy, NT}$ is increased with increasing $G_{max} \& \Delta G_{max}$. The conformity of the prescribed

isodose line differs by maximum of 0.01, except for case A, where it decreases by 0.04 from VMAT to DTRT-1. Improved conformity for the 50% isodose line is observed for the DTRT plans (table 3.3).

Table 3.3: Low dose bath $V_{5Gy,NT}$ and $V_{10Gy,NT}$, and conformity (PI and $PI_{50\%}$) comparison of the different treatment plans of case A, B and C. The best values (smallest volume or greatest PI and $PI_{50\%}$) are marked in bold.

	VMAT	DTRT-1	DTRT-2	DTRT-3	DTRT-4
Case A					
V_{PTV} 63.7 cm ³					
$V_{10Gy,NT}$ [cm ³]	801.1	639.7	608.8	574.8	619.5
$V_{5Gy,NT}$ [cm ³]	1469.2	1539.2	1492.4	1423.7	1477.9
PI	0.83	0.79	0.81	0.81	0.81
$PI_{50\%}$	0.25	0.30	0.31	0.31	0.31
Case B					
V_{PTV} 272.4 cm ³					
$V_{10Gy,NT}$ [cm ³]	1520.4	1325.9	1260.8	1341.1	1371.3
$V_{5Gy,NT}$ [cm ³]	1887.2	2057.4	2154.5	2325.6	2402.2
PI	0.48	0.49	0.49	0.49	0.49
$PI_{50\%}$	0.41	0.48	0.48	0.49	0.49
Case C					
V_{PTV} 410.8 cm ³					
$V_{10Gy,NT}$ [cm ³]	2188.5	2409.7	3074.1	3248.6	3282.3
$V_{5Gy,NT}$ [cm ³]	2897.8	4583.0	5310.6	5459.4	5383.2
PI	0.84	0.84	0.83	0.84	0.84
$PI_{50\%}$	0.29	0.31	0.31	0.31	0.31

The dosimetric robustness (figure 3.7) to patient setup uncertainties is similar between all plans for all cases. Furthermore, there is no clear trend of dosimetric robustness with respect to the GT rotation gradient. The DTRT plans of case A and B are more robust to machine uncertainties than the VMAT plans. For case C, dosimetric robustness to the investigated machine uncertainties decreases with increasing freedom in the GT rotation gradient.

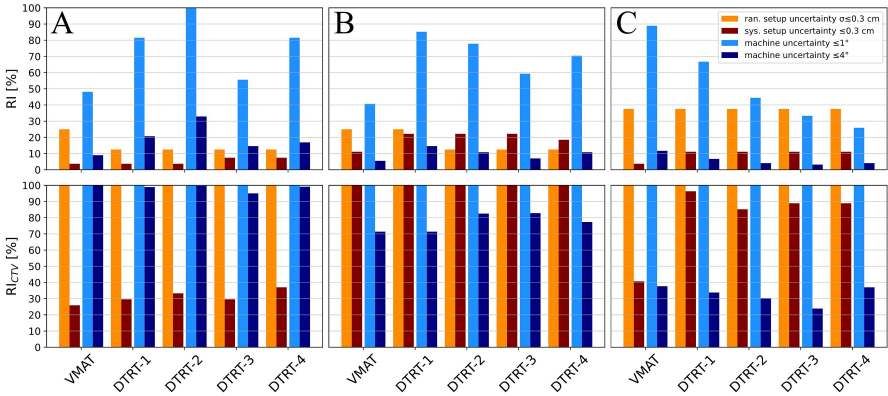


Figure 3.7: Dosimetric robustness, expressed in terms of RI and RI_{CTV} to random and systematic patient setup uncertainties in lateral, longitudinal, and vertical direction up to ± 0.3 cm, as well as systematic uncertainties in gantry, table and collimator rotation between $\pm 1^\circ$ and $\pm 4^\circ$ for the plans of case A (A, left), case B (B, middle) and case C (C, right).

When considering only the CTV robustness criteria (RI_{CTV}), the RI_{CTV} for systematic (random) setup uncertainties for case A, B and C are $>25\%$ (100%), 100% (100%) and $>40\%$ (100%), respectively. The robustness of the CTV for the VMAT plan of case C to systematic setup uncertainties is substantially worse (40%) as compared to the DTRT plans ($>88\%$). Regarding machine uncertainties up to $\pm 4^\circ$, the CTV robustness of the plans for case A is little influenced and have an $RI_{CTV} >95\%$. The larger targets of case B and C have an $RI_{CTV} >71\%$ and $>24\%$. For uncertainties up to $\pm 1^\circ$ RI_{CTV} is 100% for all plans and cases.

3.4.3 Deliverability

Logfile analysis & film measurements

The distributions of table rotation, gantry rotation and MLC position uncertainties retrieved from the recorded logfiles are shown in figure 3.8. The observed increase of the average G and ΔG from DTRT-1 to DTRT-4 has no substantial

effect on the uncertainty distribution of the gantry, table and collimator rotation. The average root-mean-square (RMS) uncertainty of the moving MLC leaves decreases with increasing G_{max} & ΔG_{max} . A correlation analysis of machine component speed and uncertainty in the respective machine component is found in the Supplementary Material 7.

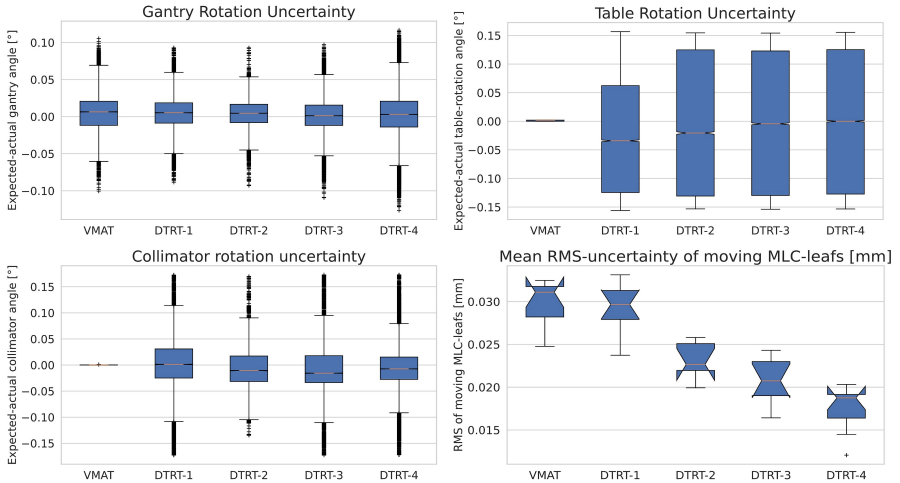


Figure 3.8: TrueBeam machine logfile analysis for the VMAT and DTRT plans. Small offsets for table and collimator rotation, observed in the VMAT plans, are not corrected, as they are within the precision limit of the respective machine component.

The film measurements for the DTRT plans of case A agree with the respective dose calculations by $>96\%$ Gamma passing rate (Supplementary Material 3). No substantial differences between the measurements of the DTRT-1 to DTRT-4 plans are observed.

Delivery time

With increasing G_{max} & ΔG_{max} , the mean time to deliver one arc/dynamic trajectory increases by a factor of 2 from 1.05 to 2.1 min (figure 3.9). Of note is that VMAT and DTRT-1 have similar delivery times. In our institution, the

TrueBeam has a maximal gantry rotation and table rotation speed of $6^\circ/\text{s}$ and $3^\circ/\text{s}$, respectively, leading to a G_{max} of 0.5 (as in DTRT-1), so that the table rotation does not slow down the delivery.

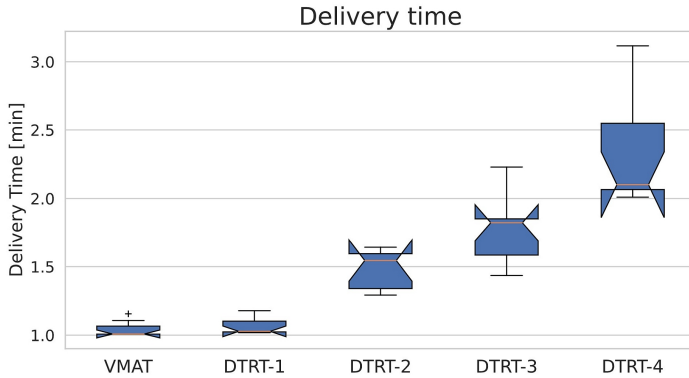


Figure 3.9: Delivery time per arc and dynamic trajectory of the VMAT and DTRT-1 to DTRT-4 plans.

3.5 Discussion

The impact of the GT rotation gradient on plan quality was comprehensively assessed by evaluation of dosimetric plan quality, complexity, dosimetric robustness, deliverability, and delivery time for three cases in the head and neck, and brain region.

Path generation and complexity

With the extended DTRT TPP, the dynamics of DTRT can be characterized and the user has more control of DTRT path generation. This developed approach has three main benefits: *First*, it provides a fast and optimal path finding solution on a given cost map. For the presented cases, path finding took less than 4 min to provide the path with the minimal cost [34]. *Second*, G_{max} and ΔG_{max} enable user control over the dynamics of the determined paths, tailoring DTRT plans to machine and institution specific requirements. G_{max} controls delivery slow-down due to the finite table rotation speed. ΔG_{max} regulates the smoothness of the path and enables to avoid multiple disruptive directional changes in table rotation. It is expected that a smoother path has a beneficial effect on the lifespan of the machine components. *Third*, the developed approach is applicable to a variety of path finding strategies and is not limited to a specific type of cost map (e.g., target-OAR overlap as presented in this work). The cost map is interchangeable and could for instance also comprise dosimetric information for dosimetric guided path finding [35]. However, approaches that include dosimetric information [36] need considerably more computation time. The path finding would also include the computationally expensive dose calculation or even intensity optimization.

G and ΔG complement the frequently used MCS, which has been related to delivery accuracy [28, 37], in characterizing the dynamics and complexity of DTRT plans. While MCS decreases slightly from VMAT to DTRT-1 for the investigated cases, it does not decrease further with increasing G_{max} & ΔG_{max} .

Dosimetric plan quality and robustness

The applied TPP in this work is sequential: first, target-OAR overlap maps generation and path finding, and second, the intensity optimization along the DTRT path. Due to this sequential nature, the dosimetric plan quality does not necessarily correlate with the decrease in path finding cost. Other approaches employ simultaneous optimization of path and intensity modulation at the cost of increased optimization times [38–40]. However, regarding dosimetric plan quality, this work agrees with previous findings [19, 41]. The generated DTRT plans of this work have the potential to substantially spare OARs as compared to the VMAT reference plans, particularly the ones considered in the target-OAR overlap maps. Increasing G_{max} & ΔG_{max} , enables improved sparing for these OARs, especially for case A and B. For case C, the DTRT plans also reduce dose to OARs considered in the target-OAR overlap, but at the cost of increased mean dose to the brain due to the large size and location of the target (lower head and neck area). Little variation in the dose conformity to the target is observed [41], with PI differing at most by 0.01, except for case A where the PI decreased by 0.04 from VMAT to DTRT-1. However, $PI_{50\%}$ is reduced for all cases from VMAT to DTRT. Furthermore, concerns regarding an increased low dose bath for non-coplanar delivery techniques [8] might not be justified, as for the DTRT plans a reduction up to 3% of $V_5 Gy, NT, caseA$, 28% of $V_{10 Gy, NT, caseA}$, and 17% of $V_{10 Gy, NT, caseB}$ is achieved compared to the respective VMAT plans.

Previous robustness considerations for non-coplanar photon-based treatment techniques are limited and have primarily focused on patient-setup uncertainties [8, 22, 23] and on the evaluation of the target dose. In these previous studies, it is indicated that non-coplanar techniques, are equally or more robust than coplanar VMAT. This work agrees by confirming that, except for case C, there is no substantial difference in the dosimetric target robustness for the investigated plans and setup uncertainties, regardless their GT rotation gradient. This work further extends these investigations by evaluating the robustness of OAR sparing

and the impact of uncertainties in gantry, table and collimator, on the planned dose distribution. The investigated machine uncertainties are several magnitudes larger than the uncertainties reported in the machine logfiles. However, systematic miscalibration of the treatment machines are not reported in the machine logfiles. Miscalibrations might be only detectable during machine QA. Furthermore, they are chosen for exploratory purposes to simulate scenarios that surpass the published machine tolerance limits [42]. On a different note, concerns about the robustness to rotational setup uncertainties are addressed by interpreting the table rotation uncertainty as patient-setup uncertainty. Plans of case A and B with increased G_{max} & ΔG_{max} show improved robustness to machine uncertainties, which is linked to their lower low dose bath. The impact of the uncertainties on the dose distribution happens on a smaller dose scale. The results of case C confirm this explanation, as the VMAT plan has the smallest low dose bath and the highest RI. The CTV robustness is hardly sensitive to random patient-setup uncertainties up to 0.3 cm and to machine uncertainties up to 1°. The PTV margin prevents a deterioration of the CTV dose in most cases. Of note is that in a clinical DTRT delivery setting, patient and machine uncertainties would occur together and a robustness evaluation would need to consider both uncertainty types in combination. Furthermore, uncertainties in patient setup might be influenced by the GT rotation gradient.

Deliverability and delivery time

This work focuses on plan deliverability, and all created plans have been delivered interlock-free. Additionally, film measurements confirm the accuracy of the dose calculation algorithm²⁶ for the extended TPP and verify the accurate delivery of the plans of different GT rotation gradient on the TrueBeam by means of an end-to-end test. Analysis of the machine logfiles confirmed the results of previous assessments [43]. Uncertainties in MLC leaf position are correlated to the leaf speed. Additionally, strong correlations are observed between table/collimator rotation uncertainty and rotation speed. However, an increase in G_{max} & ΔG_{max}

is not accompanied by greater mean uncertainties in the respective machine components for the investigated plans. The average RMS error for the moving MLC leaves even decreases with increasing G_{max} and ΔG_{max} and lower MCS. One possible explanation is that the MLC leaves have more time to achieve the desired apertures when there is more table rotation, as the table rotation speed with $3^\circ/s$ can slow the treatment delivery down.

The delivery time increases with increasing GT rotation gradient for the investigated cases. However, by setting G_{max} to 0.5, the additional dynamic table rotation does not slow the delivery down, while the plan quality still profits from the dosimetric benefits of the non-coplanar beam directions. In the context of overall treatment time, which includes the setup and positioning of the patient, also the delivery times of the DTRT-2 trajectories are comparably small [44, 45].

3.6 Conclusion

This work presents a method to generate DTRT plans with user-defined GT rotation gradients. The impact of this gradient on plan quality is comprehensively analyzed and the trade-offs between dosimetric plan quality, complexity, deliverability, delivery time and dosimetric robustness are highlighted. A small increase in this gradient, from VMAT to DTRT-1 ($G_{max}=0.5$), can already improve OAR sparing due to the non-coplanar beam directions. Furthermore, smooth delivery (by $\Delta G_{max}=0.125$) and similar delivery times as VMAT are maintained. Increasing the gradient and its change further shows no substantial improvements in dosimetric plan quality. Considering that the GT rotation gradient can impact patient comfort and machine durability, it is critical to have the option to limit G and ΔG for clinically acceptable delivery times and smooth delivery. Finally, this research confirms the feasibility of planning, accurately calculating, and delivering DTRT plans of different GT rotation gradients.

3.7 Acknowledgements

This work was supported by Varian Medical Systems. The MC dose calculations were performed on UBELIX (www.id.unibe.ch/hpc), the high-performance-computing cluster at the University of Bern.

3.8 Conflict of interest statement

The authors have no relevant conflicts of interest to disclose. In his role as deputy editor for Medical Physics, author M.K.F. was blinded to the review process and had no role in decisions pertaining to this manuscript.

REFERENCES

1. Otto, K. Volumetric modulated arc therapy: IMRT in a single gantry arc. *Medical Physics* **35**, 310–317. ISSN: 2473-4209 (Aug. 2008).
2. Verbakel, W. F. A. R. *et al.* Volumetric Intensity-Modulated Arc Therapy Vs. Conventional IMRT in Head-and-Neck Cancer: A Comparative Planning and Dosimetric Study. *International Journal of Radiation Oncology Biology Physics* **74**, 252–259. ISSN: 03603016 (Aug. 2009).
3. Teoh, M., Clark, C. H., Wood, K., Whitaker, S. & Nisbet, A. Volumetric modulated arc therapy: A review of current literature and clinical use in practice. *Brit J Radiol* **84**, 967–996. ISSN: 00071285 (2011).
4. Smyth, G. *et al.* Non-coplanar trajectories to improve organ at risk sparing in volumetric modulated arc therapy for primary brain tumors. *Radiotherapy and Oncology* **121**, 124–131. ISSN: 0167-8140 (Aug. 2016).
5. Park, J., Park, J. W. & Yea, J. W. Non-coplanar whole brain radiotherapy is an effective modality for parotid sparing. *Yeungnam University Journal of Medicine* **36**, 36 (Aug. 2019).
6. Fogliata, A., Clivio, A., Nicolini, G., Vanetti, E. & Cozzi, L. A treatment planning study using non-coplanar static fields and coplanar arcs for whole breast radiotherapy of patients with concave geometry. *Radiotherapy and Oncology* **85**, 346–354. ISSN: 0167-8140 (Aug. 2007).

7. Sheng, K. & Shepard, D. M. Point/Counterpoint. Noncoplanar beams improve dosimetry quality for extracranial intensity modulated radiotherapy and should be used more extensively. *Medical physics* **42**, 531–533. ISSN: 2473-4209 (Aug. 2015).
8. Gayen, S., Kombathula, S. H., Manna, S., Varshney, S. & Pareek, P. Dosimetric comparison of coplanar and non-coplanar volumetric-modulated arc therapy in head and neck cancer treated with radiotherapy. *Radiation Oncology Journal* **38**, 138. ISSN: 22343156 (2020).
9. Ohira, S. *et al.* HyperArc VMAT planning for single and multiple brain metastases stereotactic radiosurgery: a new treatment planning approach. *Radiation Oncology 2018 13:1* **13**, 1–9. ISSN: 1748-717X (Aug. 2018).
10. Kadoya, N. *et al.* Automated noncoplanar treatment planning strategy in stereotactic radiosurgery of multiple cranial metastases: HyperArc and CyberKnife dose distributions. *Medical Dosimetry* **44**, 394–400. ISSN: 0958-3947 (Aug. 2019).
11. Tran, A. *et al.* Treatment planning comparison of IMPT, VMAT and 4π radiotherapy for prostate cases. *Radiation Oncology 2017 12:1* **12**, 1–9. ISSN: 1748-717X (Aug. 2017).
12. Rwigema, J. C. M. *et al.* 4π Noncoplanar Stereotactic Body Radiation Therapy for Head-and-Neck Cancer: Potential to Improve Tumor Control and Late Toxicity. *International Journal of Radiation Oncology, Biology, Physics* **91**, 401–409. ISSN: 0360-3016 (Aug. 2015).
13. Dong, P. *et al.* 4π Non-Coplanar Liver SBRT: A Novel Delivery Technique. *International Journal of Radiation Oncology, Biology, Physics* **85**, 1360–1366. ISSN: 0360-3016 (Aug. 2013).
14. Murzin, V. L. *et al.* 4π plan optimization for cortical-sparing brain radiotherapy. *Radiotherapy and Oncology* **127**, 128–135. ISSN: 0167-8140 (Aug. 2018).

15. Woods, K. *et al.* Viability of Noncoplanar VMAT for liver SBRT compared with coplanar VMAT and beam orientation optimized 4π IMRT. *Advances in Radiation Oncology* **1**, 67–75. ISSN: 2452-1094 (Aug. 2016).
16. Yu, V. Y. *et al.* A Prospective 4π Radiation Therapy Clinical Study in Recurrent High-Grade Glioma Patients. *International Journal of Radiation Oncology, Biology, Physics* **101**, 144–151. ISSN: 0360-3016 (Aug. 2018).
17. Papp, D., Bortfeld, T. & Unkelbach, J. A modular approach to intensity-modulated arc therapy optimization with noncoplanar trajectories. *Physics in medicine and biology* **60**, 5179–5198. ISSN: 1361-6560 (Aug. 2015).
18. Smyth, G., Evans, P. M., Bamber, J. C. & Bedford, J. L. Recent developments in non-coplanar radiotherapy. *Brit J Radiol* **92**. ISSN: 1748880X (Aug. 2019).
19. Fix, M. K. *et al.* Part 1: Optimization and evaluation of dynamic trajectory radiotherapy. *Medical Physics* **45**, 4201–4212. ISSN: 00942405 (Aug. 2018).
20. Manser, P. *et al.* Dose calculation of dynamic trajectory radiotherapy using Monte Carlo. *Zeitschrift fur Medizinische Physik* **29**. ISSN: 18764436 (2019).
21. Hernandez, V. *et al.* What is plan quality in radiotherapy? The importance of evaluating dose metrics, complexity, and robustness of treatment plans. *Radiother Oncol* **153**, 26–33. ISSN: 18790887 (2020).
22. Sagawa, T. *et al.* Dosimetric effect of rotational setup errors in stereotactic radiosurgery with HyperArc for single and multiple brain metastases. *Journal of Applied Clinical Medical Physics* **20**, 84–91. ISSN: 1526-9914 (Aug. 2019).
23. Calmels, L. *et al.* Single-isocenter stereotactic non-coplanar arc treatment of 200 patients with brain metastases: multileaf collimator size and setup

- uncertainties. *Strahlentherapie und Onkologie* **198**, 436–447. ISSN: 0179-7158 (Aug. 2022).
24. González, Á. Measurement of Areas on a Sphere Using Fibonacci and Latitude–Longitude Lattices. *Mathematical Geosciences 2009 42:1* **42**, 49–64. ISSN: 1874-8953 (Aug. 2009).
25. Hart, P. E., Nilsson, N. J. & Raphael, B. A Formal Basis for the Heuristic Determination of Minimum Cost Paths. *IEEE Transactions on Systems Science and Cybernetics* **4**, 100–107 (1968).
26. Fix, M. K. *et al.* An efficient framework for photon Monte Carlo treatment planning. *Physics in Medicine and Biology* **52**, 425–437. ISSN: 00319155 (2007).
27. Kawrakow, I. & Fippel, M. VMC, a fast MC algorithm for Radiation Treatment planning. *The Use of Computers in Radiation Therapy*, 126–128 (2000).
28. McNiven, A. L., Sharpe, M. B. & Purdie, T. G. A new metric for assessing IMRT modulation complexity and plan deliverability. *Medical Physics* **37**, 505–515. ISSN: 2473-4209 (Aug. 2010).
29. Masi, L., Doro, R., Favuzza, V., Cipressi, S. & Livi, L. Impact of plan parameters on the dosimetric accuracy of volumetric modulated arc therapy. *Medical Physics* **40**, 71718. ISSN: 2473-4209 (Aug. 2013).
30. Paddick, I. A simple scoring ratio to index the conformity of radiosurgical treatment plans. Technical note. *Journal of neurosurgery* **93 Suppl 3**, 219–222. ISSN: 0022-3085 (2000).
31. Loebner, H. A. *et al.* Development of a Monte Carlo based robustness calculation and evaluation tool. *Medical Physics* **49**, 4780–4793. ISSN: 24734209 (2022).

32. Kanakavelu, N. & Samuel, J. J. Determination of patient set-up error and optimal treatment margin for intensity modulated radiotherapy using image guidance system. *J BUON* **2**, 505–511. ISSN: 1107-0625 (2016).
33. Delishaj, D. *et al.* Set-up errors in head and neck cancer treated with IMRT technique assessed by cone-beam computed tomography: a feasible protocol. *Radiation Oncology Journal* **36**, 54–62. ISSN: 22343164 (Aug. 2018).
34. Mathew, G. E. Direction Based Heuristic for Pathfinding in Video Games. *Procedia Computer Science* **47**, 262–271. ISSN: 1877-0509 (Aug. 2015).
35. Mackeprang, P. *et al.* MO-0544 4pi-IMRT based path-finding for dynamic trajectory radiotherapy. *Radiotherapy and Oncology* **170**, S469–S470. ISSN: 01678140 (Aug. 2022).
36. Rocha, H., Dias, J., Ventura, T., Ferreira, B. & do Carmo Lopes, M. An Optimization Approach for Noncoplanar Intensity-Modulated Arc Therapy Trajectories. *Lecture Notes in Computer Science (including subseries Lecture Notes in Artificial Intelligence and Lecture Notes in Bioinformatics)* **11621 LNCS**, 199–214. ISSN: 16113349 (2019).
37. Jubbier, O. N., Abdullah, S. S., Alabedi, H. H., Alazawy, N. M. & Al-Musawi, M. J. The Effect of Modulation Complexity Score (MCS) on the IMRT Treatment Planning Delivery Accuracy. *Journal of Physics: Conference Series* **1829**, 12017. ISSN: 1742-6596 (Aug. 2021).
38. Meedt, G., Alber, M. & Nüsslin, F. Non-coplanar beam direction optimization for intensity-modulated radiotherapy. *Physics in Medicine & Biology* **48**, 2999. ISSN: 0031-9155 (Aug. 2003).
39. Dong, P., Liu, H. & Xing, L. Monte Carlo tree search -based non-coplanar trajectory design for station parameter optimized radiation therapy (SPORT). *Physics in Medicine & Biology* **63**, 135014. ISSN: 0031-9155 (Aug. 2018).

40. Mullins, J., Renaud, M. A., Serban, M. & Seuntjens, J. Simultaneous trajectory generation and volumetric modulated arc therapy optimization. *Medical Physics* **47**, 3078–3090. ISSN: 2473-4209 (Aug. 2020).
41. Bertholet, J. *et al.* Organ-at-risk sparing with dynamic trajectory radiotherapy for head and neck cancer: comparison with volumetric arc therapy on a publicly available library of cases. *Radiation oncology (London, England)* **17**, 122. ISSN: 1748-717X (Aug. 2022).
42. Barnes, M. P. & Greer, P. B. Evaluation of the truebeam machine performance check (MPC): mechanical and collimation checks. *Journal of Applied Clinical Medical Physics* **18**, 56–66. ISSN: 1526-9914 (Aug. 2017).
43. Olasolo-Alonso, J., Vázquez-Galiñanes, A., Pellejero-Pellejero, S. & Pérez-Azorín, J. F. Evaluation of MLC performance in VMAT and dynamic IMRT by log file analysis. *Phys Med* **33**, 87–94. ISSN: 1120-1797 (Aug. 2017).
44. Studenski, M. T. *et al.* Clinical experience transitioning from IMRT to VMAT for head and neck cancer. *Medical Dosimetry* **38**, 171–175. ISSN: 0958-3947 (Aug. 2013).
45. Ballangrud, Å. *et al.* Institutional experience with SRS VMAT planning for multiple cranial metastases. *Journal of Applied Clinical Medical Physics* **19**, 176–183. ISSN: 1526-9914 (Aug. 2018).

3.9 Appendix

Supplementary Material 0

```

position          //3d vector of point in 3d-map. First coordinate refers to
                  gantry angle, second coordinate refers to table angle and
                  third coordinate refers to change in table angle.
start             //3d vector.
goal             //3d vector.
3d-map = {position} //3d map consisting of a set of 3d vectors
                  describing the map.
Gmax             //maximal allowed gantry-table rotation gradient between
                  two adjacent points along a path.
ΔGmax           //maximal allowed change of gantry-table rotation gradient
                  between two adjacent points along a path.
frontier = PriorityQueue({}, sort to return position with lowest
                       path_cost)
frontier.add(start)
came_from = {}
came_from[start] = None
get_cost(start, start) = 0
path_cost = {}
path_cost[start] = 0
total_path = {}

//Returns neighbors of position in 3d-map.
def get_neighbors(position):
    neighbors = {}
    for point in 3d-map:
        if get_gantry_angle(point) = get_gantry_angle(position) +
           gantry_angle_resolution
           and
           if get_Gradient_G(position, point) < Gmax and
              get_change_of_Gradient_G(came_from[position], position,
                                       point) < ΔGmax:
                neighbors.add(point)
    return neighbors

//Reconstruct path from a given position in the 3d-map.
def reconstruct_path(came_from, current):
    total_path = {}
    while current in came_from:
        current = came_from[current]
        total_path.add(current)
    return total_path.reverse()

//Path finding.
while frontier not empty:
    current = frontier.get()

    if current = goal:
        total_path = reconstruct_path(came_from, current)
        continue

    neighbors = get_neighbors(current)

    for neighbor in neighbors:
        tentative_cost = path_cost[current] + get_cost(current, neighbor)

        //The first condition allows to expand the path finding to all
        neighbouring candidates, the second condition "overwrites" a
        path when a path up to this point with lower path cost is
        found.
        if (neighbor not in path_cost)
           or (tentative_cost < path_cost[neighbor]):

            path_cost[neighbor] = tentative_cost
            frontier.add(neighbor)
            came_from[neighbor] = current

```


Supplementary Material 1

Table 3.4: Optimization objectives for case A, B and C. Priorities taken from Eclipse Photon Optimizer v15.6.

Case A		
Structure	Objective	Priority
CTV	D100% > 50 Gy	110
PTV	D0% < 50.75 Gy	110
	D100% > 50 Gy	110
	D100% > 47.5 Gy	300
	D95% > 50 Gy	300
Brainstem	D0% < 10 Gy	70
	D37.3% < 7 Gy	60
Cochlea R/L	D0% < 3 Gy	60
Eye L	D0% < 16 Gy	70
	D15.5% < 10 Gy	60
Eye R	D0% < 7 Gy	60
	D12.7% < 5 Gy	60
Lacrimal L	D0% < 3 Gy	60
Lacrimal R	D0% < 5 Gy	60
Optic Chiasm	D0% < 20 Gy	60
	D6% < 15 Gy	60
	D44.8% < 10 Gy	60
OpticN L	D0% < 35 Gy	70
	D8.7% < 30 Gy	60
	D53.2% < 25 Gy	60
OpticN R	D0% < 10 Gy	60
	D24.8% < 7.5 Gy	60
Parotid L/R	D0% < 5 Gy	60
	Distance from target border 0.25 cm,	
Normal Tissue	Start Dose 99.0%,	70
	End Dose 30.0%,	
	Fall-off 0.25	

Case B		
Structure	Objective	Priority
CTV	D100% > 60.0 Gy	100
PTV	D0% < 60.40 Gy	120
	D100% > 60.0 Gy	120
	D98% > 57.0 Gy	300
Optic Chiasm	D0% < 13.81 Gy	80
	D7.8% < 7.84 Gy	60
	D42.2% < 4.1 Gy	50
Eye L	D0% < 2.1 Gy	50
Eye R	D0% < 3 Gy	50
Brain	Dmean < 15 Gy	50
Brainstem	D0% < 32.9 Gy	80
	D5.6% < 4.7 Gy	70
Lacrimal L	D0% < 3.0 Gy	50
Lacrimal R	D0% < 4.5 Gy	50
Lense L/R	D0% < 0.1 Gy	50
OpticN L	D0% < 3.9 Gy	50
OpticN R	D0% < 14.2 Gy	70
	D29.7% < 6.1 Gy	70
Normal Tissue	Distance from target border 0.25 cm,	100
	Start Dose 99.0%,	
	End Dose 30.0%,	
	Fall-off 0.25	

Case C		
Structure	Objective	Priority
CTV	D100% > 50 Gy	120
PTV	D0% < 52.3 Gy	300
	D100% > 50 Gy	300
	D100% > 47.5 Gy	300
	D95% > 50 Gy	300
	Brain	D0% < 30 Gy
Brainstem	D0% < 14.0 Gy	80
Cochlea L	D0% < 10 Gy	80
Cochlea R	D0% < 5 Gy	80
Esophagus	Dmean < 15 Gy	80
Eye L	D0% < 8 Gy	80
Eye R	D0% < 5 Gy	80
Hippocampus L/R	D37% < 5 Gy	90
LarynxGSL	D0% < 50 Gy	60
	Dmean < 25 Gy	80
Lense L/R	D0% < 2 Gy	80
Lips	D0% < 36.5 Gy	80
	Dmean < 10 Gy	80
	Mandible	D0% < 50 Gy
Oral Cavity	D85% < 20 Gy	80
	Dmean < 30 Gy	80
Parotid L	Dmean < 30 Gy	80
Parotid R	Dmean < 0.1 Gy	80
Pharynx	D24% < 49.6 Gy	80
	D49% < 22 Gy	80
	Dmean < 20 Gy	80
PRV Brainstem	D0% < 16 Gy	80
PRV Spinal Cord	D0% < 22 Gy	80
Submand R	Dmean < 5 Gy	80
Normal Tissue	Distance from target border 0.25 cm,	100
	Start Dose 99.0%,	
	End Dose 30.0%,	
	Fall-off 0.25	

Supplementary Material 2

In figure 3.10 the objective function values (OFVs) of the dose distributions after optimization and final dose calculation are compared for each case. The objective

function value is a calculated scalar quantity that represents the correspondence of a dose distribution to treatment planning objectives, and is defined by dose-volume, mean dose, and dose fall-off objectives. Case A and case B profit from the increased freedom in the GT rotation gradient: the OFV is reduced by up to 72% compared to the worst performing plan (VMAT). Small improvements (7% and 10%) from the worst performing DTRT plan (DTRT-1 and DTRT-1) to the best performing DTRT plan (DTRT-4 and DTRT-2) are observed for case A and B, respectively. No major improvements on the OFVs are visible for the plans of case C with increasing GT rotation gradient.

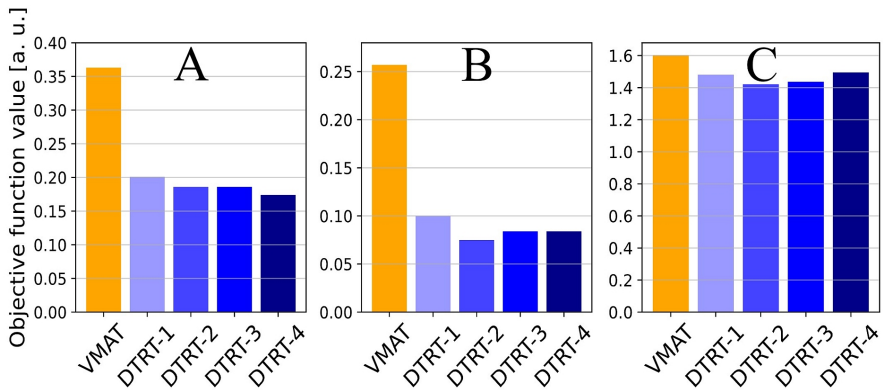


Figure 3.10: OFVs for case A (A), case B (B) and case C (C).

Supplementary Material 3

The accuracy of the dose calculation for the extended TPP is verified by means of an End-To-End test using film validation measurements for all DTRT plans of case A. To this end, two Gafchromic EBT-3 films (Ashland Advanced Materials, Bridgewater, New Jersey, USA) are placed orthogonally into a cubic polymethyl methacrylate (PMMA) phantom [1] for each plan measurement. The phantom is placed on the treatment table and the DTRT plans are delivered. Using a triple channel calibration [2], the film measurements are converted to absolute

dose, evaluated using a one scan protocol [3] and are compared against the MC dose calculation by means of 2D Gamma analysis (2% global / 2 mm with 10% dose threshold). The film measurements for the DTRT plans of case A agree with the respective dose calculations by >96% Gamma-passing-rate. No substantial differences between the measurements of the DTRT-1 to DTRT-4 plans are observed.

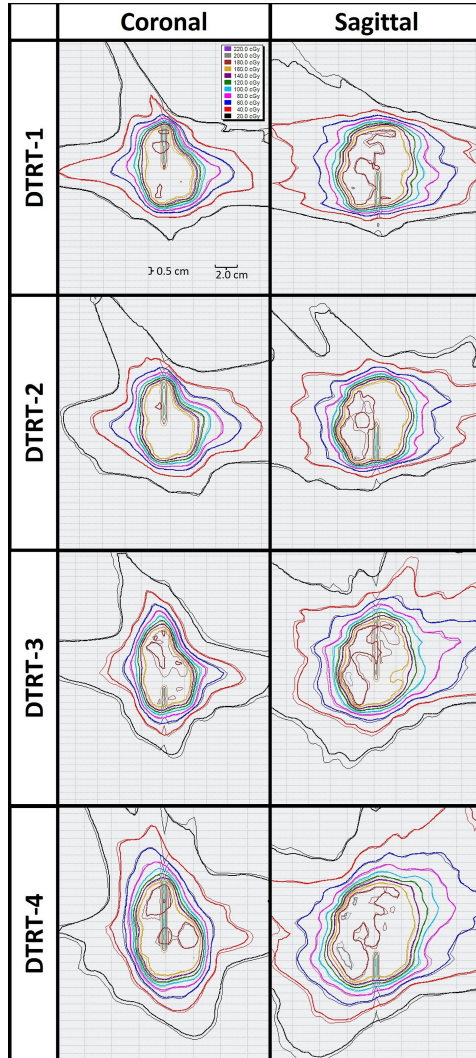


Figure 3.11: Film measurements of the coronal and sagittal plane of case A of DTRT-1, DTRT-2, DTRT-3 and DTRT-4. The thick lines correspond to the planned dose distribution and the thin lines correspond to the measurements. The discrepancies at the vertical line in the center correspond to the slit in the film, where the film of the coronal and sagittal plane intersected.

Supplementary Material 4

The complexity assessed by G , ΔG and MCS of the VMAT and DTRT treatment plans is visualized in figure 3.12.

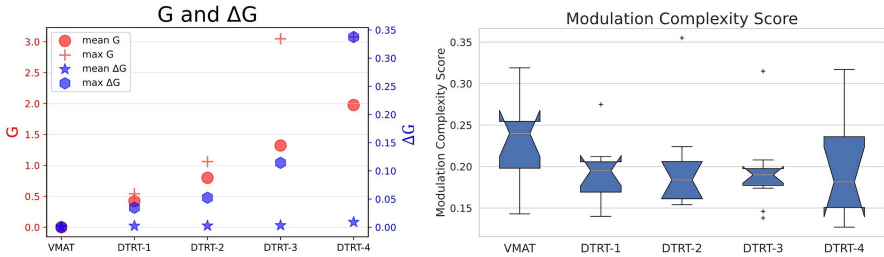


Figure 3.12: Complexity assessed by G , ΔG and MCS for all generated plans of all cases. For the boxplots: the median is depicted in orange, the notch defines medians confidence interval, the box indicates the interquartile range (IQR, $Q3-Q1$), whiskers extend to the last (first) datum less (greater) than $Q3+1.5*IQR$ ($Q1-1.5*IQR$). Outliers are marked with a plus sign.

Supplementary Material 5

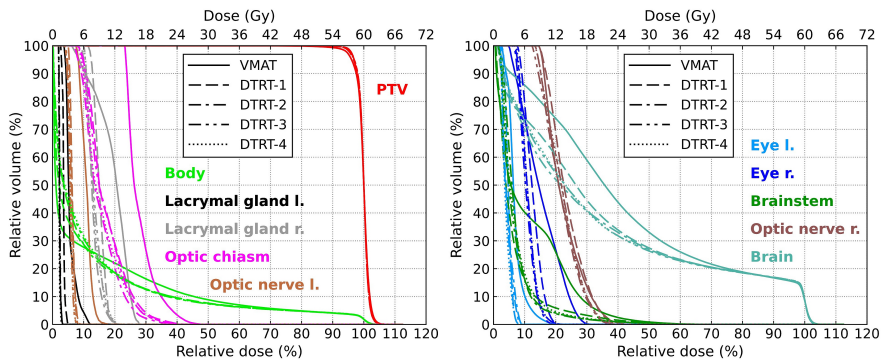


Figure 3.13: DVH comparison of the VMAT and DTRT plans of case B.

Supplementary Material 6

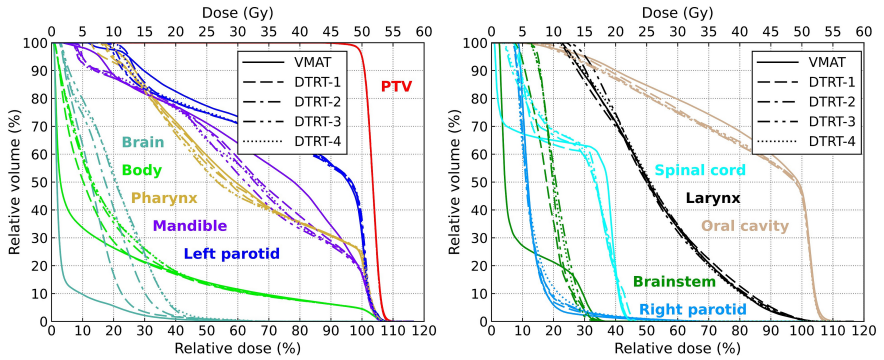


Figure 3.14: DVH comparison of the VMAT and DTRT plans of case C.

Supplementary Material 7

The following correlations are observed over all DTRT plans and cases (figure 3.15). Table, collimator, and MLC uncertainty correlate with the speed in the respective machine component. A non-linear correlation between gantry rotation speed and uncertainty is observed. For medium gantry speeds of approximately $\pm 4^\circ/\text{s}$, the greatest uncertainties in gantry angle are observed.

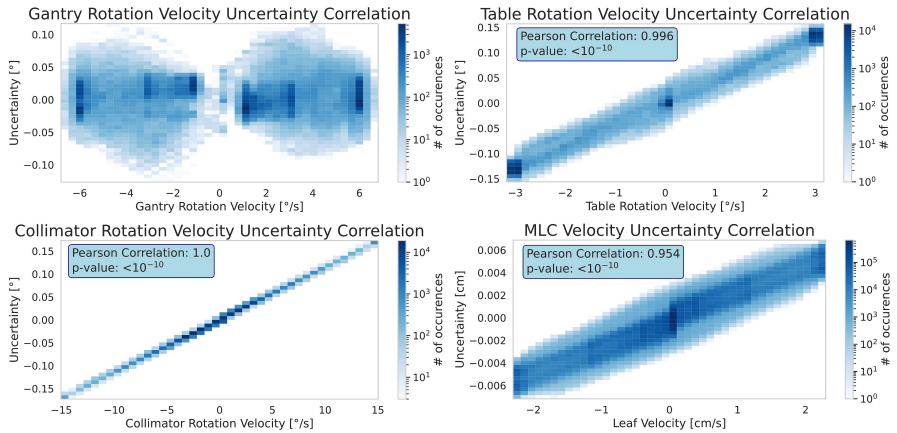


Figure 3.15: Machine component speed-uncertainty correlations: a non-linear correlation between gantry rotation speed and gantry uncertainty is observed. Strong correlation between table rotation speed, collimator rotation speed and MLC speed and the respective uncertainty is observed. P-values are $<10^{-10}$.

REFERENCES

1. Mueller, S. *et al.* *A Phantom for Dosimetric Quality Assurance of Non-Coplanar and Mixed Beam Treatment Techniques*, accessed on 26.10.2023 2022. <https://w4.aapm.org/meetings/2022AM/programInfo/programAbs.php?sid=10694&aid=65838>.
2. Micke, A., Lewis, D. F. & Yu, X. Multichannel film dosimetry with nonuniformity correction. *Medical Physics* **38**, 2523–2534. ISSN: 2473-4209 (Aug. 2011).
3. Lewis, D., Micke, A., Yu, X. & Chan, M. F. An efficient protocol for radiochromic film dosimetry combining calibration and measurement in a single scan. *Medical Physics* **39**, 6339–6350. ISSN: 2473-4209 (Aug. 2012).

ORGAN-AT-RISK SPARING WITH DYNAMIC TRAJECTORY RADIOTHERAPY FOR HEAD AND NECK CANCER: COMPARISON WITH VOLUMETRIC ARC THERAPY ON A PUBLICLY AVAILABLE LIBRARY OF CASES

J. Bertholet¹, P.-H. Mackeprang¹, S. Mueller¹, G. Guyer¹, H.A. Loebner¹, Y. Wyss¹, D. Frei¹, W. Volken¹, O. Elicin¹, D.M. Aebersold¹, M.K. Fix¹, P. Manser¹

¹ Division of Medical Radiation Physics and Department of Radiation Oncology, Inselspital, Bern University Hospital, University of Bern, Bern, Switzerland

published in
Radiation Oncology

2022, 17:122

<https://doi.org/10.1186/s13014-022-02092-5>

©2022, Springer Nature

Open access article distributed under the terms of the Creative Commons CC BY 4.0 license.

4.1 Abstract

Background

Dynamic trajectory radiotherapy (DTRT) extends volumetric modulated arc therapy (VMAT) with dynamic table and collimator rotation during beam-on. The aim of the study is to establish DTRT path-finding strategies, demonstrate deliverability and dosimetric accuracy and compare DTRT to state-of-the-art VMAT for common head and neck (HN) cancer cases.

Methods

A publicly available library of seven HN cases was created on an anthropomorphic phantom with all relevant organs-at-risk (OARs) delineated. DTRT plans were generated with beam incidences minimizing fractional target/OAR volume overlap and compared to VMAT. Deliverability and dosimetric validation was carried out on the phantom.

Results

DTRT and VMAT had similar target coverage. For three locoregionally advanced oropharyngeal carcinomas and one adenoid cystic carcinoma, mean dose to the contralateral salivary glands, pharynx and oral cavity was reduced by 2.5, 1.7 and 3.1 Gy respectively on average with DTRT compared to VMAT. For a locally recurrent nasopharyngeal carcinoma, D0.03 cc to the ipsilateral optic nerve was above tolerance (54.0 Gy) for VMAT (54.8 Gy) but within tolerance for DTRT (53.3 Gy). For a laryngeal carcinoma, DTRT resulted in higher dose than VMAT to the pharynx and brachial plexus but lower dose to the upper oesophagus, thyroid gland and contralateral carotid artery. For a single vocal cord irradiation case, DTRT spared most OARs better than VMAT. All plans were delivered successfully on the phantom and dosimetric validation resulted in gamma passing rates of 93.9% and 95.8% (2%/2 mm criteria, 10% dose threshold).

Conclusions

This study provides a proof of principle of DTRT for common HN cases with

plans that were deliverable on a C-arm linac with high accuracy. The comparison with VMAT indicates substantial OAR sparing could be achieved.

4.2 Background

Radiation therapy plays an important role in the management of head and neck (HN) cancer but is often challenging, especially for target volumes with complex shapes overlapping with organs-at-risk (OARs). The introduction of intensity-modulated radiotherapy (IMRT) has enabled clinically significant toxicity reduction through better dosimetric sparing of OARs [1] while volumetric modulated arc therapy (VMAT) improved delivery efficiency with dynamic gantry rotation [2].

Non-coplanar radiotherapy can further improve OAR sparing [3] with, e.g., 4π -IMRT using up to 30 non-coplanar beams [4], non-coplanar VMAT with multiple arcs at static non-coplanar table angles [5], or non-coplanar dynamic trajectory radiotherapy (DTRT) with simultaneous gantry and table rotation during beam-on, with [6–8] or without [9, 10] dynamic collimator rotation. The trade-of between estimated delivery time and dosimetric plan quality was explored for nasopharyngeal tumours finding non-coplanar dynamic trajectories to be dosimetrically beneficial over coplanar techniques at the cost of longer, yet acceptable, delivery times [11].

Despite encouraging dosimetric quality of DTRT plans and the promise of deliverability on standard C-arm linacs [6, 12], it remains a research topic for HN radiotherapy and is not yet clinically available. Nasopharyngeal and cranial tumours have often been investigated owing to the large collision-free space [7, 11, 12] with static non-coplanar solutions already commercially available on C-arm linacs [13, 14]. Large HN target volumes are often associated with high rates of toxicity and could benefit from DTRT but these have a more caudal isocenter. The resulting collision-free space is more restrictive than for nasopharyngeal or cranial tumours and requires careful consideration for deliverability [15].

A practical approach to determine dynamic table paths is the use of geometric criteria to minimize target/OAR overlap by combining gantry-table cost-maps of various OARs in one map where a path-finding algorithm returns the path of

lowest cost [6, 9]. However, for HN, there are many OARs that may overlap with the target, and optimal OAR selection and/or weighting at the path-finding stage remains unclear. Additionally, this provides only one path whereas multiple arcs are recommended for VMAT [16, 17]. Selecting and grouping OARs in different maps to generate more than one path for DTRT planning would enable to better exploit the collision-free space.

The aim of this proof-of-principle study was to establish path-finding strategies for DTRT of HN cases, evaluate OAR sparing compared to state-of-the-art VMAT, and demonstrate DTRT deliverability and dosimetric accuracy. For this purpose, a publicly available library covering all common HN cases was created on an anthropomorphic phantom.

4.3 Methods

Library of cases and clinical goals

The library of HN cancer cases was created on an axial computed tomography (CT) scan of the Alderson phantom (Radiology Support Devices Inc., USA). The phantom was immobilized in a 5-point thermoplastic mask (Posifix, civco Radiotherapy Inc., USA) and scanned on a Philips Brilliance Big Bore CT-scanner (Philips Healthcare, Amsterdam, The Netherlands) with 2 mm slices and 512×512 pixels in-plane resolution. All relevant OARs were delineated according to guidelines [18, 19]. Both hippocampi were additionally contoured [20].

Seven typical HN cases were identified, six of whom had elective nodal volumes treated to 50.00 Gy in 2 Gy fractions. Sequential boost volumes are prescribed a total of 66.00 Gy for any post-operative positive margin and nodal levels with extranodular extension and to 70.00 Gy for non-operated primary tumour and involved lymph nodes [21–28].

The clinical target volumes (CTV) were delineated on the phantom based on commonly observed clinical cases and relevant guidelines [29–31]. Water density was assigned to air in the CTVs or where tumour infiltration would replace bone.

Corresponding planning target volumes (PTV) were obtained by applying a 3 mm isotropic margin around the CTV, trimmed 3 mm from body contour according to institutional practice. Plans for individual phases were normalized such that $PTV_{D_{95\%}} = 100\%$ of the prescribed dose. OAR clinical goals are summarized in Additional file 1: table 4.4 [32]. The hippocampus constraint was set at $D_{40\%} < 7.3$ Gy [33]. All OARs were the same for these six cases.

The seventh case was an early stage glottic laryngeal carcinoma treated with single vocal cord irradiation (SVCI) to 58.08 Gy in 16 fractions [34]. OAR delineation and planning protocol are described elsewhere (VoiceS NCT04057209) and summarized in Additional file 1: table 4.6.

DTRT paths and VMAT arcs set-up

All treatment plans were created for 6 MV-fattened beam on a TrueBeam linac (Varian Medical Systems) equipped with a 120-leaf Millennium multi-leaf collimator (MLC) and a PerfectPitch 6-degree-of-freedom table.

DTRT plans were created based on Fix et al. [6]. In short, target and OAR contours are exported from Eclipse (Varian, research version 15.6) to an in-house path-finding software using the research Eclipse Scripting Application Programming Interface (ESAPI). For each OAR, a gantry-table (GT) cost-map is generated quantifying the fractional target/OAR volume-overlap in beam's eye view for each combination of gantry-table angle, accounting for the relative position of the OAR with respect to the target. OAR maps are combined in a weighted sum and exclusion zones are determined based on collision and CT-scan length restrictions.

An A* path-finding algorithm is used to determine the GT-path of lowest cost for a given range of gantry rotation. For the chosen GT-path, a collimator-gantry (GC) map is created that quantifies field width in the x-direction. The A* is used to determine the GC-path of lowest cost, thereby reducing the range of possible leaf-travel. The selected gantry-table-collimator (GTC)-paths are imported back into Eclipse via ESAPI for intensity modulation optimization.

In this study, case-specific collision maps were determined based on a validated virtual linac model using Blender [35, 36]. The model detects possible collisions between the gantry and the table-top/table-stand and a patient model. A reference point on the headrest and the plan isocenter coordinates are used to estimate the table position in the room. An additional safety margin of 2 cm on each component was used.

All DTRT paths covered a full gantry rotation with control points every 2°. The A* algorithm was restricted to find GT and GC-paths with a maximum gradient of 3° table/collimator rotation per degree gantry rotation and paths were smoothed using a 10-points (20°) moving average to avoid abrupt table motion. Different paths per plan were created by selecting different OARs to generate each

map. Individual OAR-maps were equally weighted. To increase the degrees-of-freedom at the intensity optimization stage, some paths were duplicated either by field-splitting in the x-direction using the secondary collimator jaws or by applying a constant 90° collimator offset to the A*-determined GC-path.

For each DTRT plan, a VMAT plan was created with the same number of full arcs as GT-paths, the same field-splitting strategy, and collimator angle of 5 or 95°.

Intensity optimization and dose calculation

Research version of the Eclipse photon optimizer (PO) and the Anisotropic Analytical Algorithm (AAA) version 15.6 were used for intensity modulation optimization and dose calculation with a 2.5 mm grid. Intermediate dose calculation was used, "convergence mode" was on, and "aperture shape controller" set to moderate [37].

A set of manual planning rules was designed to minimize planner bias (Additional file 1), where the optimization objectives are found during interactive planning, but only certain parameters can be changed. Each plan was optimized once and then re-optimized without any manual interaction. Objective tweaking and re-optimization without manual interaction was allowed if clinical goals were nearly reached. After final dose calculation with AAA, plans were normalized. All plans were optimized by the same planner.

Treatment technique comparison

Plans were reviewed for clinical acceptability by a radiation oncologist. PTV coverage, homogeneity index ($HI_{95\%} = V_{95\%} - V_{105\%}$), and Paddick conformity index ($CI_{Paddick}$ [38]) for each individual dose level were evaluated, but technique comparison focused on OAR dose in the dose distributions for the combined plans.

Delivarability of DTRT plans

To demonstrate deliverability of DTRT, all plans were delivered in developer mode

using xml files and machine log-files were recorded to evaluate mechanical accuracy and the possible correlation between speed and mechanical deviations for each dynamic axis. Prior to delivery, the phantom was positioned on the True-Beam PerfectPitch table with the thermoplastic mask. Orthogonal kV imaging was used to adjust patient positioning with 5 degrees-of-freedom. Rotation was not corrected because the dynamic table rotation is encoded for each control point in the xml files and any correction would be overridden during delivery.

Dosimetric validation with film measurement was performed for one case as described in Additional file 1: [39–42].

Recently, the Radiotherapy Treatment plannINg study Guidelines (RATING) were proposed to evaluate the quality of planning studies and there reporting. The guidelines were followed and the RATING score was calculated [43].

4.4 Results

The seven HN cases are presented in Table 4.1. The library consisting of the Alderson CT-scan and structure-sets for each case is publicly available in DICOM format on the BORIS repository (<https://dx.doi.org/10.48350/159243>).

OAR selection strategies for each case were determined empirically to obtain DTRT paths covering the 4π -space while avoiding the most relevant OARs (Table 4.1). Example GT-maps and paths are shown in Fig. 4.1 with the corresponding individual OAR GT-maps in Additional file 1: Fig. 4.6. The process from contour export to the in-house software to paths import in Eclipse currently takes approximately 8-12 min for a 2-4 paths plan.

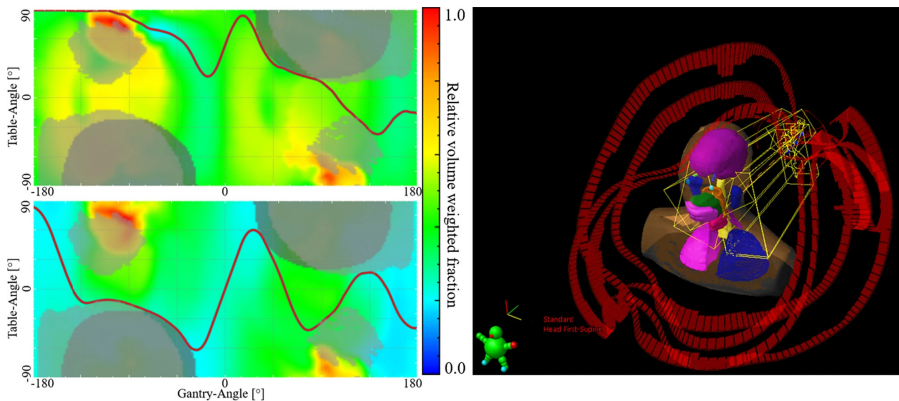


Figure 4.1: Example GT-maps with A*-determined paths (red curve) in the path-finder framework (left) and imported into Eclipse for the 50 Gy dose level of HN2. Light grey areas indicate collision zones, dark grey areas indicate end-of-CT restrictions. OAR selection for each map is detailed in Table 4.1. Individual OAR maps are shown in Additional file 1.

Table 4.1: Library of case, DTRT paths and VMAT arc setup, and delivery time. Normal tissue is the body volume excluding PTV, R right, L left, hippo. hip-pocampus, submand. submandibular gland, C collimator, SF split field, CRot collimator rotation, i.e. offset of 90° between the 2 paths

Case/dose level	PTV volume (cc)	DTRT paths and OAR selection	VMAT arcs	Delivery time DTRT (min)	Delivery time VMAT (min)
HN1					
50.00 Gy	592.6	Locoregionally advanced oropharyngeal carcinoma (bilateral elective nodal irradiation) 2 × hippo. R + L, oral cavity, parotid R + L, brain stem PRV (SF)	2 × C 5° (SF)	10.4	4.0
70 Gy	64.0	2 × hippo. R + L, pharynx, contr. submand., spinal cord PRV (SF) Same as 50 Gy level	2 × C 95° (SF)	9.2	4.2
HN2					
50.00 Gy	560.8	Locoregionally advanced oropharyngeal carcinoma (bilateral elective nodal irradiation) 2 × hippo. R + L, oral cavity, parotid R + L, brain stem PRV (SF) (see Fig. 4.1, top left)	2 × C 5° (SF)	9.6	4.0
66.00 Gy	189.5.0	2 × hippo. R + L, pharynx, contr. submand., spinal cord PRV (SF) (see Fig. 4.1, bottom left) 2 × hippo. R + L, oral cavity, parotid R + L, brain stem PRV (SF) 1 × hippo. R + L, pharynx, contr. submand., spinal cord PRV	2 × C 95° (SF) 2 × C 5° (SF) 1 × C 95°	6.9	3.0
70.00 Gy	134.4	2 × hippo. R + L, pharynx, oral cavity, parotid R + L, contr. submand., spinal cord PRV, brain stem PRV (CRot)	1 × C 5° 1 × C 95°	5.0	2.0
HN3					
50.00 Gy	279.3	Locoregionally advanced oropharyngeal carcinoma (unilateral elective nodal irradiation) 2 × hippo. R + L, pharynx, oral cavity, parotid R + L, submand. R + L, spinal cord PRV, brain stem PRV (SF)	2 × C 5° (SF)	7.5	3.0
70 Gy	47.3	1 × hippo. R + L, pharynx, contr. carotid PRV 1 × hippo. R + L, pharynx, oral cavity, parotid R + L, submand. R + L, spinal cord PRV, brain stem PRV (SF) 1 × hippo. R + L, pharynx, contr. carotid PRV	1 × C 95° (SF) 1 × C 95° (SF) 1 × C 95° (SF)	5.0	2.0
HN4					
50.00 Gy	96.1	Adenoid cystic carcinoma of the left parotid gland (postoperative) (ACC) 2 × hippo. R + L, oral cavity, pharynx, contr. parotid, submand. R + L, spinal cord PRV, brain stem PRV (CRot)	1 × C 5° 1 × C 95°	5.6	2.0
66.00 Gy	32.8	Same as 50 Gy level		4.5	2.0
HN5					
50.00 Gy	66.7	Locally recurrent nasopharyngeal carcinoma 1 × hippo. R + L, eye R + L 1 × hippo. R + L, optic nerve R + L, chiasm, lens R + L 1 × hippo. R + L, carotid PRV R + L, lens R + L	1 × C 5° 1 × C 5° 1 × C 95°	6.5	3.0
66.00 Gy	55.7	Stage II laryngeal carcinoma (no elective neck volume) Same as 50 Gy level		7.1	3.0
HN6					
50.00 Gy	39.1	2 × normal tissue*, pharynx, contr. carotid PRV, upper oesophagus, thyroid (CRot)	1 × C 5° 1 × C 95°	4.9	2.0
70.00 Gy	20.7	Same as 50 Gy level		4.9	2.0
HN7					
59.08 Gy	9.7	Early stage glottic laryngeal carcinoma (single vocal cord irradiation, SVC) 2 × normal tissue*, inferior constrictor (CRot)	1 × C 5° 1 × C 95°	4.9	2.3

Each individual plan and dose distributions from all combined plans were considered clinically acceptable by a radiation oncologist. Target coverage were similar between DTRT and VMAT. For conventional fractionation (HN1-6) CIPaddick were between 0.82 and 0.92 differing at most by 0.03 between DTRT and VMAT. $HI_{95\%}$ were between 74.5% and 99.2% with a mean absolute difference of 3.2% between DTRT and VMAT (VMAT being generally more homogeneous).

Target coverage in the dose distributions for the combined plans were similar for the high dose volume but differences were observed for lower dose volumes depending on the direction in which the elective volume extended the high dose volume (Additional file 1: Fig. 4.7).

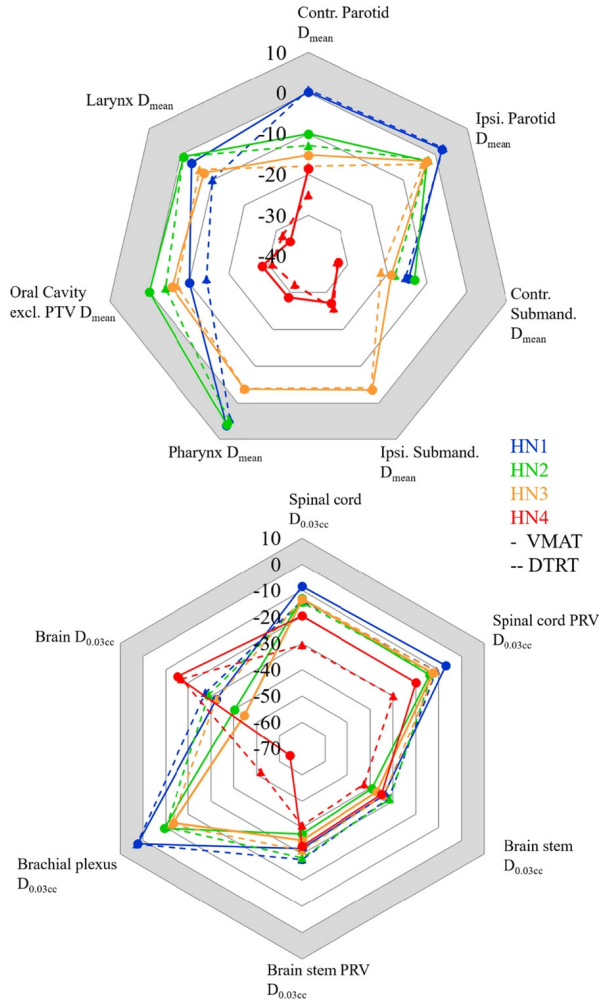


Figure 4.2: Radar plots showing the difference in OAR dose compared to tolerance for HN 1–4 for VMAT (solid lines) and DTRT (dashed lines). Mean doses are considered for the salivary glands, pharynx, oral cavity and larynx (top) and near max doses are considered for the nervous system (bottom). Negative values indicate better sparing than tolerance. Positive values (grey shaded area) indicate doses above tolerance. Ipsi: ipsilateral, Contr: contralateral, Submand: Submandibular (gland), excl: excluding.

Dosimetric endpoints of the dose distributions for the combined plans are re-

ported in Additional file 1: table 4.5 and 4.6. All plans had acceptable target coverage and near-max dose. Mandatory clinical goals were fulfilled without compromising target coverage. For some OARs, the dose was above tolerance but within acceptable deviations.

For the oropharyngeal cases and the ACC (HN1-4), challenging OARs were the salivary and swallowing structures. Mean dose to the contralateral salivary glands was on average 2.5 Gy lower for DTRT than for VMAT; it was on average 1.7 Gy and 3.1 Gy lower for the pharynx and oral cavity respectively (Fig. 4.2). Dose to the auditory or optic structures was generally higher for DTRT than VMAT (Additional file 1: table 4.6) but at least 22 Gy below tolerance except for the lenses where it was at least 0.4 Gy below the tolerance of $D_{0.03cc} \leq 6$ Gy. $V_{7.3 Gy}$ to the hippocampi was higher for DTRT than for VMAT but remained well below tolerance (maximum 28.5%). Dose volume histograms (DVHs) for HN4 are shown in Fig. 4.3 (top).

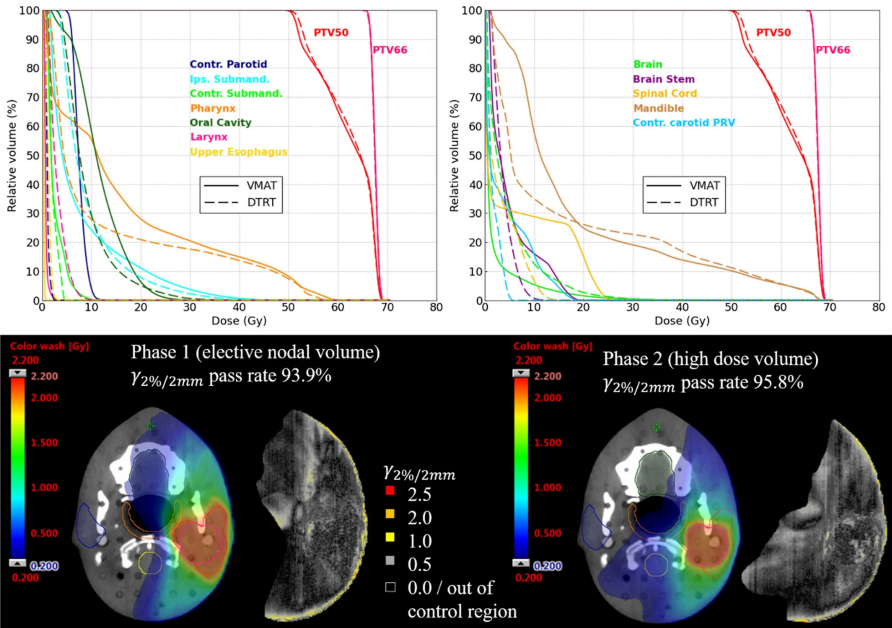


Figure 4.3: DVHs for HN4 (top) for VMAT (solid line) and DTRT (dashed line). Dose distribution from Eclipse and corresponding gamma maps (2%/2 mm, threshold: 10% of maximum dose) comparing film dose to AAA-calculated dose in Eclipse for DTRT for both dose levels (bottom).

For the nasopharyngeal case (HN5), challenging OARs were the optic and visual structures. DVHs are shown in Fig. 4.4. Near maximum dose to the ipsilateral optic nerve was above tolerance (54.0 Gy) for VMAT (54.8 Gy) but within tolerance for DTRT (53.3 Gy). Better OAR sparing for DTRT compared to VMAT was achieved for most endpoints (Additional file 1: table 4.5).

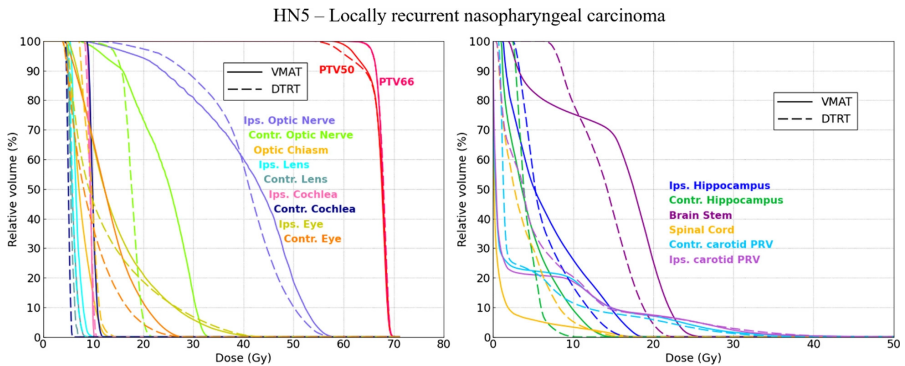


Figure 4.4: DVHs plots for HN5, locally recurrent nasopharyngeal carcinoma.

DVHs for the laryngeal cases (HN6-7) are shown in Fig. 4.5. For HN6, mean dose to the pharynx was 10.4 Gy (DTRT) and 9.3 Gy (VMAT); it was 15.5 Gy (DTRT) and 17.9 Gy (VMAT) for upper oesophagus. $D_{50\%}$ to the contralateral carotid PRV was 14.0 Gy (DTRT) and 15.0 Gy (VMAT). For the SVCI case, HN7, the plan was normalized such that $PTV_{D97\%}=99\%$ to fulfil the prescription for both plans. $CI_{Paddick}$ and $HI_{95\%}$ were 0.71 and 96.0% for DTRT and 0.77 and 96.8% for VMAT. DTRT achieved better OAR sparing than VMAT for most OARs (Additional file 1: table 4.6).

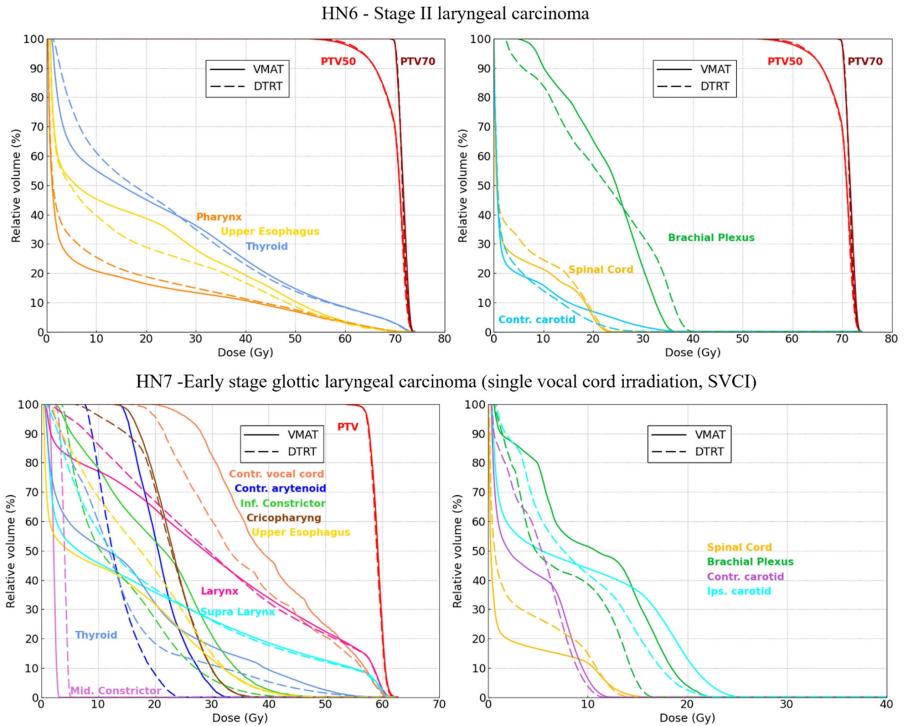


Figure 4.5: DVH plots for the laryngeal cases HN6 and HN7 (SVCI). Parallel OARs are shown on the left, serials OARs are shown on the right.

All plans were successfully delivered on the Alderson phantom in developer mode (Additional file 3: video). Delivery times, calculated from the machine log-files, were on average 2.4 (range: 2.1–2.8) times longer for DTRT compared to VMAT (Table 4.1). The mechanical accuracy for each moving component is reported as the difference between expected and actual value in the machine log-files in Table 4.2. There was a high correlation (Pearson's correlation coefficient) between speed and deviations for table and collimator angles, indicating that the table and collimator tend to lag behind their respective expected position, however correlation between speed and deviations was low for gantry angle.

Table 4.2: Deviations between expected and actual angle/position for DTRT deliveries

Axis	Root-mean-square (RMS) difference	Maximum difference	Correlation between speed and deviation
Gantry angle (°)	0.02	0.13	0.16, $p \ll 0.01$
Table angle (°)	0.12	0.16	< -0.99 , $p \ll 0.01$
Collimator angle (°)	0.03	0.17	< -0.99 , $p \ll 0.01$
	<i>RMS deviation over all moving leaves</i>		
	Mean RMS	Max RMS	
MLC leaves position (mm)	0.17	0.28	

Figure 4.3 shows the results of the dosimetric validation for HN4. The gamma passing rates (global 2%/2 mm, 10% dose threshold) were 93.9% and 95.8% with failing pixels located mostly at the film border. The overall RATING score was 96%. RATING scores were verified during review. (Additional file 2)

4.5 Discussion

This proof-of-principle study indicates substantially improved OAR sparing with equivalent target coverage may be achieved for HN radiotherapy with DTRT compared to VMAT. For three oropharyngeal carcinomas (HN1-3) and one adenoid cystic carcinoma (HN4), the reduction in mean dose to the contralateral salivary glands (2.5 Gy, average), pharynx (1.7 Gy), and oral cavity (3.1 Gy) has the potential to reduce xerostomia and dysphagia, with a positive impact on quality of life [44].

Few studies had previously investigated non-coplanar radiotherapy for HN cases with bilateral elective nodal irradiation volumes. Krayenbuehl et al. [10] reported improvement in OAR sparing of 2.9 Gy on average for parotid glands, 2.4 Gy for the oral mucosa and 6.9 Gy for the larynx using non-coplanar arcs compared to 5-beam IMRT in ten patients. Gayen et al. [45] have found non-coplanar VMAT to be advantageous over coplanar VMAT both in sequential boost and simultaneous integrated boost techniques for sparing the shoulders and improving target coverage in 22 patients. Subramanian et al. [5] compared coplanar VMAT to multi-isocentric non-coplanar VMAT in 25 patients obtaining average reductions in mean dose to the parotids, larynx, oral cavity and pharyngeal muscle between 3 and 5 Gy. This improved sparing may be partly because non-coplanar plans had 1.5–3 times as many arcs as coplanar ones whereas, in the present study, DTRT and VMAT plans had the same number of arcs/paths.

For a nasopharyngeal case (HN5), DTRT resulted in lower dose to the optic structures compared to VMAT. In particular, near-max dose to the ipsilateral optic nerve was above tolerance for VMAT but within tolerance for DTRT, where the dose-volume effect for radiation-induced optic neuropathy risk is rapidly increasing [46]. Near-max dose to the lenses was slightly reduced with DTRT but above tolerance for both plans. The volume of the ipsilateral hippocampus receiving more than 7.3 Gy was 38.0% for VMAT and 30.5% for DTRT. Tolerance would

have likely been exceeded for VMAT in a clinical setting where this OAR is generally not considered with an associated risk of neurocognitive impairment [33]. The hippocampus should be considered in the planning of nasopharyngeal cases with both coplanar and non-coplanar techniques.

The dosimetric benefit of DTRT for stage II laryngeal carcinoma (HN6) was unclear with DTRT resulting in higher doses than VMAT for the pharynx and brachial plexus but improved sparing for upper oesophagus, thyroid gland, and contralateral carotid artery. A recent analysis found no difference in survival for IMRT or 3D-conformal radiotherapy for early-stage laryngeal carcinoma but toxicity was not reported [47]. For the more advanced SVCI technique in early stage glottic cancer (HN7), DTRT resulted in improved sparing for most OARs compared to VMAT. Historically, transoral surgery and standard radiotherapy have been associated with comparable morbidity [48, 49] indicating that improved OAR sparing with DTRT and SVCI could surpass surgery.

One possible limitation of this study is planner bias due to manual planning [43]. All VMAT plans were created for the purpose of this study using the same number of arcs as DTRT paths and comparable field-splitting and collimator angle offset strategies. To further mitigate planner bias during intensity optimization, strict manual planning rules were set before planning commenced (Additional file 1: A.I) and all plans were created by the same planner. Although using the same optimization objectives for both plans could be perceived as bias mitigation and would enable to compare the objective function value [11], this would not allow to explore the true potential for OAR sparing of one technique over the other. Automated planning is an attractive approach to mitigate bias [50] but no suitable method is currently available for DTRT on our system.

To exploit the OAR sparing potential of DTRT, OAR grouping strategies to obtain different non-coplanar paths were developed through trial-and-error. This approach is a priori applicable to other geometry-based path-finding approaches [7, 9] but intensity modulation is not considered at the path-finding stage. Other approaches use 4π fluence-based optimization to inform path-finding [11, 50, 51]

or simultaneous path and intensity modulation optimization [52, 53] which may further improve dosimetric plan quality. However, the two-step geometry-based DTRT treatment planning process is less complex and compatible with Eclipse making it potentially easier to implement clinically.

All DTRT paths were created using case-specific collision models automatically generated on a virtual linac and patient model [35] to optimally yet safely exploit the 4π -space around the patient. All plans were deliverable on the anthropomorphic phantom. The model could be refined using patient-specific body contours and mensuration or surface scanning [15].

Deliverability and dosimetric accuracy of dynamic trajectory delivery was previously demonstrated in cubic or cylindrical phantoms [6, 12, 54] and on an anthropomorphic prostate phantom [54] while Mueller et al. demonstrated deliverability of dynamic mixed beam radiotherapy (DYMBER), combining DTRT with electron fields, on a head phantom [55]. Here, deliverability of DTRT for HN was demonstrated with the full Alderson phantom on the table. Delivery times were on average 2.4 times longer for DTRT than VMAT for the same number of full gantry rotations but remain clinically acceptable. Mechanical accuracy of the delivery was assessed as the deviations between expected and actual values in machine log-files for all mechanical components, with root-mean-square (RMS) deviation of 0.02° , 0.12° and 0.03° for the gantry, table and collimator angles respectively. Film measurements resulted in gamma passing rates of 93.9% and 95.8% (2%/2 mm criteria, 10% dose threshold) confirming that DTRT is deliverable with high mechanical and dosimetric accuracy and clinically acceptable delivery times.

There were several motivations to conduct this study on a phantom. First, patient CTs do not always extend to the vertex restricting possible beam incidences and preventing dose reporting in cut regions. Second, deliverability and dosimetric validation could be performed directly on the phantom, therefore enabling comprehensive end-to-end testing. Finally, the anthropomorphic phantom solution allowed to create a publicly available library of all common HN cases. The

CT and contours can be directly used for in silico planning studies or users can register the contours to their own Alderson phantom (available in many clinics) for measurements. Given the anthropomorphism of the phantom, the proposed DTRT planning strategy is expected to be applicable to real patients presenting with similar target shapes and location to these available in the library. On the other hand, it may be possible to favour sparing specific OARs on a case-by-case basis.

4.6 Conclusion

This study showed substantial improvement in OAR sparing for HN cancer radiotherapy using DTRT compared to VMAT with plans that are deliverable on standard linacs. Film measurements for one case showed good agreement with the calculated dose. A publicly available library of all common HN cancer cases was created and the treatment planning strategy applied on these cases can be applied to similar cases in future clinical studies, therefore bringing DTRT closer to clinical practice.

4.7 Acknowledgements

Not applicable

4.8 Author contributions

JB PHM SM MKF PM designed the study and contributed to the methods and data analysis. JB performed the treatment planning, data analysis and prepared the manuscript. PHM delineated the OARs and target structure on the dataset. JB PHM GG HL performed the experimental validation. GG HL YW WV DF participated in the development of the methods. PHM OE DMA participated in data collection and provided advice on the clinical aspects of the project. All authors read and approved the final manuscript

4.9 Funding

This work was supported by Varian Medical Systems.

4.10 Availability of data and materials

The datasets generated and analysed during the current study are available on the BORIS repository. <https://dx.doi.org/10.48350/159243>

4.11 Declarations

Ethics approval and consent to participate

Not applicable.

Consent for publication

Not applicable.

Competing interests

This work was supported by Varian Medical Systems. SM and GG received funding from the Swiss National Science Foundation award number (200021_185366) outside the submitted work.

REFERENCES

1. Nutting, C. M. *et al.* Parotid-sparing intensity modulated versus conventional radiotherapy in head and neck cancer (PARSPORT): A phase 3 multicentre randomised controlled trial. *The Lancet Oncology* **12**, 127–136. ISSN: 14702045 (2011).
2. Otto, K. Volumetric modulated arc therapy: IMRT in a single gantry arc. *Medical Physics* **35**, 310–317. ISSN: 2473-4209 (Aug. 2008).
3. Smyth, G., Evans, P. M., Bamber, J. C. & Bedford, J. L. Recent developments in non-coplanar radiotherapy. *Brit J Radiol* **92**. ISSN: 1748880X (Aug. 2019).
4. Rwigema, J. C. M. *et al.* 4π Noncoplanar Stereotactic Body Radiation Therapy for Head-and-Neck Cancer: Potential to Improve Tumor Control and Late Toxicity. *International Journal of Radiation Oncology, Biology, Physics* **91**, 401–409. ISSN: 0360-3016 (Aug. 2015).
5. Subramanian, V. S. *et al.* Multi-isocentric 4π volumetric-modulated arc therapy approach for head and neck cancer. *Journal of Applied Clinical Medical Physics* **18**. ISSN: 15269914 (2017).
6. Fix, M. K. *et al.* Part 1: Optimization and evaluation of dynamic trajectory radiotherapy. *Medical Physics* **45**, 4201–4212. ISSN: 00942405 (Aug. 2018).

7. Yang, Y. *et al.* Choreographing couch and collimator in volumetric modulated arc therapy. *International Journal of Radiation Oncology Biology Physics* **80**. ISSN: 03603016 (2011).
8. Locke, C. B. & Bush, K. K. Trajectory optimization in radiotherapy using sectioning (TORUS): *Medical Physics* **44**. ISSN: 24734209 (2017).
9. Smyth, G., Bamber, J. C., Evans, P. M. & Bedford, J. L. Trajectory optimization for dynamic couch rotation during volumetric modulated arc radiotherapy. *Physics in Medicine and Biology* **58**. ISSN: 13616560 (2013).
10. Kraysenbuehl, J., Davis, J. B. & Ciernik, I. F. Dynamic intensity-modulated non-coplanar arc radiotherapy (INCA) for head and neck cancer. *Radiotherapy and Oncology* **81**. ISSN: 01678140 (2006).
11. Wild, E., Bangert, M., Nill, S. & Oelfke, U. Noncoplanar VMAT for nasopharyngeal tumors: Plan quality versus treatment time. *Medical Physics* **42**, 2157–2168. ISSN: 2473-4209 (Aug. 2015).
12. Smyth, G. *et al.* Dosimetric accuracy of dynamic couch rotation during volumetric modulated arc therapy (DCR-VMAT) for primary brain tumours. *Physics in Medicine and Biology* **64**. ISSN: 13616560 (2019).
13. Kadoya, N. *et al.* Automated noncoplanar treatment planning strategy in stereotactic radiosurgery of multiple cranial metastases: HyperArc and CyberKnife dose distributions. *Medical Dosimetry* **44**, 394–400. ISSN: 0958-3947 (Aug. 2019).
14. Ho, H. W. *et al.* Dosimetric comparison between RapidArc and HyperArc techniques in salvage stereotactic body radiation therapy for recurrent nasopharyngeal carcinoma. *Radiation Oncology* **15**. ISSN: 1748717X (2020).
15. Yu, V. Y. *et al.* The development and verification of a highly accurate collision prediction model for automated noncoplanar plan delivery. *Medical Physics* **42**, 6457–6467. ISSN: 2473-4209 (Aug. 2015).

16. Guckenberger, M. *et al.* Is a single arc sufficient in volumetric-modulated arc therapy (VMAT) for complex-shaped target volumes? *Radiotherapy and Oncology* **93**. ISSN: 01678140 (2009).
17. Tol, J. P., Dahele, M., Slotman, B. J. & Verbakel, W. F. Increasing the number of arcs improves head and neck volumetric modulated arc therapy plans. *Acta Oncologica* **54**. ISSN: 1651226X (2015).
18. Brouwer, C. L., Steenbakkers, R. J., Langendijk, J. A. & Sijtsema, N. M. Identifying patients who may benefit from adaptive radiotherapy: Does the literature on anatomic and dosimetric changes in head and neck organs at risk during radiotherapy provide information to help? *Radiother Oncol* **115**, 285–294. ISSN: 18790887 (2015).
19. Sun, Y. *et al.* Recommendation for a contouring method and atlas of organs at risk in nasopharyngeal carcinoma patients receiving intensity-modulated radiotherapy. *Radiother Oncol* **110**, 390–397. ISSN: 18790887 (2014).
20. Scoccianti, S. *et al.* Organs at risk in the brain and their dose-constraints in adults and in children: A radiation oncologist's guide for delineation in everyday practice. *Radiotherapy and Oncology* **114**. ISSN: 18790887 (2015).
21. Caudell, J. J. *et al.* Volume, Dose, and Fractionation Considerations for IMRT-based Reirradiation in Head and Neck Cancer: A Multi-institution Analysis. *International Journal of Radiation Oncology Biology Physics* **100**. ISSN: 1879355X (2018).
22. Liu, Y. P. *et al.* Endoscopic surgery compared with intensity-modulated radiotherapy in resectable locally recurrent nasopharyngeal carcinoma: a multicentre, open-label, randomised, controlled, phase 3 trial. *The Lancet Oncology* **22**. ISSN: 14745488 (2021).

REFERENCES

23. Mendenhall, W. M., Werning, J. W., Hinerman, R. W., Amdur, R. J. & Villaret, D. B. Management of T1-T2 Glottic Carcinomas. *Cancer* **100**. ISSN: 0008543X (2004).
24. Deschuymer, S. *et al.* Randomized clinical trial on reduction of radiotherapy dose to the elective neck in head and neck squamous cell carcinoma; update of the long-term tumor outcome. *Radiotherapy and Oncology* **143**. ISSN: 18790887 (2020).
25. Rosenthal, D. I. *et al.* Final Report of a Prospective Randomized Trial to Evaluate the Dose-Response Relationship for Postoperative Radiation Therapy and Pathologic Risk Groups in Patients With Head and Neck Cancer. *International Journal of Radiation Oncology Biology Physics* **98**. ISSN: 1879355X (2017).
26. Bourhis, J. *et al.* Concomitant chemoradiotherapy versus acceleration of radiotherapy with or without concomitant chemotherapy in locally advanced head and neck carcinoma (GORTEC 99-02): An open-label phase 3 randomised trial. *The Lancet Oncology* **13**. ISSN: 14702045 (2012).
27. Lacas, B. *et al.* Meta-analysis of chemotherapy in head and neck cancer (MACH-NC): An update on 107 randomized trials and 19,805 patients, on behalf of MACH-NC Group. *Radiotherapy and Oncology* **156**. ISSN: 18790887 (2021).
28. Terhaard, C. H. *et al.* The role of radiotherapy in the treatment of malignant salivary gland tumors. *International Journal of Radiation Oncology Biology Physics* **61**. ISSN: 03603016 (2005).
29. Grégoire, V. *et al.* Delineation of the primary tumour Clinical Target Volumes (CTV-P) in laryngeal, hypopharyngeal, oropharyngeal and oral cavity squamous cell carcinoma: AIRO, CACA, DAHANCA, EORTC, GEORCC, GORTEC, HKNPCSG, HNCIG, IAG-KHT, LPRHHT, NCIC CTG, NCRI,

- NRG Oncology, PHNS, SBRT, SOMERA, SRO, SSHNO, TROG consensus guidelines. *Radiotherapy and Oncology* **126**. ISSN: 18790887 (2018).
30. Lee, A. W. *et al.* International guideline for the delineation of the clinical target volumes (CTV) for nasopharyngeal carcinoma. *Radiotherapy and Oncology* **126**. ISSN: 18790887 (2018).
31. Biau, J. *et al.* Selection of lymph node target volumes for definitive head and neck radiation therapy: a 2019 Update. *Radiotherapy and Oncology* **134**. ISSN: 18790887 (2019).
32. Lee, A. W. *et al.* International Guideline on Dose Prioritization and Acceptance Criteria in Radiation Therapy Planning for Nasopharyngeal Carcinoma. *International Journal of Radiation Oncology Biology Physics* **105**. ISSN: 1879355X (2019).
33. Gondi, V., Hermann, B. P., Mehta, M. P. & Tomé, W. A. Hippocampal dosimetry predicts neurocognitive function impairment after fractionated stereotactic radiotherapy for benign or low-grade adult brain tumors. *International Journal of Radiation Oncology Biology Physics* **85**. ISSN: 03603016 (2013).
34. Al-Mamgani, A. *et al.* Single vocal cord irradiation: Image guided intensity modulated hypofractionated radiation therapy for T1a glottic cancer: Early clinical results. *International Journal of Radiation Oncology Biology Physics* **93**. ISSN: 1879355X (2015).
35. Guyer, G. *et al.* *Development of a Collision Prediction Tool between Gantry and Table Using Blender*, accessed on 26.10.2023 2021. <https://w4.aapm.org/meetings/2021AM/programInfo/programAbs.php?sid=9375&aid=58124>.
36. Community, B. O. *Blender - a 3D modelling and rendering package*, accessed on 26.10.2023 2018. <http://www.blender.org>.

REFERENCES

37. Rossi, M. & Boman, E. The use of aperture shape controller and convergence mode in radiotherapy treatment planning. *Journal of Radiotherapy in Practice*. ISSN: 14671131 (2020).
38. Paddick, I. A simple scoring ratio to index the conformity of radiosurgical treatment plans. Technical note. *Journal of neurosurgery* **93 Suppl 3**, 219–222. ISSN: 0022-3085 (2000).
39. Lewis, D. & Chan, M. F. Correcting lateral response artifacts from flatbed scanners for radiochromic film dosimetry. *Medical Physics* **42**. ISSN: 24734209 (2015).
40. Micke, A., Lewis, D. F. & Yu, X. Multichannel film dosimetry with nonuniformity correction. *Medical Physics* **38**, 2523–2534. ISSN: 2473-4209 (Aug. 2011).
41. Lewis, D., Micke, A., Yu, X. & Chan, M. F. An efficient protocol for radiochromic film dosimetry combining calibration and measurement in a single scan. *Medical Physics* **39**, 6339–6350. ISSN: 2473-4209 (Aug. 2012).
42. Low, D. A., Harms, W. B., Mutic, S. & Purdy, J. A. A technique for the quantitative evaluation of dose distributions. *Medical Physics* **25**. ISSN: 00942405 (1998).
43. Hansen, C. R. *et al.* Radiotherapy Treatment planning study Guidelines (RATING): A framework for setting up and reporting on scientific treatment planning studies. *Radiotherapy and Oncology* **153**. ISSN: 18790887 (2020).
44. Dirix, P., Nuyts, S., Poorten, V. V., Delaere, P. & Bogaert, W. V. D. The influence of xerostomia after radiotherapy on quality of life: Results of a questionnaire in head and neck cancer. *Support Care Cancer* **16**, 171–179. ISSN: 09414355 (Aug. 2008).
45. Gayen, S., Kombathula, S. H., Manna, S., Varshney, S. & Pareek, P. Dosimetric comparison of coplanar and non-coplanar volumetric-modulated arc

- therapy in head and neck cancer treated with radiotherapy. *Radiation Oncology Journal* **38**, 138. ISSN: 22343156 (2020).
46. Mayo, C. *et al.* Radiation Dose-Volume Effects of Optic Nerves and Chiasm. *International Journal of Radiation Oncology Biology Physics* **76**. ISSN: 03603016 (2010).
47. Wegner, R. E., Abel, S., Bergin, J. J. & Colonias, A. Intensity-modulated radiation therapy in early stage squamous cell carcinoma of the larynx: Treatment trends and outcomes. *Radiation Oncology Journal* **38**. ISSN: 22343156 (2020).
48. Williamson, A. J. & Bondje, S. *Glottic Cancer* (StatPearls Publishing, 2023).
49. Kinshuck, A. J., Shenoy, A. & Jones, T. M. Voice outcomes for early laryngeal cancer. *Current Opinion in Otolaryngology & Head and Neck Surgery* **25**. ISSN: 15316998 (2017).
50. Langhans, M., Unkelbach, J., Bortfeld, T. & Craft, D. Optimizing highly noncoplanar VMAT trajectories: the NoVo method. *Physics in Medicine & Biology* **63**, 25023. ISSN: 0031-9155 (Aug. 2018).
51. Papp, D., Bortfeld, T. & Unkelbach, J. A modular approach to intensity-modulated arc therapy optimization with noncoplanar trajectories. *Physics in medicine and biology* **60**, 5179–5198. ISSN: 1361-6560 (Aug. 2015).
52. Mullins, J., Renaud, M. A., Serban, M. & Seuntjens, J. Simultaneous trajectory generation and volumetric modulated arc therapy optimization. *Medical Physics* **47**, 3078–3090. ISSN: 2473-4209 (Aug. 2020).
53. Dong, P., Liu, H. & Xing, L. Monte Carlo tree search -based non-coplanar trajectory design for station parameter optimized radiation therapy (SPORT). *Physics in Medicine & Biology* **63**, 135014. ISSN: 0031-9155 (Aug. 2018).

REFERENCES

54. Manser, P. *et al.* Dose calculation of dynamic trajectory radiotherapy using Monte Carlo. *Zeitschrift fur Medizinische Physik* **29**. ISSN: 18764436 (2019).
55. Mueller, S. *et al.* Part 2: Dynamic mixed beam radiotherapy (DYMBER): Photon dynamic trajectories combined with modulated electron beams. *Medical Physics* **45**, 4213–4226. ISSN: 00942405 (Aug. 2018).

4.12 Appendix

Manual planning rules

These rules apply to the use of the Eclipse photon optimizer (PO) (Varian Medical Systems) [1]. The goal is to minimize planner bias while enabling to exploit the OAR-sparing potential of each technique by determining objectives that are challenging but nearly achievable

Before plan optimization

Before plan optimization, the user should choose the number of VMAT arcs or DTRT paths and their associated collimator angle or dynamic collimator paths. The user should decide if parameters such as jaw tracking, avoidance sectors or avoidance structure are to be used. Setting such as convergence mode and aperture shape controller should be clearly selected. In the present study, convergence mode on and aperture shape controller was set to “moderate”. The dose grid was set to 2.5 mm and automatic intermediate dose calculation was used at the multi-resolution (MR) level 4.

Mandatory clinical goals and priorities should be agreed upon prior to optimizations.

Starting objectives

The objectives in table 4.3 are set before the beginning of the optimization, and it is not allowed to modify them during interactive optimization.

Table 4.3: Optimization objectives for target coverage and conformity.

Organ	Objective type	Parameters	Priority
	Normal Tissue Objective (NTO)	Manual - Distance f. target border = 0.25 cm - Start dose = 99% - End dose = 30% - Fall-off = 0.25%	100
CTV	Lower	$D_{100\%}$ to $V_{100\%}$	200
PTV	Lower	$D_{100\%}$ to $V_{100\%}$	200
PTV	Lower	$D_{100\%}$ to $V_{95\%}$	200
PTV	Upper	$D_{105\%}$ to $V_0\%$	200
Normal Tissue (Body-PTV)	Upper	$D_{100\%}$ to $V_0\%$	200

Optimization objectives for the OARs are also set before the optimization based on the clinical goals (Table 4.4) but with a priority 0. For the phase 2 and 3 plans, the dose is reduced proportionately to the ratio of prescription dose (e.g. 32% for phase 2 delivering 16 Gy). The objectives in Table 4.4 are presented in order of priority. Only the spinal cord, brain stem and their respective PRVs have higher priority than target coverage. For all other OARs, if the clinical goals cannot be met, the dose should be reduced as much as possible. The PRV margins were 5 and 3 mm isotropically for spinal cord and brain stem respectively. Carotid arteries are only considered if outside the target volume with an isotropic PRV margin of 5 mm.

Table 4.4: Clinical goals and starting optimization objectives for OARs. Only the dose can be modified manually during the interactive optimization phase.

Organ	Clinical goal	Opt. objective type	Volume [%]	Dose [Gy]
Spinal cord	D0.03 cc \leq 45 Gy ¹	Upper	0	35
PRV spinal cord	D0.03 cc \leq 48 Gy ¹	Upper	0	38
Brainstem	D0.03 cc \leq 54 Gy ¹	Upper	0	43
PRV brainstem	D0.03 cc \leq 54 Gy ¹	Upper	0	43
Hippocampus (R/L)	V7.3 Gy \leq 40% ²	Upper	35	7
Parotid gland (R/L)	Dmean \leq 26 Gy ³	Mean		25/20
Pharynx	Dmean \leq 45 Gy	Mean		45
	D50 Gy \leq 33%	Upper	33	50
Larynx GSL	Dmean \leq 35 Gy	Mean		35
Cochlea (R/L)	Dmax \leq 45 Gy	Upper	0	35
Upper Oesophagus	Dmean \leq 40 Gy	Mean		40
Lips	Dmean \leq 20 Gy	Mean		20
	Dmax \leq 30 Gy	Upper	0	30
Oral cavity - PTV	Dmean \leq 40 Gy ⁴	Mean		40
Mandible	D2% \leq 70 Gy	Upper	0	50
Brachial Plexus	D0.03 cc \leq 66 Gy	Upper	0	50
Brain	D0.03 cc \leq 65 Gy	Upper	0	50
			0.1	40
Eye (R/L)	D0.03 cc \leq 45 Gy	Upper	0	35
	Dmean \leq 35 Gy	Mean		35
Lachrymal gland (R/L)	Dmean \leq 30 Gy	Mean		30
Submandibular gland (R/L)	Dmean \leq 35 Gy	Mean		35
Lens (R/L)	D0.03 cc \leq 6 Gy	Upper	0	4
Optic chiasm	D0.03 cc \leq 54 Gy	Upper	0	43
Optic nerve (R/L)	D0.03 cc \leq 54 Gy	Upper	0	43
Inner ear (R/L)	Dmean \leq 45 Gy	Mean		22
Thyroid gland	V 50 Gy \leq 60%	Upper	60	50
		Mean		35
PRV carotid (R/L)	D50% \leq 5 Gy	Upper	47	5
	D30% \leq 10 Gy	Upper	27	10
	D10% \leq 15 Gy	Upper	7	15

¹: higher priority than target coverage

¹: introduced for this study

¹: 20 Gy if only one gland can be spared. Keep below 30 Gy for at least one gland.

¹: Optimization is performed on oral cavity but plan evaluation is performed on oral cavity excluding PTV

Interactive optimization

Optimization is started in Eclipse with only the objectives of table 4.3 with non-zero priority. No interaction is permitted until the PO reaches MR level 1, step 3/5. The user then pauses the optimization and sets a priority of 80 to all OAR objectives. Exceptions are made for OARs that have a minimum dose objective (Upper objective to 0% volume) and overlap with the PTV or for OARs with a mean dose objective having a major overlap with the PTV. In this case, the dose value is set to the prescription dose and the priority to 50.

The user resumes the optimization and is allowed only to change the dose value of the OAR objectives. The goal of these interactions is to fulfil the clinical goals and to reduce the dose to the OARs as much as possible, i.e. the objectives must contribute to the objective function value. After the intermediate dose calculation at MR level 4, the user once again pauses the optimization and can make final adjustments to the dose values of the OAR objectives. The user resumes the optimization again until it completes. Final dose calculation is performed and the user evaluates whether the clinical goals are fulfilled.

Tweaking the objective and re-optimization without manual interaction was allowed if clinical goals were nearly reached. All plans were re-optimized without any manual interaction and the plans were normalized.

Film measurement protocol

Film measurements were conducted in one end-to-end test on the Alderson phantom. Two Gafchromic EBT3 films (Ashland Advanced Materials, Bridgewater, NJ) were laser-cut to fit between the Alderson slabs closest to target isocenter. The films were scanned 21 hours after irradiation on an Epson XL 10000 flatbed scanner. The scanned films were corrected for lateral response artefact using a one-dimensional linear correction function [2]. Triple channel calibration was used to convert colour values to absolute dose [3]. Dose rescaling was applied according to the one-scan protocol using two addition film strips [4]. The resulting dose to the red channel was used for comparison with the corresponding 2D calculated dose plane in Eclipse using gamma evaluation with a 2% (global)/2mm criterion and a 10% dose threshold of the maximum dose [5].

DVH endpoints

Table 4.5 reports clinical goals and DVH endpoints for HN1-6 treated with sequential boost techniques. Table 4.6 reports clinical goals and DVH endpoints for HN7, single vocal cord irradiation treated according to the VoiceS protocol

(NCT04057209, available upon request). Endpoints above tolerance are shown in red. As per institutional guidelines, these clinical goals are not mandatory but the dose should be reduced as much possible and the following variations are acceptable:

- Parotid glands: mean dose below 30 Gy for at least one gland,
- Pharynx: mean dose below 55 Gy,
- Oral cavity (excluding PTV): mean dose below 50 Gy,
- Brachial plexus and brain: $D_{0.03cc}$ below 70 Gy,
- Mandible: $D_{2\%}$ below 75 Gy

Table 4.5: DVH endpoints for HN1-6.

OAR	Endpoint/goal [Gy/%]	Dose [Gy] or volume [%] - VMAT / DTRT					
		HN1	HN2	HN3	HN4	HN5	HN6
Target							
PTV70 D95%	70.0 Gy ¹	71.0 / 71.0	70.5 / 70.7	70.3 / 70.1	NA	NA	70.2 / 70.3
PTV70 D5%	≤ 74.9 Gy	73.9 / 74.0	73.3 / 73.5	73.5 / 73.7	NA	NA	73.1 / 72.9
PTV66 D95%	≤ 66.0 Gy ²	NA	69.5 / 69.4	NA	66.5 / 66.4	66.0 / 65.9 NA	
PTV66 D98%	≤ 62.7 Gy	NA	68.6 / 68.4	NA	66.2 / 66.1	65.2 / 65.1	NA
PTV66 D5%	≤ 70.6 Gy	NA	NA	NA	68.6 / 68.6	69.1 / 69.2	NA
PTV50 D95%	≤ 50.0 Gy	51.5 / 52.8	51.1 / 50.4	50.5 / 51.1	51.6 / 52.4	62.4 / 60.5	63.4 / 63.6
PTV50 D98%	≥ 47.5 Gy	50.9 / 51.9	50.4 / 51.3	50.0 / 50.6	51.0 / 51.7	60.7 / 58.1	60.0 / 60.9
Salivary and swallowing							
Contr. parotid	Dmean ≤ 26	26.3 / 26.8	16.0 / 13.1	10.8 / 8.1	7.5 / 1.1	4.6 / 2.2	0.3 / 0.3
Ips. parotid	Dmean ≤ 26	28.1 / 28.5	23.4 / 23.8	23.3 / 2.2	Resected	7.4 / 4.0	0.3 / 0.3
Contr. submand.	Dmean ≤ 35	20.4 / 19.5	21.8 / 16.9	16.0 / 13.4	2.6 / 2.2	0.5 / 3.2	1.4 / 1.5
Ips. submand.	Dmean ≤ 35	NA	Resected	31.4 / 31.4	7.9 / 9.3	0.5 / 4.4	1.2 / 1.2
Pharynx	Dmean ≤ 45	51.3 / 49.4	51.0 / 49.8	41.2 / 41.1	16.3 / 12.8	1.4 / 6.7	9.2 / 10.6
Oral cavity - PTV	Dmean ≤ 40	29.9 / 25.6	40.1 / 36.0	34.4 / 33.0	11.6 / 9.1	2.0 / 11.2	0.4 / 0.4
Larynx GSL	Dmean ≤ 35	31.6 / 25.1	34.1 / 34.2	27.7 / 29.1	0.7 / 3.1	0.3 / 2.7	NA
Auditory and optical							
Contr. cochlea	D0.03 cc ≤ 45	6.5 / 11.8	3.5 / 8.6	1.8 / 4.3	3.9 / 2.3	12.0 / 5.9	≤ 0.1
Ips. cochlea	D0.03 cc ≤ 45	11.2 / 18.6	4.3 / 13.2	2.9 / 17.4	16.3 / 15.5	9.7 / 9.7	≤ 0.1
Contr. inner ear	Dmean ≤ 45	5.5 / 10.2	3.0 / 8.4	1.6 / 3.9	3.1 / 2.0	9 / 4.2	≤ 0.1
Ips. inner ear	Dmean ≤ 45	7.7 / 16.3	3.6 / 12.8	2.6 / 14.4	14.8 / 14.4	9.6 / 8.6	≤ 0.1
Contr. eye	D0.03 cc ≤ 45	7.8 / 8.4	4.1 / 11.4	2.2 / 5.0	6.6 / 3.7	26.9 / 26.3	≤ 0.1
Contr. eye	Dmean ≤ 35	3.2 / 6.1	1.8 / 6.8	1.2 / 3.5	2.3 / 2.1	12.9 / 9.6	≤ 0.1
Ips. eye	D0.03 cc ≤ 45	7.0 / 7.1	4.2 / 7.5	2.6 / 6.7	10.7 / 10.5	41.0 / 41.7	≤ 0.1
Ips. eye	Dmean ≤ 35	2.9 / 4.7	1.8 / 4.3	1.3 / 4.3	3.1 / 5.8	14.5 / 12.8	≤ 0.1
Contr. lachrymal	Dmean ≤ 30	1.9 / 5.8	1.2 / 6.9	0.8 / 4.6	1.2 / 1.1	11.4 / 5.6	≤ 0.1
Ips. lachrymal	Dmean ≤ 30	1.9 / 4.0	1.3 / 3.3	0.9 / 3.5	1.5 / 7.7	11.6 / 7.7	≤ 0.1
Contr. lens	D0.03 cc ≤ 6	3.4 / 5.4	1.8 / 5.5	1.2 / 2.9	2.2 / 2.6	7.2 / 6.4	≤ 0.1
Ips. lens	D0.03 cc ≤ 6	3.0 / 4.7	1.8 / 3.6	1.3 / 3.4	2.7 / 4.4	8.2 / 7.2	≤ 0.1
Optic chiasm	D0.03 cc ≤ 54	1.9 / 9.9	1.4 / 8.7	1.1 / 9.8	1.2 / 3.7	10.7 / 11.4	≤ 0.1
Contr. optic nerve	D0.03 cc ≤ 54	2.1 / 10.9	1.6 / 10.4	1.3 / 6.0	1.3 / 3.1	31.4 / 20.2	≤ 0.1
Ips. optic nerve	D0.03 cc ≤ 54	2.5 / 11.0	1.8 / 13.1	1.3 / 10.2	1.8 / 13.8	54.8 / 53.3	≤ 0.1
Nervous and circulatory							
Spinal cord	D0.03 cc ≤ 45	36.5 / 31.3	32.0 / 30.5	31.6 / 31.8	25.4 / 14.3	17.1 / 15.7	22.9 / 23.4
PRV spinal cord	D0.03 cc ≤ 48	41.1 / 36.9	34 / 35.1	35.4 / 36.8	28 / 18.1	18.3 / 16.8	27.6 / 26.7
Brainstem	D0.03 cc ≤ 54	19.8 / 22.1	14.7 / 22.5	16.9 / 19.9	19.0 / 11.3	25.8 / 22.0	0.2 / 0.2
PRV brainstem	D0.03 cc ≤ 54	22.0 / 26.2	16.4 / 25.5	18.9 / 22.7	21.1 / 13.2	26.9 / 23.7	0.2 / 0.2
Brachial Plexus	D0.03 cc ≤ 66	68.3 / 68.7	56.6 / 55.8	52.6 / 53.6	1.4 / 14.1	0.3 / 3.0	35.7 / 39.2
Brain	D0.03 cc ≤ 65	32.6 / 37.5	24.7 / 36.0	20.4 / 32.7	49.8 / 47.9	69.7 / 69.1	0.2 / 0.2
Contr. carotid PRV	D50% ≤ 5	NA	NA	5.1 / 5.6	0.9 / 1.0	0.3 / 1.3	0.7 / 0.8
Contr. carotid PRV	D30% ≤ 10	NA	NA	7.5 / 6.8	5.0 / 2.1	0.8 / 1.7	1.4 / 2.0
Contr. carotid PRV	D10% ≤ 15	NA	NA	13.8 / 12.1	11.7 / 3.8	14.7 / 11.1	15.0 / 13.5
Ips. carotid PRV	D50% ≤ 5	NA	NA	NA	NA	0.4 / 6.2	
Ips. carotid PRV	D30% ≤ 10	NA	NA	NA	NA	0.9 / 3.8	
Ips. carotid PRV	D10% ≤ 15	NA	NA	NA	NA	14.7 / 14.2	
Other structures							
Contr. hippo.	V7.3 Gy ≤ 40	0 / 8.8	0 / 3.3	0 / 0	0 / 0	20.5 / 3.4	0 / 0
Ips. hippo.	V7.3 Gy ≤ 40	0 / 3.4	0 / 28.5	0 / 22.2	0 / 6.9	38.0 / 30.5	0 / 0
Upper oesophagus	Dmean ≤ 40	12.0 / 14.4	14.3 / 13.5	8.6 / 8.7	0.3 / 1.3	0.1 / 2.0	18.0 / 15.4
Mandible	D2% ≤ 70	72.2 / 72.6	72.4 / 72.9	61.4 / 59.3	66.7 / 66.0	31.4 / 19.7	0.6 / 0.6
Lips	Dmean ≤ 20	19.8 / 16.3	24.6 / 21.9	17.8 / 14.9	8.0 / 6.3	1.1 / 6.4	0.2 / 0.2
Lips	Dmax ≤ 30	39.3 / 35.2	71.5 / 74.5	30.5 / 28.2	17.6 / 23.0	2.6 / 17.0	0.4 / 0.4
Thyroid	V50 Gy ≤ 60	15.3 / 20.1	18.5 / 26.9	3.1 / 5.1	0 / 0	0 / 0	14.7 / 13.8

¹: within1/-2%, ²: within +/-2% for HN 4-5

Abbreviations: contr.: contralateral, ips.: ipsilateral, submand.: submandibular gland. PRV: planning at risk volume.

Table 4.6: Dosimetric endpoints for HN7 (single vocal cord irradiation)

PTV objective	Deviation acceptable	Dose [Gy] VMAT / DTRT
D99% = 58.08 Gy	≥ 55.176 Gy (95%)	56.34 / 56.34
D1% ≤ 60.98 Gy	≤ 62.15 Gy	61.52 / 61.34
D0.03cc ≤ 62.15 Gy	≤ 63.89 Gy	61.97 / 61.61
OAR	Endpoint/ objective	
Normal Tissue	D0.03cc ≤ 60.98 Gy (62.15 Gy acceptable)	54.96 / 55.15
Spinal cord*	Dmax ≤ 30 Gy	16.2 / 14.9
PRV spinal cord*	Dmax ≤ 35 Gy	18.4 / 17.8
Contr. Vocal cord	Dmean ≤ 50 Gy	40.7 / 36.4
Larynx	Dmean ≤ 40 Gy	29.6 / 31.1
Contr. Arytenoid	Dmean ≤ 40 Gy	21.1 / 13.3
Mid constrictor	Dmean ≤ 40 Gy	2.2 / 4.0
Inf constrictor	Dmean ≤ 40 Gy	20.5 / 13.8
Supra-larynx	Dmean ≤ 20 Gy	17.8 / 20.0
Cricopharyngeal muscle	Dmean ≤ 40 Gy	23.4 / 22.7
Brachial plexus*	Dmax ≤ 45 Gy	22.6 / 16.9
Ipsi. Carotid	Dmax ≤ 30 Gy	26.4 / 23.2
Contr. carotid	Dmax ≤ 15 Gy	12.9 / 11.7
Thyroid gland	Dmean ≤ 15 Gy	15.2 / 14.4
* mandatory goal		

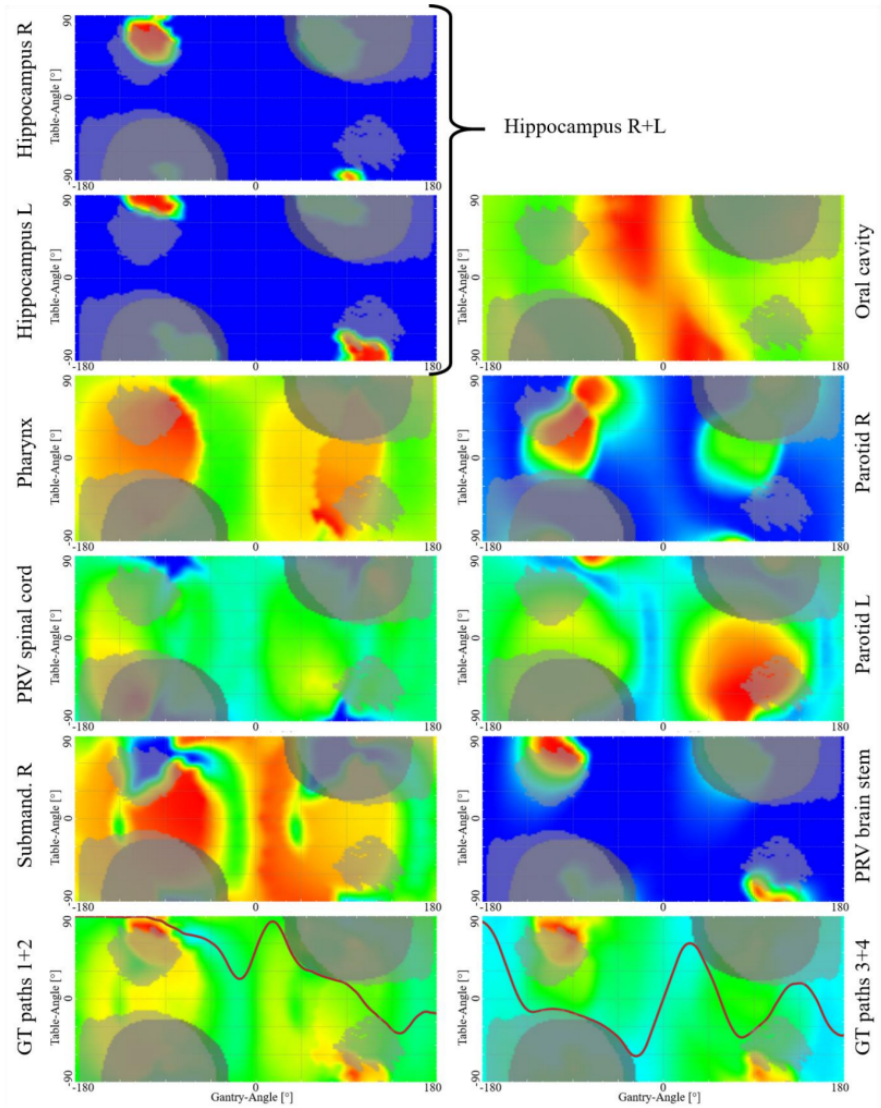


Figure 4.6: Individual OAR GT-maps and map sum for each path for HN2. The hippocampus R+L was included in both maps.

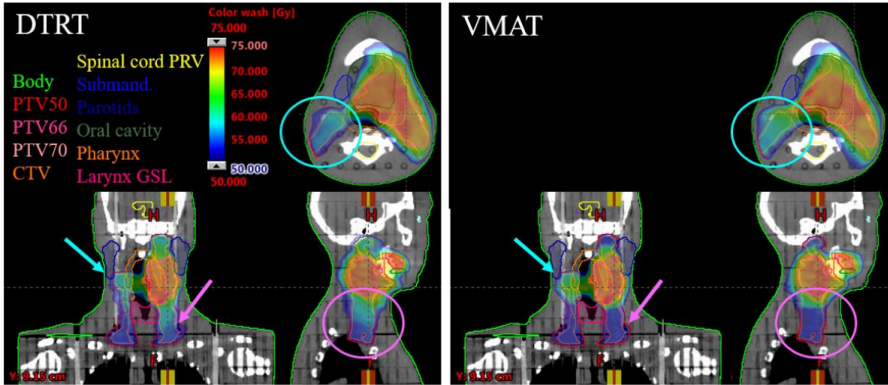


Figure 4.7: Dose distribution for HN2. Where the elective nodal volume (PTV50) extends the high dose volume (PTV66/70) in the axial direction, PTV50 receives more dose with VMAT than DTRT (cyan circle and arrow). On the contrary, where PTV50 extends PTV66/70 inferiorly, PTV50 receives more dose with DTRT than VMAT (magenta circle and arrows).

RATiNG

The RATiNG guidelines for treatment planning studies [6] were followed and the final score was 96%. The score sheet is attached below.

RATING score sheet		Points	Applicable/ relevant	Answer yes
Questions for the Introduction				
<i>The study aim formulated by research questions</i>				
1	Does the study have a concise and precise study aim, defined with a restricted number of interconnected questions?	10		<input checked="" type="checkbox"/>
<i>The motivation for the research questions</i>				
2	Has relevant up to date literature been included to support the need for the current study?	5		<input checked="" type="checkbox"/>
3	Does the study address an existing knowledge gap?	10		<input checked="" type="checkbox"/>
Questions for Materials and Methods				
4	Is the global study design adequate for answering the posed research questions?	10		<input checked="" type="checkbox"/>
5	Is the global study design described in sufficient detail for others to interpret and reproduce the results?	5		<input checked="" type="checkbox"/>
<i>Patient cohort</i>				
6	Are the inclusion and exclusion criteria of the patient cohort described?	1	<input checked="" type="checkbox"/>	<input type="checkbox"/>
7	Is the clinical patient information of the cohort presented, including disease type, site(s) and clinical staging?	1	<input checked="" type="checkbox"/>	<input type="checkbox"/>
8	Is the included number of patients stated, explained and justified?	1	<input checked="" type="checkbox"/>	<input checked="" type="checkbox"/>
9	Has there been consideration of the need for ethical and/or legal approval for the study and if needed, is there a statement about this?	5		<input checked="" type="checkbox"/>
<i>Imaging procedures</i>				
10	Have the scanning parameters been reported in sufficient detail (image modalities, equipment model, slice thickness, voxel size, patient position (e.g. head first, supine, etc.) etc.)?	1	<input checked="" type="checkbox"/>	<input checked="" type="checkbox"/>
11	Has the applied immobilisation equipment been described, (e.g. vendor and type, standard settings, etc.) where relevant?	1	<input checked="" type="checkbox"/>	<input checked="" type="checkbox"/>
<i>Treatment machine and settings</i>				
12	Have the treatment machine and relevant parameters been described with sufficient detail (model, beam energy, MLC, etc.)?	1	<input checked="" type="checkbox"/>	<input checked="" type="checkbox"/>
13	Have the monitor unit reference conditions been defined, where relevant?	1	<input type="checkbox"/>	<input type="checkbox"/>
<i>Definition of targets and OARs</i>				
14	Has GTV definition been described in sufficient detail, with references if possible?	1	<input type="checkbox"/>	<input type="checkbox"/>
15	Has CTV definition been described in sufficient detail, with references if possible?	1	<input checked="" type="checkbox"/>	<input checked="" type="checkbox"/>
16	Has the establishment of PTVs (or alternatively robustness settings) been described in sufficient detail?	1	<input checked="" type="checkbox"/>	<input checked="" type="checkbox"/>
17	Have PTV sizes in the patient cohort been described?	1	<input checked="" type="checkbox"/>	<input checked="" type="checkbox"/>
18	Have OAR definitions been described in sufficient detail, with references if possible?	1	<input checked="" type="checkbox"/>	<input checked="" type="checkbox"/>
19	Have PRV margins been described in sufficient detail, with references if available?	1	<input checked="" type="checkbox"/>	<input checked="" type="checkbox"/>
<i>Treatment planning system and dose calculation</i>				

20	Have all applied dose calculation algorithms been described in sufficient detail?	1	<input type="checkbox"/>	<input type="checkbox"/>
21	For any commercial software used, have the manufacturer, algorithms and specific versions been stated?	1	<input type="checkbox"/>	<input type="checkbox"/>
22	Have all relevant user parameters and settings in the TPS been reported, e.g. beams, dose grid, control point spacing?	1	<input type="checkbox"/>	<input type="checkbox"/>
23	Have all volumes been evaluated with the same software/methodology?	1	<input type="checkbox"/>	<input type="checkbox"/>
<i>Planning aims and optimisation</i>				
24	Are clear planning aims defined, including imposed hard constraints and planning objectives (with or without soft constraints)?	5	<input type="checkbox"/>	<input type="checkbox"/>
25	Has the ranking of planning objectives (priorities) been described?	5	<input type="checkbox"/>	<input type="checkbox"/>
26	Is the dose prescription clearly defined?	10	<input type="checkbox"/>	<input type="checkbox"/>
27	Is there a narrative description of the applied optimisation process, including the handling of all objectives with their ranking?	5	<input type="checkbox"/>	<input type="checkbox"/>
28	If manual intervention during or after optimisation is allowed, has this been described?	1	<input type="checkbox"/>	<input type="checkbox"/>
<i>Bias mitigation</i>				
29	Have enough study details been provided such that bias issues could be noted?	5	<input type="checkbox"/>	<input type="checkbox"/>
30	Has bias been sufficiently mitigated to reliably answer the posed research question?	10	<input type="checkbox"/>	<input type="checkbox"/>
<i>Plan acceptability – minor and major protocol deviations</i>				
31	Was the procedure for assessment of plan acceptability well-described?	1	<input type="checkbox"/>	<input type="checkbox"/>
32	Was the procedure for assessment of minor and major protocol deviations well described?	1	<input type="checkbox"/>	<input type="checkbox"/>
<i>Plan (re-)normalisation for plan comparisons</i>				
33	Has plan (re-)normalisation been described sufficiently?	1	<input type="checkbox"/>	<input type="checkbox"/>
<i>Dose-volume parameters for plan evaluation and comparison</i>				
34	Have sufficiently comprehensive dose-volume parameters been used for plan evaluations and comparisons?	5	<input type="checkbox"/>	<input type="checkbox"/>
<i>Population-mean DVHs</i>				
35	Has the algorithm for creating population-mean/median DVHs been reported?	1	<input type="checkbox"/>	<input type="checkbox"/>
36	Have the definitions of confidence intervals been included?	1	<input type="checkbox"/>	<input type="checkbox"/>
<i>Plan evaluations by clinicians</i>				
37	Have clinicians scored plans to assess quality?	1	<input type="checkbox"/>	<input type="checkbox"/>
38	Were plan comparisons by clinicians blinded?	1	<input type="checkbox"/>	<input type="checkbox"/>
<i>Predicted tumour control probability and normal tissue complication probabilities for plan evaluation and comparison</i>				
39	Have any applied TCP models been described and referenced?	1	<input type="checkbox"/>	<input type="checkbox"/>
40	Have any applied NTCP models been described and referenced?	1	<input type="checkbox"/>	<input type="checkbox"/>
<i>Plan deliverability and complexity</i>				
41	Have methods used to assess plan deliverability and complexity been described in sufficient detail?	1	<input type="checkbox"/>	<input type="checkbox"/>
<i>Composite plan quality metrics</i>				
42	Is there a sufficient basis (e.g. in the literature) for any selected composite plan quality metrics?	1	<input type="checkbox"/>	<input type="checkbox"/>

43	Is there an adequate description of the calculation of the composite plan quality metrics?	1	<input type="checkbox"/>	<input type="checkbox"/>
<i>Planning and delivery times</i>				
44	Has measurement of planning times been described in sufficient detail?	1	<input checked="" type="checkbox"/>	<input checked="" type="checkbox"/>
45	Has the establishment of delivery times been described in sufficient detail?	1	<input checked="" type="checkbox"/>	<input checked="" type="checkbox"/>
<i>Statistical analysis</i>				
46	Have proper statistical methods been used and described in sufficient detail?	5	<input checked="" type="checkbox"/>	<input type="checkbox"/>
47	In case of multiple testing for research questions, has this been handled appropriately?	1	<input type="checkbox"/>	<input type="checkbox"/>
Questions for Results				
48	Does the provided data contribute to (at least partly) answering all aspects of the research questions, e.g. plan acceptability, dosimetric quality, deliverability and planning and delivery times?	10	<input checked="" type="checkbox"/>	<input checked="" type="checkbox"/>
<i>Dose distribution reporting</i>				
49	Are complete summaries of the dose distributions in the patient cohort provided (low doses, high doses, OARs, PTV, patient, etc.)?	5	<input checked="" type="checkbox"/>	<input checked="" type="checkbox"/>
50	Are tables and figures optimised to clearly present the results obtained?	1	<input checked="" type="checkbox"/>	<input checked="" type="checkbox"/>
51	Have the answers to the research questions been illustrated for an example patient by providing dose distributions, DVHs, etc.?	1	<input checked="" type="checkbox"/>	<input checked="" type="checkbox"/>
<i>Plan acceptability reporting – minor and major protocol deviations</i>				
52	In case of treatment technique or planning technique comparisons, was plan acceptability reported separately for each technique?	1	<input checked="" type="checkbox"/>	<input checked="" type="checkbox"/>
53	Has plan acceptability been reported in sufficient detail: how many plans were acceptable, how many were not and for what reasons (e.g. violation of hard constraints, violation of soft constraints, other reasons)?	1	<input checked="" type="checkbox"/>	<input checked="" type="checkbox"/>
54	Was there adequate reporting of minor and major protocol deviations?	1	<input checked="" type="checkbox"/>	<input checked="" type="checkbox"/>
<i>Deliverability and complexity reporting</i>				
55	Has the deliverability of the plans been adequately reported?	1	<input checked="" type="checkbox"/>	<input checked="" type="checkbox"/>
56	Have plan deliverability and complexity been investigated in sufficient detail in relation to the posed research questions?	1	<input checked="" type="checkbox"/>	<input checked="" type="checkbox"/>
<i>Planning and delivery times reporting</i>				
57	Have planning and delivery times been adequately evaluated and reported?	1	<input checked="" type="checkbox"/>	<input checked="" type="checkbox"/>
<i>Patient-specific analyses reporting</i>				
58	Is there sufficient description of inter-patient variations in the results presented?	1	<input checked="" type="checkbox"/>	<input checked="" type="checkbox"/>
59	Have outlier patients been reported and has any exclusion from population analyses been sufficiently motivated and explained?	1	<input checked="" type="checkbox"/>	<input checked="" type="checkbox"/>
<i>Statistical reporting</i>				
60	Are the p-values reported appropriately?	1	<input type="checkbox"/>	<input type="checkbox"/>
61	Are there confidence intervals for the appropriate parameters?	1	<input type="checkbox"/>	<input type="checkbox"/>
Questions for discussions				

62	Is there an overall interpretation of the data presented in the Results section as to how the posed research questions are answered?	10		<input type="checkbox"/>
<i>Comparison with literature</i>				
63	Has the study been sufficiently discussed in the context of existing literature?	5		<input type="checkbox"/>
<i>Clinical and statistical significance</i>				
64	Does the discussion focus on statistically significant results?	1	<input type="checkbox"/>	<input type="checkbox"/>
65	Is the potential clinical significance of the results clearly discussed (assuming practical application would be feasible)?	5		<input type="checkbox"/>
<i>Clinical applicability of the study</i>				
66	Is future the clinical applicability sufficiently discussed?	1	<input type="checkbox"/>	<input type="checkbox"/>
<i>Study limitations</i>				
67	Has the impact of the study limitations on the provided answers to the research questions been sufficiently discussed?	10		<input type="checkbox"/>
<i>Future work</i>				
68	Has the potential future work arising from the study been discussed?	1	<input type="checkbox"/>	<input type="checkbox"/>
Questions for conclusions				
69	Do the presented conclusions represent answers to the posed research questions?	5		<input type="checkbox"/>
70	Are the conclusions fully supported by the results?	5	<input type="checkbox"/>	<input type="checkbox"/>
71	Are the conclusions a fair summary of all results?	5	<input type="checkbox"/>	<input type="checkbox"/>
Questions for supplementary				
<i>Supplementary materials</i>				
72	Is the information presented in the supplementary material of sufficient relevance?	1	<input type="checkbox"/>	<input type="checkbox"/>
73	Is the presentation of the included information of sufficient quality, including readability?	1	<input type="checkbox"/>	<input type="checkbox"/>
74	Has sufficient underlying data been made available or a willingness to share data been indicated, within local data sharing restrictions?	5		<input type="checkbox"/>
RATING remarks				
75	Is the RATING score added to the manuscript?	5		<input type="checkbox"/>
76	Is the accompanying question table added to the cover letter or the supplementary material?	1	<input type="checkbox"/>	<input type="checkbox"/>

RATING score

RATING fraction

96%

195 of 203

REFERENCES

1. Varian Medical Systems. Varian Medical Systems. Eclipse 15.5 Photon and Electron Algorithms Reference Guide (2017).
2. Lewis, D. & Chan, M. F. Correcting lateral response artifacts from flatbed scanners for radiochromic film dosimetry. *Medical Physics* **42**. ISSN: 24734209 (2015).
3. Micke, A., Lewis, D. F. & Yu, X. Multichannel film dosimetry with nonuniformity correction. *Medical Physics* **38**, 2523–2534. ISSN: 2473-4209 (Aug. 2011).
4. Lewis, D., Micke, A., Yu, X. & Chan, M. F. An efficient protocol for radiochromic film dosimetry combining calibration and measurement in a single scan. *Medical Physics* **39**, 6339–6350. ISSN: 2473-4209 (Aug. 2012).
5. Low, D. A., Harms, W. B., Mutic, S. & Purdy, J. A. A technique for the quantitative evaluation of dose distributions. *Medical Physics* **25**. ISSN: 00942405 (1998).
6. Hansen, C. R. *et al.* Radiotherapy Treatment planning study Guidelines (RATING): A framework for setting up and reporting on scientific treatment planning studies. *Radiotherapy and Oncology* **153**. ISSN: 18790887 (2020).

ROBUSTNESS ANALYSIS OF DYNAMIC TRAJECTORY RADIO-THERAPY AND VOLUMETRIC MODULATED ARC THERAPY PLANS FOR HEAD AND NECK CANCER

H.A. Loebner¹, J. Bertholet¹, P.-H. Mackeprang¹, W. Volken¹,
O. Elicin¹, S. Mueller¹, G. Guyer¹, D.M. Aebersold¹,
M.F.M. Stampanoni², M.K. Fix¹, P. Manser¹

¹ Division of Medical Radiation Physics and Department of Radiation
Oncology, Inselspital, Bern University Hospital, University of Bern, Bern,
Switzerland

² Institute for Biomedical Engineering, ETH Zürich and PSI, Villigen,
Switzerland

published in

Physics and Imaging in Radiation Oncology

May 2024, Available Online

<https://doi.org/10.1016/j.phro.2024.100586>

©European Society of Radiotherapy & Oncology

Open access article distributed under the terms of the Creative Commons CC BY-NC-ND 4.0 license.

5.1 Abstract

Background and purpose

Dynamic trajectory radiotherapy (DTRT) has been shown to improve healthy tissue sparing compared to volumetric arc therapy (VMAT). This study aimed to assess and compare the robustness of DTRT and VMAT treatment-plans for head and neck (H&N) cancer to patient-setup (PS) and machine-positioning uncertainties.

Methods

The robustness of DTRT and VMAT plans previously created for 46 H&N cases, prescribed 50–70 Gy to 95 % of the planning-target-volume, was assessed. For this purpose, dose distributions were recalculated using Monte Carlo, including uncertainties in PS (translation and rotation) and machine-positioning (gantry-, table-, collimator-rotation and multi-leaf collimator (MLC)). Plan robustness was evaluated by the uncertainties' impact on normal tissue complication probabilities (NTCP) for xerostomia and dysphagia and on dose-volume endpoints. Differences between DTRT and VMAT plan robustness were compared using Wilcoxon matched-pair signed-rank test ($\alpha = 5\%$).

Results

Average NTCP for moderate-to-severe xerostomia and grade \geq II dysphagia was lower for DTRT than VMAT in the nominal scenario (0.5 %, $p = 0.01$; 2.1 %, $p < 0.01$) and for all investigated uncertainties, except MLC positioning, where the difference was not significant. Average differences compared to the nominal scenario were ≤ 3.5 Gy for rotational PS ($\leq 3^\circ$) and machine-positioning ($\leq 2^\circ$) uncertainties, < 7 Gy for translational PS uncertainties (≤ 5 mm) and < 20 Gy for MLC-positioning uncertainties (≤ 5 mm).

Conclusions

DTRT and VMAT plan robustness to the investigated uncertainties depended on uncertainty direction and location of the structure-of-interest to the target.

NTCP remained on average lower for DTRT than VMAT even when considering uncertainties.

5.2 Introduction

The treatment of loco-regionally advanced head and neck (H&N) cancer typically necessitates a multi-disciplinary approach involving chemotherapy, surgery, and radiation therapy (RT) [1]. This usually imposed toxicities such as xerostomia and dysphagia [2, 3].

For this treatment site, intensity modulated RT (IMRT) improved dosimetric sparing for organ-at-risk (OAR) adjacent to the target compared to 3D conformal RT and reduced toxicities [4]. Volumetric modulated arc therapy (VMAT) improved delivery efficiency compared to IMRT, by dynamic gantry rotation during beam-on [5]. IMRT and VMAT are today's state-of-the-art techniques for H&N cancer [6]. Recent developments extended these techniques by incorporating additional degrees-of-freedom: The research technique dynamic trajectory radiotherapy (DTRT) [7, 8] includes dynamic table and collimator rotation during beam-on. Compared to VMAT, DTRT has been shown to improve OAR sparing, while maintaining similar target coverage [9]. However, it was unclear if these dosimetric advantages persist amid uncertainties.

Uncertainties in patient-setup [10, 11] or in the mechanical accuracy of the beam defining machine components (such as gantry, table, collimator or multi-leaf collimator, MLC) [12] influence the delivered dose distribution. Despite using patient immobilization devices or patient-setup techniques (e.g., laser alignment, image-guidance, or surface-monitoring), intrafraction motion and patient-setup uncertainties persevered [13–15]. Kanakavelu et al. reported, that 35.2 %, 38.6 % and 4.8 % of their H&N cancer patients had setup uncertainties > 2 mm in lateral, longitudinal, and vertical direction, respectively [13]. Moreover, setup uncertainties < 3 mm were typically not corrected with daily image guidance RT protocols [16]. On the machine side, logfile analysis has been employed to study machine delivery uncertainties [17, 18]. Compared to patient-setup uncertainties, these were generally small (sub-degree, sub-mm). Studies showed

similar logfile-reported delivery uncertainties for DTRT and VMAT, indicating maintained mechanical accuracy for DTRT [9, 19, 20]. However, logfiles are insensitive to miscalibrations [21].

Patient-setup or machine-related uncertainties are included in planning target volume (PTV) margin concepts, which are designed to ensure acceptable target coverage for a majority of the patients, even under uncertainties. Margin concepts were developed for IMRT/VMAT but their appropriateness for DTRT must be validated, considering the use of additional beam directions and dynamic machine axes compared to VMAT. The impact of patient-setup or machine miscalibration uncertainties on DTRT plan quality should be comprehensively evaluated.

Robustness analysis to determine the uncertainties' impact on the dose distribution is common in proton therapy [22]. Data from photon treatment techniques is more limited, generally only focusing on the impact of patient-setup uncertainties on target coverage [23, 24]. However, uncertainties also impact OAR dose, frequently neglected in robustness studies [25]. Normal tissue complication probability (NTCP) models are based on OAR dose metrics and are clinically relevant, e.g. in the patient selection for proton- or photon-based treatments [26]. Uncertainties therefore impact also the NTCP. A previous large plan comparison for H&N cancer showed that DTRT improves OAR sparing for salivary glands and swallowing structures compared to VMAT, resulting in statistically significant lower NTCP for xerostomia and dysphagia [27]. However, the impact of patient- or machine-related uncertainties on the dosimetric plan quality was not investigated. Therefore, a comprehensive robustness assessment was needed to conclusively compare DTRT and VMAT and assess the potential clinical impact of uncertainties.

Consequently, the objective of this study was twofold: first, to conduct a comprehensive robustness assessment of DTRT and VMAT plans for H&N cancer cases, including the uncertainties' impact on the dose to target and OARs and on NTCP. Second, to compare the robustness of DTRT to VMAT plans, to identify the potential strengths and limitations of each technique in the presence

of uncertainties.

5.3 Materials and Methods

Patient cohort and treatment plans

This robustness study was based on DTRT and VMAT plans previously created for a treatment planning comparison for 46 patients with loco-regionally-advanced oropharyngeal carcinoma (supplementary table 5.1) [27], enrolled in the UPFRONT-NECK trial (NCT02918955) between 12.2016 and 4.2022. The patients provided informed consent. The robustness study extended the analysis of the planning study by assessing the impact of uncertainties on the plan quality to compare the robustness DTRT and VMAT plans.

The prescription was 50 Gy in 2 Gy fractions to the elective nodal volume and up to 70 Gy in the sequential boost phases. The doses were calculated using the Anisotropic Analytical Algorithm (AAA). The clinical target volume (CTV) and all OARs (including those above the plane defined by the VMAT beam directions (VMAT beam-plane)) were delineated following international guidelines [28, 29] and were included in the robustness assessment. Planning target volumes (PTVs) expanded the CTV by a 3 mm isotropic margin with a minimum 3 mm distance from the body contour. This PTV design aligned with international recommendations [28], accounting for our setup and IGRT technique (mask and CBCT) and considered setup uncertainties observed at our hospital and in literature [13, 14, 16]. Further beam set-up and planning details are available in the supplementary material. Fig. 5.1 shows the dynamic trajectory/arc setup for one of the 46 cases planned with DTRT/VMAT in three sequential phases.

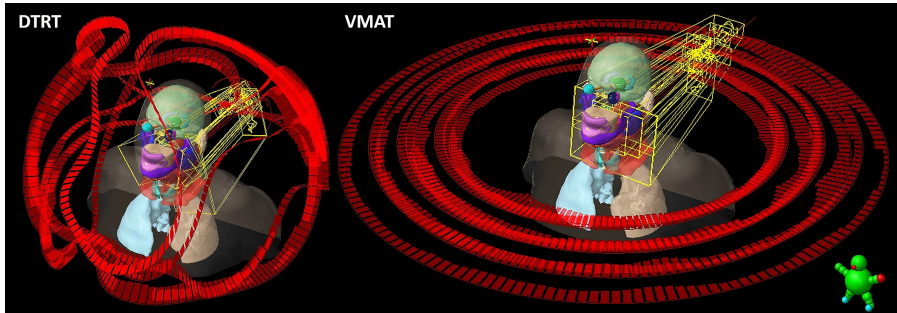


Figure 5.1: Dynamic trajectories (left) and arcs (right) for a H&N cancer case, planned with three phases. The red bands indicated the dynamic trajectories of the DTRT plans and VMAT arcs. The PTVs are shown in red, the OARs in other colors.

Robustness analysis

For the present study, robustness analysis including patient-setup and machine miscalibration uncertainties was performed with a previously developed robustness tool [12] interfaced with the Swiss Monte Carlo Plan (SMCP) and using Monte Carlo (MC) for dose calculation [30, 31] on a high-performance computing cluster. The dose was recalculated with MC for the nominal scenario (no uncertainty, without renormalization) and for each uncertainty scenario described below. The statistical uncertainty was $< 1.1\%$ for voxels with dose values higher than 50 % of the maximum dose.

The considered patient-setup uncertainty scenarios included a random component, to simulate intrafraction motion and inter-fraction setup uncertainties and different systematic components to simulate systematic setup uncertainties.

The random uncertainties were sampled from a Gaussian distribution with σ of 2 mm in anterior-posterior (AP), superior-inferior (SI) and left-right (LR) direction and σ of 0.5° in pitch, yaw and roll [23, 24]. For each case and plan, one uncertainty scenario including only random setup uncertainties was evaluated. Additionally, uncertainty scenarios combining the random setup uncertainties with

each of the following systematic uncertainties were considered: six systematic translational setup uncertainties (± 2 mm, ± 3 mm, ± 5 mm) in SI, AP or LR direction (6×3 uncertainty scenarios) and eight systematic rotational setup uncertainties ($\pm 0.5^\circ$, $\pm 1.0^\circ$, $\pm 2.0^\circ$, $\pm 3.0^\circ$) in pitch, yaw and roll (8×3 uncertainty scenarios).

The systematic uncertainties were based on literature but also included worst case scenarios [13, 14, 32]. This resulted in 43 uncertainty scenarios for random and systematic setup uncertainties per case and plan.

Furthermore, uncertainties in mechanical machine components were investigated. DTRT extends state-of-the-art treatment techniques by the combination of dynamic gantry, table and collimator rotation, along with MLC movement during delivery. The combined dynamic movement of these machine components increases the plan and delivery complexity compared to VMAT and makes it difficult to predict the impact of an uncertainty in the mechanical accuracy of these machine components on the dose distribution. It was therefore necessary to investigate these uncertainties before introducing DTRT into the clinics. The machine-related uncertainty scenarios included no random component, as previous machine logfile analysis found minimal delivery uncertainties [9, 20] with negligible impact on the dose distribution [12]. Miscalibrations were simulated by systematic uncertainties [21, 33–35]. Four systematic uncertainties ($\pm 1.0^\circ$, $\pm 2.0^\circ$) in gantry, table and collimator angle (4×3 uncertainty scenarios) and twelve systematic uncertainties (± 0.2 mm, ± 0.5 mm, ± 1.0 mm, ± 2.0 mm, ± 3.0 mm, ± 5.0 mm) in MLC position (12×1 uncertainty scenarios) were investigated.

MLC uncertainties were simulated by opening (positive)/closing (negative) all leaves at all controlpoints of the treatment plan. Already closed leaves remained unaffected by a negative uncertainty. This resulted in 24 uncertainty scenarios for machine uncertainties per case and plan.

Over all cases, dose distributions for 6164 uncertainty scenarios were calculated using approximately 140.000 CPU hours. The robustness of the DTRT and VMAT plans to the above-mentioned uncertainty scenarios was assessed and

compared by quantifying the uncertainties' impact on the fulfillment of treatment planning-goals (supplementary table) and the NTCP for xerostomia and dysphagia [36]. Additionally, a detailed robustness analysis of dose-volume endpoints for target and OARs was conducted.

Differences in DTRT and VMAT plan robustness were compared using Wilcoxon matched-pair signed rank test at 5 % significance level. Levene test with 5 % significance level was conducted to test for equal variances in endpoint differences. No correction for multiple testing was applied, exact p values were reported.

5.4 Results

Robustness of planning-goals

DTRT met more planning-goals for OARs in the VMAT beam-plane were in general better as compared to VMAT (Fig. 5.2 and supplementary material). Especially, when considering no or only random patient-setup uncertainties, DTRT plans fulfilled more planning-goals than VMAT plans. The difference was statistically significant for the oral cavity mean dose ($p = 0.05$): over all uncertainty scenarios and cases, the oral cavity mean-dose goal was respected for 2618 (DTRT) compared to 2352 (VMAT) uncertainty scenarios.

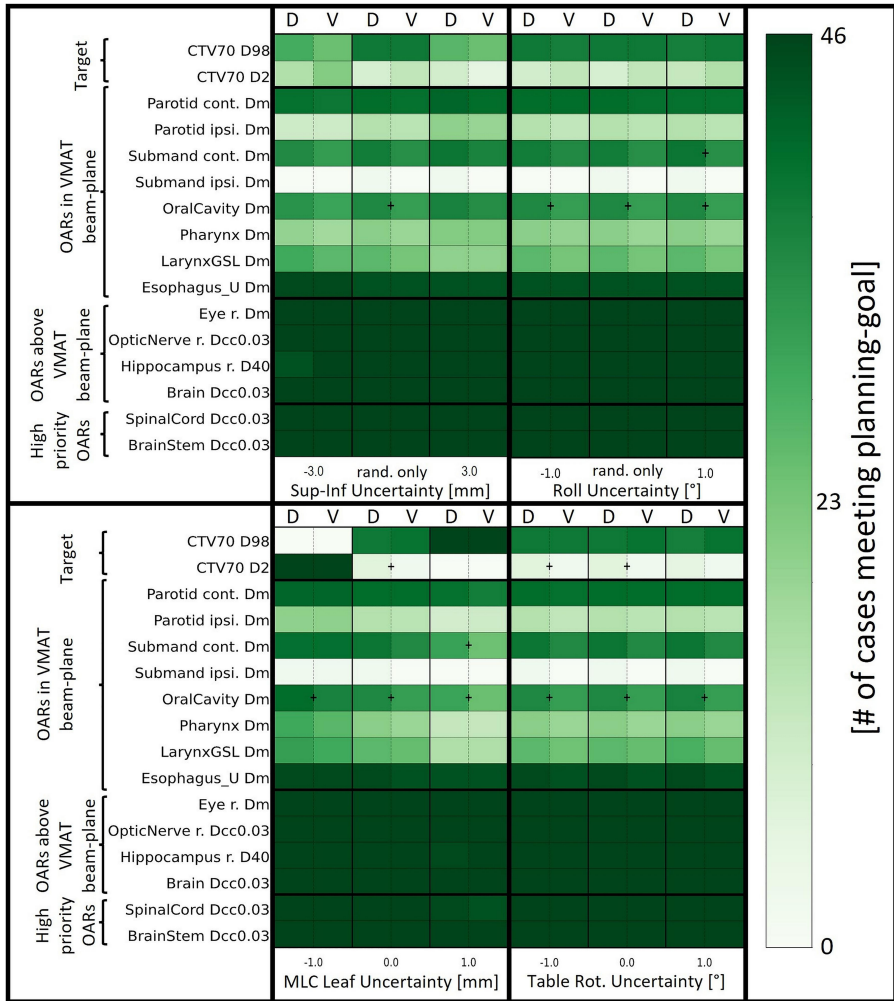


Figure 5.2: Number of DTRT (left facet, D) and VMAT (right facet, V) plans fulfilling representative planning-goals for selected uncertainty scenarios related to superior-inferior and roll patient-setup (top) and MLC position and table rotation (bottom). Significant ($\alpha < 5\%$) differences are indicated with a “+” sign. (Dm, mean dose; D2 and D98, dose to 2 % or 98 % of the structure volume; Dcc0.03, near max dose with volume 0.03 cm³).

Robustness of NTCP

The DTRT plans had significantly lower NTCP for moderate-to-severe xerostomia and grade \geq II dysphagia in both the nominal (0.5 and 2.1 percentage-points lower, respectively) and uncertainty scenarios, compared to VMAT (Fig. 5.3). Mean NTCP values for DTRT and VMAT plans were within 0.8 percentage-points of the nominal scenario values, except for uncertainty scenarios including MLC positions uncertainties, which deteriorated NTCP substantially more (> 3.3 and > 5.6 percentage-points for moderate-to-severe xerostomia and grade ≥ 2 dysphagia for DTRT and VMAT alike). The rainbow color-code indicates consistent NTCP order across cases, treatment technique and uncertainty scenarios. Similar trends were observed for severe xerostomia and dysphagia grade \geq III (supplementary material).

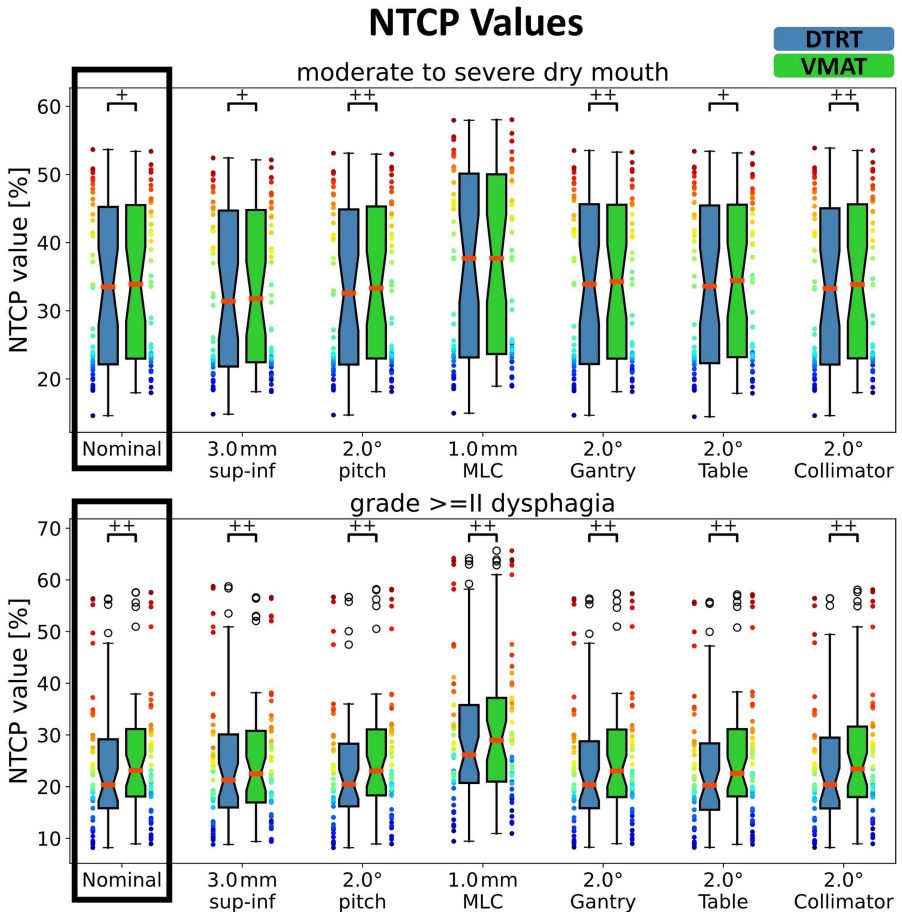


Figure 5.3: NTCP values of the DTRT and VMAT plans for the nominal scenario and representative uncertainty scenarios. Significant differences between DTRT and VMAT are indicated by: $\alpha < 0.05$ “+” and $\alpha < 0.01$ “++”. There is no significant difference in variance. Each of the rainbow colored dots corresponds to a datapoint of a single case. The color-code identifies the plans for the same case across the treatment techniques and uncertainty scenarios.

Detailed robustness analysis

The MC dose recalculation led to an average [minimum, maximum] PTV underdosage of 1.9 Gy [-0.1, 5.4] for DTRT and 1.9 Gy [0.5, 5.6] for VMAT, compared

to the AAA dose calculation of the nominal scenario ($D95\%_{PTV70}$, $p = 0.05$).

Degradation of $D98\%_{CTV70}$ due to random patient-setup uncertainties was not statistically significant ($p > 0.43$) for both DTRT and VMAT (Fig. 5.4). MLC miscalibration uncertainties resulted in the largest average differences, with an average 5 Gy increase of $D98\%_{CTV70}$ for a 1 mm opening for DTRT and VMAT. Statistically significant differences in robustness between DTRT and VMAT were observed for systematic uncertainties (e.g. a 3 mm uncertainty in superior-direction, $p < 0.01$).

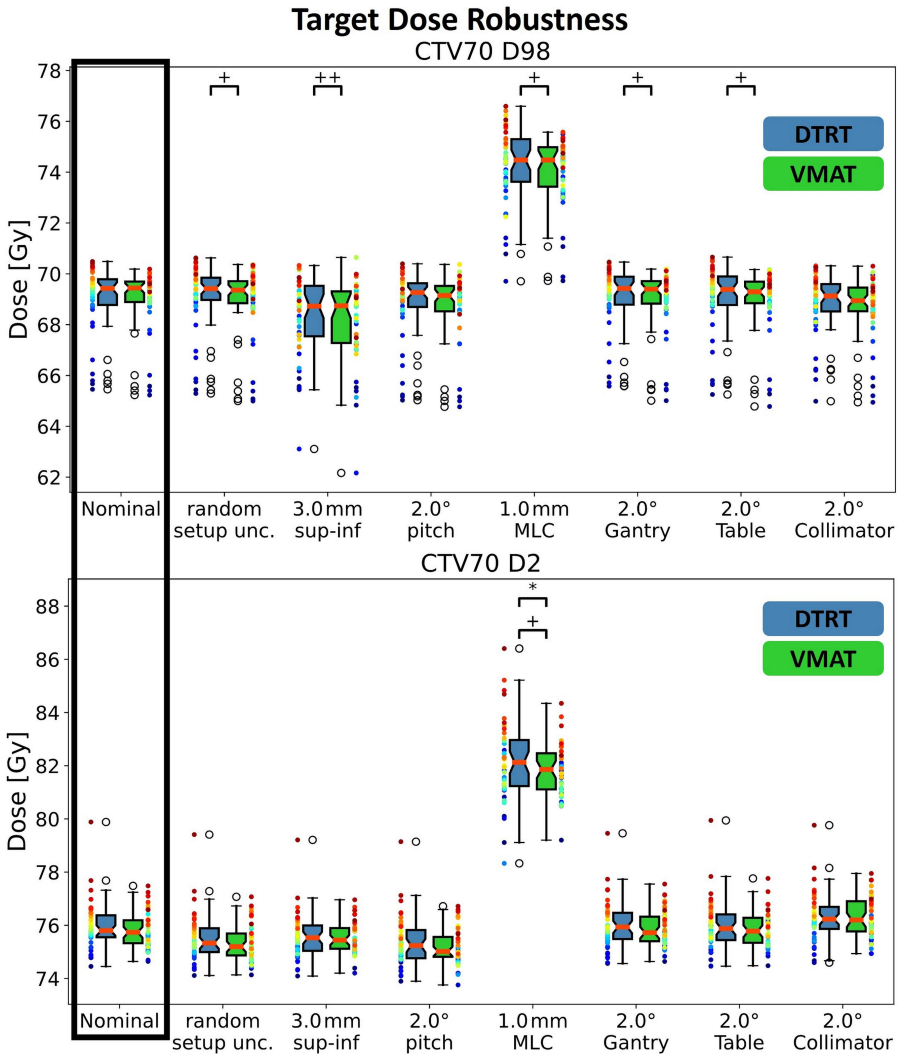


Figure 5.4: Impact of representative uncertainty scenarios on CTV70 endpoints. Significant ($\alpha < 5\%$) differences in robustness and in the variance between DTRT and VMAT plans are indicated by “+” and “*” respectively. “++” indicates significance with $\alpha < 1\%$. Scenarios 3 mm sup-inf and 2.0° pitch also include random uncertainties. Each of the rainbow colored dots corresponds to a datapoint of a single case. The color-code identifies the plans for the same case across the treatment techniques and uncertainty scenarios.

OAR robustness to the investigated dose-volume endpoints was depended on the location of the OAR with respect to the VMAT beam plane (Fig. 5.5 and supplementary material). The differences in mean dose to OARs for the DTRT and VMAT plans in the VMAT beam-plane caused by random patient-setup uncertainties were within 0.8 Gy on the average. The difference between DTRT and VMAT was not statistically significant, except for the contralateral submandibular gland, $p < 0.01$ (Fig. 5.5 and supplementary material). For patient-setup uncertainties, the largest differences were observed in the SI direction: a 5 mm systematic uncertainty in inferior direction increases the ipsilateral parotid mean dose by 3.7 Gy [-5.2, 13.3] (DTRT) and 4.1 Gy [-5.7, 14.4] (VMAT, $p < 0.01$). The nominal dose to OARs above the VMAT beam-plane was close to zero for VMAT and significantly higher for DTRT: The mean dose to both eyes was on average 2.8 Gy ($p < 0.01$) higher and D0.03 cc to both optic nerves was on average 5.4 Gy ($p < 0.01$) higher. For all patient-setup uncertainty scenarios the dose difference to the nominal scenario for above-mentioned OARs remained below < 0.9 Gy (< 3.6 Gy) for VMAT (DTRT).

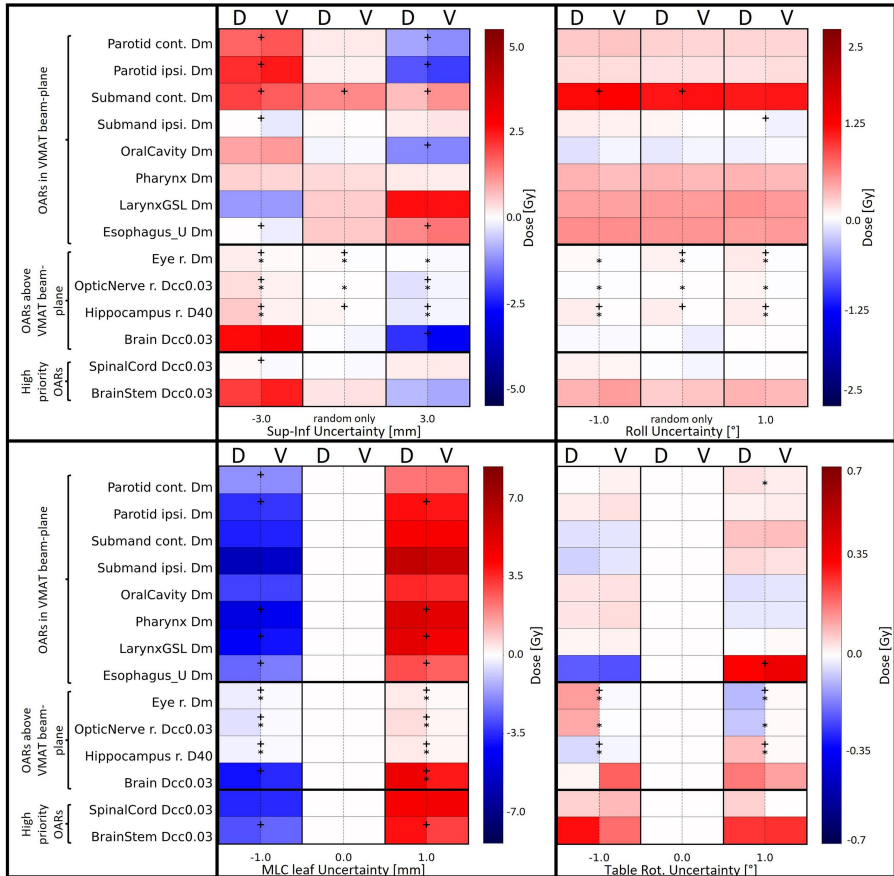


Figure 5.5: Average difference with respect to the nominal scenario for DTRT (left facet, D) and VMAT (right facet, V) for patient-setup and machine position uncertainties. Depending on the uncertainty, different ranges for the differences are given, with the largest one for MLC uncertainties and the smallest one for table rotation uncertainties. Significant ($\alpha < 5\%$) differences in robustness of the dose-volume endpoints between DTRT and VMAT are indicated by a “+” sign; significant ($\alpha < 5\%$) differences in the variance of the DTRT and VMAT robustness are indicated by a “*”. OARs in the VMAT beam-plane are shown in the upper part, followed by representative OARs above the VMAT beam-plane and the brain stem and spinal cord. (Dm, mean dose; D2 and D98, dose to 2% or 98% of the structure volume; Dcc0.03, near max dose with volume 0.03 cm³)

Gantry, table, and collimator angle uncertainties of $\pm 1^\circ$ resulted in average differences of < 0.7 Gy for all investigated OAR endpoints for both, DTRT and VMAT. MLC uncertainties resulted in substantially increased (opening) or decreased (closing of the leaves) dose.

For OARs in the VMAT beam-plane, the variance in robustness was not significantly different between DTRT and VMAT. For most OARs above the VMAT beam-plane, except for the brain, the dose difference to the nominal scenario varied for most uncertainty scenarios significantly ($p < 0.05$) between DTRT and VMAT.

Two example cases, case (A) and (B) with a CTV50 of 406 cm^3 and 59 cm^3 , are analyzed in Fig. 5.6. For case (A), the DTRT plan met more planning-goals than VMAT for the investigated uncertainties. The opposite was true for case (B). The largest differences were observed for the oral cavity mean dose (case A, 2.9 Gy lower for DTRT) and hippocampus D40% (case B, 7.2 Gy lower for VMAT), indicated by white arrows.

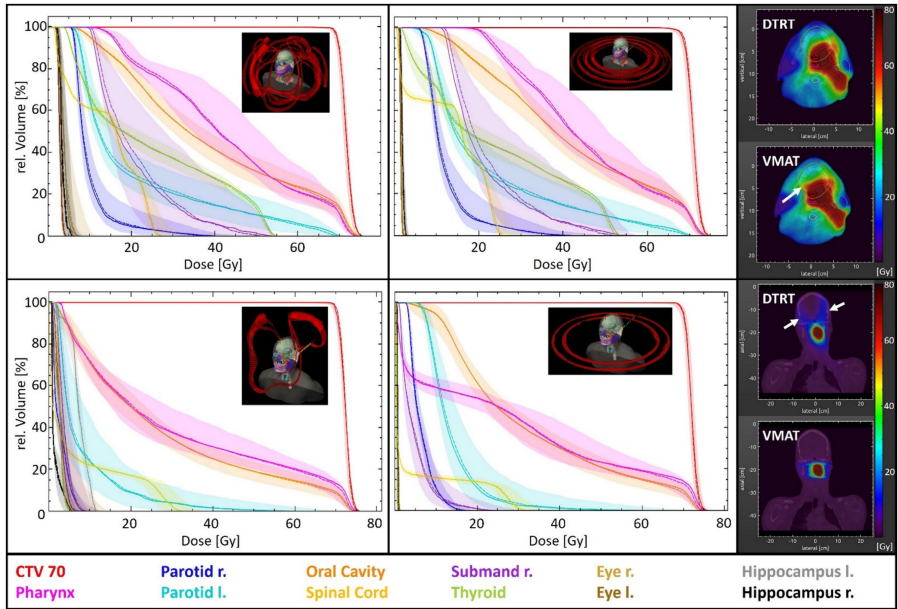


Figure 5.6: DVH and nominal dose distribution comparison of the DTRT and VMAT plan for two example cases (A) and (B). Additionally, the dynamic trajectory/arc setup is shown by the red bands around the patient. The solid DVH lines represents the nominal scenario. The dashed line represents the uncertainty scenario with only random setup uncertainties, and the DVH bands include all random plus systematic patient-setup uncertainties. The arrows indicate the location of the greatest differences in the dose distribution between the DTRT and VMAT plan.

For both cases, DTRT had lower NTCP values than VMAT. The largest differences were observed for moderate to severe dry mouth and grade \geq II dysphagia, where the difference in NTCP was 1.7 and 3.5 percentage-points for case (A), and 3.4 and 0.7 percentage-points for case (B). The largest difference in NTCP robustness evaluated on all uncertainty scenarios was observed for grade \geq II dysphagia and 1 mm MLC uncertainties, where the DTRT (VMAT) plans varied by 9.6 and 4.2 (9.3 and 3.7) percentage-points for case A and case B, respectively.

5.5 Discussion

The present robustness analysis was the first study to systematically analyze DTRT and VMAT plan robustness for a large cohort. Comparing their robustness enabled to assess if the dosimetric and NTCP benefits of DTRT persisted in the presence of uncertainties. The robustness analysis included three major novel aspects: First, clinical relevance was investigated by assessing the impact of uncertainties on planning-goals and NTCP for xerostomia and dysphagia. Second, next to target also OAR robustness was evaluated. Third, alongside patient-setup, machine-related uncertainties were investigated. This study substantially added to our treatment plan comparison [27] by extending the evaluation from the nominal to realistic uncertainty scenarios, recognizing robustness as an integral part of plan quality [37].

For 46 H&N cases, DTRT and VMAT planning-goal robustness showed no significant difference, except for oral cavity mean dose (favoring DTRT) and hippocampus D40% (favoring VMAT). Generally, DTRT plans respected more planning-goals compared to VMAT across all uncertainty scenarios except for the CTV70 near max dose, brachial plexus and hippocampus. Planning-goal robustness further depended on the structures location with respect to the VMAT beam-plane: those above received only scattered dose with VMAT but could be in the primary beam path for DTRT. Thus, uncertainties were likely to induce greater absolute changes in dose in these regions for DTRT than for VMAT. Nonetheless, doses to optical and auditory structures remained well below planning-goals, even with uncertainties. This was not the case for the hippocampus; hence the use of planning organ at risk volumes (PRVs) for DTRT is recommended. Structures in the VMAT beam-plane (parotids, submandibular glands and oral cavity) benefited from improved sparing with DTRT, facilitating planning-goal fulfillment. It should be noted that cases meeting one planning-goal could differ from those meeting another. Furthermore, the OAR planning-goals vary in importance and should only

serve as an initial evaluation point, while focusing on the “as low as reasonably achievable” (ALARA) principle [38].

While NTCP robustness has been mainly studied in the context of proton therapy [39, 40], the present study confirmed and complemented these findings with patient-setup and machine-related uncertainties for state-of-the-art VMAT and novel DTRT photon-based treatments. Our results were in line with previous findings [39]: patient- and machine-related uncertainties (except MLC uncertainties) had little influence on the average NTCP (within 0.8 percentage-points on average) over all patients. Importantly, DTRT had on average, lower NTCP than VMAT for all considered uncertainty scenarios, except for MLC position uncertainties, where predicted xerostomia for DTRT was slightly higher than for VMAT. However, this difference was not statistically significant.

In the detailed investigation, we found that CTV coverage was lower when calculated with MC than with AAA. Target coverage robustness was similar between DTRT and VMAT, indicating that the PTV design was appropriate for DTRT. DTRT plans had steeper dose gradients in the VMAT beam-plane at the cost of increased dose to OARs above it. Furthermore, a directional trend, especially for non-central structures, was observed. For instance, contralateral parotid mean dose was more robust for DTRT with SI setup uncertainties but less for uncertainties in AP direction, partially due to VMAT’s steeper dose gradients in the SI direction. The individual robustness analysis of the two cases highlighted the robustness tool’s [12] applicability to evaluate plan robustness prior to delivery. Moreover, in the clinic, it could serve as an independent dose calculation for the generated plans. In such a case-by-case usage, also the combination of uncertainties could be evaluated, similar to previous studies [12, 19]. In clinical practice, patient-setup and machine uncertainties can occur simultaneously. A comprehensive robustness assessment would therefore need to consider both uncertainty types in combination.

In the uncertainty scenario selection, we included random and systematic patient-setup uncertainties observed in clinical practice, as well as worst-case

scenarios. The magnitudes of the patient-setup uncertainties were based on literature [13–16, 23, 24, 32]. Machine uncertainties (e.g., MLC position uncertainty [21, 35]) were selected according to tolerance limits [41, 42], to investigate the effect of realistic miscalibrations. For investigative purposes, additional uncertainty scenarios beyond those limits that are commonly found in literature were assessed but should be considered extreme scenarios [21, 33–35]. In a clinical delivery setting, routine QA checks, as well as patient-specific QA are performed [43], aiming to detect machine miscalibrations outside the tolerance limits. Regarding dosimetric impact, we observed that rotational patient-setup uncertainties ($\leq 3^\circ$) had less impact than uncertainties in AP, SI or LR (≤ 5 mm) on the investigated endpoints. Similarly, uncertainties in the rotational machine components of up to $\pm 2^\circ$ had less impact, than the investigated uncertainties in the MLC positions.

Apart from standard margins for the target, brainstem and spinal cord, no specific robustness measures were taken in this study, which could be seen as a limitation. While proton treatments are usually robustly optimized [44, 45], robust optimization for photon-based treatments is not state-of-the-art yet. In future, patient- and machine-related uncertainties could be considered during robust optimization. Additionally, because DTRT paths were based on individual patient anatomy, robustness could be considered at the path-finding step of the treatment planning process.

In conclusion, this study thoroughly analyzed the robustness of DTRT and VMAT plans for 46 H&N cancer cases and a large range of uncertainty scenarios. Generally, no significant difference in planning-goal robustness between DTRT and VMAT was observed for the investigated uncertainties. DTRT had significantly lower NTCP for xerostomia and dysphagia than VMAT and this advantage generally remained for the investigated uncertainties.

5.6 CRediT authorship contribution statement

HAL: Conceptualization, Formal analysis, Investigation, Methodology, Software, Visualization, Writing – original draft, Writing – review & editing. JB: Conceptualization, Investigation, Methodology, Supervision, Writing – review & editing. P-HM, WV, OE, SM, GG, DMA: Methodology, Writing – review & editing. MFMS: Supervision, Writing – review & editing. MKF, PM: Conceptualization, Methodology, Project administration, Resources, Supervision, Writing – review & editing.

5.7 Declaration of competing interest

The authors declare that they have no known competing financial interests or personal relationships that could have appeared to influence the work reported in this paper.

5.8 Acknowledgements

This work was supported by Varian, a Siemens Healthineers Company. The MC dose calculations were performed on UBELIX (www.id.unibe.ch/hpc), the HPC cluster at the University of Bern.

5.9 Data statement

Research data are not available at this time.

REFERENCES

1. Lo Nigro, C., Denaro, N., Merlotti, A. & Merlano, M. Head and neck cancer: Improving outcomes with a multidisciplinary approach. *Cancer Management and Research* **9**, 363–371. ISSN: 11791322 (2017).
2. Dirix, P., Nuyts, S., Poorten, V. V., Delaere, P. & Bogaert, W. V. D. The influence of xerostomia after radiotherapy on quality of life: Results of a questionnaire in head and neck cancer. *Support Care Cancer* **16**, 171–179. ISSN: 09414355 (Aug. 2008).
3. Baudalet, M. *et al.* Very late xerostomia, dysphagia, and neck fibrosis after head and neck radiotherapy. *Head and Neck* **41**, 3594–3603. ISSN: 10970347 (2019).
4. Nutting, C. M. *et al.* Parotid-sparing intensity modulated versus conventional radiotherapy in head and neck cancer (PARSPORT): A phase 3 multicentre randomised controlled trial. *The Lancet Oncology* **12**, 127–136. ISSN: 14702045 (2011).
5. Otto, K. Volumetric modulated arc therapy: IMRT in a single gantry arc. *Medical Physics* **35**, 310–317. ISSN: 2473-4209 (Aug. 2008).
6. Teoh, M., Clark, C. H., Wood, K., Whitaker, S. & Nisbet, A. Volumetric modulated arc therapy: A review of current literature and clinical use in practice. *Brit J Radiol* **84**, 967–996. ISSN: 00071285 (2011).

7. Fix, M. K. *et al.* Part 1: Optimization and evaluation of dynamic trajectory radiotherapy. *Medical Physics* **45**, 4201–4212. ISSN: 00942405 (Aug. 2018).
8. Smyth, G., Evans, P. M., Bamber, J. C. & Bedford, J. L. Recent developments in non-coplanar radiotherapy. *Brit J Radiol* **92**. ISSN: 1748880X (Aug. 2019).
9. Bertholet, J. *et al.* Organ-at-risk sparing with dynamic trajectory radiotherapy for head and neck cancer: comparison with volumetric arc therapy on a publicly available library of cases. *Radiation oncology (London, England)* **17**, 122. ISSN: 1748-717X (Aug. 2022).
10. Hunt, M. A. *et al.* The effect of setup uncertainties on the treatment of nasopharynx cancer. *International Journal of Radiation Oncology, Biology, Physics* **27**, 437–447. ISSN: 03603016 (1993).
11. Stroom, J. C. & Heijmen, B. J. M. Geometrical uncertainties, radiotherapy planning margins, and the ICRU-62 report. *Radiother Oncol* **64**, 75–83. ISSN: 01678140 (2002).
12. Loebner, H. A. *et al.* Development of a Monte Carlo based robustness calculation and evaluation tool. *Medical Physics* **49**, 4780–4793. ISSN: 24734209 (2022).
13. Kanakavelu, N. & Samuel, J. J. Determination of patient set-up error and optimal treatment margin for intensity modulated radiotherapy using image guidance system. *J BUON* **2**, 505–511. ISSN: 1107-0625 (2016).
14. Boda-Heggemann, J. *et al.* Repositioning accuracy of two different mask systems-3D revisited: Comparison using true 3D/3D matching with cone-beam CT. *International Journal of Radiation Oncology Biology Physics* **66**, 1568–1575. ISSN: 03603016 (2006).

15. Billiet, C. *et al.* Precision of image-guided spinal stereotactic ablative radiotherapy and impact of positioning variables. *Physics and imaging in radiation oncology* **22**, 73–76. ISSN: 2405-6316 (Apr. 2022).
16. Delishaj, D. *et al.* Set-up errors in head and neck cancer treated with IMRT technique assessed by cone-beam computed tomography: a feasible protocol. *Radiation Oncology Journal* **36**, 54–62. ISSN: 22343164 (Aug. 2018).
17. Qian, J. *et al.* Dose reconstruction for volumetric modulated arc therapy (VMAT) using cone-beam CT and dynamic log files. *Physics in Medicine & Biology* **55**, 3597–3610. ISSN: 0031-9155 (Aug. 2010).
18. Olasolo-Alonso, J., Vázquez-Galiñanes, A., Pellejero-Pellejero, S. & Pérez-Azorín, J. F. Evaluation of MLC performance in VMAT and dynamic IMRT by log file analysis. *Phys Med* **33**, 87–94. ISSN: 1120-1797 (Aug. 2017).
19. Loebner, H. A. *et al.* Impact of the gradient in gantry-table rotation on dynamic trajectory radiotherapy plan quality. *Medical Physics* **50**, 7104–7117. ISSN: 2473-4209 (Sept. 2023).
20. Loebner, H. A. *et al.* Technical note: Feasibility of gating for dynamic trajectory radiotherapy – Mechanical accuracy and dosimetric performance. *Medical Physics* **50**, 6535–6542. ISSN: 0094-2405 (Aug. 2023).
21. Katsuta, Y. *et al.* Log file-based patient dose calculations of double-arc VMAT for head-and-neck radiotherapy. *Phys Med* **48**, 6–10. ISSN: 1120-1797 (Aug. 2018).
22. Malyapa, R. *et al.* Evaluation of Robustness to Setup and Range Uncertainties for Head and Neck Patients Treated with Pencil Beam Scanning Proton Therapy. *International Journal of Radiation Oncology Biology Physics* **95**, 154–162. ISSN: 1879355X (2016).
23. Verma, M. *et al.* An audit of setup reproducibility in radiotherapy of head and neck cancers. *J Radiat Cancer Res* **7**, 85–89. ISSN: 0973-0168 (2016).

24. Dzierma, Y. *et al.* Set-up errors and planning margins in planar and CBCT image-guided radiotherapy using three different imaging systems: A clinical study for prostate and head-and-neck cancer. *Phys Med* **31**, 1055–1059. ISSN: 1724191X (2015).
25. Herk, M. V. Errors and Margins in Radiotherapy. *Seminars in Radiation Oncology* **14**, 52–64. ISSN: 10534296 (2004).
26. Langendijk, J. A. *et al.* Clinical Trial Strategies to Compare Protons With Photons. *Seminars in Radiation Oncology* **28**, 79–87. ISSN: 15329461 (2018).
27. Bertholet, J. *et al.* Organs-at-risk dose and normal tissue complication probability with dynamic trajectory radiotherapy (DTRT) for head and neck cancer. *Radiotherapy and Oncology* **195**. ISSN: 18790887 (June 2024).
28. Sun, Y. *et al.* Recommendation for a contouring method and atlas of organs at risk in nasopharyngeal carcinoma patients receiving intensity-modulated radiotherapy. *Radiother Oncol* **110**, 390–397. ISSN: 18790887 (2014).
29. Brouwer, C. L., Steenbakkers, R. J., Langendijk, J. A. & Sijtsema, N. M. Identifying patients who may benefit from adaptive radiotherapy: Does the literature on anatomic and dosimetric changes in head and neck organs at risk during radiotherapy provide information to help? *Radiother Oncol* **115**, 285–294. ISSN: 18790887 (2015).
30. Fix, K. *et al.* Efficient photon treatment planning by the use of Swiss Monte Carlo Plan. *Journal of Physics: Conference Series* **74**, 21004. ISSN: 1742-6596 (Aug. 2007).
31. Fix, M. K. *et al.* An efficient framework for photon Monte Carlo treatment planning. *Physics in Medicine and Biology* **52**, 425–437. ISSN: 00319155 (2007).

32. Rodrigues, M. F. *et al.* The influence of a six degrees of freedom couch and an individual head support in patient positioning in radiotherapy of head and neck cancer. *Physics and Imaging in Radiation Oncology* **11**, 30–33 (2019).
33. LoSasso, T., Chui, C.-S. & Ling, C. C. Physical and dosimetric aspects of a multileaf collimation system used in the dynamic mode for implementing intensity modulated radiotherapy. *Medical Physics* **25**, 1919–1927. ISSN: 2473-4209 (Aug. 1998).
34. May, L. *et al.* Multi-institutional investigation into the robustness of intracranial multi-target stereotactic radiosurgery plans to delivery errors. *Medical Physics* **51**, 910–921. ISSN: 2473-4209 (Feb. 2024).
35. Katsuta, Y. *et al.* Quantification of residual dose estimation error on log file-based patient dose calculation. *Phys Med* **32**, 701–705. ISSN: 1120-1797 (Aug. 2016).
36. Nederslandse Vereniging voor Radiotherapie en Oncologie. *Landelijk Indicatie Protocol Protonentherapie (versie 2.2) (LIPPv2.2)*, accessed on 25.10.2023 2019. <https://docplayer.nl/195792198-Landelijk-indicatie-protocol-protonentherapie-versie-2-2-lippv2-2.html>.
37. Hernandez, V. *et al.* What is plan quality in radiotherapy? The importance of evaluating dose metrics, complexity, and robustness of treatment plans. *Radiother Oncol* **153**, 26–33. ISSN: 18790887 (2020).
38. Hendee, W. R. & Edwards, F. M. ALARA and an integrated approach to radiation protection. *Seminars in Nuclear Medicine* **16**, 142–160. ISSN: 00012998 (1986).
39. Hamming-Vrieze, O. *et al.* Impact of setup and range uncertainties on TCP and NTCP following VMAT or IMPT of oropharyngeal cancer patients. *Physics in Medicine and Biology* **64**. ISSN: 13616560 (2019).

REFERENCES

40. Smolders, A. *et al.* Inter- and intrafractional 4D dose accumulation for evaluating Δ NTCP robustness in lung cancer. *Radiother Oncol* **182**. ISSN: 18790887 (2023).
41. Barnes, M. P. & Greer, P. B. Evaluation of the truebeam machine performance check (MPC): mechanical and collimation checks. *Journal of Applied Clinical Medical Physics* **18**, 56–66. ISSN: 1526-9914 (Aug. 2017).
42. Palta, J. R., Kim, S., Li, J. G. & Liu, C. in *Intensity-modulated radiation therapy: the state of the art* (eds Palta, J. R. & Mackie, T. R.) 593–612 (2003). ISBN: 9781930524163.
43. Klein, E. E. *et al.* Task Group 142 report: quality assurance of medical accelerators. *Medical physics* **36**, 4197–4212. ISSN: 0094-2405 (2009).
44. Unkelbach, J. *et al.* Robust radiotherapy planning. *Physics in Medicine and Biology* **63**. ISSN: 13616560 (Aug. 2018).
45. Liu, W., Zhang, X., Li, Y. & Mohan, R. Robust optimization of intensity modulated proton therapy. *Medical Physics* **39**, 1079–1091. ISSN: 00942405 (2012).

5.10 Appendix

Patients characteristics

Table 5.1: Patients characteristics used in this study.

Age	median (range)	62 (50-70)
Sex	N (%)	
M		30 (65.2)
F		16 (34.2)
HPV status	N (%)	
Positive		24 (52.5)
Negative		22 (47.8)
T stage	N (%)	
1		6 (13.0)
2		22 (47.8)
3		11 (23.9)
4a		7 (15.2)
N stage	N (%)	
1		5 (10.9)
2a		6 (13.0)
2b		26 (56.5)
2c		9 (19.6)
Primary tumor localization	N (%)	
Hypopharynx		5 (10.9)
Oropharynx		37 (80.4)
Larynx		4 (8.7)
Neck dissection	N (%)	
Yes		22 (47.8)
No		24 (52.2)
Baseline xerostomia	N (%)	
None		46 (100.0)
Mild		0 (0.0)
Moderate or severe		0 (0.0)
Baseline dysphagia	N (%)	
0-I (solid food)		41 (89.1)
II (soft food)		4 (8.7)
III-IV (liquid food or SV)		1 (2.2)
PTV volume (cc)	median (range)	
Phase I (50 Gy)		416.77 (83.68 – 800.23)
Phase II (66 Gy, n = 15)		137.63 (77.38 – 222.67)
Phase II (70 Gy, n = 31)		96.47 (19.23 – 402.70)
Phase III (70 Gy, n = 15)		74.01 (39.45 – 157.52)

The patients were enrolled in the prospective clinical UPFRONT-NECK trial (NTC02918955) [1].

Treatment planning process

DTRT and VMAT plans were created for a prescription dose of 50 Gy delivered in 2 Gy fractions to the elective nodal volume, with sequential boost to 66 Gy for nodal levels with extra nodular extension and to 70 Gy for non-operated primary tumor and involved lymph nodes. DTRT plans were created using a geometric based planning approach [2] with particular focus on sparing of OARs close to the PTV including oral cavity and salivary glands.

DTRT and VMAT treatment plans were generated for a 6 MV-flattened beam on a TrueBeam linac (Varian Medical Systems) equipped with a 120-leaf Millennium MLC and a PerfectPitch 6-degree-of-freedom table. For DTRT and VMAT plan generation, the planning procedure described in [3] is followed. In short: DTRT plans include intensity modulation by the MLC, dynamic gantry, table, and collimator rotation during beam-on. The gantry-table path minimizes the fractional volume overlap, weighted according to a depth dose curve of a 6 MV photon beam in water of selected OARs with the target in beam's eye view. Details of OAR selection for path-finding can be found in [3]. Gantry-table-path-finding accounts for restriction zones due to end of CT stack and case-specific collision maps [4]. The dynamic collimator rotation minimizes the field width in leaf travel direction along the gantry-table path. VMAT plans use the same number of arcs as paths in the DTRT plans. Collimator angle for the VMAT plans were set to 5° or 95°. Depending on the size of the PTV, DTRT and VMAT treatment plans with 2-4 arcs/dynamic trajectories were created. Field-splitting in leaf-travel direction using the secondary collimator jaws (for large targets) or 90° collimator rotation offset (for small targets) was applied to duplicate arcs/paths.

DTRT and VMAT plans were optimized by the same planner in Eclipse, using the photon optimizer and the analytical anisotropic algorithm for intermediate and

final dose calculation (Research version embedded in the Aria 15.6 framework, Varian) following the manual planning guidelines to mitigate planner bias [3]. The plans were normalized to $PTV_{D95\%} = 100\%$ of the prescription. The aim was to obtain similar target coverage for DTRT and VMAT; techniques were then compared based on OAR sparing and NTCP. All plans were reviewed by a radiation oncologist for clinical acceptability, ensuring that target coverage and mandatory OAR constraints of our internal guidelines were fulfilled. Based on the nominal scenario (no uncertainties), the resulting plans are compared for OAR sparing in a planning comparison study [5].

Planning goals

Table 5.2: Planning-Goals

Organ	Goal
Spinal Cord	Dcc0.0345 Gy
Brainstem	Dcc0.0354 Gy
Hippocampus (l./r.)	D40% \leq 7.3 Gy
Pharynx	Dmean \leq 45 Gy D50Gy \leq 33%
Larynx GLS	Dmean \leq 35 Gy
Cochlea (l./r.)	Dcc0.03 \leq 45 Gy
Esophagus u.	Dmean \leq 40 Gy
Lips	Dmean \leq 20 Gy Dmax \leq 30%
Oral cavity – PTV	Dmean \leq 40 Gy
Mandible	D2% \leq 70 Gy
Brachial Plexus	Dcc0.03 \leq 66 Gy
Brain	Dcc0.03 \leq 45 Gy
Eye (l./r.)	Dcc0.03 \leq 45 Gy Dmean \leq 35 Gy
Lachrymal gland (l./r.)	Dmean \leq 30 Gy
Submandibular gland (l./r.)	Dmean \leq 35 Gy
Lens (l./r.)	Dcc0.03 \leq 6 Gy
Optic chiasm	Dcc0.03 \leq 54 Gy
Optic nerve (l./r.)	Dcc0.03 \leq 54 Gy
Inner ear (l./r.)	Dmean \leq 45 Gy
Thyroid	V50Gy \leq 60%

Additionally, D98% \geq 68.6 Gy and D2% \leq 74.9Gy are introduced for CTV70 to evaluate target robustness. Spinal cord and brain stem including their planning at risk volume (PRVs) had priority over the target planning goals during planning.

As the VMAT plans always respected the planning goals for optical and auditory structures, and the hippocampus, they were considered mandatory planning

goals during planning. The other planning goals were respected as good as possible and the dose was reduced as much as possible with particular focus on reducing dose to oral cavity, pharynx and salivary glands.

Robustness of with respect to planning goals

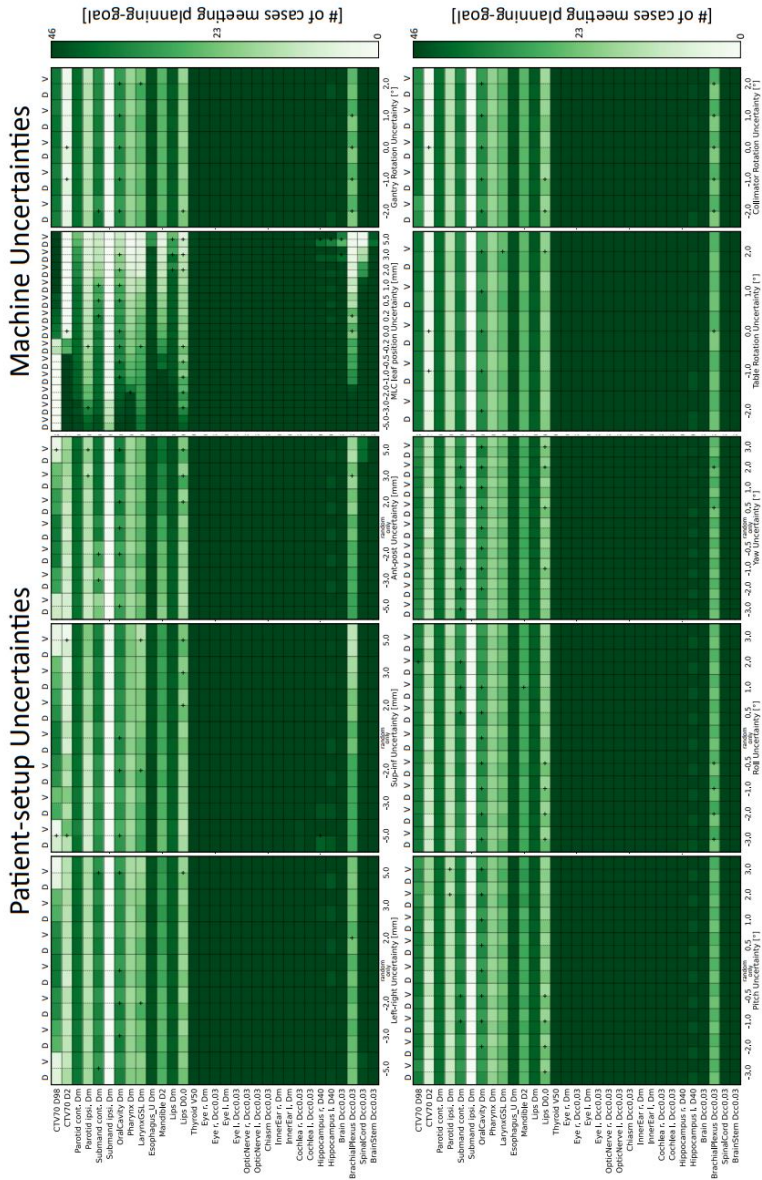


Figure 5.7: Number of DTRT (left panel) and VMAT (right panel) plans fulfilling planning-goals for the investigated uncertainty scenarios related to patient setup (left) and machine position (right). Significant ($\alpha < 5\%$) differences are indicated with a "+" sign.

Robustness of NTCP

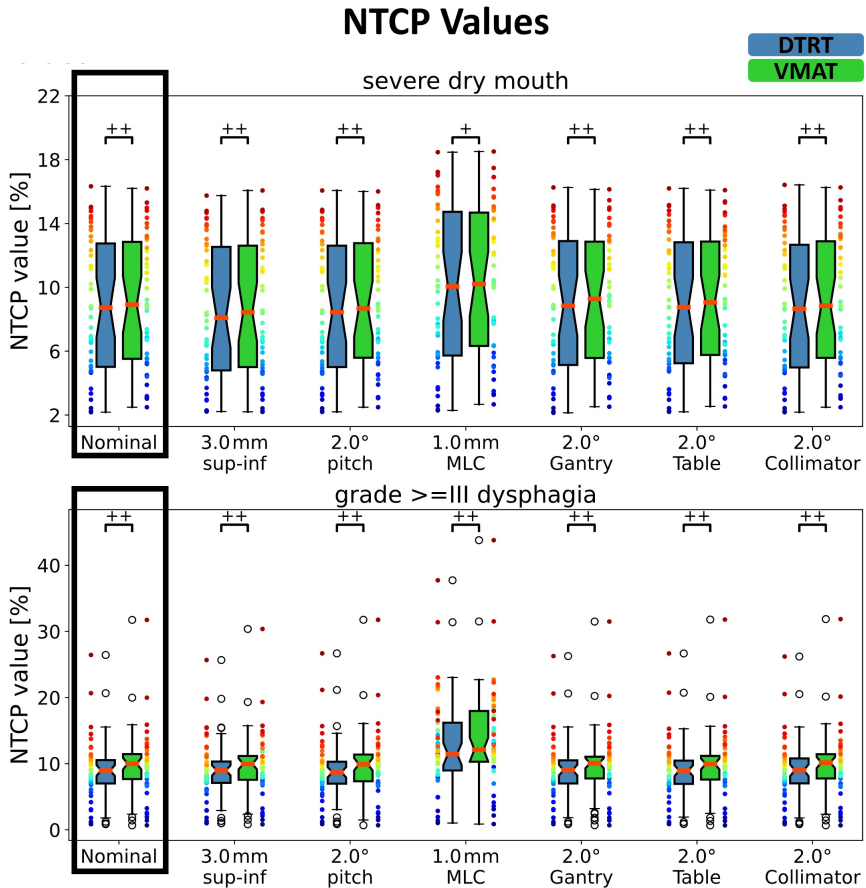


Figure 5.8: NTCP values of the DTRT and VMAT plans for the nominal scenario and representative uncertainty scenarios for severe dry mouth and grade \geq III dysphagia. Significant differences between DTRT and VMAT are indicated by: $\alpha < 0.05$ “+” and $\alpha < 0.01$ “++”. There is no significant difference in variance. Each of the “rainbow” colored dots corresponds to a datapoint of a single case. The colorcode identifies the plans for the same case across the treatment techniques and uncertainty scenarios.

Robustness of OARs

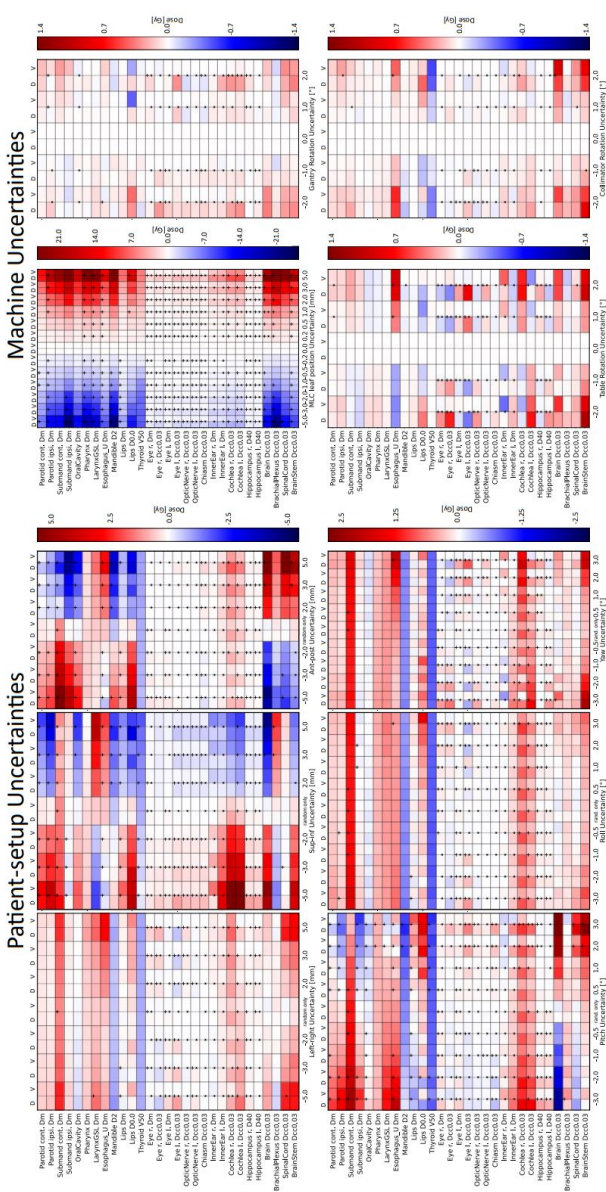


Figure 5.9: Average difference of DTRT (left panel) and VMAT (right panel) for the patient setup and machine position uncertainties as compared to the nominal scenario. A deeper color indicates a greater difference with lower dose in blue and higher dose in red. Significant ($\alpha < 5\%$) differences in robustness of the dose-volume parameter between DTRT and VMAT are indicated by a “+” sign, significant ($\alpha < 5\%$) differences in the variance of the DTRT and VMAT robustness are indicated by a “*”.

REFERENCES

1. Insel Gruppe AG. *Definitive Chemo-Radiotherapy for Regionally Advanced Head and Neck Cancer With or Without Up-front Neck Dissection*, accessed on 26.10.2023 2023. <https://classic.clinicaltrials.gov/ct2/show/NCT02918955>.
2. Fix, M. K. *et al.* Part 1: Optimization and evaluation of dynamic trajectory radiotherapy. *Medical Physics* **45**, 4201–4212. ISSN: 00942405 (Aug. 2018).
3. Bertholet, J. *et al.* Organ-at-risk sparing with dynamic trajectory radiotherapy for head and neck cancer: comparison with volumetric arc therapy on a publicly available library of cases. *Radiation oncology (London, England)* **17**, 122. ISSN: 1748-717X (Aug. 2022).
4. Guyer, G. *et al.* Technical note: A collision prediction tool using Blender. *Journal of Applied Clinical Medical Physics*, e14165. ISSN: 1526-9914 (Oct. 2023).
5. Bertholet, J. *et al.* Comparison of Dynamic Trajectory Radiotherapy and Volumetric Modulated Arc Therapy for Loco-Regionally Advanced Oropharyngeal Cancer. *International Journal of Radiation Oncology Biology Physics* **117**, 644. ISSN: 03603016 (Oct. 2023).

6

TECHNICAL NOTE: FEASIBILITY OF GATING FOR DYNAMIC TRAJECTORY RADIOTHERAPY - MECHANICAL ACCURACY AND DOSIMETRIC PERFORMANCE

H.A. Loebner¹, D. Frauchiger¹, S. Mueller¹, G. Guyer¹, P.-H. Mackeprang¹, M.F.M. Stampanoni², M.K. Fix¹, P. Manser¹, J. Bertholet¹

¹ Division of Medical Radiation Physics and Department of Radiation Oncology, Inselspital, Bern University Hospital, University of Bern, Bern, Switzerland

² Institute for Biomedical Engineering, ETH Zürich and PSI, Villigen, Switzerland

published in
Medical Physics

July 2023, Volume 50, Issue 10

<https://doi.org/10.1002/mp.16533>

©American Association of Physicists in Medicine

Open access article distributed under the terms of the Creative Commons CC BY-NC-ND 4.0 license.

6.1 Abstract

Background

Dynamic trajectory radiotherapy (DTRT) extends state-of-the-art volumetric modulated arc therapy (VMAT) by dynamic table and collimator rotations during beam-on. The effects of intrafraction motion during DTRT delivery are unknown, especially regarding the possible interplay between patient and machine motion with additional dynamic axes.

Purpose

To experimentally assess the technical feasibility and quantify the mechanical and dosimetric accuracy of respiratory gating during DTRT delivery.

Methods

A DTRT and VMAT plan are created for a clinically motivated lung cancer case and delivered to a dosimetric motion phantom (MP) placed on the table of a TrueBeam system using Developer Mode. The MP reproduces four different 3D motion traces. Gating is triggered using an external marker block, placed on the MP. Mechanical accuracy and delivery time of the VMAT and DTRT deliveries with and without gating are extracted from the logfiles. Dosimetric performance is assessed by means of gamma evaluation (3% global/2 mm, 10% threshold).

Results

The DTRT and VMAT plans are successfully delivered with and without gating for all motion traces. Mechanical accuracy is similar for all experiments with deviations $<0.14^\circ$ (gantry angle), $<0.15^\circ$ (table angle), $<0.09^\circ$ (collimator angle) and <0.08 mm (MLC leaf positions). For DTRT (VMAT), delivery times are 1.6-2.3 (1.6-2.5) times longer with than without gating for all motion traces except one, where DTRT (VMAT) delivery is 5.0 (3.6) times longer due to a substantial uncorrected baseline drift affecting only DTRT delivery. Gamma passing rates with (without) gating for DTRT/VMAT were $\geq 96.7\%/98.5\%$ ($\leq 88.3\%/84.8\%$). For one VMAT arc without gating it was 99.6%.

Conclusions

Gating is successfully applied during DTRT delivery on a TrueBeam system for the first time. Mechanical accuracy is similar for VMAT and DTRT deliveries with and without gating. Gating substantially improved dosimetric performance for DTRT and VMAT.

6.2 Introduction

Intensity modulated radiotherapy (IMRT) and volumetric modulated arc therapy (VMAT) are considered state-of-the-art radiotherapy treatment techniques for external radiation therapy with C-arm linear accelerators (linacs). Building on the C-arm linacs potential to dynamically move multiple machine axes, previous studies demonstrated the potential of non-coplanar radiotherapy [1] to improve organ-at-risk (OAR) sparing and/or dose conformity to the target compared to coplanar techniques by avoiding OARs in the beam path [2–6]. Efficient non-coplanar delivery, such as in dynamic trajectory radiotherapy (DTRT, [2]), can be obtained by combination of dynamic gantry and table rotation with intensity modulation, with or without dynamic collimator rotation [7, 8].

Regardless of the chosen treatment technique, respiratory motion in the thorax [9–13] and abdomen requires motion management to mitigate the degradation of the delivered dose distribution [14]. Motion management techniques include breath-hold, free-breathing gating, or MLC or couch tracking [15].

Dedicated systems such as the CyberKnife[®] (Accuray, Sunnyvale, CA, USA) or the discontinued VERO[®] (Brainlab, Munich, Germany and Mitsubishi Heavy Industries, Tokyo, Japan) are specifically designed to make use of non-coplanar beam angles with dynamic tumor tracking for motion mitigation [16, 17]. However, these systems are not as widely available as C-arm linacs where motion mitigation strategies such as gating are applied in clinical practice [15]. Free-breathing gating, however, imposes frequent beam-on/off switching, making it potentially more difficult to deliver for dynamic techniques [18, 19]. To apply free-breathing gating for DTRT, several challenges and questions need to be answered:

- *Is the machine capable of applying free-breathing gating DTRT for realistic motion traces?*
- *Can the machine deliver the intended dynamic trajectory with sufficient*

mechanical accuracy despite gating events?

- *What is the dosimetric accuracy of DTRT delivery with gating?*

The aim of this work is therefore to investigate the technical feasibility of gating during DTRT delivery, with additional dynamic table and collimator rotation compared to VMAT, and to evaluate mechanical accuracy, delivery time and dosimetric performance of DTRT delivery with and without gating. Mechanical accuracy and dosimetric performance for DTRT and VMAT deliveries with and without gating are compared for one case and four patient-recorded motion traces.

6.3 Materials and Methods

6.3.1 Treatment planning and patient case

Free-breathing gating for DTRT is tested for a clinically motivated lung cancer case prescribed 60 Gy in 20 fractions to the median planning target volume (PTV). The target has a volume of 190 cm³. The treatment planning process of Fix et al. [2] is followed to generate a DTRT treatment plan with dynamic gantry, table and collimator rotation during beam-on. The gantry-table path minimizes the target-OAR (heart and spinal cord) overlap in the beam's eye view. For collision prevention, an inhouse developed Blender [20] model of the motion phantom is used [21]. Dynamic collimator rotation minimizes field width in the leaf-travel direction. The obtained gantry-table-collimator path has 178 control points corresponding to a 2° gantry control point resolution and is duplicated by applying a 90° collimator angle offset on the second path. The DTRT treatment plan thus consists of two paths, each covering a full gantry rotation and a table rotation range of 56.4° (figure 6.1, A). The paths are imported into Eclipse® (Varian Medical Systems, Palo Alto, CA, USA) using the Eclipse Scripting Application Programming Interface. For comparison, a VMAT plan with two partial arcs covering a total range of 195° gantry rotation each with collimator angles of 2° and 88° is created (figure 6.1, B). Both plans are optimized according to clinical standards using a research version of the Eclipse Photon Optimizer and the Analytical Anisotropic Algorithm (AAA) dose calculation algorithm v15.6. The two DTRT trajectories deliver 373 MU and 369 MU with mean dose rates of 299 and 291 MU/min and the two VMAT arcs, deliver 369 MU and 213 MU with nominal mean dose rates of 551, 313 MU/min. The resulting dose distributions conform to clinical standards and have been accepted by a clinician.

For each plan, a verification plan is created for a cylindrical polymethylmethacrylate (PMMA) motion phantom representing the Delta4+ (ScandiDos, Uppsala, Sweden) measurement device, and dose is recalculated on the motion

phantom geometry (figure 6.1, C). For DTRT, a verification plan without table rotation is also created to distinguish the impact of potential table rotation errors. On this plan, dynamic gantry and collimator rotation and MLC movement is maintained.

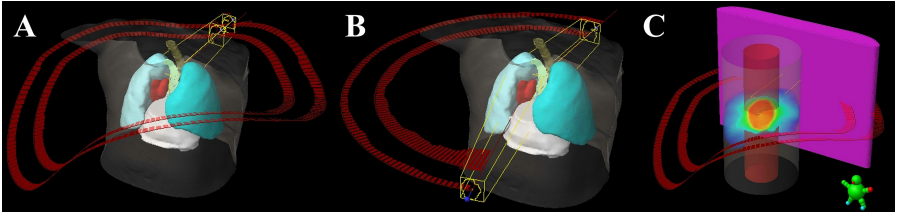


Figure 6.1: DTRT trajectories (A), VMAT arcs (B) and motion phantom with DTRT trajectories (C) for the lung cancer case. The PTV is shown in red, lungs in blue, spinal cord in yellow, oesophagus in green, heart in white and the body surface in translucent grey. The red bands indicate the beam incidences of the DTRT and VMAT plan respectively.

6.3.2 Respiratory motion

Gating is tested for four different breathing motion traces of lung tumors from a publicly available dataset recorded in patients [22, 23], denoted as: typical, high frequency, left right and baseline shifts, given after the predominant motion type. Each trace contains combined motion in superior-inferior, anterior-posterior, and left-right directions. Gating is applied at end-exhale. The amplitude gating windows are selected on the main motion axis (either superior-inferior or anterior-posterior) with gating windows between 4 and 6 mm depending on the motion trace. For the typical motion trace, two gating windows (2 and 4 mm) are tested (supplementary material A1).

6.3.3 Experimental setup and plan delivery

The experimental setup is shown in figure 6.2. For dosimetric verification, a Delta4+ motion phantom is used. It has two orthogonal planes of 1069 p-type

silicon diodes with a resolution of 5 mm at isocenter. The Delta4+ motion phantom is positioned in the HexaMotion (ScandiDos) stage on the PerfectPitch 6-degree-of-freedom treatment table of the TrueBeam system (Varian). The motion stage can rigidly move the Delta4+ to reproduce the motion traces shown in the supplementary material A1. Amplitude gating is triggered using the three-camera infrared-based Real-time Position Management respiratory gating system (RPM, Varian) with the marker block on top of the phantom (figure 6.2).

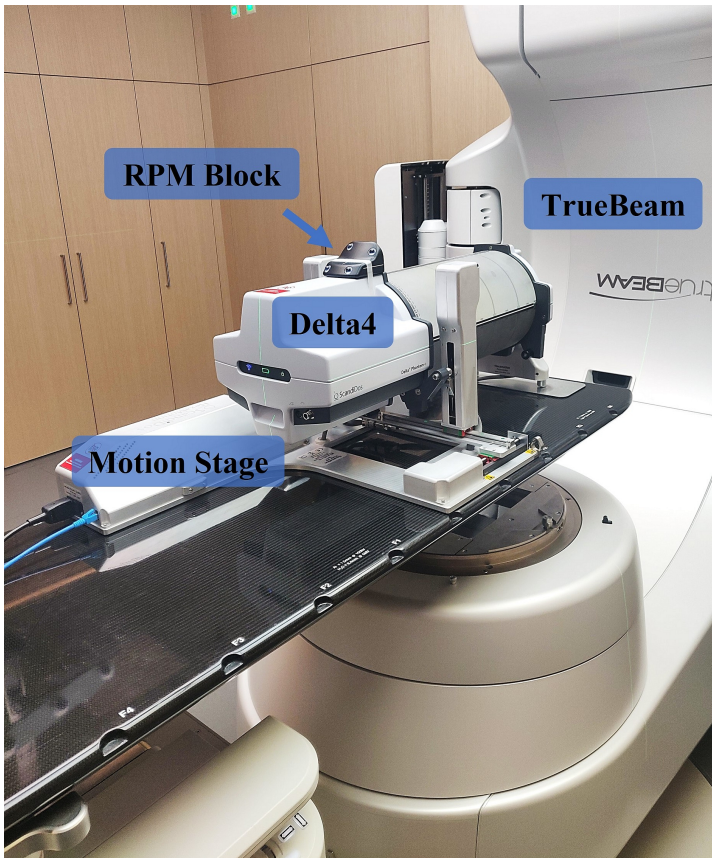


Figure 6.2: Experimental setup of motion stage, Delta4+ and RPM Marker Block on the treatment table.

The DTRT and VMAT plans are delivered at the machine with and without gating for all motion traces using Developer Mode. Developer Mode enables the delivery of experimental treatment techniques, by use of XML files which describe the plan. The gating latency of the TrueBeam system using the RPM signal has been recently reported to be 84 ms for beam-on and 44 ms for beam-off [24]. Delivery is started approximately ten seconds after the motion stage is set in motion. For each trajectory/arc, the motion trace is recycled until the MUs are fully delivered.

6.3.4 Data analysis

Mechanical accuracy

During delivery, motion along all mechanical axes is interpolated between control-points (every 2° gantry angle) by the TrueBeam supervisor and machine logfiles are collected to assess the mechanical accuracy as the deviation between actual and expected machine positions for gantry, table and collimator angle and moving MLC leaf positions in 20 ms intervals. Additionally, the MU delivery is assessed. Delivery time, duty cycle (DC) and beam-holds are extracted from the logfiles and compared for the deliveries with and without gating.

Dosimetric accuracy

Dosimetric accuracy of the deliveries with and without gating is assessed using the Delta4+ motion phantom. For reference, dosimetric accuracy is also assessed in the static case (no motion, without gating) for VMAT and for DTRT with and without table rotation. Gamma passing rate (3% global/2 mm, 10% threshold) and dose difference are used for evaluation following the patient specific quality assurance criteria recommended for IMRT measurement-based verification QA [25] and MLC tracking [26].

6.4 Results

Gating is successfully applied during DTRT and VMAT deliveries, with the gantry (VMAT and DTRT), table (DTRT) and collimator (DTRT) automatically rotating back during beam-hold and resuming motion at beam-on, i.e., when entering the gating window (figure 6.3). This correction is completed within <1 s. Maximal overshooting due to gating-triggered beam-hold is $<1.5^\circ$ for the gantry (VMAT and DTRT) and $<0.2^\circ$ for the table and $<0.02^\circ$ for the collimator rotation. In the supplementary material A2 a recording of a DTRT delivery with gating can be found. No loss of RPM signal is observed for the investigated case and motion traces and the RPM block is accurately tracked (supplementary material A3). The gantry-table (GT) and gantry-collimator (GC) path for the DTRT delivery with and without gating during the "typical" motion trace agree within $\pm 0.2^\circ$ (supplementary material A4).

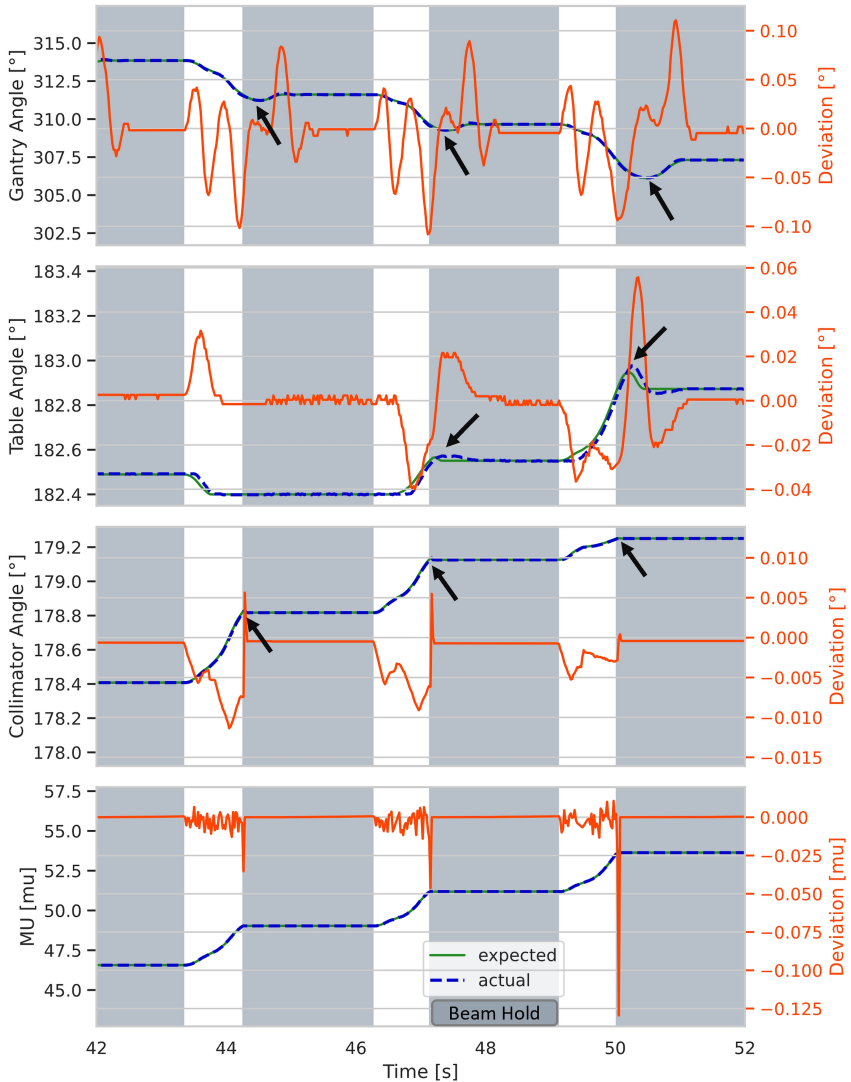


Figure 6.3: Zoom in on TrueBeam logfile of a gated DTRT delivery. The “overshoot” and “rotating back” is indicated by arrows during beam-hold (grey). The delivery is resumed when entering the gating window again.

6.4.1 Mechanical accuracy

The mean root-mean-square (RMS) deviation between expected and actual position was below 0.1° for gantry, table and collimator rotation and 0.023 mm for moving leaf position for all deliveries.

The mechanical deviation distributions are shown in figure 6.4. Greater variations (interquartile range) are observed for the deviations in table and collimator angle for DTRT deliveries without gating than for the deliveries with gating. Small systematic offsets for table/collimator angle observed in the delivery of the VMAT plans are not corrected, as they are within the precision limit of the machine component.

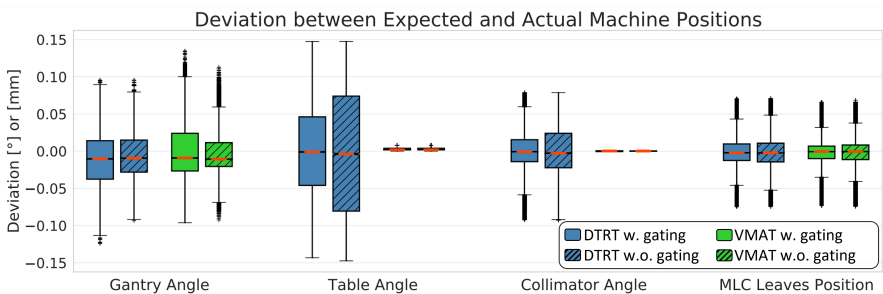


Figure 6.4: Deviation (expected-actual positions) in gantry, table and collimator angle and moving MLC leaf positions for DTRT (blue) and VMAT (green) delivery with (full) and without (dashed) gating. Deviations are only computed when the beam is on. The median is depicted in red, the notch defines the 95% confidence interval of the median, the box extends to the interquartile range (IQR, $Q3 - Q1$), whiskers extend to the last (first) data point less (greater) than $Q3 + 1.5 * IQR$ ($Q1 - 1.5 * IQR$). Outliers are marked with the plus sign.

Delivery of the DTRT and VMAT plans takes 2.5 and 1.4 min without gating. Of note, total gantry angle ranges are 720° for DTRT and 390° for VMAT. The delivery time and number of beam-holds of the gated deliveries depend on the gating window and motion traces: For the selected gating windows the total delivery time increases for the gated DTRT (VMAT) delivery by a factor of 2.3

(2.0) for lung typical with a ± 2 mm gating window and 3.4 (3.2) with a ± 1 mm gating window, 1.6 (1.6) for predominantly left right and 2.3 (2.5) for baseline shift motion trace. This led likewise to a decrease in the DC for the gated DTRT (VMAT) deliveries to 43% (50%) for lung typical with a ± 2 mm gating window and 29% (31%) with a ± 1 mm gating window, 63% (63%) for predominantly left right and 43% (40%) for baseline shift motion trace. For the high frequency motion trace, delivery time is increased by a factor of 5.0 (3.6), DC 20%, for DTRT (VMAT) which corresponds to a DC of 20% (28%). This is because the VMAT delivery is completed before reaching a baseline drift in the motion trace which affects the duty cycle of the DTRT delivery (see supplementary material A5). The number of beam-holds for DTRT (VMAT) deliveries are 173 (93) for lung typical with a ± 1 mm gating window and 122 (54) with a ± 2 mm gating window, 56 (31) for predominantly left right, 57 (38) for baseline shift and 358 (112) for the high frequency motion trace.

6.4.2 Dosimetric accuracy

Gamma passing rates are reported in table 6.3 and supplementary material A6. All gated deliveries achieve passing rates $>95.0\%$, All deliveries without gating result in passing rates $<88.3\%$, except for one arc of one VMAT plan where it was 99.6% . Gamma passing rates for the deliveries on static phantom are above 99.5% for static table plans and above 98.7% for DTRT deliveries. Figure 6.5 shows the Delta4+ measurement on one of the two orthogonal planes with dose profiles for the DTRT delivery with and without gating with the lung typical motion.

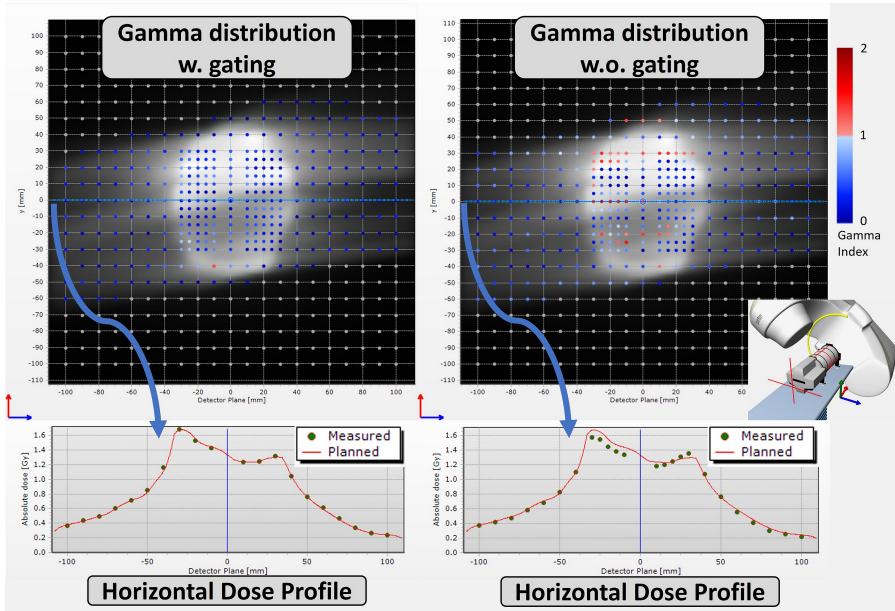


Figure 6.5: Deviation (expected-actual positions) in gantry, table and collimator angle and moving MLC leaf positions for DTRT (blue) and VMAT (green) delivery with (full) and without (dashed) gating. Deviations are only computed when the beam is on. The median is depicted in red, the notch defines the 95% confidence interval of the median, the box extends to the interquartile range (IQR, $Q3-Q1$), whiskers extend to the last (first) data point less (greater) than $Q3+1.5 \cdot IQR$ ($Q1-1.5 \cdot IQR$). Outliers are marked with the plus sign.

Table 6.1: Gamma passing rates (3% global dose difference / 2 mm distance, 10% threshold) for the DTRT (T1: first DTRT trajectory, T2: second DTRT trajectory) and the VMAT (V1: first VMAT arc, V2: second VMAT arc) deliveries with and without gating for the different motion traces. Values above 95% are indicated in bold.

Motion Trace	T1	T2	V1	V2
Typical				
Gating ± 1 mm	99.5	99.7	99.9	99.6
Gating ± 2 mm	99.5	97.1	99.3	99.8
No Gating	88.3	81.3	77.0	99.6
High frequency				
Gating $+1/-3$ mm	99.7	97.9	98.5	99.8
No Gating	55.4	48.6	55.3	50.6
Baseline shift				
Gating ± 3 mm	99.2	97.4	98.7	98.8
No Gating	84.3	82.1	72.8	76.9
Pred. left right				
Gating ± 2 mm	96.7	98.0	99.3	99.1
No Gating	79.3	85.3	84.8	76.2
No motion				
No Gating	99.7	98.7	100.0	100.0
No motion				
Static table	100.0	99.5	NA	NA

6.5 Discussion

Free-breathing gating is successfully applied during delivery of a DTRT treatment plan for the first time, demonstrating its technical feasibility for this highly complex and dynamic treatment technique on a standard C-arm linear accelerator.

For the investigated case and motion traces, the mechanical accuracy of the TrueBeam system delivering a DTRT treatment plan gated by the RPM signal is within sub-mm and sub-degree accuracy, similar to VMAT. When the beam is held, the positions of certain machine components (such as gantry angle) may overshoot the planned value. The machine, however, automatically corrects for these overshoots during the beam hold within the physical machine limits (including adaptation of the expected machine positions). The machine waits to resume delivery as soon as all machine components are in the correct positions and the signal of the RPM indicates that the target is within the gating window. Similar deviations between gantry angle or MLC leaf positions are observed between the VMAT and the DTRT deliveries, indicating that the addition of dynamic table and collimator rotation does not influence the accuracy of these common dynamic axes. The observed deviations are similar compared to previous logfile analyses [3, 27, 28]. For DTRT, it is worth noting, that the spread in the deviations of table and collimator angle are lower with gating than without gating. This is probably because the mechanical axes have time to go back to the expected position at the beam hold and to accelerate when the beam is turned on again and MU output is ramping-up. It has been observed that for continuous delivery, table and collimator rotation tend to slightly lag behind [3], whereas with gated delivery, lag can be eliminated at each gating event. It has to be noted that this mechanical accuracy evaluation is based on logfiles. These logfiles are not independent from the treatment machine and accurate calibration and routine QA are essential [29] and performed at our institute.

Dosimetric measurements for DTRT and VMAT showed that gating partially

restores the planned dose distribution for common respiratory motion traces. Residual motion during beam-on depends on the gating window with a trade-off between residual motion and delivery time. In addition, the gating window is defined for one direction of motion and substantial, uncorrelated, motion in the other axes is still possible and will not trigger a beam hold. Despite these effects, deliveries with gating had high dosimetric accuracy with gamma passing rates $>96.7\%$.

DTRT is currently a research technique and not available for patient treatments. However, only commercially available and adequate [30] equipment, widely employed during clinical PSQA, is used for the motion experiments. It is important to test the treatment machine capability to apply gating for real motion traces to test the technique for clinical practice [31, 32]. As in previous studies on motion management system performance [23, 33], we used four different motion traces that are representative of common lung motion types [22, 23]. No loss of RPM signal is observed for the investigated case and motion traces, despite the non-coplanar table positions during DTRT.

The dosimetric benefit of gating is directly related to the gating window and motion trace, which in turn influence DC and thus the delivery time. In clinical practice, the selection of the gating window and the PTV margins would be based on balancing accurate tumor targeting, DC and PTV margins, considering the inherent uncertainty of correlating the surface motion to the actual tumor motion. The total delivery time without gating for DTRT and VMAT is 2.5 min and 1.4 min respectively, with VMAT having slightly more than half the gantry angle range of the DTRT plan. With exception of the lung high frequency motion trace, delivery time increased by up to a factor of 2.5 for the gated deliveries (VMAT and DTRT), similar to the results of Chin et al. [19]. For the lung high frequency motion trace, the delivery time increased by a factor of 5.0 for DTRT delivery with gating compared to delivery without gating due to an uncorrected baseline drift. For this motion trace, gating enabled dosimetric accuracy similar to the other motion traces for both treatment techniques. Without gating, dosimetric

accuracy is substantially lower to approximately 50% gamma passing rate. This shows the need to monitor the motion during delivery and adapt in case of baseline drift. A potential solution would be to interrupt treatment and apply set-up correction as proposed in other gating studies [34].

Our results show that motion mitigation, e.g., free-breathing gating, is needed to ensure that the favourable dose distributions achievable with DTRT [2, 3] are accurately delivered to the patient in treatment sites affected by breathing motion. In these cases, PSQA can also be performed with realistic motion traces or using the motion recorded at 4DCT using the experimental setup proposed in this study.

6.6 Conclusion

In this work, the technical feasibility of gating for DTRT on a TrueBeam is successfully demonstrated for the first time. The mechanical accuracy in terms of gantry, table and collimator angle and MLC leaf position is similar with and without gating and to VMAT delivery for the investigated case and motion traces. Comparable to VMAT, gating substantially improves the dosimetric plan quality, at the cost of increased delivery time.

6.7 Acknowledgements

This work was supported by Varian Medical Systems. Open access funding provided by Inselspital Universitatsspital Bern.

6.8 Conflict of interest statement

The authors have no relevant conflicts of interest to disclose.

REFERENCES

1. Webb, S. *The physics of three-dimensional radiation therapy : conformal radiotherapy, radiosurgery, and treatment planning* 373. ISBN: 9780750302548 (Taylor & Francis, 1993).
2. Fix, M. K. *et al.* Part 1: Optimization and evaluation of dynamic trajectory radiotherapy. *Medical Physics* **45**, 4201–4212. ISSN: 00942405 (Aug. 2018).
3. Bertholet, J. *et al.* Organ-at-risk sparing with dynamic trajectory radiotherapy for head and neck cancer: comparison with volumetric arc therapy on a publicly available library of cases. *Radiation oncology (London, England)* **17**, 122. ISSN: 1748-717X (Aug. 2022).
4. Kim, S.-T. *et al.* Non-coplanar VMAT plans for lung SABR to reduce dose to the heart: a planning study. *The British Journal of Radiology* **93**, 20190596. ISSN: 0007-1285 (Aug. 2020).
5. Sheng, K. & Shepard, D. M. Point/Counterpoint. Noncoplanar beams improve dosimetry quality for extracranial intensity modulated radiotherapy and should be used more extensively. *Medical physics* **42**, 531–533. ISSN: 2473-4209 (Aug. 2015).
6. Park, J., Park, J. W. & Yea, J. W. Non-coplanar whole brain radiotherapy is an effective modality for parotid sparing. *Yeungnam University Journal of Medicine* **36**, 36 (Aug. 2019).

7. Papp, D., Bortfeld, T. & Unkelbach, J. A modular approach to intensity-modulated arc therapy optimization with noncoplanar trajectories. *Physics in medicine and biology* **60**, 5179–5198. ISSN: 1361-6560 (Aug. 2015).
8. Smyth, G., Evans, P. M., Bamber, J. C. & Bedford, J. L. Recent developments in non-coplanar radiotherapy. *Brit J Radiol* **92**. ISSN: 1748880X (Aug. 2019).
9. Seppenwoolde, Y. *et al.* Precise and real-time measurement of 3D tumor motion in lung due to breathing and heartbeat, measured during radiotherapy. *International Journal of Radiation Oncology, Biology, Physics* **53**, 822–834. ISSN: 0360-3016 (Aug. 2002).
10. Mishra, P. *et al.* Changes in lung tumor shape during respiration. *iop-science.iop.org* **57**, 919–935 (2012).
11. Huang, C. Y., Tehrani, J. N., Ng, J. A., Booth, J. & Keall, P. Six Degrees-of-Freedom Prostate and Lung Tumor Motion Measurements Using Kilo-voltage Intrafraction Monitoring. *International Journal of Radiation Oncology, Biology, Physics* **91**, 368–375. ISSN: 0360-3016 (Aug. 2015).
12. Schmidt, M. L. *et al.* Cardiac and respiration induced motion of mediastinal lymph node targets in lung cancer patients throughout the radiotherapy treatment course. *Radiotherapy and Oncology* **121**, 52–58. ISSN: 0167-8140 (Aug. 2016).
13. Shah, A. P. *et al.* Real-time tumor tracking in the lung using an electromagnetic tracking system. *International Journal of Radiation Oncology Biology Physics* **86**, 477–483. ISSN: 1879355X (Aug. 2013).
14. Keall, P., Poulsen, P. & Booth, J. T. See, Think, and Act: Real-Time Adaptive Radiotherapy. *Seminars in Radiation Oncology* **29**, 228–235. ISSN: 1053-4296 (Aug. 2019).

15. Anastasi, G. *et al.* Patterns of practice for adaptive and real-time radiation therapy (POP-ART RT) part I: Intra-fraction breathing motion management. *Radiotherapy and Oncology* **153**, 79–87. ISSN: 0167-8140 (Aug. 2020).
16. Hoogeman, M. *et al.* Clinical Accuracy of the Respiratory Tumor Tracking System of the CyberKnife: Assessment by Analysis of Log Files. *International Journal of Radiation Oncology, Biology, Physics* **74**, 297–303. ISSN: 0360-3016 (Aug. 2009).
17. Depuydt, T. *et al.* Initial assessment of tumor tracking with a gimbaled linac system in clinical circumstances: A patient simulation study. *Radiotherapy and Oncology* **106**, 236–240. ISSN: 0167-8140 (Aug. 2013).
18. Snyder, J. E., Flynn, R. T. & Hyer, D. E. Implementation of respiratory-gated VMAT on a Versa HD linear accelerator. *Journal of applied clinical medical physics* **18**, 152–161. ISSN: 1526-9914 (Aug. 2017).
19. Chin, E., Loewen, S. K., Nichol, A. & Otto, K. 4D VMAT, gated VMAT, and 3D VMAT for stereotactic body radiation therapy in lung. *Physics in Medicine & Biology* **58**, 749. ISSN: 0031-9155 (Aug. 2013).
20. Community, B. O. *Blender - a 3D modelling and rendering package, accessed on 26.10.2023* 2018. <http://www.blender.org>.
21. Guyer, G. *et al.* *Development of a Collision Prediction Tool between Gantry and Table Using Blender, accessed on 26.10.2023* 2021. <https://w4.aapm.org/meetings/2021AM/programInfo/programAbs.php?sid=9375&aid=58124>.
22. Suh, Y., Dieterich, S., Cho, B. & Keall, P. J. An analysis of thoracic and abdominal tumour motion for stereotactic body radiotherapy patients. *Physics in medicine and biology* **53**, 3623–3640. ISSN: 0031-9155 (Aug. 2008).

23. Colvill, E. *et al.* A dosimetric comparison of real-time adaptive and non-adaptive radiotherapy: A multi-institutional study encompassing robotic, gimbaled, multileaf collimator and couch tracking. *Radiotherapy and Oncology* **119**, 159–165. ISSN: 0167-8140 (Aug. 2016).
24. Worm, E., Thomsen, J. B., Johansen, J. G. & Poulsen, P. R. OC-0040 Gating latencies and resulting geometrical errors at clinical proton and photon accelerators. *Radiotherapy and Oncology* **170**, S13–S15. ISSN: 0167-8140 (Aug. 2022).
25. Miften, M. *et al.* Tolerance limits and methodologies for IMRT measurement-based verification QA: Recommendations of AAPM Task Group No. 218. *Medical Physics* **45**, e53–e83. ISSN: 2473-4209 (Aug. 2018).
26. Keall, P. J. *et al.* AAPM Task Group 264: The safe clinical implementation of MLC tracking in radiotherapy. *Medical Physics* **48**, e44–e64. ISSN: 2473-4209 (Aug. 2021).
27. Olasolo-Alonso, J., Vázquez-Galiñanes, A., Pellejero-Pellejero, S. & Pérez-Azorín, J. F. Evaluation of MLC performance in VMAT and dynamic IMRT by log file analysis. *Phys Med* **33**, 87–94. ISSN: 1120-1797 (Aug. 2017).
28. Smyth, G. *et al.* Dosimetric accuracy of dynamic couch rotation during volumetric modulated arc therapy (DCR-VMAT) for primary brain tumours. *Physics in Medicine and Biology* **64**. ISSN: 13616560 (2019).
29. Agnew, A., Agnew, C. E., Grattan, M. W. D., Hounsell, A. R. & McGarry, C. K. Monitoring daily MLC positional errors using trajectory log files and EPID measurements for IMRT and VMAT deliveries. *Physics in medicine and biology* **59**. ISSN: 1361-6560 (Aug. 2014).
30. Huang, C. Y. *et al.* Performance assessment of a programmable five degrees-of-freedom motion platform for quality assurance of motion management techniques in radiotherapy. *Australasian Physical and Engineering Sciences in Medicine* **40**, 643–649. ISSN: 18795447 (Aug. 2017).

31. Malinowski, K. *et al.* Development of the 4D Phantom for patient-specific end-to-end radiation therapy QA. *Journal of Medical Imaging* **6510**, 174–182. ISSN: 16057422 (Aug. 2007).
32. Mukumoto, N. *et al.* Development of a four-axis moving phantom for patient-specific QA of surrogate signal-based tracking IMRT. *Medical Physics* **43**, 6364–6374. ISSN: 2473-4209 (Aug. 2016).
33. Hansen, R. *et al.* Electromagnetic guided couch and multileaf collimator tracking on a TrueBeam accelerator. *Medical Physics* **43**, 2387–2398. ISSN: 2473-4209 (Aug. 2016).
34. Nankali, S. *et al.* Geometric and dosimetric comparison of four intrafraction motion adaptation strategies for stereotactic liver radiotherapy. *Physics in Medicine & Biology* **63**, 145010. ISSN: 0031-9155 (Aug. 2018).

6.9 Appendix

A1 Motion traces

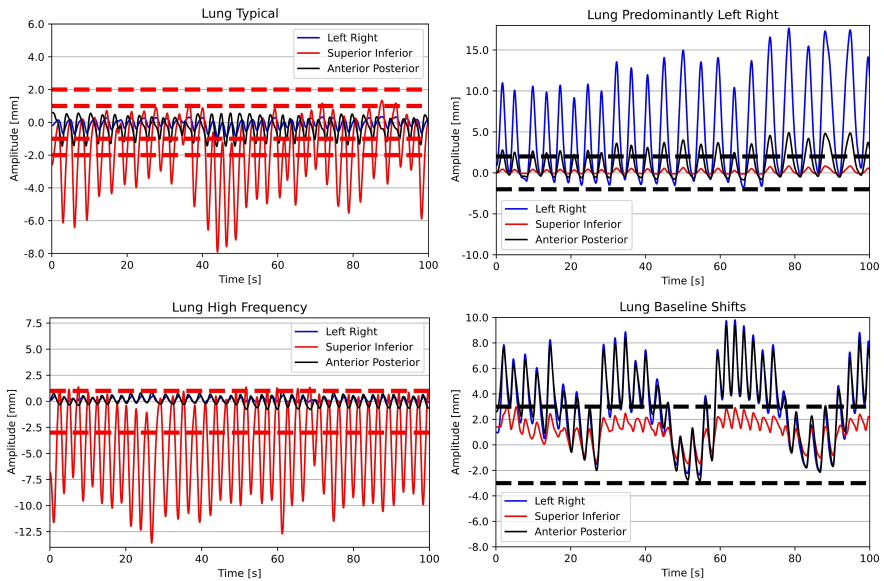


Figure 6.6: Respiratory motion traces from Suh et al.1. The dashed lines represent the amplitude gating window. Gating is applied at end-exhale only on the main motion axis (either maxima of superior-inferior or minima of anterior-posterior, indicated by the colour of the dashed line).

A2 Video material

In the supporting material, there is a video of a gated DTRT delivery during a sinusoidal motion in anterior-posterior direction.

A3 RPM signal

To verify the accuracy of RPM Block tracking during DTRT, beam-on/-holds patterns are compared for DTRT deliveries with and without table rotation for

gating on a regular sinusoidal motion in superior-inferior and anterior-posterior direction, respectively. The gating pattern is unaffected by table rotation as shown in figure 6.7.

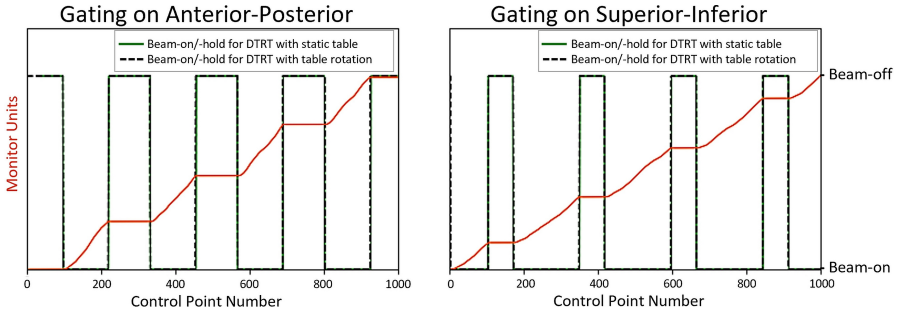


Figure 6.7: Beam-hold and beam-on (indicated by the green and black curve) for gating of regular sinusoidal motion in anterior-posterior and superior-inferior directions for DTRT deliveries with a static and with a rotating table. For clarification, the Monitor Units are shown in orange and increase if there is no beam-hold.

A4 Mechanical accuracy

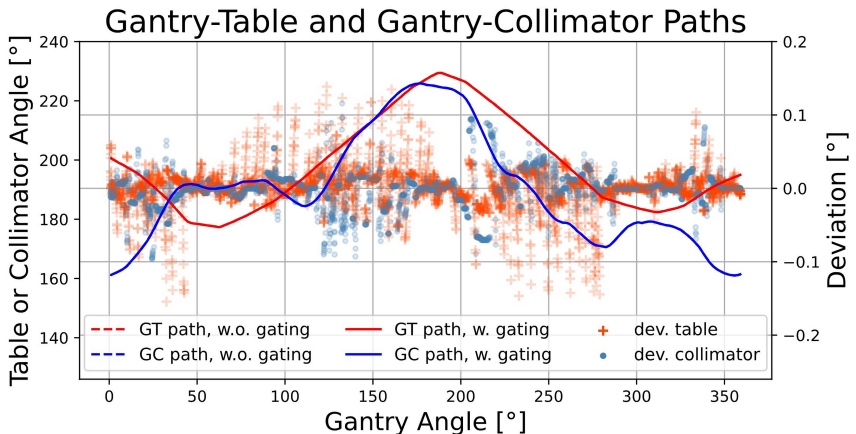


Figure 6.8: Comparison of the GT and GC path of a DTRT delivery with and without gating during the lung typical motion.

A5 Lung high frequency motion trace

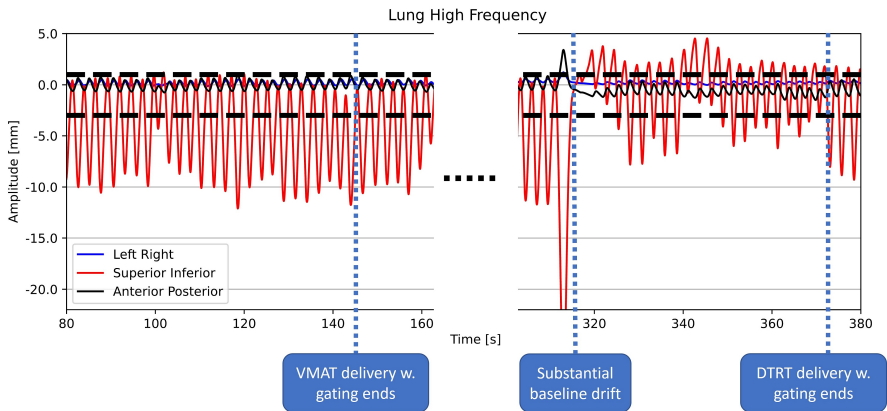


Figure 6.9: Lung high frequency motion trace. The dashed lines represent the amplitude gating window. The end of the VMAT and DTRT delivery with gating is indicated, as well as the substantial baseline drift.

A6 Dosimetric accuracy

Table 6.2: Gamma passing rates (2% global dose difference / 2 mm distance, 10% threshold) for the DTRT (T1: first DTRT trajectory, T2: second DTRT trajectory) and the VMAT (V1: first VMAT arc, V2: second VMAT arc) deliveries with and without gating for the different motion traces.

Motion Trace	T1	T2	V1	V2
Typical				
Gating ± 1 mm	96.3	90.7	96.0	98.6
Gating ± 2 mm	95.8	91.7	96.8	98.1
No Gating	80.2	76.6	68.9	96.7
High frequency				
Gating $+1/-3$ mm	95.0	92.4	95.0	98.6
No Gating	44.6	40.2	44.7	38.0
Baseline shift				
Gating ± 3 mm	96.8	92.6	96.7	97.4
No Gating	75.0	69.8	61.4	68.4
Pred. left right				
Gating ± 2 mm	93.5	92.7	96.8	96.7
No Gating	69.4	79.4	77.0	68.3
No motion				
No Gating	99.5	96.6	99.5	99.3
No motion				
Static table	99.1	96.2	NA	NA

Table 6.3: Gamma passing rates (3% global dose difference / 1 mm distance, 10% threshold) for the DTRT (T1: first DTRT trajectory, T2: second DTRT trajectory) and the VMAT (V1: first VMAT arc, V2: second VMAT arc) deliveries with and without gating for the different motion traces.

Motion Trace	T1	T2	V1	V2
Typical				
Gating ± 1 mm	98.7	93.6	96.8	97.9
Gating ± 2 mm	97.6	92.2	97.2	98.2
No Gating	74.9	70.4	69.4	97.0
High frequency				
Gating +1/-3 mm	97.7	93.7	97.5	98.2
No Gating	46.0	40.5	48.2	38.3
Baseline shift				
Gating ± 3 mm	93.2	90.5	96.0	92.3
No Gating	75.6	70.6	62.1	64.1
Pred. left right				
Gating ± 2 mm	93.7	92.2	96.6	94.4
No Gating	72.3	79.2	76.1	65.3
No motion				
No Gating	94.8	92.9	96.0	96.1
No motion				
Static table	94.7	94.2	NA	NA

7

DISCUSSION AND OUTLOOK

The presented studies contribute to the advancement of external radiotherapy, in particular, DTRT. They are oriented towards addressing the open questions regarding the different aspects of DTRT plan quality [1–3], with a special focus on robustness and motion management of DTRT.

One of the cornerstones of this thesis is the development of the robustness tool and its application in the second and fourth study. It enabled to investigate and to compare the robustness of different treatment plans using different treatment techniques on an individual patient level as well as in a large-scale robustness study - an aspects of DTRT plan quality which has not been explored before to this extent. The dynamic table rotation is a main characteristic of DTRT. Based on the results of the second study, suitable parameters for the gantry-table rotation gradient for the DTRT path generation were chosen in the following studies, enabling a reasonable trade-off especially between dosimetric plan quality and delivery time. In addition, this work presents a standardized but nevertheless patient-specific protocol to generate DTRT treatment plans. The presented protocol facilitates DTRT treatment planning, minimizes planner bias and enabled the treatment planning for the large-scale robustness comparison of DTRT and VMAT. Finally, this thesis investigated the dosimetric performance and deliverability aspect of DTRT plan quality in the presence of intra-fraction patient motion. In a world's first, the technical feasibility of free-breathing gating for DTRT is demonstrated, thus providing an active motion management strategy for this novel technique.

While the context of each of the studies is explained and discussed in the respective sections, the following discussion is a guide for the interpretation of the studies within the context of this thesis and provides an outlook on their prospective applications.

7.1 Robustness assessments in the clinical context

As highlighted in the introduction, robustness is an integral part of radiotherapy plan quality [1, 2]. While robustness assessments are common in proton therapy [4, 5], they are scarce for photon-based treatment techniques. In-depth robustness assessments as presented in this thesis of photon-based treatment plans are usually not routinely conducted in daily clinical practice. Furthermore, when performed, robustness assessments often focus solely on patient-setup uncertainties and target robustness, with OAR robustness frequently overlooked or addressed only through initial margins. The developed robustness tool presented in the first study addresses these challenges. It enables a flexible selection of patient- and machine-related uncertainty scenarios and allows to evaluate target and OAR robustness. Its application in the subsequent studies brought about a thorough robustness assessment of DTRT treatment plans, particularly regarding the question if the dosimetric benefits of DTRT, when compared to state-of-the-art VMAT, are not lost in the presence of uncertainties. This assessment is a pre-requisite for the introduction of DTRT in the clinics. A shortcoming of the developed tool is that biological uncertainties [6], imaging uncertainties (e.g., imaging artefacts and range uncertainties [7]), and uncertainties related to deformation due to patient-motion (e.g., breathing [8, 9]), can only be indirectly considered. While the evaluation of dose distributions including such uncertainties is possible, models to simulate these uncertainties are not implemented yet.

Some clinically employed treatment planning systems offer the possibility to

perform a robustness assessment, usually focusing on systematic patient-setup or range (in the case of proton-based treatments) uncertainties and do not include random patient-setup or other types of uncertainties. This possibility is seldom used in clinics due to the substantial computational burden involved to calculate the multiple dose distributions of the treatment plan each including one of the uncertainties. Rather a visual inspection of the dose distribution is conducted, e.g., to assess the proximity of a high-dose region to an OAR. It is because of this substantial computational burden that the presented robustness assessments in this work have been performed on a high performance computing cluster.

In research there exists several approaches to reduce the computational burden, usually at the cost of decreasing accuracy. One approach, which has also been implemented and can be used in the developed robustness tool is to base the robustness assessment on interpolating the desired dose quantities of a few uncertainty scenarios to simulate additional uncertainty scenarios. Another approach, already mentioned in the introduction, is the static dose cloud approximation [10, 11]. In the static dose cloud approximation, only one dose distribution is calculated and shifted/turned according to the uncertainty. The "improved static dose cloud approximation" [11] additionally accounts for changed the patient surface with respect to the beam incidence due to a patient-setup uncertainty. While these two approximations are deemed sufficiently accurate for tumors in homogeneous density regions, e.g., in the pelvic region, they are not appropriate for heterogeneous density regions, e.g., in the lung region [12, 13]. Furthermore, the accuracy decreases with increasing level of the uncertainty. Moreover, not all uncertainties can be simulated using this approximation, such as MLC leaf position uncertainty or collimator rotation uncertainty. To circumvent these problems, machine learning algorithms can be employed in the dose calculation. There exist approaches which use deep-learning to either predict the dose distribution based on CT, structure set and information about the treatment plan [14–17] or to denoise computationally inexpensive MC dose distributions of high statistical uncertainty [18]. To use these deep-learning techniques, the uncertainty could be

directly included at the stage of dose prediction, by modifying the plan information, shifting the CT or adapting the contours of the structures according to the uncertainty. The machine-learning based dose prediction is usually performed within less than a second and also denoising is performed within minutes [14–18], thus, substantially reducing the calculation time for the calculation of the dose distribution of the uncertainty scenarios. The developed robustness tool is extendable to include these deep-learning techniques in the dose distribution calculation step to reduce the computational cost. Building up on such extensions or provided that there is enough computational power available to compute the dose distributions of a large number of uncertainty scenarios, and assuming that there is knowledge about the probability of how often and to which extent a type of uncertainty occurs, the robustness assessment can be extended by confidence intervals for relevant dose quantities as suggested in several studies [19, 20]. Including them in the robustness assessment, provides more information about the likelihood of the impact of an uncertainty.

The robustness assessments presented in the studies of this thesis, lead to the conclusion that even a sparse sampling of the robustness space allows for a valuable overview of the dosimetric plan robustness. Routinely applied in clinical practice, treatment planners or clinical personnel could be prompted in difficult cases to consider additional measures, such as margins to spare critical organs or extra imaging to increase patient-setup accuracy [21]. The application of the tool in the presented studies makes it clear, that the impact of the investigated uncertainties is non-negligible for photon-based treatments. Moreover, when the dosimetric benefits of one treatment technique over the other are lost in the presence of common uncertainties, they can impact clinical decisions (e.g., the NTCP-based selection of the treatment technique [22, 23]). Hence, the findings of our studies encourage robustness assessments, particularly before the introduction of novel treatment techniques and for critical cases where target or OAR constraints are barely met.

A different approach to robustness is to include uncertainty scenarios directly

at the optimization stage. Robust optimization [24], allows to generate treatment plans which are robust to a pre-defined set of uncertainties. The dose is usually optimized directly on the CTV instead of the PTV, including the uncertainties [25]. Similar to robustness assessments, robust optimization is however connected with increased computational burden due to the pre-calculation of the beamlets for each uncertainty scenario. Up to now, robust optimization is only common in clinical practice for proton-based treatments [26].

Lastly, we should bear in mind that evaluating treatment plan robustness is a complex topic. In addition to a great variety of uncertainties, also different endpoints can be evaluated. Taking up the idea of a summarizing plan quality index [27], the robustness index introduced in the studies of this work condenses robustness into one number, thus facilitating the robustness comparison of different treatment plans. Future clinical implementation of robustness assessments will benefit from such index by streamlining the workflow to evaluate robustness and to evaluate plan quality.

7.2 Paving the way for DTRT delivery in the clinics

Up to this date, DTRT is still a research technique and has not been implemented in clinics yet. Although, there are promising results regarding the dosimetric benefits of DTRT [28–31] and DTRT is deliverable on the most commonly used treatment devices for external photon-based radiotherapy, a standard C-arm linac [32] (although only in a research mode called "Developer Mode"), several questions regarding the different aspects of plan quality remain. In this thesis, particularly in the second to fifth study, the author aimed to answer some of these questions, with the goal to pave the way for a clinical implementation of DTRT.

In the second presented study, several aspects of plan quality have been investi-

gated as a function of freedom in the gantry-table rotation gradient. For non-coplanar treatments, such as DTRT, quickly the question of how to select the non-coplanar paths to deliver the radiation, and how such selection influences the plan quality, arises. In other words, these questions relate to the beam-angle optimization problem [29, 33], with respect to the different aspects of plan quality. In the presented study, this problem is partly answered by providing a path finding algorithm, that returns the optimal path on a given map under user-defined restrictions in the gantry-table rotation gradient. This algorithm enables the planner to consider restrictions related to delivery time, patient comfort and machine durability at the path finding stage by restricting the gantry-table rotation gradient and thus tailor the DTRT plan generation to the specific needs of the patient and the clinic. For the implementation of non-coplanar treatment techniques in the clinics, particularly the delivery efficiency has been identified as an obstacle. Long delivery times lead to limited patient throughput and can negatively impact patient comfort [29, 34, 35]. Furthermore, having control over the path finding potentially enables to reduce table rotation-induced setup uncertainties and increase machine durability: multiple directional changes in the table rotation are avoided, by limiting the change in the gantry-table rotation gradient. Another idea is to switch the gantry and table axis during path finding in order to completely exclude back- and forth movement of the table for benefits regarding patient comfort and machine durability and generate so-called coronal-VMAT plans [29, 36]. On a different note, only dynamic trajectories with a full gantry rotation are considered in the presented study. It can be speculated, that partial arcs [37], might be beneficial dosimetrically and with regard to delivery efficiency. To find promising partial arcs, the developed algorithm can be employed on a trimmed gantry-table map according to the desired gantry- or table-range. Another approach is to extend the path finding algorithm to consider additional constraint such as the maximal gantry or table rotation range.

In the third study, the need for standardized protocols as an integral part of plan quality is answered [3]. These protocols minimize planner bias and facili-

tate clinical implementation by aiming for consisting plan quality and thus help to ensure patient safety. In the presented study, a protocol for the geometric path finding approach of DTRT is presented and investigated. An OAR grouping strategy, as well as manual planning rules for the intensity optimization are introduced. The developed protocol paves the way to standardized DTRT treatment planning by serving as a basis for the DTRT plan generation. Upon achieving the minimal planning goals, the protocol recommends continuing the intensity modulation optimization until no further improvements are possible. While the developed protocol is specific to the head and neck treatment site, it can be extended and developed for other treatment sites as well. In the presented study, the patient-machine collision space has been considered by including information about potential collisions between machine and patient based on a generic patient model. However, this approach can be extended in the future by replacing the generic patient model with patient-specific information from the CT or from surface imaging of the patient. Surface imaging of the patient on the treatment table further allows to obtain real-time information about potential collisions [38, 39] and therefore increase the safety of the patients upon a future clinical implementation of DTRT.

The robustness comparison of DTRT versus state-of-the-art VMAT for head and neck cancer answers one of the remaining questions regarding DTRT plan quality. The findings from the second and the fourth study result in the following conclusion. Although there are statistically significant differences in robustness between DTRT and VMAT, the dosimetric benefits of DTRT over VMAT are mostly maintained in the presence of the investigated patient-setup and machine-position uncertainties. Based on these studies, the author believes, that with regard to robustness to the investigated uncertainties, DTRT can be employed in the clinics for head and neck cancer with one exception: special attention needs to be paid to structures outside the plane defined by the VMAT beam directions. In the fourth study it was shown, that these structures receive more dose due to the non-coplanar beam directions. When uncertainties are considered,

the respective dose limits can be breached. Due to this reason, we recommend considering planning at risk volumes (PRVs), particularly for the hippocampus, to mitigate the dosimetric impact of the uncertainties on these structures. A shortcoming of the presented studies is the selection of uncertainty scenarios. Although the most evident and commonly investigated uncertainties are considered (i.e., patient-setup and machine position uncertainties), intra-fraction motion is not discussed [40]. Bearing in mind that standard fixation devices include masks, such motion is limited. However, to improve patient comfort, minimal mask solutions are pursued [41]. In this context, volunteer studies [42] with "dry-runs", where no radiation is delivered and only the machine movements are executed, combined with surface imaging of the volunteer on the treatment table, provide a solution to determine the extent of involuntary motion caused by the table rotation of DTRT. Before implementing DTRT for other treatment sites, the respective uncertainty scenarios should be identified (e.g, breathing-induced uncertainties in the thorax region), their extent should be determined and their impact should be assessed.

Historically, the potential of non-coplanar treatment techniques has been mostly investigated for treatment sites in the brain or in the head and neck region [30, 31, 34], mostly due to the large collision-free space. Nonetheless, also other treatment sites can benefit from the improved healthy tissue sparing of DTRT as compared to state-of-the-art treatment techniques. For these other treatment sites, particularly in the thorax and pelvis region, new challenges arise: intra-fraction motion is more pronounced as compared to the head and neck region [43, 44], and needs to be managed to ensure accurate dose delivery to the tumor. As a world's first, the last study confirms the technical feasibility of gating during DTRT delivery. In detail, the machine is able to accurately initiate gating and resume delivery according to the gating signal. Dosimetric measurements showed that gating for DTRT partially (depending on the gating window) restores the planned dose distribution for patient-recorded respiratory motion traces, with similar dosimetric performance as gating for VMAT. Two strong points of

this study are the use of clinically available QA equipment and real-life patient-recorded motion traces. The use of clinically available QA equipment facilitates a future implementation of gating for DTRT in common radiotherapy centers, as no additional measurement equipment or complicated measurement setup is needed to verify the accuracy and performance of gating during DTRT delivery. The patient-recorded motion traces confirm the feasibility of gating during DTRT also for irregular motion traces. In this study a real-time position management system (RPM) including a marker block was used to monitor the motion. In the future, the RPM and the marker block can be replaced with surface monitoring systems to monitor the patient motion to initiate gating to improve accuracy and patient comfort. First experiments already confirmed the feasibility to monitor moving surfaces during DTRT delivery [45]. Another motion mitigation strategy is tracking. The potential of tracking during DTRT has not been investigated yet. However, this approach faces additional challenges. On the one hand, tracking using the treatment table [46] potentially counteracts the planned table rotation and subsequently increases the risk of patient-machine collision. Moreover, in DTRT, the table rotation defines the beam direction and is thus involved in the intensity modulation of the beam. It is not clear, how tracking impacts the resulting dose distribution. On the other hand, tracking using the MLC [47], faces difficulties due to DTRTs dynamic rotation of the collimator which continuously changes the orientation of the MLC leaves. Besides, the MLC would be involved in both, intensity modulation and active motion compensation. MLC tracking overrides the planned MLC pattern thus invalidating pre-treatment QA measurements. However, perhaps the greatest obstacle on the way to clinical implementation of tracking for DTRT and in general, and thus the key difference to gating, is that tracking on a standard C-arm treatment machine is currently not clinically available and, to the best of our knowledge, the different companies developing linacs do not show an interest in pursuing developments towards the implementation of tracking.

As a last point, to pave the way for DTRT to the clinics, the author wants to

mention the need for routinely employable QA methods for DTRT. Particularly, efficient pre-treatment and patient-specific QA methods are needed. There is the trend to perform only logfile-based pre-treatment QA [48–50], however, logfiles do not record miscalibrations of the respective machine components. Additionally, it has been shown that the logfile reported machine positions do not necessarily coincide with the actual machine positions [51]. For these reasons and to gain experience with new treatment techniques, such as DTRT, fast, reliable and measurement-based QA methods are preferred. There exist already several measurement based QA approaches for DTRT. For instance, film measurements have been used in the presented second and third and other studies [52, 53] to verify the accurate DTRT delivery. Although they allow fine resolved measurements, film measurements have the drawback of a delayed result. The films require time between the measurement and the read-out for the radiation induced darkening of the film to stabilize. Moreover, they are only usable once. In the first and last study, the Delta4+ (ScandiDos, Uppsala, Sweden) is used as QA device. While this measurement device provides a fast and reliable readout, attention needs to be paid due to the increased collision risk with this device, especially when mounted in the HexaMotion stage as in the last study. Furthermore, depending on the gantry-table path of the DTRT plan, the non-coplanar angles lead to radiation beaming through the electronics of the Delta4+. The attenuation through these electronics is not well characterized so far and in the long run, this might lead to problems regarding the functionality of this QA device. Summarizing these points, the author concludes that new QA methods and devices need to be designed and investigated with the goal to provide fast and reliable QA methods for DTRT.

First patients

Finally, to treat first patients with DTRT, a promising indication is needed. The presented and previous mentioned studies found in literature, focus mainly on

clinically motivated cases in the brain or head and neck region. The motivation to investigate the potential of DTRT for these treatment sites is two-fold. First, the poor prognosis and the radiation related toxicities for state-of-the-art techniques for these cancer entities [54, 55] are a motivation to employ a technique which has the potential to spare more healthy tissue and thus to reduce the toxicities. Second, these treatment sites offer an increased collision-free space as compared to treatment sites located in the middle and lower body, thus allowing for more non-coplanarity and thus more possibility to spare healthy tissue [29, 56, 57]. For these reasons, the author believes, that these cancer entities serve as a good starting point for a clinical implementation of DTRT.

7.3 On the future of DTRT

The research presented in this thesis focuses on advancing DTRT. So far, in all investigated aspects, DTRT seems promising. The question is now, how can DTRT be advanced further, beyond the scope of the investigations conducted in this thesis? What can the future bring for DTRT?

Plan generation

A first point that comes to mind is the geometric-based treatment planning approach of DTRT. The dosimetric plan quality might profit from a dosimetrically motivated planning approach [58, 59]. While geometric considerations of target-OAR overlap have the advantage of providing computationally cheap and intuitive solutions for the gantry-table paths, first investigations regarding dosimetrically motivated approaches [60] showed promising results. However, we do not expect a paradigm change with regard to the dosimetric plan quality to the current geometrically motivated approach, due to the already observed high dosimetric plan quality. Nonetheless, the dosimetric approach can facilitate the implementation of planning protocols. Dosimetric approaches have the flexibility to include new

planning objectives on the fly, instead of defining fixed OAR grouping strategies. However, dosimetrically motivated approaches come at the cost of a substantial computational burden as mentioned before. Furthermore, they require the definition of a metric which includes the dosimetric information to quantify promising beam directions.

Another point to advance the DTRT plan generation, is to include robust optimization strategies in the DTRT planning process. While conventional robust optimization usually considers only the intensity optimization [24, 26], the DTRT paths can be also robustly optimized, similarly to uncertainty incorporated beam angle optimization [61]. To this end, the map on which the gantry-table path is found, would already include uncertainties. For both geometric and dosimetric path finding approaches multiple maps would be generated before path finding, with each map including a different uncertainty. The dimensionality during path finding would therefore be extended by the number of maps.

In contrast to the first points, the author wants to mention, that reducing complexity or improving delivery efficiency of DTRT is also considered an advancement. In this context, the design of class solutions for the trajectories, similarly to HyperArc [62], is promising. Instead of patient-specific gantry-table paths, treatment site-specific paths can be designed, which have the additional advantage of reducing the risk of collisions when including appropriate safety margins. Another approach to reduce complexity is avoiding the dynamic table rotation, while maintaining the dosimetric benefits from the non-coplanar beam-angles. In colli-DTRT, multiple static non-coplanar partial arcs with dynamic collimator rotation are used to deliver the radiation and first results even show reduced delivery times as compared to DTRT [63].

As a last point regarding advancing DTRT plan generation, the author wants to comment on the "hot-topic" of adaptive radiotherapy [64]. Over the course of the treatment, there can be changes in the patient anatomy stemming from tumor shrinkage, weight loss or emptying/filling of organs such as the bladder or rectum [65–67]. Adaptive radiotherapy aims to account for these changes.

Compared to VMAT, DTRT includes the additional dynamic table and collimator rotation. The corresponding additional steps in the current DTRT treatment planning process (see figure 1.6), are patient anatomy specific. It might therefore be beneficial to involve table and collimator rotation in the adaptive radiotherapy workflow. Based on repeat CTs, new gantry-table and gantry-collimator maps can be generated and new adapted gantry-table and/or gantry-collimator paths can be found.

Increasing the degrees of freedom

DTRT is based on the idea of increasing the degrees of freedom in treatment plan generation to improve the dosimetric plan quality, in particular by adding dynamic table and collimator rotation compared to VMAT. The author wants to ask the question of what can be included to improve DTRT plan quality and increase the freedom in DTRT treatment planning?

Next to dynamically rotating the table, table translations can be included. First investigations showed promising results with regard to collision risk prevention, increasing delivery efficiency and improving dosimetric plan quality [53]. Apart from including additional movements of different machine components in the treatment planning, different radiation types can be added. In dynamic mixed beam radiotherapy (DYMBER) [52], DTRT is extended by electron fields. A further extension with electron and proton beams to triple beam radiotherapy (TriB-Rt) [68] is also possible for DTRT. Beyond machine equipment and radiation type, the time- and space-component of the treatment plan can be explored. In temporally feathered radiotherapy [69], the tissue biology is exploited. By using different iso-curative plans to deliver the radiation to the tumor and spare different OARs in each session, this technique offers the OARs more regeneration time, thus reducing healthy tissue damage. Similarly in spatiotemporal fractionated radiotherapy [70], the biological dose to the healthy tissue is lowered, by treating different metastasis in each treatment fraction. For these treatment techniques,

DTRT has the advantage to provide different gantry-table paths for each treatment fraction, to feather different OARs, spare healthy tissue or to treat different parts of the tumor.

Motion management

DTRT also has the potential to further develop in the field of motion management. In this context, the author wants to take up the topic of tracking again. As previously discussed, there are several challenges to implementing tracking for this technique. However, there is the possibility to make use of one of the "free" machine components for tracking. Similar to the principles of the CyberKnife or VERO, where the linac head can tilt to account for motion, the pitch and roll possibilities of the treatment table can be used to mitigate small intra-fraction motions. However to apply such strategies, studies need to verify the patients compatibility with these tracking techniques and that no additional setup uncertainties are introduced because of these tracking movements. Another possibility is to make use of the dynamic collimator rotation. Instead of aiming for minimization of potential leaf travel as in this thesis [28], the collimator can be rotated to align with the principle motion axis [71], thus facilitating MLC tracking.

Recent advances in surface monitoring can also further advance DTRT. Gating or tracking could be triggered by a surface monitoring signal. Currently available kV or MV based motion monitoring methods on a standard C-arm linac [72, 73] cannot be straightforwardly employed for DTRT. Gantry-mounted, fully extended kV or MV systems substantially reduce the collision-free space between patient-machine and machine-machine, thus limiting the capabilities of DTRT. Even when there is enough room for kV or MV imaging, the image quality might be reduced due to the increased path length of the imaging beam through the patient [74]. Therefore, surface monitoring techniques are promising candidates to further advance DTRT in the context of gating or tracking. Moreover, surface monitoring allows to detect anatomy deformations such as weight loss without

the need for repeat CT or MRI [75]. Upon the implementation of action levels regarding the observed deformations, re-planning or plan adaptation can be triggered.

The author believes that the design of appropriate QA methods, reliable collision prevention, and additional analysis of more extensive planning studies and feasibility studies on motion management, similar to the ones presented in this thesis, are a pre-requisite to the introduction of DTRT in clinics. Furthermore, a successful outcome of volunteer studies confirming the volunteers tolerance with the DTRT machine movements is needed. Based on these future investigations, the author is convinced, that the implementation of DTRT to treat patients, potentially with one of the indications mentioned before, will be a two step process. First, incorporating only one dynamic machine axis additional to VMAT presents the opportunity to gain experience with a "light" version of DTRT, thereby rendering colli-DTRT [63] a promising candidate for study and application. In a second step, based on the clinical experiences of the "light" version of DTRT, the transition to DTRT plans including dynamic table rotation can be suggested.

REFERENCES

1. Hernandez, V. *et al.* What is plan quality in radiotherapy? The importance of evaluating dose metrics, complexity, and robustness of treatment plans. *Radiother Oncol* **153**, 26–33. ISSN: 18790887 (2020).
2. Kaplan, L. P. *et al.* Plan quality assessment in clinical practice: Results of the 2020 ESTRO survey on plan complexity and robustness. *Radiotherapy and Oncology* **173**. ISSN: 18790887 (2022).
3. Hansen, C. R., Hussein, M., Bernchou, U., Zukauskaitė, R. & Thwaites, D. *Plan quality in radiotherapy treatment planning – Review of the factors and challenges 2022*.
4. Mohan, R. & Grosshans, D. Proton therapy – Present and future. *Advanced Drug Delivery Reviews* **109**. ISSN: 18728294 (2017).
5. Malyapa, R. *et al.* Evaluation of Robustness to Setup and Range Uncertainties for Head and Neck Patients Treated with Pencil Beam Scanning Proton Therapy. *International Journal of Radiation Oncology Biology Physics* **95**, 154–162. ISSN: 1879355X (2016).
6. Van der Merwe, D. *et al.* Accuracy requirements and uncertainties in radiotherapy: a report of the International Atomic Energy Agency. *Acta Oncologica* **56**. ISSN: 1651226X (2017).
7. Rousselle, A. *et al.* Metallic implants and CT artefacts in the CTV area: Where are we in 2020? *Cancer/Radiotherapie* **24**. ISSN: 17696658 (2020).

8. Lu, X. Q. *et al.* Organ Deformation and Dose Coverage in Robotic Respiratory - Tracking Radiotherapy. *International Journal of Radiation Oncology Biology Physics* **71**. ISSN: 03603016 (2008).
9. Velec, M., Moseley, J. L., Craig, T., Dawson, L. A. & Brock, K. K. Accumulated dose in liver stereotactic body radiotherapy: Positioning, breathing, and deformation effects. *International Journal of Radiation Oncology Biology Physics* **83**. ISSN: 03603016 (2012).
10. Karlsson, K., Lax, I., Lindbäck, E. & Poludniowski, G. Accuracy of the dose-shift approximation in estimating the delivered dose in SBRT of lung tumors considering setup errors and breathing motions. *Acta Oncologica* **56**. ISSN: 1651226X (2017).
11. Unkelbach, J., Bortfeld, T., Martin, B. C. & Soukup, M. Reducing the sensitivity of IMPT treatment plans to setup errors and range uncertainties via probabilistic treatment planning. *Medical Physics* **36**. ISSN: 00942405 (2009).
12. Craig, T., Battista, J. & Van Dyk, J. Limitations of a convolution method for modeling geometric uncertainties in radiation therapy. I. The effect of shift invariance. *Medical Physics* **30**. ISSN: 00942405 (2003).
13. Fredriksson, A. & Bokrantz, R. The scenario-based generalization of radiation therapy margins. *Physics in Medicine and Biology* **61**. ISSN: 13616560 (2016).
14. Bakx, N. *et al.* Development and evaluation of radiotherapy deep learning dose prediction models for breast cancer. *Physics and Imaging in Radiation Oncology* **17**. ISSN: 24056316 (2021).
15. Osman, A. F. & Tamam, N. M. Attention-aware 3D U-Net convolutional neural network for knowledge-based planning 3D dose distribution prediction of head-and-neck cancer. *Journal of Applied Clinical Medical Physics* **23**. ISSN: 15269914 (2022).

16. Xing, Y., Nguyen, D., Lu, W., Yang, M. & Jiang, S. Technical Note: A feasibility study on deep learning-based radiotherapy dose calculation. *Medical Physics* **47**. ISSN: 24734209 (2020).
17. Poel, R. *et al.* Deep-Learning-Based Dose Predictor for Glioblastoma – Assessing the Sensitivity and Robustness for Dose Awareness in Contouring. *Cancers* **15**. ISSN: 20726694 (2023).
18. Neph, R., Lyu, Q., Huang, Y., Yang, Y. M. & Sheng, K. DeepMC: a deep learning method for efficient Monte Carlo beamlet dose calculation by predictive denoising in magnetic resonance-guided radiotherapy. *Physics in Medicine and Biology* **66**. ISSN: 13616560 (2021).
19. Sobotta, B., Söhn, M. & Alber, M. Accelerated evaluation of the robustness of treatment plans against geometric uncertainties by Gaussian processes. *Physics in Medicine and Biology* **57**. ISSN: 00319155 (2012).
20. Sterpin, E. *et al.* Development of robustness evaluation strategies for enabling statistically consistent reporting. *Physics in Medicine & Biology* **66**, 45002. ISSN: 0031-9155 (Aug. 2021).
21. Pisani, L. *et al.* Setup error in radiotherapy: On-line correction using electronic kilovoltage and megavoltage radiographs. *International Journal of Radiation Oncology, Biology, Physics* **47**. ISSN: 03603016 (2000).
22. Nederslandse Vereniging voor Radiotherapie en Oncologie. *Landelijk Indicatie Protocol Protontherapie (versie 2.2) (LIPPv2.2)*, accessed on 25.10.2023 2019. <https://docplayer.nl/195792198-Landelijk-indicatie-protocol-protontherapie-versie-2-2-lippv2-2.html>.
23. Palma, G., Monti, S., Conson, M., Pacelli, R. & Cella, L. *Normal tissue complication probability (NTCP) models for modern radiation therapy* 2019.

24. Unkelbach, J. *et al.* Robust radiotherapy planning. *Physics in Medicine and Biology* **63**. ISSN: 13616560 (Aug. 2018).
25. Biston, M. C., Chiavassa, S., Grégoire, V., Thariat, J. & Lacornerie, T. Time of PTV is ending, robust optimization comes next. *Cancer/Radiotherapie* **24**. ISSN: 17696658 (2020).
26. Unkelbach, J. & Paganetti, H. Robust Proton Treatment Planning: Physical and Biological Optimization. *Seminars in Radiation Oncology* **28**. ISSN: 15329461 (2018).
27. Giglioli, F. R. *et al.* Dosimetric Multicenter Planning Comparison Studies for Stereotactic Body Radiation Therapy: Methodology and Future Perspectives. *International Journal of Radiation Oncology Biology Physics* **106**, 403–412. ISSN: 1879355X (Aug. 2020).
28. Fix, M. K. *et al.* Part 1: Optimization and evaluation of dynamic trajectory radiotherapy. *Medical Physics* **45**, 4201–4212. ISSN: 00942405 (Aug. 2018).
29. Smyth, G., Evans, P. M., Bamber, J. C. & Bedford, J. L. Recent developments in non-coplanar radiotherapy. *Brit J Radiol* **92**. ISSN: 1748880X (Aug. 2019).
30. Smyth, G. *et al.* Non-coplanar trajectories to improve organ at risk sparing in volumetric modulated arc therapy for primary brain tumors. *Radiotherapy and Oncology* **121**, 124–131. ISSN: 0167-8140 (Aug. 2016).
31. Smyth, G., Bamber, J. C., Evans, P. M. & Bedford, J. L. Trajectory optimization for dynamic couch rotation during volumetric modulated arc radiotherapy. *Physics in Medicine and Biology* **58**. ISSN: 13616560 (2013).
32. Thwaites, D. I. & Tuohy, J. B. Back to the future: The history and development of the clinical linear accelerator. *Physics in Medicine and Biology* **51**. ISSN: 00319155 (2006).

33. Bortfeld, T. & Schlegel, W. Optimization of beam orientations in radiation therapy: Some theoretical considerations. *Physics in Medicine and Biology* **38**. ISSN: 00319155 (1993).
34. Thomas, E. M. *et al.* Comparison of plan quality and delivery time between volumetric arc therapy (rapidarc) and gamma knife radiosurgery for multiple cranial metastases. *Neurosurgery* **75**. ISSN: 15244040 (2014).
35. Sheng, K. & Shepard, D. M. Point/Counterpoint. Noncoplanar beams improve dosimetry quality for extracranial intensity modulated radiotherapy and should be used more extensively. *Medical physics* **42**, 531–533. ISSN: 2473-4209 (Aug. 2015).
36. Shaitelman, S. F. *et al.* Continuous arc rotation of the couch therapy for the delivery of accelerated partial breast irradiation: A treatment planning analysis. *International Journal of Radiation Oncology Biology Physics* **80**. ISSN: 03603016 (2011).
37. Yang, Y. *et al.* Choreographing couch and collimator in volumetric modulated arc therapy. *International Journal of Radiation Oncology Biology Physics* **80**. ISSN: 03603016 (2011).
38. Padilla, L., Pearson, E. & Pelizzari, C. Patient-Specific Collision Detection Package Using Surface Imaging. *International Journal of Radiation Oncology, Biology, Physics* **90**. ISSN: 03603016 (2014).
39. Padilla, L., Pearson, E. A. & Pelizzari, C. A. Collision prediction software for radiotherapy treatments. *Medical Physics* **42**. ISSN: 24734209 (2015).
40. Bruijnen, T. *et al.* Intrafraction motion quantification and planning target volume margin determination of head-and-neck tumors using cine magnetic resonance imaging. *Radiotherapy and Oncology* **130**. ISSN: 18790887 (2019).

41. Zhao, B., Maquilan, G., Jiang, S. & Schwartz, D. L. Minimal mask immobilization with optical surface guidance for head and neck radiotherapy. *Journal of Applied Clinical Medical Physics* **19**. ISSN: 15269914 (2018).
42. Pollock, S., Keall, R. & Keall, P. Breathing guidance in radiation oncology and radiology: A systematic review of patient and healthy volunteer studies. *Medical Physics* **42**. ISSN: 24734209 (2015).
43. Suh, Y., Dieterich, S., Cho, B. & Keall, P. J. An analysis of thoracic and abdominal tumour motion for stereotactic body radiotherapy patients. *Physics in medicine and biology* **53**, 3623–3640. ISSN: 0031-9155 (Aug. 2008).
44. Colvill, E. *et al.* A dosimetric comparison of real-time adaptive and non-adaptive radiotherapy: A multi-institutional study encompassing robotic, gimbaled, multileaf collimator and couch tracking. *Radiotherapy and Oncology* **119**, 159–165. ISSN: 0167-8140 (Aug. 2016).
45. Loebner, H. A. *et al.* *Surface Monitoring for Dynamic Trajectory Radiotherapy - A Feasibility Study*, accessed on 26.10.2023 2022. <https://w4.aapm.org/meetings/2022AM/programInfo/programAbs.php?sid=10716&aid=64982>.
46. Keall, P. J. *et al.* The management of respiratory motion in radiation oncology report of AAPM Task Group 76. *Medical physics* **33**, 3874–3900. ISSN: 0094-2405 (2006).
47. Keall, P. J. *et al.* AAPM Task Group 264: The safe clinical implementation of MLC tracking in radiotherapy. *Medical Physics* **48**, e44–e64. ISSN: 2473-4209 (Aug. 2021).
48. Katsuta, Y. *et al.* Log file-based patient dose calculations of double-arc VMAT for head-and-neck radiotherapy. *Phys Med* **48**, 6–10. ISSN: 1120-1797 (Aug. 2018).

49. Sun, B. *et al.* Initial experience with TrueBeam trajectory log files for radiation therapy delivery verification. *Practical Radiation Oncology* **3**. ISSN: 18798500 (2013).
50. Rangaraj, D. *et al.* Catching errors with patient-specific pretreatment machine log file analysis. *Practical Radiation Oncology* **3**. ISSN: 18798500 (2013).
51. Agnew, A., Agnew, C. E., Grattan, M. W. D., Hounsell, A. R. & McGarry, C. K. Monitoring daily MLC positional errors using trajectory log files and EPID measurements for IMRT and VMAT deliveries. *Physics in medicine and biology* **59**. ISSN: 1361-6560 (Aug. 2014).
52. Mueller, S. *et al.* Part 2: Dynamic mixed beam radiotherapy (DYMBER): Photon dynamic trajectories combined with modulated electron beams. *Medical Physics* **45**, 4213–4226. ISSN: 00942405 (Aug. 2018).
53. Guyer, G. *et al.* Enabling non-isocentric dynamic trajectory radiotherapy by integration of dynamic table translations. *Physics in Medicine and Biology* **67**. ISSN: 13616560 (2022).
54. Tewarie, I. A. *et al.* *Survival prediction of glioblastoma patients—are we there yet? A systematic review of prognostic modeling for glioblastoma and its clinical potential* 2021.
55. Tsao, M. N. *et al.* *Radiotherapeutic management of brain metastases: A systematic review and meta-analysis* 2005.
56. Podgorsak, E. B., Olivier, A., Pla, M., Lefebvre, P. Y. & Hazel, J. Dynamic stereotactic radiosurgery. *International Journal of Radiation Oncology, Biology, Physics* **14**. ISSN: 03603016 (1988).
57. Kraysenbuehl, J., Davis, J. B. & Ciernik, I. F. Dynamic intensity-modulated non-coplanar arc radiotherapy (INCA) for head and neck cancer. *Radiotherapy and Oncology* **81**. ISSN: 01678140 (2006).

58. Bangert, M. & Oelfke, U. Spherical cluster analysis for beam angle optimization in intensity-modulated radiation therapy treatment planning. *Physics in Medicine and Biology* **55**. ISSN: 00319155 (2010).
59. Llacer, J., Li, S., Agazaryan, N., Promberger, C. & Solberg, T. D. Non-coplanar automatic beam orientation selection in cranial IMRT: A practical methodology. *Physics in Medicine and Biology* **54**. ISSN: 00319155 (2009).
60. Mackeprang, P. *et al.* MO-0544 4pi-IMRT based path-finding for dynamic trajectory radiotherapy. *Radiotherapy and Oncology* **170**, S469–S470. ISSN: 01678140 (Aug. 2022).
61. Cao, W. *et al.* Uncertainty incorporated beam angle optimization for IMPT treatment planning. *Medical Physics* **39**. ISSN: 00942405 (2012).
62. Ohira, S. *et al.* HyperArc VMAT planning for single and multiple brain metastases stereotactic radiosurgery: a new treatment planning approach. *Radiation Oncology 2018 13:1* **13**, 1–9. ISSN: 1748-717X (Aug. 2018).
63. Bertholet, J. *et al.* Development of Colli-DTRT: A Non-Coplanar Intensity Modulated Arc Therapy Technique with Dynamic Collimator Rotation. *Medical Physics* **49**. ISSN: 0094-2405 (June 2022).
64. Sonke, J. J., Aznar, M. & Rasch, C. Adaptive Radiotherapy for Anatomical Changes. *Seminars in Radiation Oncology* **29**, 245–257. ISSN: 1053-4296 (Aug. 2019).
65. Erridge, S. C. *et al.* Portal imaging to assess set-up errors, tumor motion and tumor shrinkage during conformal radiotherapy of non-small cell lung cancer. *Radiotherapy and Oncology* **66**. ISSN: 01678140 (2003).
66. O'Doherty, Ú. M. *et al.* Variability of bladder filling in patients receiving radical radiotherapy to the prostate. *Radiotherapy and Oncology* **79**. ISSN: 01678140 (2006).

67. Chao, M., Xie, Y., Moros, E. G., Le, Q. T. & Xing, L. Image-based modeling of tumor shrinkage in head and neck radiation therapy. *Medical Physics* **37**. ISSN: 00942405 (2010).
68. Kueng, R. *et al.* TriB-RT: Simultaneous optimization of photon, electron and proton beams. *Physics in Medicine & Biology* **66**, 45006. ISSN: 0031-9155 (Aug. 2021).
69. López Alfonso, J. C. *et al.* Temporally feathered intensity-modulated radiation therapy: A planning technique to reduce normal tissue toxicity. *Medical Physics* **45**. ISSN: 24734209 (2018).
70. Torelli, N., Papp, D. & Unkelbach, J. Spatiotemporal fractionation schemes for stereotactic radiosurgery of multiple brain metastases. *Medical Physics* **50**. ISSN: 24734209 (2023).
71. Murtaza, G., Toftegaard, J., Khan, E. U. & Poulsen, P. R. Volumetric modulated arc therapy with dynamic collimator rotation for improved multileaf collimator tracking of the prostate. *Radiotherapy and Oncology* **122**. ISSN: 18790887 (2017).
72. Nguyen, D. T. *et al.* The first clinical implementation of a real-time six degree of freedom target tracking system during radiation therapy based on Kilovoltage Intrafraction Monitoring (KIM). *Radiotherapy and Oncology* **123**. ISSN: 18790887 (2017).
73. Worm, E. S., Høyer, M., Fledelius, W. & Poulsen, P. R. Three-dimensional, time-resolved, intrafraction motion monitoring throughout stereotactic liver radiation therapy on a conventional linear accelerator. *International Journal of Radiation Oncology Biology Physics* **86**. ISSN: 03603016 (2013).
74. Carucci, L. R. Imaging obese patients: Problems and solutions. *Abdominal Imaging* **38**. ISSN: 09428925 (2013).
75. Freislederer, P. *et al.* Recent advanced in Surface Guided Radiation Therapy. *Radiation Oncology* **15**, 1–11. ISSN: 1748717X (July 2020).

REFERENCES

8

CONCLUDING REMARKS

This work advances DTRT by addressing open questions about DTRT plan quality beyond the dosimetric aspects of the planned dose distribution. While the dosimetric benefits and deliverability of DTRT have been demonstrated previously for several indications, this work confirms them and expands on them. This work focuses especially on exploring DTRT robustness and managing motion during DTRT delivery.

The developed MC-based robustness tool allows to perform in-depth robustness assessments of different treatment techniques to a great variety of uncertainties. The tool enabled the comparison of DTRT with state-of-the-art techniques like VMAT in the following studies. Furthermore, based on the extended gantry-table path finding algorithm, DTRT plans with user-specified restrictions in the gantry-table rotation gradient can be generated. This offers greater control to the planner to tailor the treatment plan to the patient's and clinic's needs. It further enabled to investigate DTRT plan quality according to the freedom in this key characteristic, the gantry-table rotation gradient, and find an appropriate trade-off between dosimetric plan quality, complexity, deliverability, delivery time and robustness for the subsequent studies. Next to these investigations, a planning protocol was introduced for the head and neck treatment site, which can be extended in future to other treatment sites. It improves DTRT plan quality by standardizing DTRT treatment planning and reducing planner bias. The protocol further allowed to perform the large-scale robustness study between DTRT and VMAT. The findings from this robustness study underline that robustness is an

integral part of photon-based radiotherapy treatment plan quality. The robustness assessments also demonstrated, that DTRT is affected in a similar manner by the investigated patient and machine related uncertainties as VMAT, except for organs located outside the VMAT beam-plane, defined by the coplanar beam directions of the VMAT arc. The non-coplanar beam directions of DTRT can result in increased dose to these organs as compared to VMAT. In combination with uncertainties, this can lead to exceeding the respective dose limits of these organs. Therefore, they need to be considered carefully during planning, possibly by extra margins and PRVs for sensitive OARs (e.g., for the hippocampus). Nonetheless, it is important to note that the dosimetric benefits of DTRT of lower NTCP values for dysphagia and xerostomia compared to VMAT are maintained, even in the presence of the investigated uncertainties. With our study on motion management, we demonstrated in a world's first that gating is feasible for DTRT and successfully mitigates the detrimental effects of breathing motion on the planned dose distribution. This study served as a proof of concept study, and while it successfully showed the potential of this motion management strategy for DTRT, more cases need to be explored, to confirm the feasibility and dosimetric benefits for a larger cohort.

In conclusion, the outcomes of this work provide comprehensive answers and insights to the various aspects of DTRT plan quality. These findings are a substantial step forward, advancing and positioning DTRT as a next-generation treatment technique for external photon-based radiotherapy treatments. The author is curious what the future might hold for DTRT.

STUDENT PROJECTS

As part of my work, I had the opportunity to advise and mentor following students and their semester and master's projects:

2020 - Semester project

"Impact of the source-to-surface distance of electron beams on dynamic mixed beam radiotherapy (DYMBER) plans"

Yannik Wyss, master's program at ETH Zürich in Physics, co-supervision with Dr. Silvan Mueller, Prof. Dr. Marco F.M. Stampanoni, Prof. Dr. Peter Manser and Prof. Dr. Michael K. Fix

2021 - Semester project

"Quality Assurance for Dynamic Trajectory Radiotherapy"

Jean Radig, master's program at ETH Zürich in Physics, co-supervision with Prof. Dr. Marco F.M. Stampanoni, Prof. Dr. Peter Manser and Prof. Dr. Michael K. Fix

2022 - Semester project

"Robustness of Normal Tissue Complication Probability to Patient-Setup and Contouring Uncertainties"

Lisa Fankhauser, master's program at ETH Zürich in Biomedical Engineering, co-supervision with Dr. Paul-Henry Mackeprang, Prof. Dr. Marco F.M. Stampanoni, Prof. Dr. Peter Manser and

Prof. Dr. Michael K. Fix

2023 - Master's project

"Monte Carlo Dose Calculation for Moving and Deforming Anatomy"

Björn Zobrist, master's program at ETH Zürich in Physics, co-supervision with Prof. Dr. Marco F.M. Stampanoni, Prof. Dr. Peter Manser and Prof. Dr. Michael K. Fix

2023 - Master's project

"Deep Learning based Monte Carlo Dose Denoising for Radiation Therapy"

Raphael Joost, master's program at University of Bern, Faculty of Medicine - Artificial Intelligence in Medicine, co-supervision with Prof. Dr. Stavroula Mougiakakou, Prof. Dr. Michael K. Fix and Prof. Dr. Peter Manser

PUBLICATIONS, CONFERENCE PROCEEDINGS, GRANTS

During the course of the PhD, work on the following publications and conference proceedings has been conducted. The list is sorted by date.

First Author Publications

Development of a Monte Carlo based robustness calculation and evaluation tool, *HA Loebner, W Volken, S Mueller, J Bertholet, P-H Mackeprang, G Guyer, DM Aebersold, MFM Stampanoni, P Manser, MK Fix*, Medical Physics, 2022

Technical note: Feasibility of gating for dynamic trajectory radiotherapy – Mechanical accuracy and dosimetric performance, *HA Loebner, D Frauchiger, S Mueller, G Guyer, P-H Mackeprang, MFM Stampanoni, MK Fix, P Manser, J Bertholet*, Medical Physics, 2023

Impact of the gradient in gantry-table rotation on dynamic trajectory radiotherapy plan quality, *HA Loebner, S Mueller, W Volken, P Wallimann, DM Aebersold, MFM Stampanoni, MK Fix, P Manser*, Medical Physics, 2023

Robustness Analysis of Dynamic Trajectory Radiotherapy (DTRT) and

Volumetric Modulated Arc Therapy (VMAT) Plans for Head and Neck cancer: A Comparative Study, HA Loebner, J Bertholet, P-H Mackeprang, W Volken, O Elicin, S Mueller, G Guyer, DM Aebersold, MFM Stampanoni, MK Fix & P Manser, submitted to the International Journal of Radiation Oncology, Biology, Physics, 2023

Co-Author Publications

Organ-at-risk sparing with dynamic trajectory radiotherapy for head and neck cancer: comparison with volumetric arc therapy on a publicly available library of cases, J Bertholet, P-H Mackeprang, S Mueller, G Guyer, HA Loebner, Y Wyss, D Frei, W Volken, O Elicin, DM Aebersold, MK Fix & P Manser, Radiation Oncology, 2022

Co-Author Publications outside the scope of this thesis

Enabling non-isocentric dynamic trajectory radiotherapy by integration of dynamic table translations, G Guyer, S Mueller, C Koechli, D Frei, W Volken, J Bertholet, P-H Mackeprang, HA Loebner, DM Aebersold, P Manser, MK Fix, Physics in Medicine and Biology, 2022

Auto-commissioning of a Monte Carlo electron beam model with application to photon MLC shaped electron fields, MK Fix, D Frei, S Mueller, G Guyer, HA Loebner, W Volken & P Manser, Physics in Medicine and Biology, 2023

Conference proceedings

The contents of this thesis and related contents have been presented at the following conferences. Only first author conference proceedings are listed. The list is sorted by date.

International Conferences

Development of a framework to assess robustness of dynamic trajectory treatment plans, *HA Loebner, W Volken, S Mueller, J Bertholet, P-H Mackeprang, G Guyer, DM Aebersold, MFM Stampanoni, P Manser, MK Fix*, American Association of Physicists in Medicine Annual Meeting & Exhibition, accepted for Oral Presentation, Virtual, 2021

Influence of the freedom in table rotation on plan quality, deliverability, delivery time and robustness of dynamic trajectory treatment plans, *HA Loebner, S Mueller, W Volken, P Wallimann, DM Aebersold, MFM Stampanoni, MK Fix, P Manser*, American Association of Physicists in Medicine Annual Meeting & Exhibition, accepted for Oral Presentation, Virtual, 2021

Monte Carlo based assessment of VMAT, HyperArc and dynamic trajectory radiotherapy plan robustness against systematic machine uncertainties, *HA Loebner, S Mueller, W Volken, J Bertholet, P-H Mackeprang, G Guyer, DM Aebersold, MFM Stampanoni, P Manser, MK Fix*, International Conference on Monte Carlo Techniques for Medical Applications, accepted for Oral Presentation, Antwerp, Belgium, 2022

Surface Monitoring for Dynamic Trajectory Radiotherapy – A Feasibility Study, *HA Loebner, J Bertholet, D Frauchiger, MFM Stampanoni, P Manser*

& MK Fix, American Association of Physicists in Medicine Annual Meeting & Exhibition, accepted for Poster Presentation, Washington, USA, 2022

Proof of Concept of Surface Monitoring for Dynamic Trajectory Radiotherapy, *HA Loebner, J Bertholet, D Frauchiger, MFM Stampanoni, P Manser & MK Fix*, European Congress of Medical Physics, accepted for Poster Presentation, Dublin, Ireland, 2022

Automated dynamic trajectory radiotherapy planning using 4pi-IMRT path-finding - proof of concept, *HA Loebner, J Bertholet, S Mueller, G Guyer, D Frei, W Volken, O Elicin, DM Aebersold, MFM Stampanoni, MK Fix, P Manser & P-H Mackeprang*, European Society for Radiotherapy and Oncology Annual Meeting, accepted for Poster Discussion, Vienna, Austria, 2023

Gated dynamic trajectory radiotherapy: feasibility, mechanical accuracy and dosimetric validation, *HA Loebner, D Frauchiger, D Terriblini, S Mueller, G Guyer, P-H Mackeprang, MFM Stampanoni, MK Fix, P Manser & J Bertholet*, European Society for Radiotherapy and Oncology Annual Meeting, accepted for Poster Presentation, Vienna, Austria, 2023

National Conferences

Development of a treatment QA framework for dynamic radiotherapy using logfile based Monte Carlo dose calculation, *HA Loebner, S Mueller, J Bertholet, MFM Stampanoni, DM Aebersold, P Manser & MK Fix*, Scientific Association of Swiss Radiation Oncology Annual Meeting, accepted for Poster Presentation, Virtual, 2020

Predicting machine uncertainties from logfile data of a radiotherapy system using machine learning, *HA Loebner, P-H Mackeprang, S Mueller, J Bertholet, MK Fix & P Manser*, Bern Data Science Days, accepted for Poster Presentation,

Bern, Switzerland, 2021

Investigating the trade-offs between plan quality, delivery time and deliverability as a function of freedom in table rotation for dynamic trajectory radiotherapy, HA Loebner, S Mueller, W Volken, G Guyer, P Wallimann, DM Aebersold, MFM Stampanoni, P Manser & MK Fix, Scientific Association of Swiss Radiation Oncology Annual Meeting, accepted for Poster Presentation, Rorschach, Switzerland, 2021

A tool to assess robustness of radiotherapy dose distributions against patient- and machine-related uncertainties, HA Loebner, W Volken, S Mueller, J Bertholet, P-H Mackeprang, G Guyer, DM Aebersold, MFM Stampanoni, P Manser, MK Fix, Bern Data Science Days, accepted for Poster Presentation, Bern, Switzerland, 2022

Feasibility and mechanical accuracy of gated dynamic trajectory radiotherapy, HA Loebner, D Frauchiger, D Terribilini, S Mueller, G Guyer, P-H Mackeprang, MFM Stampanoni, MK Fix, P Manser & J Bertholet, Swiss Society of Radiobiology and Medical Physics Annual Meeting, accepted for Oral Presentation, Thun, Switzerland, 2022

An Automatic Intensity Optimization Process for a Commercial Treatment Planning System, HA Loebner, P-H Mackeprang, J Bertholet, S Mueller, N Torelli, G Guyer, MFM Stampanoni, MK Fix & P Manser, Swiss Society of Radiobiology and Medical Physics Annual Meeting, accepted for Oral Presentation, Thun, Switzerland, 2022

Plan robustness to patient-setup uncertainties of dynamic trajectory radiotherapy and volumetric modulated arc therapy plans for head and neck cancer, HA Loebner, J Bertholet, P-H Mackeprang, W Volken, DM Aebersold,

MFM Stampanoni, P Manser & MK Fix, Scientific Association of Swiss Radiation Oncology Annual Meeting, accepted for Poster Presentation, Bern, Switzerland, 2023

Grants

Following grant was awarded by the Swiss Society of Radiobiology and Medical Physics Annual Meeting. The results will be presented at the Swiss Society of Radiobiology and Medical Physics Annual Meeting 2023 in Lucerne.

Robustness Assessment of Swiss Radiotherapy Treatment Plans,
HA Loebner (PI), P-H Mackeprang (clinical assessment), MK Fix & P Manser (scientific oversight & discussion), Research Grant of the Swiss Society of Radiobiology and Medical Physics, 2022

PEER REVIEW

During my PhD studies, I was able to participate in the peer review process of following journals:

International Journal of Radiation Oncology, Biology, Physics (4)

Radiation Oncology (3)

Medical Physics (2)

Physics and Imaging in Radiation Oncology (2)

Biomedical Physics & Engineering Express (1)



CURRICULUM VITAE

PERSONAL DATA

Name Hannes Anton Loebner
Date of Birth 28th of June 1995
Place of Birth Achern, Germany

EDUCATION

2019-present PhD candidate
*Division of Medical Radiation Physics, Inselspital, Bern,
Switzerland
ETH Zurich, Zurich, Switzerland*

2019-present Medical Physicist in Training
*Swiss Society of Radiobiology and Medical Physics,
Switzerland*

2020-2022 Master of Advanced Studies (MAS) Medical Physics
ETH Zurich, Zurich, Switzerland

2018-2019 Master of Science in Physics
ETH Zurich, Zurich, Switzerland

2014-2017 Bachelor of Science in Physics
ETH Zurich, Zurich, Switzerland

2005-2013 Abitur
Gymnasium Achern, Achern, Germany

EMPLOYMENT

2019-present PhD candidate
*Division of Medical Radiation Physics, Inselspital, Bern,
Switzerland*

2016-2019 Speaker, Lecturer, Teaching Assistant
*Experimentalphysik Vorlesung, ETH Unterwegs,
Department of Physics, ETH Zurich, Zurich,
Switzerland*